Essentials of Autopsy Practice

Updates and Reviews to Aid Practice

Guy N. Rutty
Editor

Springer

Essentials of Autopsy Practice

Guy N. Rutty
Editor

Essentials of Autopsy Practice

Updates and Reviews to Aid Practice

Springer

Editor
Guy N. Rutty
East Midlands Forensic Pathology Unit
University of Leicester
Leicester, UK

ISBN 978-3-031-11540-0 ISBN 978-3-031-11541-7 (eBook)
https://doi.org/10.1007/978-3-031-11541-7

This Springer imprint is published by the registered company Springer Nature Switzerland AG
The registered company address is: Gewerbestrasse 11, 6330 Cham, Switzerland

Preface

When I started the *Essentials* series over 20 years ago my intention was to aid practitioners keep up to date with changes within the field of death investigation and plug reference knowledge gaps that often occur with larger textbooks of medico-legal practice, which, by their nature, cannot be expected to cover all areas of practice. In this ninth edition in the series, I have yet again tried to identify subject matter and authors from across the world and bring them together to present a range of subjects where changes in practice have occurred in recent times or where I felt there was a knowledge gap in terms of an easily accessible reference source for death investigation practice. As I have spent much of the last 20 years exploring the application of cross-sectional radiology to autopsy practice, through practice and research, and as I felt that there was a growing use of cross-sectional imaging across the world, a large proportion of this edition is focused on this area of practice and its wider application. There are then chapters focusing on recent updates related to disaster victim identification as well as chapters considering the re-examination of the previously autopsied or exhumed body, deaths associated with trees as well as a continuation from the last edition with further consideration of deaths related to activities in the mountain and those associated with mass slope movement. I hope that the subject matter chosen aids practice as well as assists personal and professional development.

Leicestershire, UK

Guy N. Rutty
MBE FMedSci

Contents

Contributors

Barszcz Marta MSc Department of Forensic Medicine, Jagiellonian University Medical College, Kraków, Poland

Biggs Mike MB ChB MRCS FRCPath MFFLM MD East Midlands Forensic Pathology Unit, University of Leicester, Leicester Royal Infirmary, Leicester, UK

Blau Soren AM, BA(Hons), MSc, PhD, FFSc (RCPA), CF Victorian Institute of Forensic Medicine / Department of Forensic Medicine, Monash University Victoria, Southbank, VIC, Australia

Christensen Angi M. PhD, D-ABFA, C-FASE FBI Laboratory, Quantico, VA, USA

Clarkson Melanie Elizabeth OStJ BDS MSc (Dist) MFGDP(UK) RAF Headquarters Defence Medical Services, Lichfield, Staffordshire, United Kingdom

de Boer Hans MD, PgDipPMCT, PhD Victorian Institute of Forensic Medicine / Department of Forensic Medicine, Monash University Victoria, Southbank, VIC, Australia

Hainsworth Sarah V. OBE FREng University of Bath, Claverton Down, Bath, UK

Jackowski Christian MD, Prof., EMBA Institute of Forensic Medicine, University of Bern, Bern, Switzerland

Machin Ruth MBBS FRCR MA Msc Infirmary Square, University Hospitals of Leicester, Leicester, UK

Marsden Philip Haley BDS Lond LDS RCS Eng DipFOd MSc (Hons) DipFMS DipFHID London, United Kingdom

Moskała Artur MD PhD Department of Forensic Medicine, Jagiellonian University Medical College, Kraków, Poland

Ranson David B.Med.Sci. B.M. B.S. LLB. FRCPath. FRCPA. FACLM. FFFLM (RCP). FFCFM (RCPA). FFPMI (RCPA). DMJ (Path) Victorian Institute of Forensic Medicine / Department of Forensic Medicine, Monash University Victoria, Southbank, VIC, Australia

Rutty Guy N. MBE MBBS MD FRCPath DipRCPath(Forensic) FFFLM FCSFS AFHEA DipIMC FMedSci East Midlands Forensic Pathology Unit, University of Leicester, Leicester Royal Infirmary, Leicester, UK

Rzepecka-Woźniak Ewa MD PhD Department of Forensic Medicine, Jagiellonian University Medical College, Kraków, Poland

Weyrauch Deland MD Yale School of Medicine, New Haven, CT, USA

Woźniak Krzysztof Jerzy MD PDD Department of Forensic Medicine, Jagiellonian University Medical College, Kraków, Poland

Zech Wolf-Dieter MD, EMBA Institute of Forensic Medicine, University of Bern, Bern, Switzerland

Chapter 1
Forensic Application of "Free-D" Software

Mike Biggs

Introduction

Many practitioners will already be familiar with the use of cross-sectional imaging, such as computed tomography (CT) scanning, in forensic practice. Medically-focused imaging software packages that can recreate three-dimensional (3D) representations of the scanned data are widely available. For many years, whilst the hardware and software capability continued to improve, the standard 3D depiction of medical scan data remained largely similar in appearance. More recently, systems such as *Cinematic Rendering* (Siemens) [1] and *Global Illumination* (Canon) [2] have enabled clinicians to create more photorealistic and aesthetically-pleasing simulations. These facilities are not available to everyone, but alternatives exist. The purpose of this chapter is to tempt curious individuals into exploring what can be achieved using only software that is freely-available. A complete manual covering every aspect of this software would be beyond the scope of an introductory chapter, but online sources and textbooks already exist to fulfil this requirement (see below). Some basic direction and a few examples have been included here in the hope that others will be inspired to embrace this tool and enhance their own practice.

Blender

Many different 3D software applications are available, but one that is widely-known to 3D artists, animators, designers and 3D printers is *Blender*. This software is free to download and use for any purpose, for any computing platform,

M. Biggs (✉)
East Midlands Forensic Pathology Unit, University of Leicester, Leicester Royal Infirmary, Robert Kilpatrick Building, Leicester, UK
e-mail: mb614@le.ac.uk

G. N. Rutty (ed.), *Essentials of Autopsy Practice*,
https://doi.org/10.1007/978-3-031-11541-7_1

from www.blender.org [3], and is sufficiently comprehensive to satisfy all of the likely requirements of forensic practitioners seeking to expand beyond what standard DICOM (Digital Imaging and Communications in Medicine) viewing software currently allows. Put simply, *Blender* unlocks the potential hidden within your scan data. Learn *Blender*, and you will be able not only to view your scans, but to interact with and manipulate the 3D elements, produce higher-quality images and animations, and even potentially to conduct some types of useful analysis. Throughout this chapter, capitalisation and inverted commas have been used to emphasise specific *Blender* terminology in the hope that this will make it easier to identify the search terms to use when looking online for further resources as you begin to extend your capability.

Getting Started

Downloading and installing *Blender* are the first steps, and they should not trouble anyone who already uses a computer. When the program is started for the first time, an initial setup screen should appear. Do not worry about the various options and default settings, as everything can be changed at any time later within the preferences menu. Most importantly at this stage is the fact that for many years the default method of selecting items was to click the *right* mouse button. This often feels alien to new users, who have invariably been accustomed to using the *left* mouse button to select items ever since they first grasped a computer mouse. Following the introduction of *Blender 2.8*, which overhauled the user interface to make it more user-friendly and intuitive for new users, this default changed to selection with the *left* mouse button. If the default "select with left" is highlighted then you are safe to proceed.

The initial start-up screen may appear fairly daunting, but do not be discouraged by the interface at first glance, especially if you are new to this type of software. All of the tiny icons, numbers, headings and sub-menus can be ignored until you need to use them, and as you need to use them you will gradually find out where the important ones are, and what they do. You can customise almost every conceivable parameter using the "Preferences" menu option, and adjust the layout of the interface to suit your own specific requirements. By saving a "Startup" file (hidden under "Defaults" in the "File" menu) you can be sure that every time you open *Blender* it will appear exactly as you like to use it, rather than reverting back to the default settings.

The *Blender* workspace is easiest to navigate using a 3-button mouse, and a full-size keyboard with a dedicated numpad (i.e. the separate block of number keys to the right of a full-size keyboard, and not just the row of numbers across the top). This does not mean that you *cannot* use a laptop, but it will certainly feel more awkward, especially at first. There are often multiple methods of achieving the same effect, and personal preference will dictate whether you opt to search through menus, click on icons or use keyboard shortcuts. In practice, the keyboard shortcuts are usually the fastest, most efficient methods, so even though it may take some time to learn them, the shortcut keys will save you more time in the future once familiar.

The screen itself is divided into separate sections, and exactly how many sections are displayed, their shape, size and what is contained within each of them can be customised later, as required. For example, when previewing materials or camera views (both discussed later) you may find it helpful to split the screen and have one section for manipulating objects whilst the other section provides a real-time preview. To begin with, the majority of the screen consists of the 3D workspace, and a default cube, light and camera are preconfigured within this space. The top right section is the "Outliner", which contains a list of all objects present, shows their status and allows you to rename them and control whether or not they are visible. The lower right section is the "Properties" editor, and the vertical column of small, coloured icons at the left side of the Properties editor lets you select which property to edit (examples are given below). As mentioned above, it is not the intention of this chapter to provide a complete beginner course covering every aspect of this software. After downloading the installation package from the *Blender* website, it is well worth also clicking on the "Support" tab at the top of the website and then selecting the "Tutorials" section. Here you will find online tutorials, and watching at least the first few "Fundamentals" tutorials is highly recommended. If you look along the very bottom edge of the *Blender* window, you will notice a series of icons explaining what various mouse actions will do, and this changes as you press CTRL, ALT or SHIFT keys, for example. Keep an eye on this bar, and you will notice that as you begin to interact with objects and access different modes, the various keyboard shortcuts will be displayed here, giving you valuable hints until you become familiar.

Learning to navigate your way around the 3D workspace might feel strange initially, but controlling the view by orbiting/panning and zooming with the mouse and keyboard should quickly become intuitive. If the default cube is not interesting enough to practice with, you could instead load a skull or other anatomical object from one of your scans. It is worth noting at this stage that if you try to "open" or "save" a file, this refers to files of the *blend* format (i.e. the *whole* project, including all the objects, orientations, settings, etc.). If you intend to "load" a 3D object into *Blender* then you must actually "import" the file. Similarly, when you wish to "save" a 3D model, you will instead need to "export" it as a 3D file. (If you have made more than one object in the same workspace, there is a box to tick to export *only* the selected item, so you don't end up with a single file that includes *all* of the objects present within the scene.)

There are several different 3D file formats, but unless you have a specific reason for using one of the other types then it is recommended to use the standard "STL" file. The STL file format encodes a list of points (called "vertices") aligned in 3D space using standard x, y and z Cartesian co-ordinate axes. As illustrated in Fig. 1.1, *vertices* are joined together by *edges* to form a network (known as a "mesh") of triangular *faces*.

The production of 3D anatomical models from DICOM data has been covered elsewhere [4], but if you have not already tried this then rest assured that commonly-used viewers (such as *OsiriX* / *Horos* and *3D Slicer*) [5–8] all have the ability to

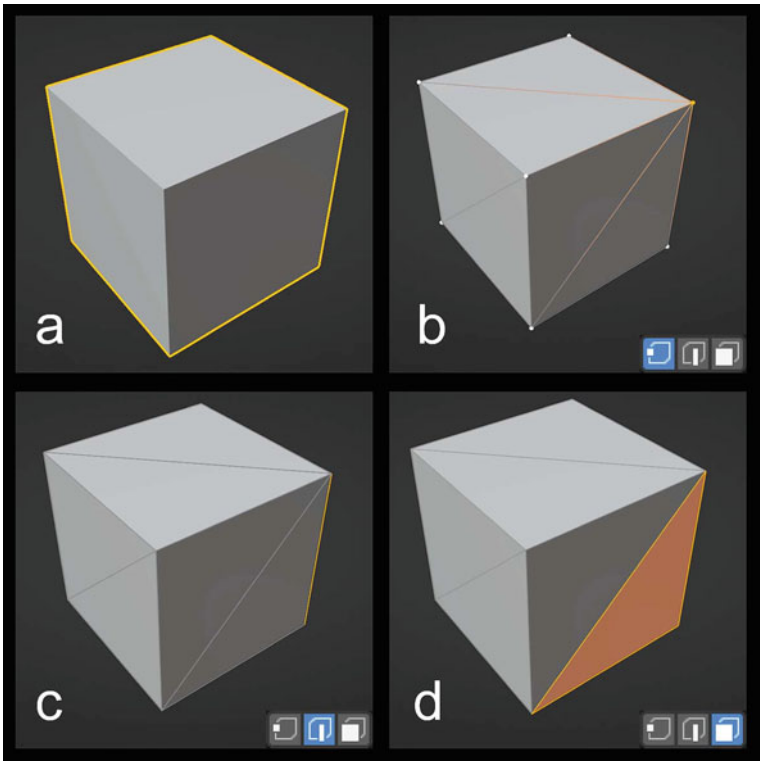

Fig. 1.1 **a** In Object mode the entire cube is selected and the underlying mesh is not visible, **b** Edit mode (vertex selection): the triangular mesh is visible and the vertices can be seen and selected, **c** Edit mode (edge selection): vertices are not directly visible and instead selection applies to whole edges, **d** Edit mode (face selection): entire faces can be selected with a single click. *Inset* within **b–d** are the icons that need to be clicked to switch between these modes

export files in the STL format. The first time you import a 3D model, you may be surprised to find that you cannot see it. This is likely to be because its "origin" (which functions as a "handle" for positioning the object) was derived from the large volume included within the whole CT scan dataset, and this will usually be far removed from the origin (i.e. middle) of the *Blender* 3D world. If you press the "." (decimal point) key on the numpad, it will align the view to the active object. Alternatively, you can move the object to the origin of the *Blender* scene. If you right click on an object (or select the "Object" menu, usually located at the top of the 3D view), you should see an option to "Set Origin". The "3D cursor" is the red and white circle that will be in the middle of the scene (unless you have inadvertently moved it already, in which case you can reset it by holding SHIFT and pressing C). By setting the origin of the object to the 3D cursor, the small orange dot that represents the origin of the object will be moved to the centre of the scene. The object itself has not moved, and its origin is now potentially a long way outside the actual shape. Now if you repeat the

origin-setting procedure, and this time set the geometry (i.e. the shape) to the origin, you will see the object jump to the centre of the scene. This process may seem overly complicated at first, but later you will appreciate that this powerful function can be used to position and control objects very precisely.

Once you have created an anatomical model and imported it into *Blender*, there are some other principles that need to be understood early on in order for more complex operations to make sense later. Pressing the TAB key toggles between "Object" mode and "Edit" mode. (There are several other modes, but you can safely ignore those until you require them for a specific reason.) You must enter edit mode to see (and edit) an object's "mesh" (its actual underlying architecture), whereas object mode restricts you to making whole-object adjustments. The mesh is a visual representation of the network of interconnected vertices, edges and faces encoded within the STL file. In edit mode, you can choose between either vertex-, edge- or face-selection methods (see Fig. 1.1), and this is important to note as there are subtle differences between what is possible with each, which can cause frustration until this is realised.

The difference between "Orthographic" and "Perspective" view (toggled between by pressing numpad key 5) might not at first seem particularly significant (Fig. 1.2). However, in perspective view mode you can zoom "inside" objects, and this can be vital in certain editing situations. Also, the Z key can be used to switch between solid and wireframe view, which not only influences how the workspace looks, but affects your ability to select vertices that might be hidden behind the front of an object whilst in solid view (Fig. 1.3).

Getting used to aligning and navigating the 3D view, importing, controlling and editing 3D objects, selecting parts of a mesh and locating options within menus takes some practice, but quickly becomes automatic (or, at least, *semi*-automatic!). If you have managed to follow up to this point then you are ready to see how and why this software might actually be of benefit to your practice. You may have noticed that a

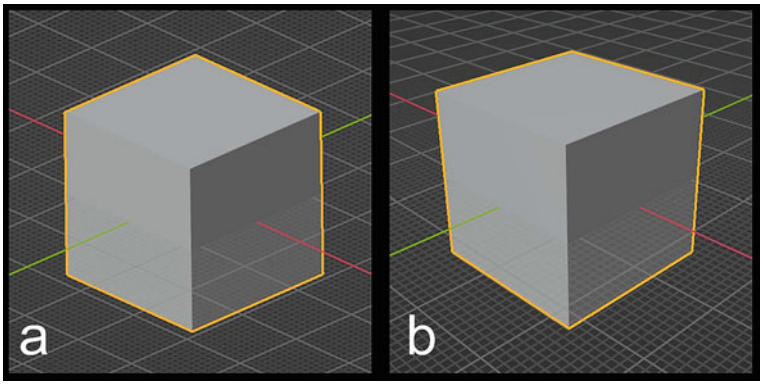

Fig. 1.2 **a** Orthographic view, **b** Perspective view. The same cube and background grid look noticeably different, depending upon which viewing mode is in use. Most importantly, if you need to zoom "inside" an object then you must first activate Perspective view (numpad key 5 toggles between the two)

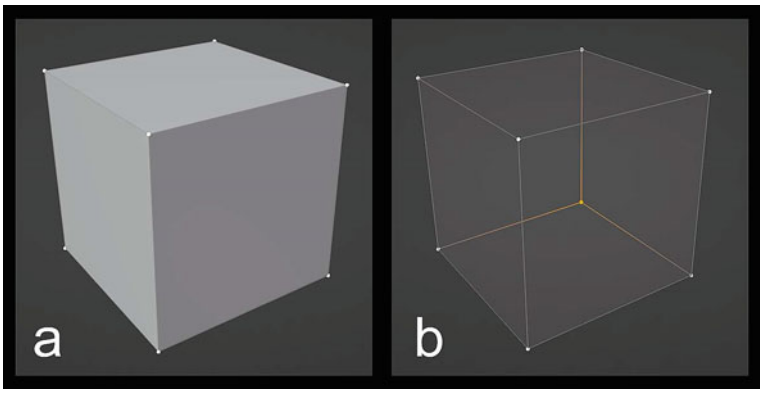

Fig. 1.3 **a** Solid view, with front faces "blocking" visibility of vertices at the back of the object, **b** Wireframe view allows you to see and select vertices (*orange*) that were obscured by other parts of the object in solid mode

side panel of values can be summoned at the right side of the 3D view, which contains a variety of parameters you might wish to adjust. This menu can be toggled in and out of view by pressing the N key. Another essential trick to know is that when you add an object or carry out an action, the so-called "Operator" panel (which contains essential variables for you to specify) may disappear before you've finished with it (or may not appear at all). Do not panic: it can be made to reappear by pressing the F9 key. This works only until you add your next object (or carry out your next action) though, so make sure you have completely finished with the Operator panel before you move on.

Basic Tidying

As mentioned in the introduction, *Blender* allows you not only to "see" your 3D anatomical models, but to interact with them. Why might this be useful? If you have a CT scan of a comminuted fracture, the individual fracture fragments might be displaced. With *Blender* you can re-approximate these fragments in order to see the fracture pattern more clearly. If you have a dismembered body that has been scanned in separate sections, you can now import the individual portions into the same workspace and place them back into continuity. If there are multiple foreign bodies and debris items, you can remove them to leave a clearer view of the anatomy that you wish to illustrate. To do all of these things, you need to be able to select and move individual parts.

Selection

You can select individual elements, using a number of tools, in both object and edit modes. Any 3D model that you have extracted from a DICOM viewer will have been imported as a single object, and in order to select individual parts of it you will first need to separate them into different objects. This can be done by pressing the P key whilst in edit mode, at which point you will see the various options available. If the parts are not touching one another, they can simply be separated as “Loose parts”. If they are touching, the software considers them as a single object, and they must first be separated manually. By selecting the parts of the mesh where contact occurs, and deleting them (either the DELETE or X key activates the delete menu), you can remove any contact between the parts, which can then be separated. (You will notice that opting to delete vertices actually deletes a wider area than your selection, and so deleting only the selected faces might be preferable in many situations.) The resulting “holes” in the separated parts can be closed later (see below).

When you first enter edit mode, you may notice that all of the vertices are already selected (highlighted orange). Pressing the A key whilst holding ALT will deselect everything, and pressing A on its own will select everything that is not already selected. Clicking on a single vertex will select only that single vertex, and holding SHIFT whilst clicking on other vertices will add them to the selection (whereas holding SHIFT whilst clicking on already-selected vertices will deselect them). Holding CTRL and clicking on a vertex some distance away from one that is already selected will select the shortest distance path between the two. This is a good technique that allows rapid encirclement of a join between two parts that you wish to separate, as you can click at a few strategic points around the perimeter whilst holding the CTRL key, rather than having to select each individual vertex as you work around the intended “cut” line (Fig. 1.4).

If the join line between two parts that you intend to separate is particularly jagged, you can use the “Knife” tool to draw a straighter line across the surface of the mesh. Pressing K whilst in edit mode activates the Knife tool, and then you can left mouse button click at your intended start point and either drag or re-click intermittently (with slightly different results) along your chosen path. If you are happy with the cut lines, press RETURN to confirm, otherwise press ESC to cancel. Once the new cut lines have been incorporated onto the surface, it will be possible to delete the unwanted parts of the mesh whilst leaving a neater edge (Fig. 1.5).

As mentioned above, separation of parts in this way will leave holes in each part. A quick way of closing these holes is to select an edge whilst holding the ALT key. If the hole is relatively straight-edged then this may select the entire hole outline in a single action, but often there are irregularities meaning that multiple sections of the edge must be selected by holding SHIFT + ALT and clicking at each unselected portion of the hole’s outline until the entire edge is selected. This can then be crudely filled by pressing ALT + F. (Alternative methods for repairing such defects will be covered in more detail below.)

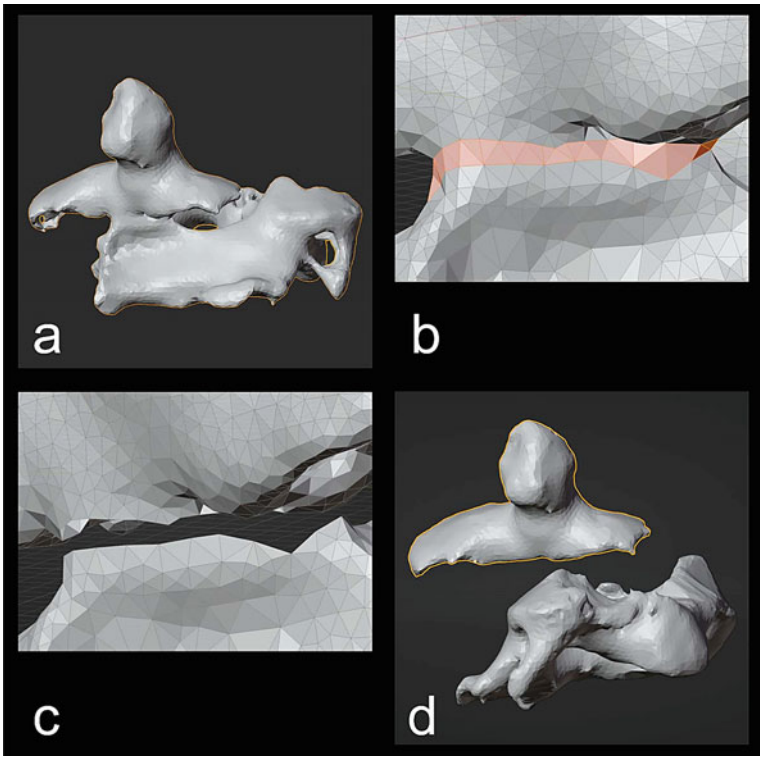

Fig. 1.4 **a** Parts that are in direct contact with each other cannot be separated automatically, and are treated as a single object, **b** In Edit mode the points of contact can be selected (*orange*) using a variety of selection methods, **c** The selected areas can be deleted to leave a clear gap between the parts to be separated, **d** Once no longer physically joined, the parts can be separated into individual objects and manipulated independently in Object mode

Different methods of selection can be used depending on the situation. Pressing B (for "box") and then "clicking and dragging" a rectangular box is a quick method of selecting items, although the geometric nature of such selection is not always ideal for precise selection in relation to complex anatomical shapes. Pressing C ("circle") gives you a circular cursor (which can be increased or decreased in size using the mouse wheel) to "paint" a selection. Holding SHIFT whilst clicking on already-selected areas will deselect them. Once finished, press ESC to exit circle selection mode. Perhaps more useful for irregular anatomical shapes is the "lasso" selection tool. By holding CTRL whilst clicking and dragging the *right* mouse button, you can draw a freehand selection around your required area. When you release the mouse button, everything within the area you have drawn will become selected. Any selections made can be fine-tuned by holding down SHIFT and clicking on additional items to add them (or clicking on selected items to deselect them).

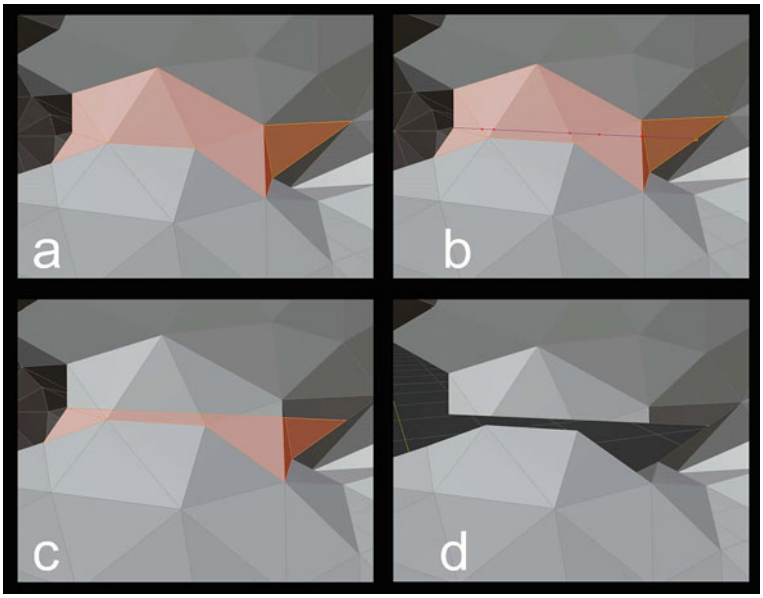

Fig. 1.5 **a** The intended line of separation (*orange*) is deemed too irregular for the intended purpose, **b** The Knife tool is used to cut a straight line directly across the faces, **c** The selection (*orange*) can now be restricted to the newly created faces to leave a straight border, **d** After deletion the cut part has a straight edge

Another selection feature allows you to select "linked" elements using the L key. If you already have some vertices selected, holding CTRL and pressing L will add all linked vertices to the current selection. Alternatively, pressing L with the mouse pointer over an object will select everything linked to that object. This method is good for removing debris or other unwanted elements quickly, simply by pressing the L key each time you place the mouse pointer over an element you intend to keep. Then, holding CTRL and pressing I ("invert") will switch the selection to everything *else* instead. These can then be deleted to leave a much cleaner 3D workspace, and selecting a small number of large items and inverting the selection is far simpler than attempting to target many small items individually (Fig. 1.6).

So far it has been assumed that the default "vertex" selection mode is being used. For various reasons it may be preferable to switch to edge or face selection mode. This can be done by clicking on the small icons (depicted in Fig. 1.1) at the top left of the 3D view, or by pressing the 1, 2 or 3 keys on the top row of the main keyboard (*not* the numpad). By holding SHIFT and clicking on more than one icon, multiple selection modes can be active simultaneously. The significance of each mode will become apparent later. Some additional specialised selection features also exist, but the above should enable most tasks to be completed successfully. If the view ever appears so cluttered as to make seeing particular items difficult, you can "Hide" unnecessary areas temporarily. Simply select any parts of the model that you do

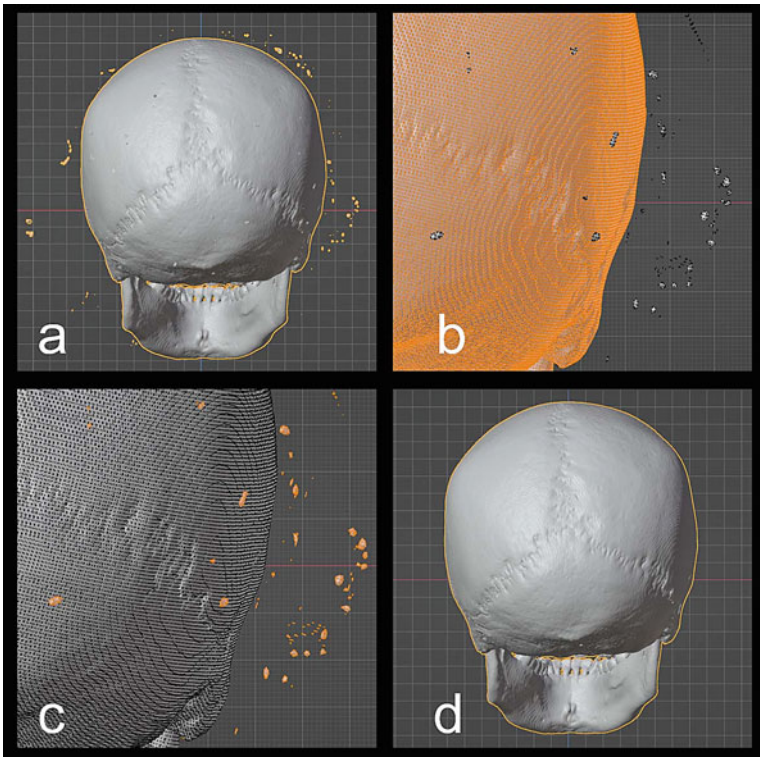

Fig. 1.6 **a** Anatomical models extracted from CT scan data may contain large numbers of unwanted small debris items, **b** Large items (*orange*) can easily be selected quickly in Edit mode, **c** Inverting the selection then highlights all of the debris items instead (*orange*), **d** These can then be deleted in a single action, which is considerably quicker than trying to edit such items out individually

not need to view, and then press the H key to make them disappear. You can keep repeating this step to remove multiple parts until the view is sufficiently clear, which should enable you to focus solely upon the important elements. (Alternatively, you can use SHIFT + H to hide everything *apart* from the current selection.) After you have completed your editing steps, you can restore all of the hidden elements by pressing ALT + H.

Removing Artefacts

This process can be very time-consuming, but can have an extreme impact in cases where there is no alternative (Fig. 1.7).

Whilst it would be possible to remove many of the unwanted items in the medical imaging software prior to exporting the 3D file, in practice this is a fairly crude method and can result in alteration of the surface of the 3D model if cropping is

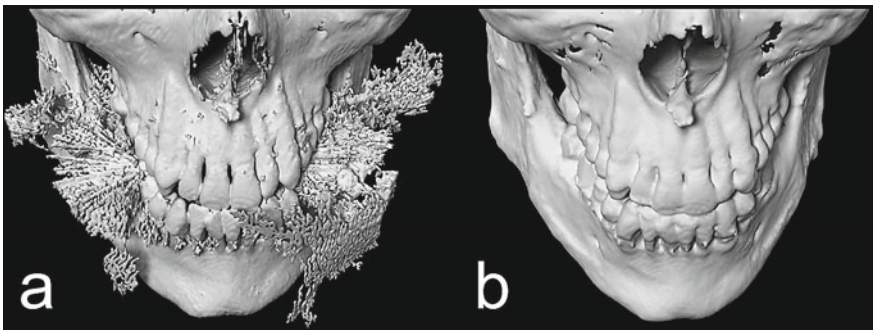

Fig. 1.7 **a** Extreme scanning artefact caused by metallic dental restorations, **b** The same case following manual removal of artefacts in Edit mode. This process consists of selecting and deleting any unwanted items, followed by repairing any holes left behind (see below)

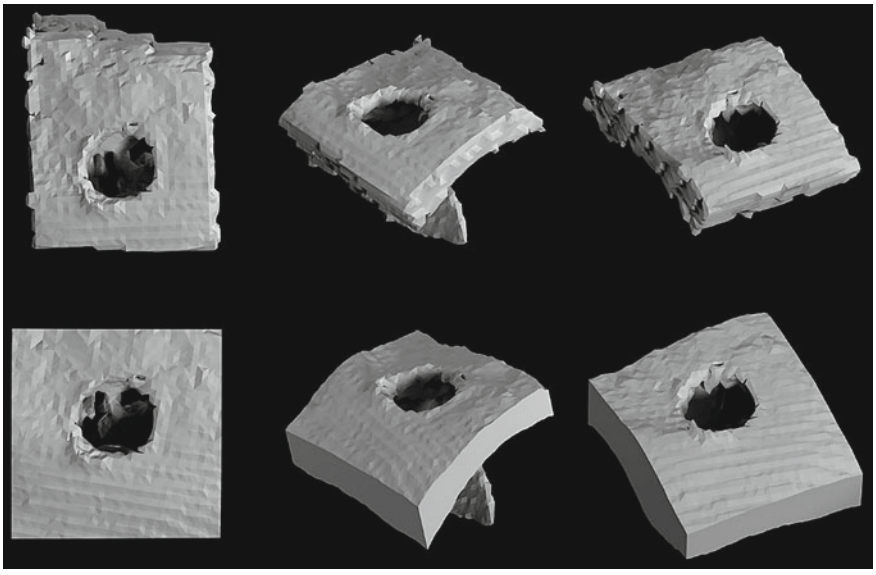

Fig. 1.8 Various views of the same segment of skull containing a penetrating projectile injury. The top row was cropped directly within the DICOM viewing software, whereas the bottom row used Blender's capability for a neater result

attempted close to the edge of an object to be retained. Editing afterwards in *Blender* affords a far greater degree of control and precision. This precision also extends to cropping. When using the medical imaging software to crop objects, the cropping plane can be controlled with relatively limited precision and the finished edges may appear roughened or incomplete. By waiting until the *Blender* editing stage to carry out any required cropping procedures, far greater control of the cropping plane is

achievable, and the edges of the cuts can be made perfectly flat and completely sealed, as illustrated in Fig. 1.8.

Other procedures, such as smoothing rough or otherwise irregular surfaces can also be carried out quickly and easily. Evidently such a process would not be appropriate where this detail is of forensic importance, but where for aesthetic or other reasons some form of smoothing is desirable then this is another example of a software feature that can be employed to good effect, and with minimal effort.

Filling Holes

If you intend to 3D print a physical model then the STL file that you export must be so-called "manifold". That is to say "watertight", with no artefacts to confuse the slicing software that converts STL files into 3D printer instructions. This does not mean that the model cannot have holes, it just means that all of the surfaces between and around the holes have to be intact. In simple terms, the slicer software needs to be able to differentiate between the "inside" and "outside" of the walls of the model. If the vertices, edges and faces that make up a surface are incomplete, duplicated or facing "inside-out", then the software may not be able to interpret the file, leading to 3D printing anomalies. This can be frustrating (and potentially expensive) if the anomaly is not revealed until it ruins a full-size skull that had been printing for 72 hours, and was *almost* finished!

Luckily, *Blender* comes with helpful 3D printing tools that help you identify and rectify such anomalies before they can cause trouble. If you enter edit mode and then ensure nothing is selected (by clicking in empty space, or pressing ALT + A), you can ask *Blender* to select any non-manifold areas of the model. This does not work in face-selection mode, so ensure that you are using either edge- or vertex-selection mode (see above). Go to the "Select" menu (located at the top of the 3D view), and from this menu choose "Select All by Trait" and then "Non Manifold". Any areas highlighted orange will need attention if you intend to 3D print the model. If you enable the "3D Print Toolbox" add-on (by searching in the "Add-ons" tab of the "Preferences" menu) you will unlock further 3D print analysis functionality, which may also be of benefit when checking models for 3D printability.

It may be obvious that there are holes in a surface that need to be filled. This can be done by selecting the outline of a hole and then filling the hole with either a face or a group of faces, depending on the shape (Fig. 1.9). As described in the selection section above, pressing ALT whilst clicking on the edge of a hole will select the entire edge in one action (but again this works only in edge- or vertex-selection modes, not face-selection). If the shape of the hole is too complex, only part of the edge may be selected. In this case, hold SHIFT whilst pressing ALT and clicking at multiple points around the hole, adding to the edge selection until the entire loop is closed. Now, if you press F the hole will be filled with a single face, but unless the defect is a simple triangle or square this is not ideal. If the hole is complex, the resulting "fill" will be a so-called "Ngon", which does not truly fill the surface defect and will cause

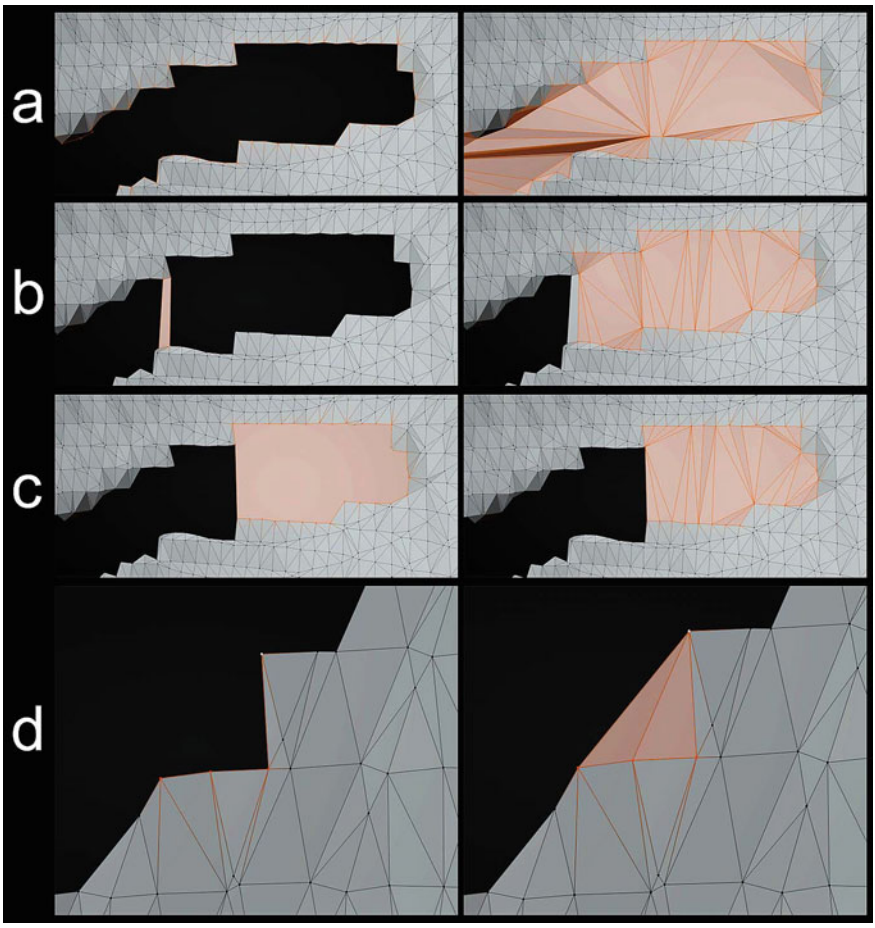

Fig. 1.9 **a** Left: in Edit mode, the boundary edge of a hole can be selected by holding ALT whilst left-clicking on an edge (in either edge or vertex selection mode, but not face selection). Right: ALT + F will then fill the selected hole with triangular faces, although the effect may produce harsh angles and awkward faces that disrupt the contour of the finished surface, **b** Left: as an alternative, individual sections can be partitioned off by creating faces (by selecting opposing pairs of vertices and then pressing the F key) at strategic points. Right: the ALT + F method of filling now produces a cleaner result, **c** Left: another method involves selecting part of an edge boundary (e.g. by holding CTRL to select the shortest path between two points) and then pressing F to fill the space with a single “Ngon”. Right: the resulting Ngon can be converted to triangular faces by pressing CTRL + T, **d** Left: jagged steps in a boundary can cause issues with hole filling, but are easily overcome by first selecting the involved vertices. Right: after pressing F (followed by CTRL + T if necessary) the jagged step has been replaced by a smooth slope, making automated edge selection and hole filling easier

issues with 3D printing. It is therefore better to press ALT + F, which will fill the space with true triangular faces. An option called "grid fill" (accessed via the "Face" menu at the top of the 3D view) can be used to fill a hole with a uniform pattern of faces, but this works better for simple geometric objects, and can cause undesirable results when applied to complicated anatomical shapes. For very complex holes, it may be necessary to fill using several smaller chunks rather than attempting a single operation. For example, by selecting only a portion of the hole (using selection tools described above), then pressing F to fill that section, followed by CTRL + T to turn the resulting Ngon into triangular faces, you can gradually fill a defect that would otherwise be too irregular for automated procedures to complete correctly. If you need to fill many holes in a model, this process will start to become both intuitive and (slightly) quicker with more practice.

Not all non-manifold areas will require a hole to be filled. In some cases, it may simply be that when the STL was being extracted from the DICOM dataset, some faces were "flipped", so that their inside surfaces were placed on the outside of the model. This will likely be visible in the 3D view as an area of the model with a darker colour (see Fig. 1.10). The property of a face that determines whether it is inside or outside is its so-called "normal", and this problem can usually be resolved simply by recalculating the normals (SHIFT + N) whilst in edit mode and with all faces selected (press A). If this does not cure the issue, then it may be that a hole or other defect has to be corrected first before the calculation can correctly interpret the appropriate inside-outside orientation.

In some cases, the cause of the non-manifold area will be two vertices occupying the same point in space, so that whilst the model appears intact, there is not a true, continuous single surface for the 3D printing software to process. These anomalies, known as "Doubles", used to be resolved using a menu option called simply "Remove Doubles". However, in the most recent versions of *Blender* this has disappeared.

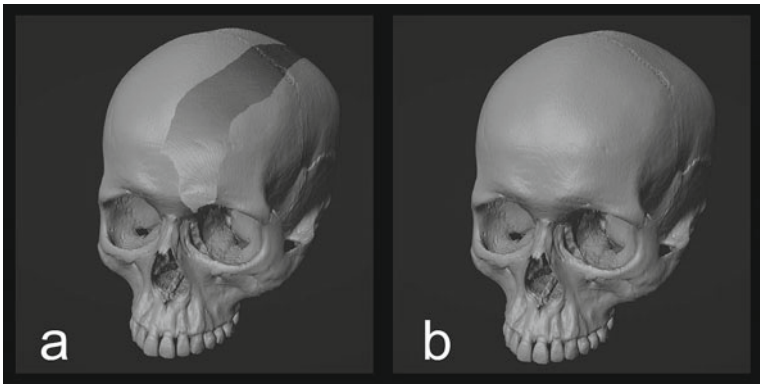

Fig. 1.10 **a** There is no physical defect in this skull, but the "normals" of some faces have been reversed, meaning that they are shaded to appear like an "inside" surface even though they are actually on the outside, **b** Simply recalculating the normals allows correct interpretation of inside and outside surfaces, with appropriate shading

Instead, you can mow "Merge" such anomalies together into a single vertex (which is in fact what the Remove Doubles tool used to do). In edit mode, select everything by pressing A, and then press M to open the merge menu. Select "By Distance", and any vertices that are sufficiently close to each other will be merged together. The merge distance can be altered, if necessary, but the default setting will remove any doubles. A message will appear at the bottom of the screen telling you how many vertices have been removed, and if you *did* have any doubles then the number that appears will be greater than zero.

The steps outlined above required to make a model manifold are essential only if you intend to 3D print the model. However, some of the anomalies, such as flipped normals or holes, can still cause unsightly effects when viewing the model and so it is always worth having the ability to repair such defects.

Manipulation

Once you have removed unwanted objects and tidied any defects or other artefacts, attention can be turned to altering the positions and alignments of the individual items that you have separated from the original single object. (These manipulations can be carried out in edit mode, without the need first to create separate objects, but such operations are more processor-intensive, and it is far quicker to manipulate in object mode.) You may of course import multiple objects from different scans, such as in the case of a dismembered body, or even a case that was scanned as different body sections rather than a whole body. If multiple 3D models have been extracted from the same scan (e.g. the skin surface and the underlying bones) then they should retain alignment with one another when you import them into *Blender*, as they will share a common origin point.

Separation of one object into multiple objects has already been discussed, and for completeness it is necessary to discuss the joining of multiple objects into a single object. As edit mode allows you to edit only the single object selected, you would first need to join separate objects together if you wished to edit them at the same time in edit mode. This is achieved simply by selecting multiple objects in object mode (by holding SHIFT and clicking on the required objects), and then pressing CTRL + J to join the objects into a single object. You will now be able to edit the separate meshes at the same time once you enter edit mode. If you encounter a situation where you wish to connect two separate meshes together in edit mode, it is possible to do this by first selecting edge loops (ALT + left click on one loop, followed by the same action on the opposite loop whilst holding SHIFT) on each mesh and then, with both edge loops selected, clicking on the "Edge" menu followed by "Bridge Edge Loops". (Alternatively, a similar process can be achieved manually in stages by adding the required faces individually using the F key after selecting appropriate vertices / edges.)

You may need to join separate fragments *physically* together (rather than just designating them as the same object), for example if you need dissociated fragments

to be in contact with one another to achieve a contiguous 3D print. In addition to the method depicted in Fig. 1.11, this can also be achieved by adding a mesh "Primitive" (such as a cylinder) in object mode using the SHIFT + A keys. Select a suitable shape from the mesh menu, scale it to the required size and move it into the necessary position so that it overlaps the fragments to be joined. A "Boolean modifier" (see below) can then be used to fuse the objects together.

If you want to move an object there are different methods available, but as with many procedures in *Blender* the keyboard shortcuts are often the most efficient… once you have learned all the shortcuts! In either edit mode or object mode, once you have selected something, pressing G ("grab") will then cause the entire selection (whether that is a single vertex, part of an object or multiple objects) to move with your mouse. Your mouse cursor does not need to be on or near the selection: as long as the cursor is within the 3D viewport (and not hovering over a menu on a different section of the screen) when you press G, the selection will simply start moving as you

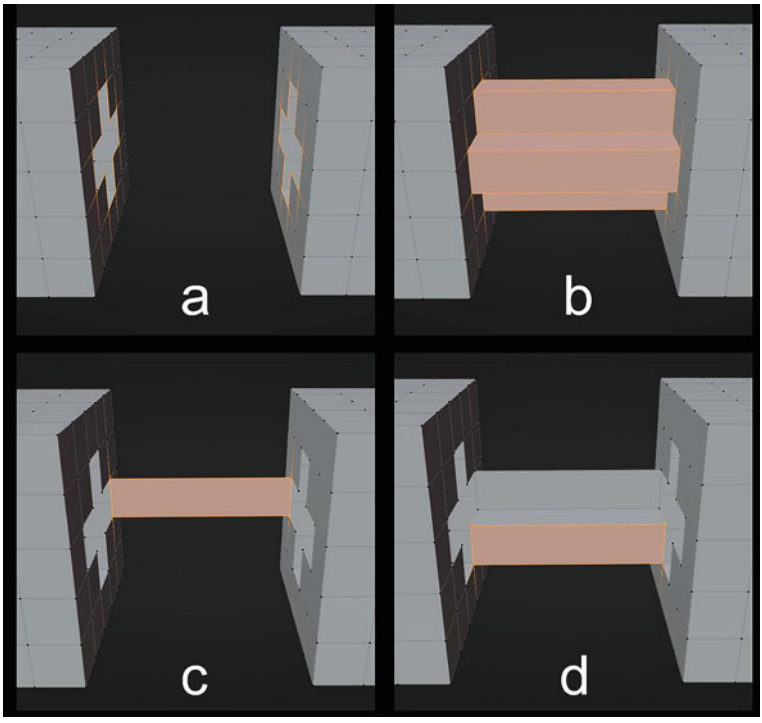

Fig. 1.11 **a** Edge loops (*orange*) around holes on opposite faces of two separate objects have been selected in Edit mode (holding CTRL to allow more than one loop to be selected simultaneously), **b** Using the "Bridge Edge Loops" option from the Edge menu (in Edit mode) creates a physical connection, bridging the gap between the two objects with a single action, **c** If this automatic function does not work, or is otherwise undesirable for a specific reason, individual faces (*orange*) can be created manually instead, **d** Simply select the vertices you wish to join and then press the F key to create each face exactly where it is required

move the mouse. Once you are satisfied with the new location, click the left mouse button (or press ENTER) to confirm the movement. If you change your mind whilst moving, you can click the right mouse button (or press the ESC key) to cancel the movement. If you change your mind *after* you have confirmed the movement, there is always the "Undo" command (CTRL + Z). You can undo any action that you have just carried out in *Blender* using this shortcut, and if you press CTRL + Z repeatedly you will notice that multiple backward steps can be taken. (The number of undo steps is yet another thing that can be specified, if necessary, within the "Preferences" menu.)

Once you have pressed the G key, you can refine the movement using other keys. For example, you can constrain the movement to a particular axis by pressing the X, Y or Z key. Alternatively, you can hold SHIFT whilst pressing one of the axis (X, Y or Z) keys to restrict movement to anything else *except* a single axis. Entering a numerical value after pressing the G key will snap the movement to the specified value (i.e. pressing 2 will move the selection exactly 2 *Blender* units). Pressing the "−" (minus) key, either before or after the numerical value, turns it negative and therefore moves the object in the opposite direction. Numerical control may not seem important when adjusting anatomical models visually, but will be of immense value if you decide later on to design custom items (see below). What may be more useful when fine-tuning the positions of anatomical models is "precision" mode, which considerably slows down the movement for as long as you hold the SHIFT key whilst moving the mouse, allowing greater precision during critical adjustments.

In addition to moving selected items, you can also rotate them. Pressing the R button activates "rotate" mode, and this functions similarly to the movement mode discussed above. This means that you can specify (or exclude) a single axis to constrain the rotation, enter a numerical value (positive or negative) for the number of degrees to rotate and slow down the rate of rotation by holding the SHIFT key. Confirming or cancelling the rotation is by the same method as before. If you simply press R and start to rotate the selection using the mouse, the direction of rotation will be determined by the starting viewpoint. Once you get used to this, you can pre-set the view (either by orbiting with the middle mouse button held down, or by using the numpad keys 1, 3, 7 or CRTL + 1, CTRL + 3, CTRL + 7) before rotating to achieve the effect you require. Eventually, through a combination of switching between viewpoints, moving and rotating objects, you will be able to position and align your objects relatively quickly and easily (Figs. 1.12 and 1.13). Of note, the rotation occurs around the specified "pivot point", which can be altered by choosing one of the options in the drop-down menu at the top of the 3D view. If you have separated objects then you may need to re-set their origins (described above) to the centre of each object in order to make any movement and rotation adjustments easier to control.

As well as G to move and R to rotate, the S key can be used to "scale" a selection, increasing or decreasing its size. This is unlikely to be useful when aligning anatomical models, and can lead to difficulties with scale mis-matches and so on,

Fig. 1.12 Fractured bone fragments can be separated into independent objects, which can then be individually moved and rotated back into their correct anatomical positions to facilitate analysis

but if a particular project would benefit from scaling a selection, then exactly the same control methods apply as have been discussed above for both movement and rotation.

Modifiers

Blender has a series of powerful functions, known as "modifiers", which can be used to alter your mesh objects in a variety of ways. Many of these will not have an immediately-apparent application for the manipulation of medical scan data, but at least a few of these are worth learning as they can convert otherwise complex procedures into relatively straightforward operations. The "Boolean" modifier allows you to perform mathematical functions such as addition and subtraction. Whilst this may not sound exciting at first, the significance of this capability should not be

Fig. 1.13 With complex cases the process of fragment isolation, separation and re-approximation can be a time-consuming undertaking, but this may be deemed worthwhile if no alternative method exists. For example, in this case no invasive autopsy had been authorised and the only material available for anthropological assessment was the original CT scan data

overlooked. If you need to fuse objects together, this modifier offers you a quick and simple method. Alternatively, subtracting the shape of one object from another can be used to create perfect-fit anatomical contours between objects.

For example, if you are dealing with excavated skeletal remains, and you wish to “repair” a fragmented bone, the separate fragments can be “added” together (Fig. 1.14).

If you then wish to produce a custom intervertebral disc, a simple sphere can be inserted into position between adjacent vertebral bodies and stretched / squashed as necessary to match the approximate antero-posterior and medio-lateral dimensions required. The Boolean modifier is then used to “subtract” the bone shapes from the sphere, leaving behind a disc with the correct upper and lower contours to fit the gap exactly (Fig. 1.15).

This process can be repeated for each articulation, allowing a complete virtual model to be assembled gradually from isolated skeletal elements, entirely within *Blender* (Fig. 1.16).

When attempting to 3D print a physical model that retains the post-injury positions of dissociated fragments, it may be helpful to incorporate a series of rods that can either be printed as a single item, or as separate elements for assembly after printing. This can easily be achieved by placing cylinders of the required size into position, and using the Boolean modifier either to fuse with a bone and add a protruding rod, or to subtract from a bone to leave a locating hole (Fig. 1.17).

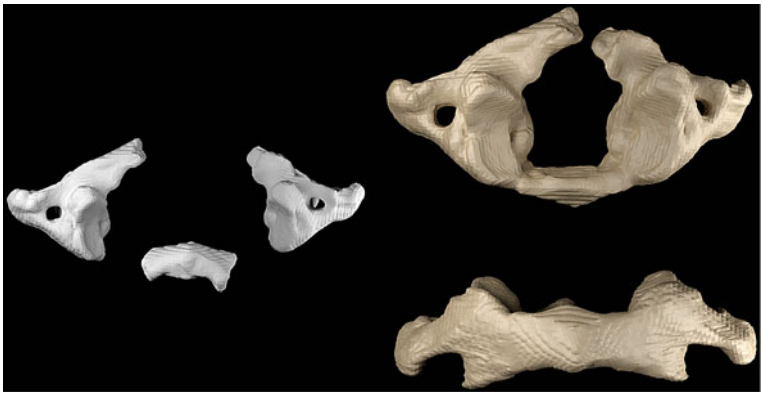

Fig. 1.14 Scans of the original fragmented parts (*left*) unearthed during an archaeological excavation were fused together digitally to create a single cervical vertebra (*right upper and lower*) as part of a spinal reconstruction project

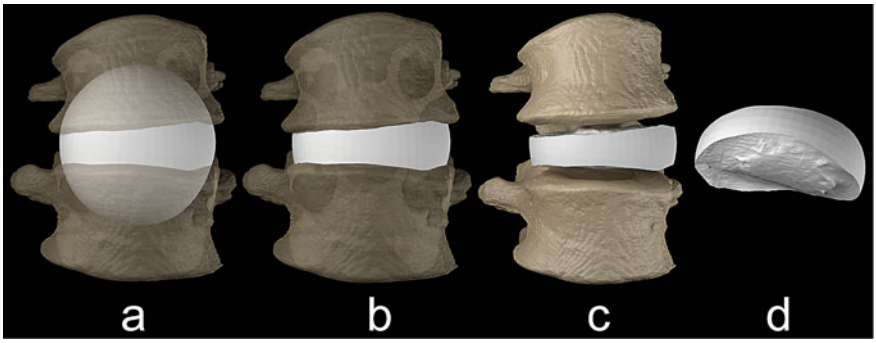

Fig. 1.15 **a** A sphere primitive mesh (*white*) is placed between two adjacent vertebral bodies and sculpted as necessary to ensure the entire intervertebral space is filled, **b** The Boolean modifier is used to subtract the vertebral body shapes from the sphere, **c** The new disc (*white*) and vertebral bodies remain as separate objects, **d** the surface contours of the custom disc's underside can be seen more clearly

Alternatively, if you wish to produce a virtual "cast" you can use the Boolean modifier to subtract a complex shape from a solid object, potentially revealing the extent of a wound track inside tissue, or the shape of a weapon that has left an indentation in a bony surface.

The modifiers are accessed by clicking on the blue spanner (wrench) icon in the vertical column of small icons between the right side of the main 3D view and the Properties editor. Clicking on the "Add Modifier" text will open the menu of all available modifiers, and the Boolean modifier can be found under the "Generate" heading. Selecting a modifier will cause a modifier control panel to appear within the Properties editor. You can add multiple modifiers to an object (creating a "stack"

Fig. 1.16 Using the methods described, an entire vertebral column model was constructed entirely from the CT scan data of disarticulated skeletal remains, including the creation of custom interverbal discs and the fusing together of fragmented bones

of modifiers), and they will affect the object in the order in which they appear (i.e. top to bottom of the stack). You can move modifiers up and down the stack so that the effects occur in the optimum order. Altering the various parameters of each modifier will change how the object appears, but nothing permanent is done to the object until you “apply” the modifier.

Once you have seen the modifiers in action a few times, it will make more sense. For now, practice with the Boolean modifier. You have options for “Difference” (i.e. subtract another object from the selected object), “Union” (fuse another object to the selected object) and “Intersect” (create an object that fills only the space where the two objects overlap). In the object selection field you can either click on the eye-dropper icon to select an object in the 3D view simply by clicking on it, or you can click into the object field to open a list of available objects, and select the required object by its name. It may be difficult to preview the effect if both objects are visible in the 3D view. In the Outliner (top right section of the screen) there is a list of all the objects in the scene. You can toggle an object’s visibility by clicking the small eye icon, and by hiding the object that you are either adding or subtracting from your selected object, it will make it easier to see whether the modifier has done what you expected of it. Until you apply the modifier, no permanent changes will be made, and if you enter edit mode you will see that the original mesh remains intact. If you move either of the objects, the modifier will update to reflect the different overlap arrangement. When you wish to apply the modifier, you must be in object mode, and then either select “Apply” from the drop-down menu within the modifier’s control panel, or press CTRL + A

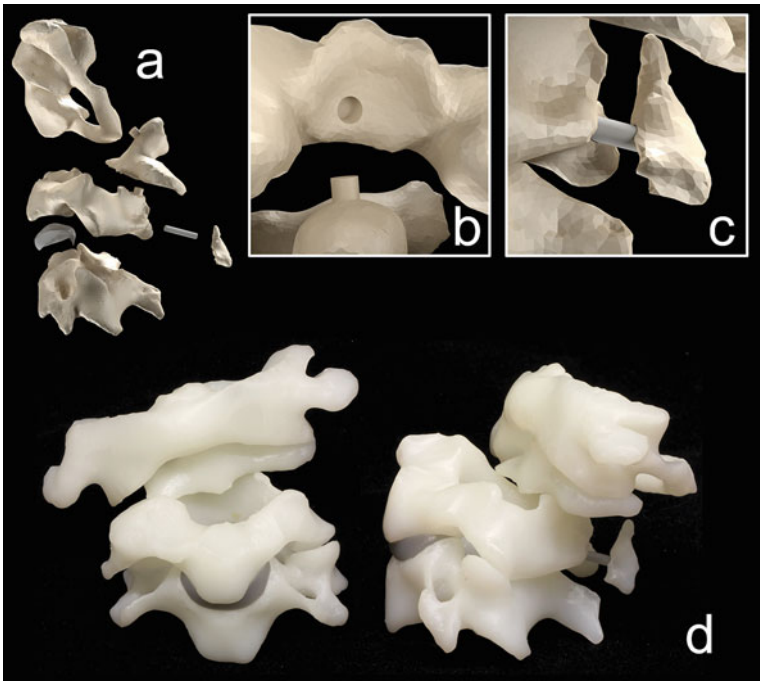

Fig. 1.17 **a** Exploded view showing individual components of proposed model, **b** Detail showing how a circular socket has been added on one side of a join, with a corresponding cylindrical stud on the opposite face of the join, **c** Detail showing how a connecting rod has been added to hold a disconnected fragment in its post-fracture position, **d** Front and side views of the completed model after assembly of the individual 3D printed elements

whilst your mouse cursor is over the modifier's control panel. The change will now become permanent, and the mesh will look different when you change back into edit mode. You can, of course, always undo with CTRL + Z if you get an unwanted result.

It is worth experimenting and practising to become familiar with the procedure. It may seem counterintuitive at first, but should soon start to make sense, and once you have mastered the technique you will be able to use it in a variety of useful situations. The list of modifiers is long and potentially confusing, but explanations of what they are all for and how to use them can be easily found online. Table 1.1 summarises how a selection of them might be of benefit in different situations. Before you commit to spending a lot of time manually editing a mesh, first consider whether an automated process (i.e. a modifier) could do this for you.

Table 1.1 Just a sample of the modifiers available, together with examples of how they might be useful

Modifier name	Example use
Array	Reproduces a specified number of identical copies of an object or feature, and arranges them in a geometric pattern. Useful when designing custom objects
Decimate	Reduces the number of vertices by a specified amount, allowing you to reduce the file size and model complexity whilst retaining sufficient detail
Lattice	Complex anatomical objects can be smoothly and evenly distorted by first placing an invisible shape such as a cube (the "lattice") around them, and then making simple adjustments to the cube
Mirror	This allows creation of symmetrical designs by mirroring geometry across an axis. More than one axis can be mirrored, and the geometry can either join across the axis or consist of separate, mirrored objects. Combining this with an Array modifier allows rapid production of repetitive, symmetrical whole parts or component features. (N.B. if you simply want to "flip" an existing model to produce a mirrored version, you do not need to use a modifier, but can instead do this by selecting "Mirror" from the Object menu in object mode, or the Mesh menu in edit mode)
Shrinkwrap	One object can be made to conform to the surface of another. A simple application might involve the wrapping of text around a cylinder, but there are many other situations in which this capability can be useful
Simple deform	Simple deformation, such as bending of an object, can be controlled precisely using this modifier
Smooth	If it is necessary to smooth surface features then this modifier can be used to control the degree of smoothing over a whole object, preserving or removing detail as required
Solidify	Flat (2D) surfaces are given a "thickness" to make them solid. Perhaps counterintuitively, this modifier can be used to convert a "solid" object into a "hollow" one (see Fig. 1.18)
Subdivision surface	Used very commonly when designing custom objects, this modifier allows you to create complex shapes with smooth, even curves, whilst working with only a basic, low-resolution underlying mesh. (Discussed in more detail below.)

Text

As well as mesh objects, *Blender* caters for the creation and manipulation of text objects (Fig. 1.19). From the Add menu (accessed by SHIFT + A) select the Text option, and a new Text object will be added at the location of the 3D cursor (usually the origin of the 3D view, unless you have previously moved it elsewhere). The default "Text" can be altered by pressing TAB to enter edit mode. Delete the word "Text" and type your own using the keyboard, then press TAB again to revert to Object mode. In the vertical column of small icons between the right of the 3D view and the Properties editor, you should see a green "a" symbol. Clicking on this will open the Text tab, allowing you to control every text attribute you might need to, as

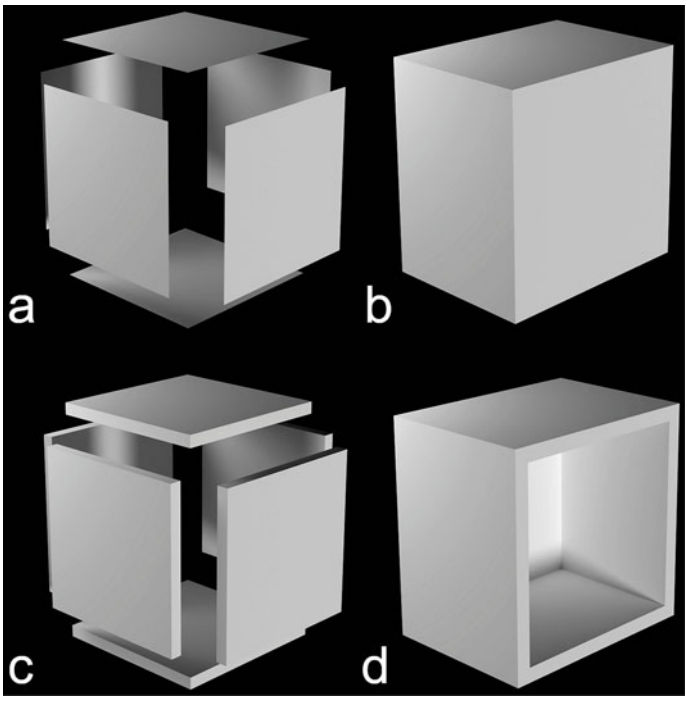

Fig. 1.18 **a** Exploded view of a cube composed of six square faces, each of which has no thickness (i.e. is 2-dimensional), **b** When such a cube is "sliced" for 3D printing it will be considered completely solid, as shown by this cross-section of the intact cube, **c** Using the Solidify modifier gives all of the faces a thickness (i.e. makes them "solid"), **b** This time the "thickness" of the faces results in an internal hollow space during the 3D printing process

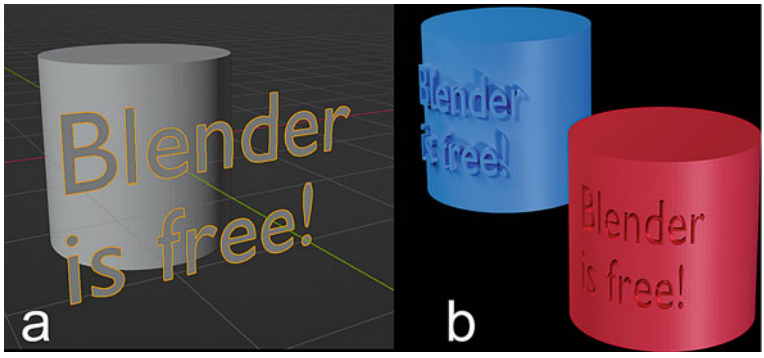

Fig. 1.19 **a** Text objects can be added, moved, rotated and scaled in the same way as 3D mesh objects, and entering Edit mode using the TAB key allows you to type directly into the 3D scene, **b** Text objects can then be converted into 3D mesh objects, enabling you to emboss (*blue*) or engrave (*red*) custom text into the surfaces of your 3D objects, even bending them to fit contoured surfaces if necessary

well as specifying any alternative font file you may wish to use instead of the default font. Importantly, for 3D work, under the Geometry heading you will see an option to "Extrude" the text. You should be able to resize and reposition your text as required using the controls you would for any other object, but if you want to add text to (or subtract it from) another object using the Boolean modifier you must first convert it into a mesh object. When in object mode, you can either right-click on the text, select "Convert To" and then "Mesh", or you can instead select "Convert" from the Object menu of the 3D view to implement the mesh conversion. If you now TAB into edit mode, you will see that the text has become a mesh, with selectable vertices, etc. Once you have converted into a mesh object, you cannot edit the text again by typing, so correct any spelling errors *before* converting! The conversion process usually generates a large number of doubles, so it is always a good idea to remove these (described above) immediately to prevent them causing any issues later on.

Designing Your Own Models

As can be seen, *Blender* is highly capable of editing anatomical models that you have exported from medical scan data. In addition, it can also be used to create entirely new designs if required. Detailed instructions covering all aspects of computer-aided design are well beyond the scope of this introductory chapter, but if this is something that is likely to be of use then step-by-step tutorials can readily be found online to guide you through the basic *Blender* modelling principles as well as the more advanced actions needed to control precisely the various dimensions and shapes needed for a particular project. Once you have mastered the ability of controlling lines, curves and dimensions by manipulating only a few key vertices, whilst letting "modifiers" and "proportional editing" automate the majority of the process, you will soon be able to create smooth, contoured shapes exactly to your specifications. You can even import background images (either reference photographs or your own hand-drawn sketches) to assist when deciding exactly where the various features should be, and how they should align. One important point that will be repeated by the majority of modelling tutorials is that when working with the "Subdivision Surface" modifier (to smooth and improve the appearance of complex shapes), four-sided faces (known as "quads") are preferable. Triangles (three-sided faces) and "Ngons" (more than four sides) cause ugly pinching and other deformities of surfaces when this modifier is used, and so are best avoided when creating your models.

Snapping

For some projects it may be sufficient to place vertices by eye alone, but if exact alignment is necessary then different methods are available to achieve precise control. As described above, holding CTRL whilst making any adjustments activates the precision mode, slowing the rate of adjustment and making fine-tuning easier. You can also make use of the "Snap" facility to assist with exact alignment. One type of Snapping can be accessed either from the "Mesh" menu in Edit mode or the "Object" menu in Object mode, and in either case the "Snap" menu will give you a list of options from which to choose. The other variation of Snapping is accessed (in either Edit mode or Object mode) by clicking and activating the small magnet icon at the top centre of the 3D view. Just to the right of this icon is a drop-down menu, which allows you to specify exactly how the "Snap To" action is to be applied. Figure 1.20 illustrates another trick that is useful to know: when you want to align different vertices together on the same plane, select the vertices in Edit mode, and then scale (S key) along the required axis (X, Y or Z key) using a value of *zero* (0 key).

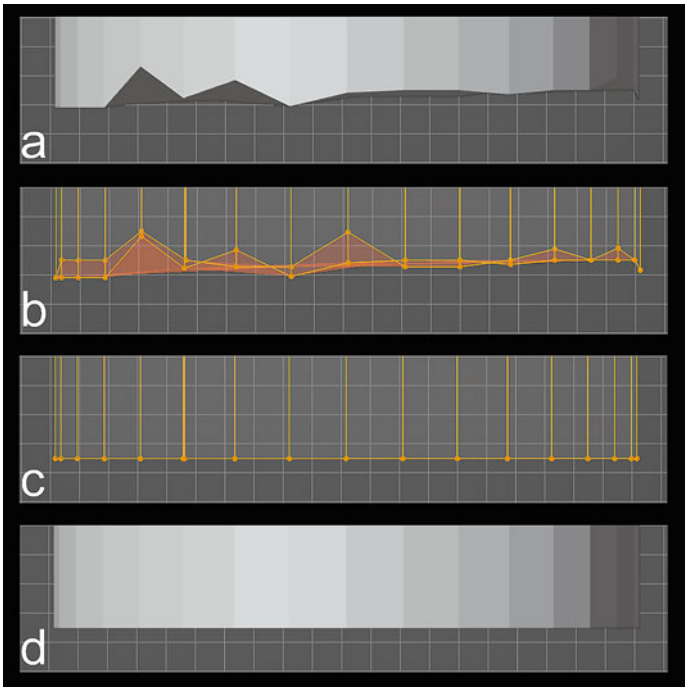

Fig. 1.20 **a** Jagged edge caused by poorly aligned vertices, **b** All of the misaligned vertices have been selected in Edit mode (*orange*), **c** Scaling the vertices along a single axis (in this case it was the Z axis) using the numerical value of zero moves all of the selected vertices into line with the "Active" object (the last object selected) along the chosen axis, **d** Back in Object mode, confirming that the edge of the object is now perfectly straight

Extrusion

"Extrusion" is one of the simplest methods of modelling. You can start by adding a basic mesh primitive, such as a cube, by selecting from the Add menu (SHIFT + A). Then, in edit mode, select a vertex, edge or face (depending upon how you want to start growing the shape). Press the E key to start extruding, and you will see that your chosen selection begins to "extrude" as you move your mouse. You can either cancel the extrusion (ESC key or right mouse button) or confirm (ENTER key or left mouse button). As with movements, extrusions can be constrained to particular axes by pressing the X, Y or Z keys, or set to particular values by entering a numerical value (including negative values). Snap options can also be used to control the end points of the extrusion, and ALT + E opens an extrusion menu with different options for special extrusions that vary depending upon what is possible with the particular selection. "Spin" allows you to create curved extrusions with precise control, although the location of the 3D cursor and the viewing angle must be used to control how the spin is executed, so the results may not appear as expected until you learn how to control this particular option. Extrusion can be used to create a quick, basic shape for subsequent refinement later.

Subdivision Surface Modifier

The "Subdivision Surface" modifier is a commonly-used method of smoothing basic shapes and improving their appearance, but the smoothing effect may produce excessive curves where you need straighter edges. You can either add "Edge Creases" to reduce this curving effect, or you can add "Control Loops" to influence the degree of curving. This is done in edit mode using a "Loop Cut and Slide" action. CTRL + R adds a "Loop Cut", the orientation of which is previewed in yellow as you move your mouse cursor over the object being edited. Scrolling the mouse wheel up and down alters the number of loop cuts to be added (if multiple cuts are required), and then an initial left mouse click confirms the cut(s), after which you can "slide" the cut(s) from side to side by moving the mouse, clicking the left mouse button a second time to finalise the location of the cut(s). This process is illustrated in Fig. 1.21.

This sounds more complicated than it actually is, so it is worth going through the process a few times with a simple mesh to understand how to apply loop cuts. Sliding a loop cut in an object that has a Subdivision Surface modifier applied will show you how the additional loop affects the smoothing curve, and with practice you will be able to control any unwanted excessive curvature. You may never attempt to create your own 3D designs, but if you do then the power of this process will rapidly be appreciated. If a suitable loop of vertices already exists then you do not need to add a new one. You can instead simply select the loop by holding ALT whilst clicking

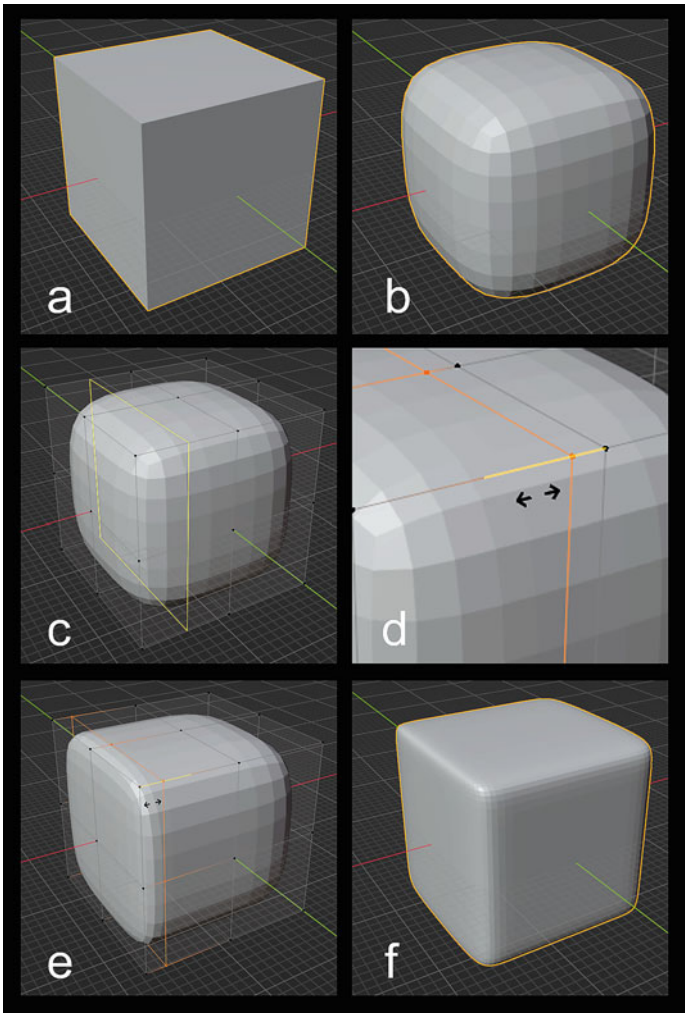

Fig. 1.21 **a** A crude design may be simple to work with, but such an appearance is not always satisfactory, **b** The Subdivision Surface modifier introduces smooth contours and improves overall appearance, but the effect can be excessive, **c** In Edit mode a "Loop Cut" (*yellow*) can be added by pressing CTRL + R, using the scroll wheel of the mouse to control the number of loops to be added and then left-clicking the mouse to confirm the cut(s), **d** Immediately after adding a Loop Cut, the mouse can be used to "Slide" the Loop Cut (*orange*) along an axis (*yellow*) by moving in the directions indicated by the mouse cursor (*black arrows*), **e** Sliding a Loop Cut towards an already existing edge will "compress" the curvature of the Subdivision Surface modifier, allowing you to control precisely how creased or smooth any edges are, **f** The interaction of "Control Loops" with the Subdivision surface modifier allows rapid fine-tuning of smooth, contoured shapes when designing custom items

on a relevant edge to select the entire loop, and then press G *twice* to start sliding the vertices along edges (rather than simply moving them, as would happen with a single press of the G key).

Proportional Editing

Another method of introducing smooth transitions to models is to make use of so-called "Proportional Editing". This can be activated by pressing the O key, or by clicking the small circular icon in the row of tools at the top of the 3D view. To its immediate right is a drop-down list allowing you to choose from a range of "fall off" patterns. Once proportional editing has been activated, you will find that the adjustments you make affect not only the selection, but a surrounding area dictated by a white circle that can be enlarged or reduced using the scroll wheel of the mouse. This is another feature that requires experimentation and practice to appreciate its full potential, but if you plan to create your own objects then this ability to create subtle gradations will greatly enhance your ability to produce professional-looking results. Temporarily hiding parts of the model, by selecting them and pressing the H key, will allow you to edit sections of the model without influencing the hidden elements. ALT + H will restore the hidden selection(s), which will not have been affected by the proportional editing, even if the circle of influence "should" have involved the hidden structures.

When modelling new items, it may be of benefit to employ certain modifiers. The Mirror modifier will allow you to produce a symmetrical model whilst designing only one half of it, and repeating patterns or features can be added using an Array modifier, for example. After you have created a model, a copy can be "flipped" using the Mirror command (not the modifier), to create a corresponding opposite item—meaning that you don't have to repeat the whole process of designing the object from start to finish, just to achieve a corresponding version for the opposite side.

Image Rendering

Whilst standard medical imaging programs allow perfectly adequate 3D representations of anatomical data to be created quickly and easily, the default colours and shading may not be ideal for all intended purposes. *Blender* can "render" a 3D scene to appear however you wish, opening up virtually limitless potential for fine-tuning the precise viewing angle, perspective and relationships between objects, as well as their colour, transparency and texture. As an example, the obviously computer-generated appearance of standard medical images can easily be improved to result in a more natural-looking aesthetic quality (Fig. 1.22).

Fig. 1.22 **a** Typical appearance achieved when viewing DICOM data using common medical imaging software, **b** The same scan data converted into a 3D file and then rendered in Blender (with complete control over lighting, colour and other factors to alter the realism or aesthetic quality as required)

Lights, Camera…

In order to render an image of any 3D scene, *Blender* needs both a camera and some lighting. Such items can be found in the Add menu (SHIFT + A), but it is worth noting that you are not restricted only to the types of lighting available in this list. *Any* object can be turned into a light simply by adding "Emission" as either all or part of its "Material" property (discussed in more detail below). It can seem cumbersome at first to control the view of the active camera. One quick and simple solution is to adjust the 3D view using the normal methods of orbiting, panning and zooming. Once you are satisfied with how things look, select "Align Active Camera to View" from the "Align View" section of the "View" menu (or press CTRL + ALT + numpad 0). This will place the camera where it needs to be to recreate the view you have just arranged, and you will be able to see the central rectangular view captured by the camera surrounded by a darker zone that will not be included in the final render.

You can adjust what the camera sees via a variety of methods, but you will find it easiest to appreciate the changes in camera view (numpad 0 toggles in and out of camera view). With the camera selected as the active object (click on "Camera" in the outliner at the top right of the screen if you can't find the camera easily in the 3D view), you can click on the small green movie camera icon in the vertical column of icons between the right side of the 3D view and the Properties editor. This will open the camera properties, and you can then "shift" the view in the X and Y directions, or adjust the focal length to "zoom" nearer to or farther from the viewpoint. Bear in mind that changing the focal length also alters the perspective of how objects appear in relation to one another, which you can use to your advantage depending on the required effect. The "clipping" start and end points define the visible zone in front of the camera, and you may need to adjust these values if any of your objects do not

appear because they are too close or far away. Other than this, the camera can be moved or rotated just like any other object in the 3D space, or there are "walk" and "fly" modes available to preview and adjust the camera's view.

Once you have a suitable view of the scene to be rendered, you will need some light within the scene to illuminate the objects. Lighting can be simple or complex, stark or subtle. Online tutorials are a good way of learning about "key", "fill" and "rim" lights if you wish to recreate a standard appearance. To get started, a "sun" light can be added to the scene to give very simple light. The brightness, colour and other properties of a light can be adjusted in the Properties editor (after clicking on the green lightbulb icon with the light selected as the active object). The angle of illumination can be adjusted by selecting any light as an object in the 3D view, and rotating its direction to point where you need it. The precise location of a "sun" light within the 3D scene is of less importance, as it is the direction of illumination that determines how the shadows are cast on (and by) objects. Other types of light will need more careful positioning, as their location will also be a factor in determining how the light interacts with the scene. If you use the Z key to select the "rendered" view, you will see a preview of how the rendered image will appear, and this will allow you to see in real-time how adjustments to the position, direction and brightness of a light source affect the objects and their shadows. (Incidentally, a slightly quicker way of switching between viewing modes is to *hold down* the Z key and then move the mouse in the direction of the intended mode before releasing the Z key, rather than pressing the Z key to activate the menu and then clicking on one of the options.)

Rendering Engine

It is worth noting that the default rendering "Engine" used to create pictures of your 3D scene is called "Eevee". This rendering method produces very fast results, but at the expense of quality and realism. You may therefore prefer to select the "Cycles" rendering engine instead (accessed within the Properties editor by clicking the white rendering tab icon, which resembles the rear of a digital camera). Also, if your computer has a powerful graphics card then you may achieve faster rendering by selecting "GPU Compute" for the Device, rather than the standard CPU setting. Rendering is a very processor-intensive task, especially if you have a detailed scene containing complex materials (see below). In-depth online tutorials are available if necessary to help set up your device for optimum rendering based upon your hardware and intended requirements. For now, simply be aware that a higher number of "Samples" will take longer to render, but will improve quality. An advanced "Denoise" algorithm has been added to recent versions of *Blender*, so you can now render with fewer samples and then dramatically reduce any persistent "noise" (pixelated, grainy appearance) afterwards. This function is added simply by ticking the Denoise box under the Sampling heading of the render settings tab of the Properties editor.

There are separate parameters for the Viewport (i.e. your 3D screen preview) and the Render (the final output). Ordinarily the Viewport settings are of lower quality to

keep the working speeds manageable. As well as the rendering option settings, the Output settings (accessed by clicking the white printer icon below the render icon) can be adjusted to control the quality of the final render. The Format heading lets you specify exact X and Y pixel dimensions of the final image, as well as a percentage quality setting. The Output heading lets you select the file type, compression and folder for saving. A balance can be struck between rendering speed (i.e. time taken) and ultimate quality, as required. Once you have organised your scene, including a camera and appropriate lighting, and you are content with the rendering and file type options, you can render an image either by pressing the F12 key or choosing Render Image from the Render menu at the top of the screen. It may take several seconds, or considerably longer, to complete the render, which you should see gradually becoming clear in a separate window called Render Result. It is important that you save any images you wish to keep by choosing a Save option from the Image menu within the Render Result window. If you do not, the rendered image will be lost when you close *Blender*.

Materials

If you do not assign a specific material to an object, it will be rendered simply as a solid white shape. This may be all that you require, but in order to enhance the appearance of your images you may prefer to impart certain qualities, such as colour, texture or a degree of transparency to an object. This is done by creating "Materials", and then applying these to the object(s). It is possible to assign more than one material to a single object (e.g. teeth can be a different colour to the rest of the skull). If you select an object in the 3D view, you can then open the Materials tab of the Properties editor by clicking on the lower red circular icon (not the upper red "World" icon). Pressing the "New" button will assign a new material to the object, which by default will be a so-called "Principled BSDF" shader. "Shaders" are things that tell *Blender* how a surface should appear, and the Principled shader is a good all-round shader that lets you easily specify the colour and other characteristics of your objects, without having to know very much about what is going on inside the machine. Many of the variables (such as "Metallic") are self-explanatory, whereas others may not seem obvious initially. For example, the "Subsurface" option allows you to control how much light is scattered internally beneath the surface of an object, rather than simply reflected from it, and this quality enables the appearance of certain substances (e.g. wax) to be simulated. Detailed documentation and tutorials are available online to explain all of the parameters of the Principled shader, and it is likely to be sufficient on its own for many applications.

However, highly complex *Blender* materials can be configured exactly to your specifications to create any visual effect that you might need. The subject of material creation is well beyond the scope of this introductory chapter, and there are abundant online sources available to demonstrate what each shader does, and how to control it. Furthermore, realistic patterns and textures can be created entirely within *Blender*

using mathematically-generated data and then manipulating it. This process is known as "procedural" texturing, and an online search for "*Blender* procedural textures" will quickly reveal a seemingly endless supply of fascinating demonstrations of how to achieve complex, realistic appearances using the algorithmic "node" system. If you do not wish to try creating your own materials, searching online will instead allow you to download ready-made materials (some of which are free, but many require payment).

There are different ways of accessing the "Node editor", but whichever way you do this the most important thing to note is that the process is far simpler than it might first appear! The node tree is essentially a flowchart (from left to right) that takes one or more inputs, modifies and combines them to achieve the desired effect, and then outputs the end result as a material surface. For example, if you wanted to make a material of a certain colour, and then give it a partially-glossy quality, you would use a "Mix" shader to combine the outputs of both a Diffuse shader (in which you can choose any colour) and a Glossy shader (in which you could also specify a particular colour, or simply leave white). Clicking on the green output dots of the Glossy and Diffuse nodes and dragging them to the green input dots of the Mix node allows you to connect the nodes in turn, and start building your flowchart. (Clicking and dragging the green output of the Mix node to the Surface input of the Material node is what actually imparts the characteristics to the object, and if you don't make this final connection then nothing you have done so far will make it through to the object and actually be visible in the final render.) You can then adjust the Factor of the Mix shader to alter how glossy or otherwise the final result is.

Adding nodes (SHIFT + A) in the node editor, dragging them around and joining them using colour-coded noodles is more intuitive than reading how to use the node editor, so it is best simply to start experimenting. If you opt to use the dedicated Shader editor (by clicking the Shading tab from the menu bar at the very top of the screen) you will see a split screen, with the node tree in the large bottom section and a material preview in the large upper section. This preview is surrounded by a background image and lighting (which can be altered) to provide a better representation of how materials will appear in "real world" settings. Alternatively, you can change what is displayed in the 3D viewport by clicking the small, drop-down list at the top left (just below the main *Blender* symbol). This menu can be used to switch between various editors, and if you split the screen into multiple areas you can choose a different editor for each, allowing simultaneous manipulation in one with real-time preview in another, for example. If you move your mouse pointer to the interface between screen areas, it will change into a double-sided arrow. Right-clicking whilst this symbol is displayed will activate a menu that lets you either "Split" or "Join" areas to customise your window layout exactly as you like.

Once you have created your own (or downloaded somebody's else's) materials, you may wish to assign multiple materials to the same object. This process may initially seem confusing, and the first time you try it, it may seem not to have worked. Once you have successfully worked out how to do it, the capability will prove extremely useful, so it is worth taking the time to master it. First of all, you need to have at least two materials. Then, and this is the important part, you need to

make sure that the object has more than one material "slot". To do this, simply click the " + " sign at the top right of the Materials section within the Properties Editor. This will generate an extra row in the list of materials slots for the selected object. You can change which material occupies each slot using the drop-down menu of available materials, or by clicking "New" and creating another one. Now, in the 3D view enter Edit mode (TAB key) and select the faces to which you intend to apply a particular material. Back in the Properties Editor, beneath the list of material slots, there will be a button marked "Assign". Click this, and all the faces currently selected will be assigned with the chosen material. Now select some different faces, choose another material slot and assign the different material to the new selection (Fig. 1.23). In this way you can control precisely how each part of an object is displayed, which could prove invaluable for highlighting features (such as emphasising a fracture line), delineating anatomical boundaries (such as separating the teeth from the rest of the skull) or creating interesting visual effects (such as incorporating a transparent window into the side of a solid object, revealing hidden internal structures).

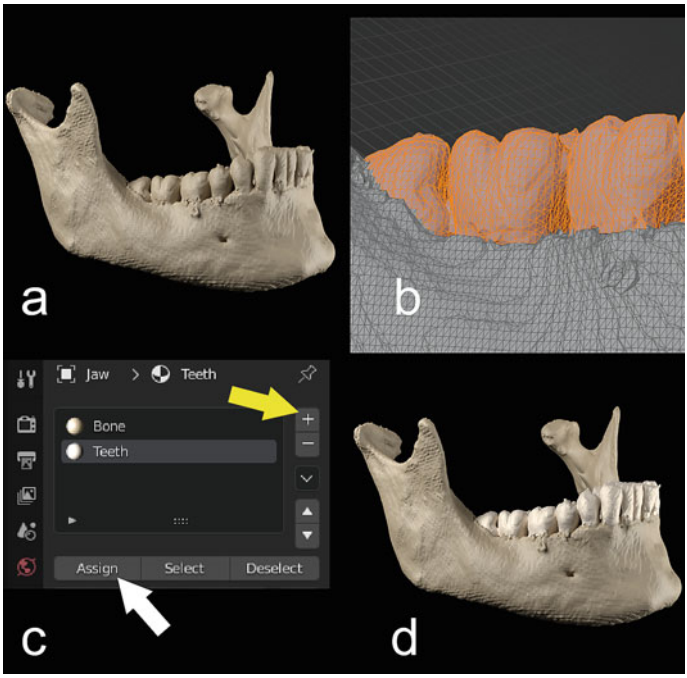

Fig. 1.23 **a** It may be necessary to assign different materials to separate parts of the same model, such as where teeth look unnatural when rendered in the same colour as the adjacent bone, **b** First select specific parts (*orange*) of the mesh in Edit mode, **c** Then use the "Assign" button (*white arrow*) in the Materials tab of the Properties Editor to apply the chosen material to those selected faces. In order for this to work, an object must have more than one material "slot", which can be added using the " + " button (*yellow arrow*), **d** If successful, the selected parts of the mesh will now have been assigned a separate material to the rest of the mesh

As you can see, *Blender* will enable you to produce professional-looking and effective visualisations that may be difficult or impossible to achieve using standard medical imaging software. As an example, Fig. 1.24 illustrates a fatal brain injury resulting from a self-inflicted air rifle discharge. The trajectory from base of skull entry wound to final resting place of the projectile was created using a simple cylinder, scaled along one axis to create a long rod. By placing the "3D Cursor" at the skull entry point, and specifying this as the "pivot point", rotational alignment was greatly simplified. The transparent skull version shows the internal trajectory, whilst the "cut away" view offers an alternate method of revealing the internal aspects of the skull. The third image includes the mandible, but this has been rotated from the scanned position to the angle where it allows the straight-line trajectory to enter the mouth. Such an extreme angle of opening suggests that the depicted line is unlikely to be the true trajectory, and that some deflection of the projectile must have occurred after entering the skull.

The "cut away" effect was achieved using the "Bisect" tool, which is another useful feature that is worth learning. In Edit mode, select the vertices that you wish to be affected (you don't need to bisect the *whole* model, and can instead specify precisely the areas to be cut). Then either choose Bisect from the Mesh menu, or choose the Bisect tool from the icons at the left side of the 3D view. After activating the Bisect tool in this way, left click and drag to draw your linear plane of bisection. Once you release the mouse button, a circle and arrow symbol will appear at the point you started dragging your mouse, and this can be used to alter both the plane position and angle of your chosen cut. The Operator panel (press F9 if this is not already visible) contains options to "Clear Inner" or "Clear Outer" (i.e. remove the vertices on one or other sides of the cut), and to "Fill" (i.e. close the gaps left by cutting across the object).

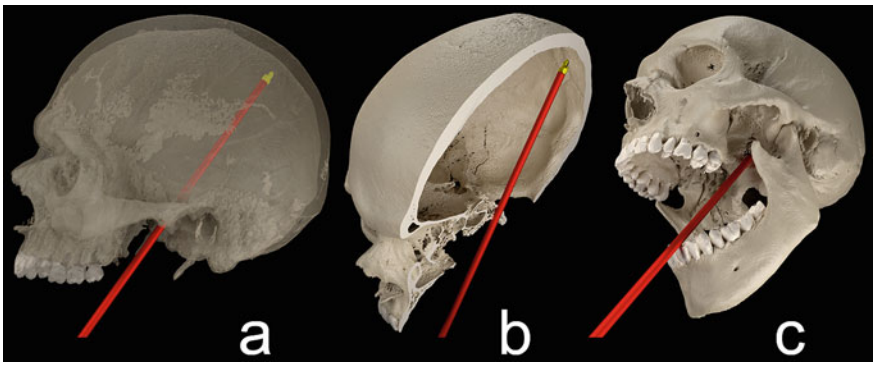

Fig. 1.24 **a** Semi-transparent skull showing the straight-line trajectory (*red*) between the skull base entry point and the final resting place of the projectile (*yellow*), **b** Alternate version of the same view, this time with a cut-away view through a solid skull, **c** Inclusion of the mandible, which has been rotated to the extent that would have been necessary to accommodate a straight linear path, indicating an unfeasibly large degree of opening and therefore likely deflection from this theoretical trajectory

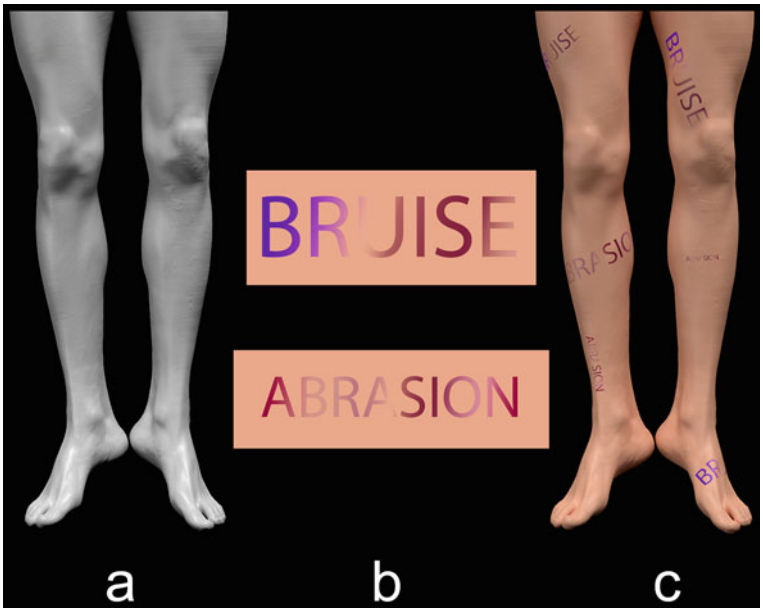

Fig. 1.25 **a** A model of the external skin surface can be extracted from the CT scan data, but it is monochrome and does not capture the appearance of surface injuries, **b** 2D photographs of injuries are represented here by simple text labels, **c** Blender can "wrap" 2D images around the 3D surface of the skin during rendering, giving you precise control over where and how injuries are depicted

Texture "Wrapping"

Further enhancement to rendering includes the ability to incorporate specific "Textures" onto rendered surfaces. As an example, the surface of the skin can be extracted as a 3D model from a CT scan, but as this surface is generated from x-ray data there is no information about the colour of the surface. If a photograph of an injury (such as a bruise) has been taken, *Blender* can "wrap" that 2D image around the 3D surface during rendering, imitating the real-world appearance more correctly than simply "cutting and pasting" a 2D image of a bruise onto a 2D image of the skin's surface. This process is illustrated schematically in Fig. 1.25, using simple text labels in lieu of genuine injury photographs.

Animation

Once you know how to render a single image, you can easily adapt to rendering a sequence of consecutive, slightly different images (i.e. an animation). Simple animations, such as an object rotating to reveal its entire surface (or a camera panning around

or zooming into a stationary object) are very straightforward, but more ambitious projects can be achieved with some perseverance. The good news is that all you have to do is specify "start" and "stop" positions, and *Blender* will interpolate every intervening frame for you, dramatically reducing the amount of work required of you. Importantly, just about *any* property can be "animated" in *Blender*, so as well as simply moving an object around the 3D space, you can also alter its colour, shape or transparency, for example, as the animation progresses.

Several other potential applications can also benefit from the *Blender's* inbuilt animation tools, and so the term "animation" should not be considered restricted to the creation of "moving images". For example, *Blender* has a method of deforming mesh objects in order to allow models to appear natural whilst moving. This capability can be used to adjust the shape of a 3D model from its position as extracted from a CT scan into one more useful to you.

Movement

The most immediately-apparent use for animation tools is the creation of moving images, and there are several potential uses for such an ability within forensic practice. A post-mortem CT scan acquires anatomical data with fractured bones in their "finish" positions. Using the methods outlined above, you can reposition those fragments into their correct anatomical (i.e. "start") positions, and *Blender* can interpolate as many frames as you require in between to produce a smooth animation demonstrating simple movement paths from start to finish. All that you need to learn is how to insert so-called "keyframes". Keyframes are simply values stored at specific points along the animation timeline, allowing *Blender* to calculate the incremental changes necessary between each frame. If you look along the bottom of the *Blender* window, you will see the animation timeline, which by default ranges from frame 1 to frame 250. You can click at any point along this timeline (or click and drag the blue frame marker) to move through the frames, or you can type directly into the frame counter window at the right-hand side just above the timeline (where you can also adjust the start and finish frame numbers of the animation). Exactly how the animation works is probably easier to *see* than to read about.

Open *Blender* and add (SHIFT + A) a mesh object, such as a cube. Ensure that the object is selected (click on it if it does not already display an orange outline). Press the I key to open the "Insert Keyframe" menu, and choose "Location, Rotation & Scale" option from the list. These values will now be stored for frame 1 (the default frame indicated on the timeline by the blue marker). You will notice a small yellow icon appear on the timeline, indicating that a keyframe has been added. Now click further along to the right of the timeline to select a higher frame number (e.g. 200). Do some interesting things to your cube (i.e. move its position, rotate it and scale its size). Then repeat the process of inserting a keyframe using the I key. You should see another yellow icon on the timeline. Press the triangular "play" icon just above the middle of the timeline, and your animation will begin to run. You will then see how

Blender smoothly animates all the incremental steps between your two keyframes. The animation can be paused, or played in reverse, or you can simply click and drag the blue marker back and forth along the timeline to see how the object's position, rotation and scale are adjusted per frame. The more keyframes you insert, the more complicated your animation will become. With the Output tab of the Properties editor (small white icon resembling a printer) you can adjust the frame rate and number of frames, giving you precise control of the length and smoothness of the animation, and you can also adjust the dimensions and resolution of the individual frames to be rendered.

By now it should be apparent how you can create animated clips of individual objects moving from start to finish positions, but note that you can also animate the position of the camera, the position and brightness of lights and the visible qualities of objects (e.g. colour or transparency) over the course of the animation. All you need to do is ensure that the required values for each are specified at each keyframe, which as before is done using the I key. As an example, when creating or editing an object's Material (see above), you can press the I key whilst hovering over any value. The value field will turn yellow, confirming that it has been "recorded" as a keyframe. Clicking on another frame in the animation timeline, you will notice that the value field is now green (indicating that it is an interpolated value, influenced by another keyframe). Enter a different value for this frame, and press I again to set this value for this keyframe. When you run the animation, you should see that whatever value you have just edited will gradually transition between the two keyframes that you have specified. It is very easy to get lost or confused, resulting in changes happening in the reverse order to what you intended, or leading to completely unexpected effects. This is a good stage to pass through, as once you understand how to control what you want to using keyframes, a whole new dimension of powerful visual impact will have been unlocked for you. Once basic animation has been mastered, further finesse can be achieved by entering the world of the "Graph Editor". This will allow you to start altering the rates of acceleration and so on to achieve greater realism, so if you feel this is necessary for a particular animation then search online for in-depth tutorials (of which there are many), as this degree of animation control is far beyond what can be covered during a brief introductory chapter.

Saving Your Animation

Rendering an animation is almost as straightforward as rendering a single image. You can simply set the file output type to one of the "Movie" file formats (such as MPEG) in the output tab of the Properties editor, and then select "Render Animation" from the Render menu (or press CTRL + F12). This will produce a finished animation that you can play straight away, but the rendering process will take a long time, and if your computer crashes partway through you will lose *everything* (and need to start again from the beginning). You will also lose the ability to alter settings such as frame rate later. The "recommended" way of rendering an animation is therefore to render the

individual frames into a temporary folder, and then create the animation afterwards using *Blender's* inbuilt Video Sequence Editor. This may sound overly complicated, but if your beautiful 4 K 60 fps animation breaks your presentation when you try to embed it into a slide, and you need to create a more presentation-friendly version, you will find it much quicker and easier to do if you had originally saved all of the individual frames in this way. If necessary, step by step instructions for using the video editor to compile an animation from individual frames can be found online.

Mesh Deformation

As mentioned briefly above, the animation tools allow you to do more than simply move objects around. You can also *deform* your objects based upon motion. The significance of this may not seem immediately obvious, and so it might be helpful to illustrate with an example. Figure 1.26 depicts a case in which a question had been asked by police about the physical possibility of storage of dismembered body parts within a particular container that had been recovered during a missing person enquiry. As no body had been recovered, an experiment was instead carried out using a "virtual cadaver". A suitably-sized body scan was obtained from a consented research database, and virtually separated at common sites of dismemberment using *Blender*. This produced the necessary body parts, but the limbs remained in the extended positions in which they had been scanned. By first "rigging" the limb meshes with "bones" (a potentially confusing term!), *Blender* was able to deform the surface skin in such a way that the limbs could be more realistically packaged as commonly seen in cases of dismemberment, allowing the theoretical question to be answered.

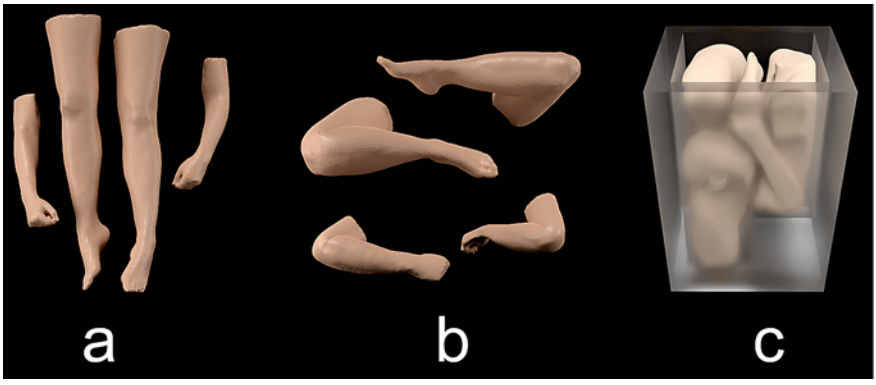

Fig. 1.26 **a** After virtually "dismembering" an intact whole body CT scan, the limbs remained straight, **b** Blender's animation capability has been used to bend the limbs into more appropriate configurations, **c** This allowed virtual confirmation of the theoretical possibility that a victim of a particular size could have been dismembered and stored within a specific container

"Rigging" using "armatures" of deforming "bones", "skinning", "constraints", "drivers" and "shape keys" are all well beyond the scope of this chapter, but as *Blender* is fully-featured 3D animation software it contains all of the tools you would need to create realistic, complex animations that can incorporate real-world physics. The take-home message is that you should not feel constrained by the limited scope of what has been covered here, but should instead assume that *Blender* can do anything that you can imagine… you just have to find out how to do it!

Summary

Blender is an immensely powerful resource that provides a free solution to a wide variety of 3D data manipulation and display requirements, which may be of benefit to forensic practitioners and associated disciplines. It has not been possible to cover every aspect of its use within this introductory chapter, but it is hoped that the descriptions and examples included here will be sufficient to prompt readers to begin exploring the software and investigating how it can be applied in casework, teaching and research. Once basic skills have been acquired, more targeted online searches can be performed in order to reveal detailed methods of using and enabling this software to accomplish increasingly sophisticated tasks. If you do achieve something useful or interesting, please share your methods with the wider community of potential users so that maximum benefit can be derived by all. And if you ever do something catastrophic to your project, remember there is always the "undo" command!

References

1. Siemens Healthineers. Cinematic Rendering. https://www.siemens-healthineers.com/medical-imaging-it/syngo-carbon-products/cinematic-rendering. Accessed 1 Apr 2022.
2. Canon Medical Systems. Global Illumination. https://global.medical.canon/products/healthcare_it/global_illumination. Accessed 1 Apr 2022.
3. Blender Foundation. https://www.blender.org/download/. Accessed 1 Apr 2022.
4. Biggs M. 3D Printing applied to forensic investigations. In: Rutty GN, editor. Essentials of Autopsy Practice: Reviews, Updates and Advances. Springer; 2019. p. 19–49.
5. Pixmeo SARL. OsiriX DICOM Viewer. https://www.osirix-viewer.com/. Accessed 1 Apr 2022.
6. Horos Project. Horos Viewer. https://horosproject.org/. Accessed 1 Apr 2022.
7. Fedorov A, Beichel R, Kalpathy-Cramer J, Finet J, Fillion-Robin J-C, Pujol S, et al. 3D Slicer as an Image Computing Platform for the Quantitative Imaging Network. Magn Reson Imaging. 2012;30(9):1323–41.
8. 3D Slicer. https://www.slicer.org/. Accessed 1 Apr 2022.

Chapter 2
Post-mortem Cardiac Magnetic Resonance Imaging

Wolf-Dieter Zech and Christian Jackowski

Introduction

In cases with a suspected cardiac cause of death, post-mortem cardiac magnetic resonance (PMCMR) imaging of the heart can be used either as an alternative in non-forensic cases or as an adjunct to forensic autopsy. Compared to cardiac post-mortem computed tomography (PMCT), PMCMR offers considerably better visualization of the anatomical heart structures such as the atria, the valves and the ventricular myocardium. Even the coronary arteries can be visualized in an unenhanced manner. Thus, PMCMR is far superior to cardiac PMCT in terms of diagnosis of relevant cardiac findings, in particular related to myocardial pathology. Compared to cardiac PMCT, the cons of PMCMR are higher costs, significantly longer examination times, dependence of image contrast and image quality on corpse temperature and image artefacts due to metallic objects or putrefactive gas. Usually, PMCT is conducted prior to PMCMR in order to detect findings compromising magnetic resonance (MR) image quality such as ferromagnetic devices (Fig. 2.1.) or putrefaction gas formations. In such cases, PMCMR may be refrained due to expectable poor image quality [1, 2].

W.-D. Zech (✉) · C. Jackowski
Institute of Forensic Medicine, University of Bern, Murtenstrasse 26, 3008 Bern, Switzerland
e-mail: wolf-dieter.zech@irm.unibe.ch

C. Jackowski
e-mail: christian.jackowski@irm.unibe.ch

G. N. Rutty (ed.), *Essentials of Autopsy Practice*,
https://doi.org/10.1007/978-3-031-11541-7_2

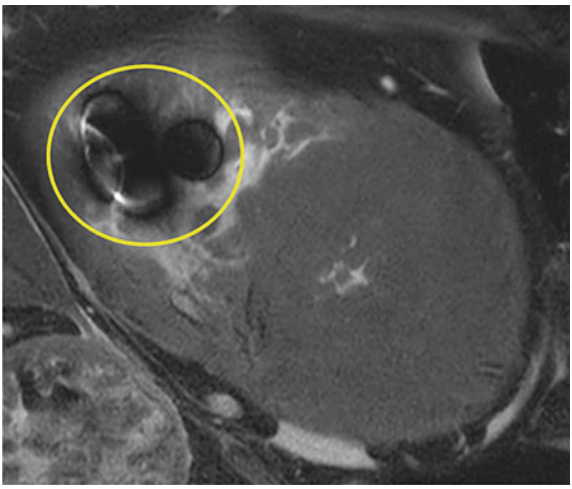

Fig. 2.1 T2 weighted cardiac short axis image showing artefacts (yellow marking) in the right heart chamber due to ferromagnetic pacemaker wire tip

Technique

MRI scanners use strong magnetic fields, magnetic field gradients, and radio waves to generate images of the organs and tissues in the human body. MRI does not involve X-rays or the use of ionizing radiation, which distinguishes it from computed tomography (CT). Post-mortem imaging uses the same MR scanners that are being used in clinical radiology (Fig. 2.2). However, based on individual vendor agreements it may be possible to exceed the specific absorption rate (SAR) limits during post-mortem imaging, which are normally put in place on these scanners for patient safety. Cross sectional MR images are generated by so-called MRI sequences. An MRI sequence is a number of radio-frequency pulses and gradients (from the MR machine) that result in a set of images with a particular appearance based on the echos deriving from body tissues (protons). When describing MRI sequences radiologists

Fig. 2.2 A corpse in body bag in a MRI scanner

refer to the shade of grey of tissues or fluids with the word *intensity*, leading to the following terms: high signal intensity: white, intermediate signal intensity: grey, low signal intensity: black. Often radiologists will refer to the image appearance by relative terms: hyperintense: brighter than compared structure, isointense: same brightness as compared structure, hypointense: darker than compared structure. The most common sequence in PMCMR is T2w since it allows for the best soft tissue contrasts at most temperature conditions.

Only a few forensic institutions rely on their own MR-machines. Mostly, MR scanners from local nearby hospitals or medical research departments are used for post-mortem examinations. In living patients MR machines with different magnetic field strength (usually 1.5 T (T) and 3 T) are used depending on the diagnostic questions. For PMCMR, both 1.5 T and 3 T MR-Machines can be used. Compared to 1.5 T scanners, 3 T scanners offer a better resolution of the myocardium and myocardial pathology in PMCMR. Unfortunately, 3 T scanners suffer from a higher sensitivity to inhomogeneity of the magnetic field due to metallic objects or air-fluid borders which results in amplified image artefacts. In contrast to clinical conditions the higher susceptibility to pulsation and motion artifacts of 3 T scanners is not an issue in PMCMR so that 3 T scanners are the state of the art for PMCMR.

PMCMR is usually conducted in a supine position in the MR scanner. To prevent image artefacts external metallic objects need to be removed from the body. If the body is scanned within a body bag, a special artefact free bag needs to be used and the zipper should be placed close to the feet. The body can also be removed from the body bag and be wrapped in a linen sheet. Scanning time is dependent on the type and number of sequences used. Using standard sequences the scanning time for PMCMR usually does not exceed 30 min. For optimal image acquisition, technical PMCMR settings of sequences need to be adapted by the operating MR technician due to specific post-mortem requirements such as differing body temperatures. The lower the temperature the less image contrast is to be expected, particularly below 10 °C [3].

Most diagnostic questions in PMCMR can be addressed with conventional T1 and T2 weighted sequences that generate cardiac cross sectional images with a slice thickness ranging from one to several millimeters. Image interpretation based on conventional MR sequences depends on the experience and subjective image interpretation of the forensic radiologist. A promising approach to a more objective image interpretation is provided by quantitative sequences. Such sequences allow measurements of MR specific parameters such as relaxation times and the proton density of tissues which enable thereby an objective and observer independent characterization of tissue alterations [4–6]. Additional MR sequences, such as fluid sensitive sequences, can be added. However, currently there is no scientific evidence that such sequences provide an additional diagnostic value to conventional or quantitative sequences.

Images generated with conventional MR sequences do not allow multiplanar viewing and the heart can only be displayed in one image plane. The desired image plane needs to be defined before the actual image acquisition by the MR operator. Standard cardiac image planes are defined to the references of the long axis of the

left ventricle. The most frequently used image planes in PMCMR are the short axis view or so-called 2-chamber view and the horizontal long axis view or the so-called 4-chamber view. The short axis view gives a cross sectional view of the left and right ventricles and often displays the cardiac skeleton and valve annuli. The 4-chamber view is a long axis view that displays all four chambers of the heart, the left and right atria and ventricles.

Image interpretation and diagnosis is based on different image contrast and signal behavior of cardiac tissue in different MR sequences. Diagnosis should only be made by radiologists or forensic pathologists with special training and experience in post-mortem cardiac MR imaging. Radiologists who are very experienced in clinical cardiac MRI may tend to misinterpret post-mortem findings since nonenhanced PMCMR is a pure anatomical visualization of cardiac findings that appears similar but is not comparable to clinically dominating enhanced cardiac MR images. For example, the early stages of myocardial infarction appear rather hypointense in post-mortem T2w images whereas in clinical radiology the area of infarction would be diagnosed based on late enhancements (hyperintensities) in the affected myocardial regions.

Furthermore, there are always some minor signal inhomogeneities within the left ventricular walls, where the right ventricular wall inserts into the left one (Fig. 2.3). This is a normal finding in PMCMR, which may be misinterpreted as an ischemic alteration by clinical radiologists not experienced in post-mortem MR examinations.

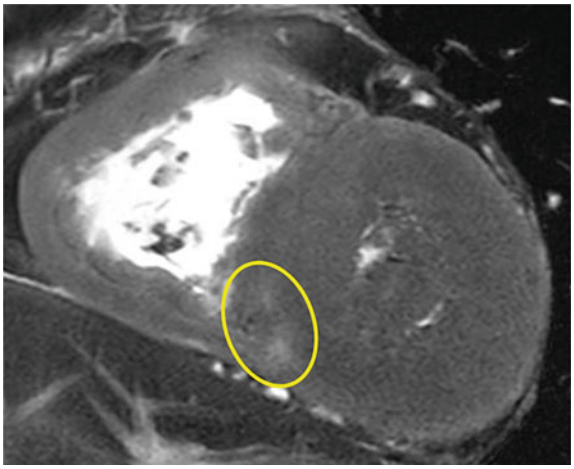

Fig. 2.3 T2 weighted cardiac short axis image showing common signal inhomogeneity (yellow marking) in the junction area of the posterior left and right ventricular wall

Diagnostic Possibilities

Compared to clinical cardiac MRI, post-mortem cardiac MRI is not influenced by breathing, cardiac motion, pulsation or further patient related motion artefacts. It can provide excellent cardiac image quality, particularly in corpses with a short post-mortem interval and those showing no putrefaction. As the MRI scanning time can be directly invested in image quality and there are no scanning time limitations due to patient constraints in PMRI a PMCMR exam may also last for 2–3 h, when an above-average image quality is desired.

Using standard imaging software, PMCMR allows for metric measurements of ventricular wall thickness (Fig. 2.4) and ventricular volume. Moreover, the circumferences of the cardiac valves can be assessed. Study results indicate that measurements of the semilunar valves are consistent with autopsy measurements while measurements of the atrioventricular valves can significantly differ to autopsy measurements. Ventricular thickness measurements in PMCMR may also differ to autopsy. Study results indicate that ventricular thickness measured in PMCMR is usually larger than the thickness measured at autopsy. Therefore, ventricular thickness measurements are not feasible for the diagnosis of hypertrophic cardiac pathology [7–9. The post-mortem phenomena of rigor mortis also effects the myocardium and may be misinterpreted as cardiac hypertrophy. It has been previously reported that the thickness of the ventricular walls in PMCMR does not correlate with post-mortem interval, sex, age, cardiac weight, body mass, body height or cause of death. Some PMCMR exams present dilated and some rather contracted left ventricles. The exact influencing factors of post-mortem cardiac myocardial contraction remain unclear to date [10].

It is possible to estimate the heart weight using PMCMR. A study reported that the calculated heart weight based on the left ventricular circumferential area in PMCMR reflected the actual heart weight. In the 4-chamber view the circumferential area of the left ventricle at mid-level corresponded to approximately one-tenth of the actual heart weight [11].

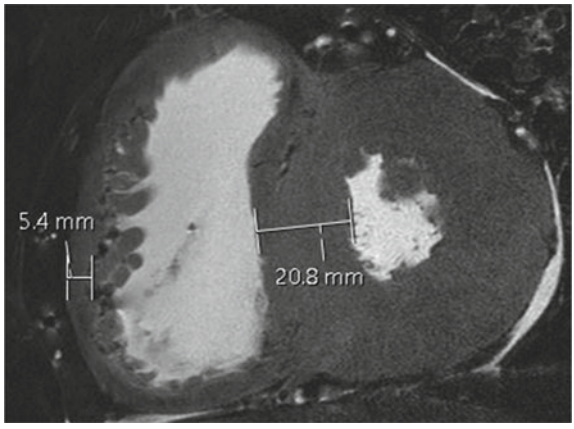

Fig. 2.4 T2 weighted cardiac short axis image showing metric measurements of the ventricular septum and the right ventricular wall

T2w PMCMR can show fatty ventricular infiltration and ventricular wall thinning.

In PMCMR blood within the heart cavities will often show sedimentation levels. Gravitational sedimentation of blood will typically exhibit a lower level erythrocyte layer and an upper level plasma layer. In T2w images the cell rich lower layer appears dark / hypointense while the upper layer appears bright / hyperintense. Depending on the actual platelet count a tiny intermediate greyish layer may be present as well containing mainly platelets and granulocytes [12]. The phenomena of post-mortem blood sedimentation is also visible in pericardial tamponade.

Often, thrombotic blood clots can be observed within the heart cavities in PMCMR. In T2w images post-mortem clots appear rather heterogeneous and may appear free-floating within the greater blood-filled cavities at the sedimentation level. In most cases post-mortem clots have a brighter mainly fibrin containing part and a darker part mainly containing platelets and erythrocytes. This phenomenon is explained by the fact that post-mortem clotting and sedimentation occur parallel but not at comparable speed. Fast clotting and slow sedimentation leads to rather homogeneous clots since the clots developed prior to sedimentation, whereas slower clotting and faster sedimentation leads to clots that have frozen the sedimentation levels already. In contrast to vital thrombi, post-mortem clots do not adhere to areas of myocardial infarction or hypokinetic myocardial regions. In addition, they do not show hemosiderin-induced signal loss as mature vital thrombi may do. Structures of homogeneous intermediate signal intensity in T2w images occluding branches of vessels are rather indicative of vital thrombosis or thromboembolism. However, a definitive diagnosis of vital thromboembolism based on these criteria is often difficult or impossible [13].

Internal livores at the heart may also be visible in PMCMR. They will typically appear as hypointense areas on T2-weighted images, usually in the region of the posterior left ventricular wall.

As a frequent finding gas formations can be found in the heart chambers. In the absence of an open trauma or other plausible explanations for gas embolism, gas accumulations within the cardiac chambers must not be misinterpreted as vital gas embolism since they are often the result of early post-mortem putrefaction. The heart is one of the organs in which putrefaction gas formations become visible first in post-mortem imaging. In bodies with only mild putrefaction, a sign hinting to vital gas embolism may be the appearance of gas in both ventricles in the absence of a septal defect or gas in the pulmonary arteries.

Only a few post-mortem case reports describe PMCMR imaged traumatic heart injuries. Myocardial lacerations due to blunt violence against the thorax will appear as focal dark / hypointense areas both in T1w and T2w images. Pericardial blood tamponade may be an indirect reference to myocardial rupture (Fig. 2.5). Since myocardial rupture may also be a complication of myocardial infarction, PMCMR diagnosis of traumatic myocardial damage should only be made in the presence of other indications of thoracic trauma [14–17]. Dissection and rupture of the ascending aorta can be the cause of pericardial tamponade. In some cases, aortic dissection may be visible with unenhanced PMCMR showing irregular wall structuring or even two separate lumina of the ascending aorta [1].

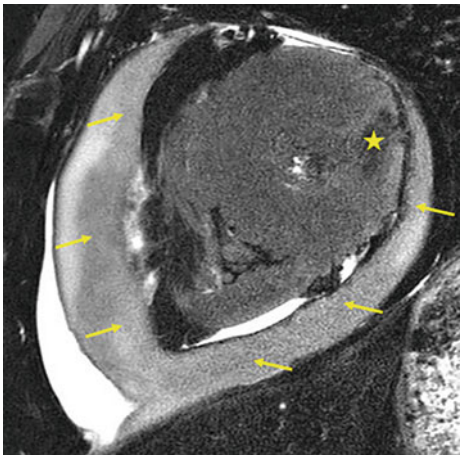

Fig. 2.5 T2 weighted cardiac short axis image of myocardial rupture (yellow star) in the left lateral wall with consecutive pericardial hemorrhage (yellow arrows)

PMCMR is well suited for the diagnosis of myocardial infarction of different ages. The sequence of choice for depiction of myocardial infarction is T2w in short axis orientation. For discrimination of the different ages of myocardial infarction a T1w sequence can be added. In T2w images acute myocardial infarction shows a focal hypointense (necrotic) area with a hyperintense (hemorrhagic and/or edema) marginal region (Fig. 2.6).

The marginal region appears hypointense in T1w images. In the further course of time, MR T1w and T2w signal behavior of the infarction area changes due to degradation and tissue remodeling processes (Fig. 2.7). Granulation tissue in subacute infarction appears hyperintense in T2w. Myocardial scarring as the final stage of infarction appears hypointense with none or only few signal both in T1w and T2w [18–22].

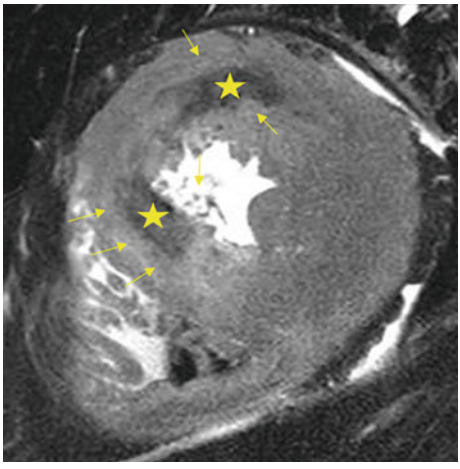

Fig. 2.6 T2 weighted cardiac short axis image with focal hypointense myocardial infarction (stars) and surrounding hyperintense hemorrhagic and/or edema margin (arrows) in the septum and left anterior wall

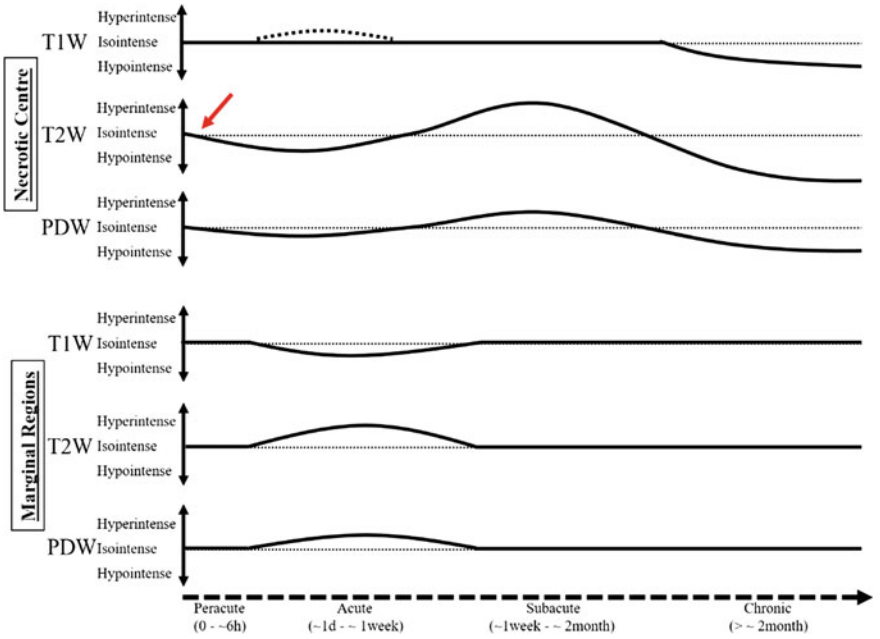

Fig. 2.7 Time course of PMCMR signal alterations in myocardial infarction. T1, T2, and PD (proton-density) weighted signal course within the necrotic center (upper graphs) and in marginal myocardial regions (lower graphs). Dashed line on the T1 graph of the necrotic center indicates the signal increase due to intramural hemorrhage. Indistinctively dropping signal on T2 without signal changes around that hypointensity indicates a very early stage of myocardial infarction not visible on macroscopic dissection (red arrow). Figure taken from Jackowski et al. [21], Licensed by Elsevier, License Number 5239250101716

Similar to the macroscopic examination of the heart at autopsy, peracute infarction aged less than 6 h old cannot be reliably recognized with PMCMR. However, focal hypointense areas without hyperintense margin in T2w images may be a sign of peracute infarction (Fig. 2.8), since they often correlate with a coronary artery thrombosis in the supplying coronary artery vessel [23].

Quantitative PMCMR is based on specific MR sequences that allow for assessment of MR derived parameters such as myocardial T1 and T2 relaxation times and proton density. These parameters can be measured in the myocardium with dedicated software. Tissue changes, such as myocardial infarction, result in changes of tissue relaxation times and proton density over the course of time. Studies have shown that in quantitative PMCMR different age stages of myocardial infarction can be characterized and discerned based on specific T1, T2 and PD values [4, 5, 24].

PMCMR studies have reported that post-mortem coronary artery MR angiography is possible and provides results comparable to post-mortem computed tomography angiography (PMCTA) [25–27]. Compared to PMCT, post-mortem MR angiography

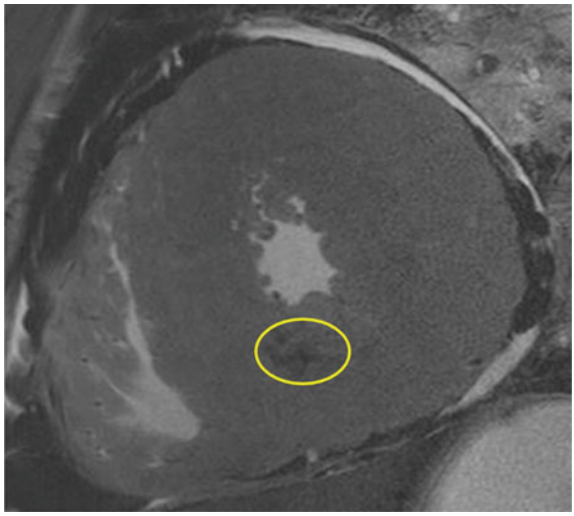

Fig. 2.8 T2 weighted cardiac short axis image showing a focal hypointense area (yellow marking) in the posterior left ventricle wall indicating early myocardial infarction

is more time consuming and needs expensive dedicated equipment. These are the main reasons why currently post-mortem coronary MR angiography is not used on a routine basis in post-mortem imaging.

In native T2w PMCMR blood in the coronary arteries may appear hypointense or hyperintense according to the intracoronary post-mortem blood condition and sedimentation effects. In PMCMR, the larger proximal coronary artery segments can be assessed for stenosis or thrombosis if a small slice thickness is chosen. Coronary artery thrombosis may appear as focal signal alteration with intermediate but homogeneous signal intensity in T2w native PMCMR images [23]. However, arteriosclerotic coronary wall changes and coronary stenosis may also cause focal signal alteration. Thus, differentiation between focal coronary artery thrombosis and arteriosclerosis may be difficult or impossible. In native PMCMR, coronaries can appear with chemical shift artifacts. Such artifacts occur at the interface between fat and water and appear as light and dark bands mimicking blood sedimentation. A study showed that the appearance of such artifacts rather occurs in the absence of coronary thrombosis or stenosis [28].

With PMCMR vegetation on the cardiac valves can be diagnosed. This may give a hint to endocarditis. However, endocarditic vegetations may be hard to discriminate from degenerative valve alterations of other causes. Currently no reliable data exist to assess if PMCMR is feasible for diagnosis of myocarditis.

Summary

Post-mortem magnetic resonance imaging of the heart (PMCMR) can be used either as an alternative in non-forensic cases or as an adjunct to forensic autopsy. Compared to cardiac post-mortem computed tomography (PMCT), PMCMR offers a considerably better visualization of the anatomical heart structures and the myocardium. PMCMR is particularly feasible for diagnosis of myocardial infarction. Moreover, PMCMR allows for cardiac metric measurements, estimation of heart weight, diagnosis of cardiac trauma and the investigation of coronary artery pathology. In the future, new technologies such as computer aided diagnosis based on quantitative PMCMR sequences and ultra-high field (≥7 T) applications may further improve PMCMR's diagnostic abilities.

References

1. Jackowski C, Schweitzer W, Thali M, Yen K, Aghayev E, Sonnenschein M, Vock P, Dirnhofer R. Virtopsy: postmortem imaging of the human heart in situ using MSCT and MRI. Forensic Sci Int. 2005;149(1):11–23.
2. Ruder TD, Thali MJ, Hatch GM. Essentials of forensic post-mortem MR imaging in adults. Br J Radiol. 2014.
3. Ruder TD, Hatch GM, Siegenthaler L, Ampanozi G, Mathier S, Thali MJ, Weber OM. The influence of body temperature on image contrast in post mortem MRI. Eur J Radiol. 2012;81(6):1366–70.
4. Persson A, Baeckmann J, Berge J, Jackowski C, Warntjes M, Zech WD. Temperature-corrected post-mortem 3-T MR quantification of histopathological early acute and chronic myocardial infarction: a feasibility study. Int J Legal Med. 2018;132(2):541–9.
5. Schwendener N, Jackowski C, Persson A, Warntjes MJ, Schuster F, Riva F, Zech WD. Detection and differentiation of early acute and following age stages of myocardial infarction with quantitative post-mortem cardiac 1.5T MR. Forensic Sci Int. 2017;270:248–254.
6. Zech WD, Schwendener N, Persson A, Warntjes MJ, Jackowski C. Temperature dependence of post-mortem MR quantification for soft tissue discrimination. Eur Radiol. 2015;25(8):2381–9.
7. Ampanozi G, Hatch GM, Flach PM, Thali MJ, Ruder TD. Post-mortem magnetic resonance imaging: Reproducing typical autopsy heart measurements. Leg Med (Tokyo). 2015;17(6):493–8.
8. Michaud K, Grabherr S, Jackowski C, Bollmann MD, Doenz F, Mangin P. Postmortem imaging of sudden cardiac death. Int J Legal Med. 2014;128(1):127–37.
9. Femia G, Langlois N, Raleigh J, Perumal SR, Semsarian C, Puranik R. Post-mortem cardiac magnetic resonance parameters in normal and diseased conditions. Cardiovasc Diagn Ther. 2021;11(2):373–82.
10. Bonzon J, Schön CA, Schwendener N, Zech WD, Kara L, Persson A, Jackowski C. Rigor mortis at the myocardium investigated by post-mortem magnetic resonance imaging. Forensic Sci Int. 2015;257:93–7.
11. Ruder TD, Stolzmann P, Thali Y, Hatch G, Somaini S, Bucher M, Alkadhi H, Thali MJ, Ampanozi G. Estimation of heart weight by post-mortem cardiac magnetic resonance imaging. J Forensic Radiol Imaging. 2013;1(1):15–8.
12. Jackowski C, Thali M, Aghayev E, Yen K, Sonnenschein M, Zwygart K, Dirnhofer R, Vock P. Post-mortem imaging of blood and its characteristics using MSCT and MRI. Int J Legal Med. 2006;120(4):233–40.

13. Jackowski C, Grabherr S, Schwendener N. Pulmonary thrombembolism as cause of death on unenhanced postmortem 3T MRI. Eur Radiol. 2013;23(5):1266–70.
14. Aghayev E, Sonnenschein M, Jackowski C, Thali M, Buck U, Yen K, Bolliger S, Dirnhofer R, Vock P. Postmortem radiology of fatal hemorrhage: measurements of cross-sectional areas of major blood vessels and volumes of aorta and spleen on MDCT and volumes of heart chambers on MRI.AJR Am J Roentgenol. 2006;187(1):209–15.
15. Aghayev E, Christe A, Sonnenschein M, Yen K, Jackowski C, Thali MJ, Dirnhofer R, Vock P. Postmortem imaging of blunt chest trauma using CT and MRI: comparison with autopsy. J Thorac Imaging. 2008;23(1):20–7.
16. Ebert LC, Schön CA, Ruder TD, Thali MJ, Hatch GM. Fatal left ventricular rupture and pericardial tamponade following a horse kick to the chest. Am J Forensic Med Pathol. 2012;33(2):167–9.
17. Crooijmans HJ, Ruder TD, Eggert S, Paula P, Thali MJ, Bieri O, Schweitzer W. Feasibility of post mortem cardiac proton density weighted fast field echo imaging in two cases of sudden death. Leg Med (Tokyo). 2013;15(6):310–4.
18. Ampanozi G, Flach PM, Ruder TD, Filograna L, Schweitzer W, Thali MJ, Ebert LC. Differentiation of hemopericardium due to ruptured myocardial infarction or aortic dissection on unenhanced postmortem computed tomography. Forensic Sci Med Pathol. 2017;13(2):170–6.
19. Jackowski C, Warntjes MJ, Berge J, Bär W, Persson A. Magnetic resonance imaging goes postmortem: noninvasive detection and assessment of myocardial infarction by postmortem MRI. Eur Radiol. 2011;21(1):70–8.
20. Jackowski C, Christe A, Sonnenschein M, Aghayev E, Thali MJ. Postmortem unenhanced magnetic resonance imaging of myocardial infarction in correlation to histological infarction age characterization. Eur Heart J. 2006;27(20):2459–67.
21. Jackowski C, Schwendener N, Grabherr S, Persson A. Post-mortem cardiac 3-T magnetic resonance imaging: visualization of sudden cardiac death? J Am Coll Cardiol. 2013;62(7):617–29.
22. Wagensveld IM, Blokker BM, Pezzato A, Wielopolski PA, Renken NS, von der Thüsen JH, Krestin GP, Hunink MGM, Oosterhuis JW, Weustink AC. Diagnostic accuracy of postmortem computed tomography, magnetic resonance imaging, and computed tomography-guided biopsies for the detection of ischaemic heart disease in a hospital setting. Eur Heart J Cardiovasc Imaging. 20181;19(7):739–748.
23. Jackowski C, Hofmann K, Schwendener N, Schweitzer W, Keller-Sutter M. Coronary thrombus and peracute myocardial infarction visualized by unenhanced postmortem MRI prior to autopsy. Forensic Sci Int. 2012;214(1–3):e16–9.
24. Zech WD, Schwendener N, Persson A, Warntjes MJ, Jackowski C. Temperature dependence of postmortem MR quantification for soft tissue discrimination. Eur Radiol. 2015;25(8):2381–9.
25. Bruguier C, Egger C, Vallée JP, Grimm J, Boulanger X, Jackowski C, Mangin P, Grabherr S. Postmortem magnetic resonance imaging of the heart ex situ: development of technical protocols. Int J Legal Med. 2015;129(3):559–67.
26. Grabherr S, Grimm J, Baumann P, Mangin P. Application of contrast media in post-mortem imaging (CT and MRI). Radiol Med. 2015;120(9):824–34.
27. Ruder TD, Hatch GM, Ebert LC, Flach PM, Ross S, Ampanozi G, Thali MJ. Whole body postmortem magnetic resonance angiography. J Forensic Sci. 2012;57(3):778–82.
28. Ruder TD, Bauer-Kreutz R, Ampanozi G, Rosskopf AB, Pilgrim TM, Weber OM, Thali MJ, Hatch GM. Assessment of coronary artery disease by post-mortem cardiac MR. Eur J Radiol. 2012;81(9):2208–14.https://doi.org/10.1016/j.ejrad.2011.06.042. Epub 2011 Jul 2.

Chapter 3
The Use of Micro–computed Tomography for Forensic Applications

Sarah V. Hainsworth

Introduction

Wilhelm Röntgen discovered the electromagnetic radiation known as X–rays in 1895. One of Röntgens first images was of his wife's hand which showed the structure of the hand and bones beneath the skin. X–rays travel from the X–ray source through the object (patient) being examined and are captured on an X–ray detector, originally a photographic plate but now using an electronic detector, to create an image known as a radiograph which gives a 2D representation of the object [1].

X–rays are absorbed in different amounts depending on the radiological density represented by the Hounsfield number, symbol HU [2] of the material being examined. Different materials therefore give different contrasts in the final image, depending on their radiological density. The radiological density is a function of the density of the material and the atomic number. The HU values are measured based on zero HU being defined as the radiodensity of distilled water at standard temperature (STP) and –1000HU being the radiodensity of air at STP. The HU value is calculated from

$$\mathrm{HU} = 1000 \times (\mu - \mu_{\mathrm{water}}/\mu_{\mathrm{water}} - \mu_{\mathrm{air}})$$

where μ = linear attenuation coefficient of substance, μ_{water} = linear attenuation coefficient of water, and μ_{air} = linear attenuation of air. Bone, which contains calcium for example, has a higher atomic number than most tissues and therefore bones absorb X–rays more readily to give a higher contrast than tissues and bony structures. This is why they appear white against a black background in a radiograph (HU cortical bone ~ +1000 or very dense bone +2000). Tissues like fat and muscle or air–cavities like the lungs give a darker grey shade on the radiograph [2]. Metals typically have

S. V. Hainsworth (✉)
University of Bath, Claverton Down, Bath, UK
e-mail: sh2933@bath.ac.uk

G. N. Rutty (ed.), *Essentials of Autopsy Practice*,
https://doi.org/10.1007/978-3-031-11541-7_3

a HU of 3000 [3]. The ability of X–rays to discriminate between fat, tissue, muscle, bone and fractures have thus meant that they have been commonly used as a medical diagnostic tool since their discovery.

The first forensic use of X–rays followed very quickly after their discovery as it was realised that foreign objects such as needles and bullets could easily be located on an X–ray radiograph [1]. Professor Arthur Schuster, a physicist at Owens College in Manchester, England used X–rays in the case of a gunshot wound to locate a bullet fired by Hargreaves Hartley, into the brain of his wife Elizabeth Ann Hartley at Nelson, Lancashire, on 23 April 1896 [4, 5]. The bullets were located but Elizabeth Hartley died shortly afterwards from her injuries.

In the early 1950s, Godfrey Hounsfield from EMI in the UK and Allan Cormack from Tufts University in the USA were separately and simultaneously instrumental in working out that the internal structure of an object could be determined from multiple X–ray images taken at various angles. They were subsequently awarded the Nobel Prize for Physiology or Medicine in 1979 [6] for the development of X–ray computed tomography. Their work showed that 3D representations of objects could be achieved by taking multiple 2D radiographs and computationally reconstructing 3D tomograms of the internal structure of the object that can be used for visualisation and quantification. The advent of storing radiographs digitally by capturing the X–rays on flat screen detectors has meant that access to computing tools to reconstruct the images in 3D becomes much more accessible than was the case with wet chemical photographic plates and along with modern computing capabilities has vastly transformed the way in which images can be recorded and manipulated to gain insights into 3D structures.

Conventional multi–detector computed tomography (MDCT) is widely used in medicine [7, 8] and has been adopted, along with MRI, as an essential tool in forensic applications for many of years [9, 10]. Computed tomography uses X–ray projections taken at multiple angles of view about an axis through an object to make a 3D reconstruction using an algorithm [11]. It is widely used in post mortem imaging and has become recognised as having the capability of allowing virtual autopsies [12], although not all forensic practices have ready access to the scanners.

One of the disadvantages of multi–detector computed tomography (MDCT) is that it has a relatively low resolution and a fixed magnification. For higher resolution X–ray imaging, Cone Beam Computed Tomography (CBCT) can image smaller areas with higher magnifications [13, 14]. This technique is commonly used for dental X–rays [15] and breast examination [16].

When higher resolution than cone beam tomography is needed then micro– or nano–CT [17] systems, often found in engineering or materials science research, can be used. Micro– and nano–CT are used for studying materials, foods, and samples from biology, geology and palaeontology. The scans can also be used for metrology and accurate characterisation of dimensions of internal structures produced during manufacturing. Nano–CT is outside the scope of this chapter as it commonly requires high–resolution X–rays from a synchrotron storage ring. Micro computed tomography (μCT) was developed in the early 1980s [17, 18]. The term applies to X–ray tomography with voxel (volume element) resolutions that are typically between 1

and 50 μm. Mini–CT typically has voxel resolutions between 50 and 200 μm and nano–CT has voxel resolutions between 0.1 and 1 μm. However, micro–, mini– and nano–CT are all often described generically as μCT. μCT has become an increasingly important technique since its inception because it has a number of advantages including:

- Quick and easy radiographic inspection
- Exceptional resolution
- Photo–realistic reconstruction
- Non–destructive
- Little or no preparation of specimens other than securely mounting
- Intuitive visualisation that brings results to life
- Ability to create 3D replicas using modern 3D printing tools.

μCT is attractive for forensic applications as it can provide images which have much higher magnifications and resolutions than that achievable in clinical CT scanners [19].

Another form of CT is industrial computed tomography [20–22] that was also developed from medical CT. It is widely used for industrial inspection, for quality control of complex three–dimensional engineering components and for inspection of assemblies of parts. There are two types of industrial CT scanners:– some use a cone–shaped X–ray beam and flat–panel type of detector as is used in μCT; whereas others use a collimated fan–shaped beam with a detector in a line–scanning mode. Industrial CT can be used for flaw detection, engineering failure analysis, and metrology (inspection of the dimensions of components and in particular internal features that cannot otherwise be measured using e.g. laser scanning or touch probes). Additionally, industrial metrology can be used for reverse engineering of components. Industrial scanning has potential forensic uses in engineering, for example, inspections of gear boxes/air bags/switches or other components that might have failed. Other forensic uses can include examination of firearms, or explosive devices, and searching for concealed compartments [23]. Industrial CT can also be used for applications in forensic anthropology when access to MDCT or μCT is not available [23].

Table 3.1 compares the typical size of objects that can be imaged, resolution, and X–ray energy for the different types of tomography. All X–ray CT systems rely on the absorption of X–ray photons. This gives limits to the volume of objects that can be scanned as if all the photons are absorbed before the detector then there are no data. Higher atomic number materials/denser materials absorb X–rays more readily than lower atomic materials/lower density materials and thus the largest volume that can be measured is limited by the volume that allows analysis of the X–rays reaching the detector.

One disadvantage of μCT techniques is that they usually require a further analysis, for example by scanning electron microscopy with energy dispersive X–ray analysis or other chemical analysis by X–ray diffraction, to determine the chemical composition or phase of a foreign material within a sample or specimen. One way in which CT can become more useful in determining the chemistry of the body is by measuring the HU values of common materials found in forensic pathology, including

Table 3.1 A comparison of the different object sizes, resolution and X–ray energy for a number of different 3D X–ray computed tomography modalities

	Object size	Resolution (Voxel size)	X–ray energy
Medical multidetector CT	Whole human body can be imaged Typical engineering component such as an automobile cylinder head which fits through scanning ring	≥100 μm	80–140 keV
Medical cone beam CT	Dental scanners will allow head and jaw to be imaged	500 μm	60–90 keV
Micro CT	Varies but 280 mm diameter by 600 mm height is typical for a cone–beam system where the specimen rotates	≥0.1 μm	30–300 keV
Industrial CT	Varies but typically 0.8 × 1.2 m part envelope	~0.5 μm	>450 keV

steels, brass, aluminium for example, glass, rocks or other man–made materials to produce a reference set of materials that can aid identification [24]. These materials can then be incorporated into phantom samples (a specially designed object with defined components and composition) that can be scanned alongside the sample of interest.

Instrumentation

Figure 3.1 illustrates the two types of arrangements that are commonly used in μCT scanners. In the first, a specimen is scanned by rotating it around a vertical axis whilst the X–ray source and detector are static. In the second (typically used for scanning small animals) the sample is positioned horizontally and the X–ray source and detector are rotated around a horizontal axis through the animal.

The size of sample that can be imaged in a μCT is determined by the space between the source and the detector. A sample must be able to sit on the rotation platform and be rotated in a stable manner without impeding (touching) the detector or source. In order to be able to exactly reconstruct the 3D image, the specimen has to stay in the field of view (FOV) for all rotations.

The time taken for a scan depends on the number of radiographs that are taken and the time for an individual radiograph to be taken. The time for an individual radiograph depends on the X–ray flux that is generated by the X–ray source and the absorption of the X–rays by the sample. The flux determines the time required to

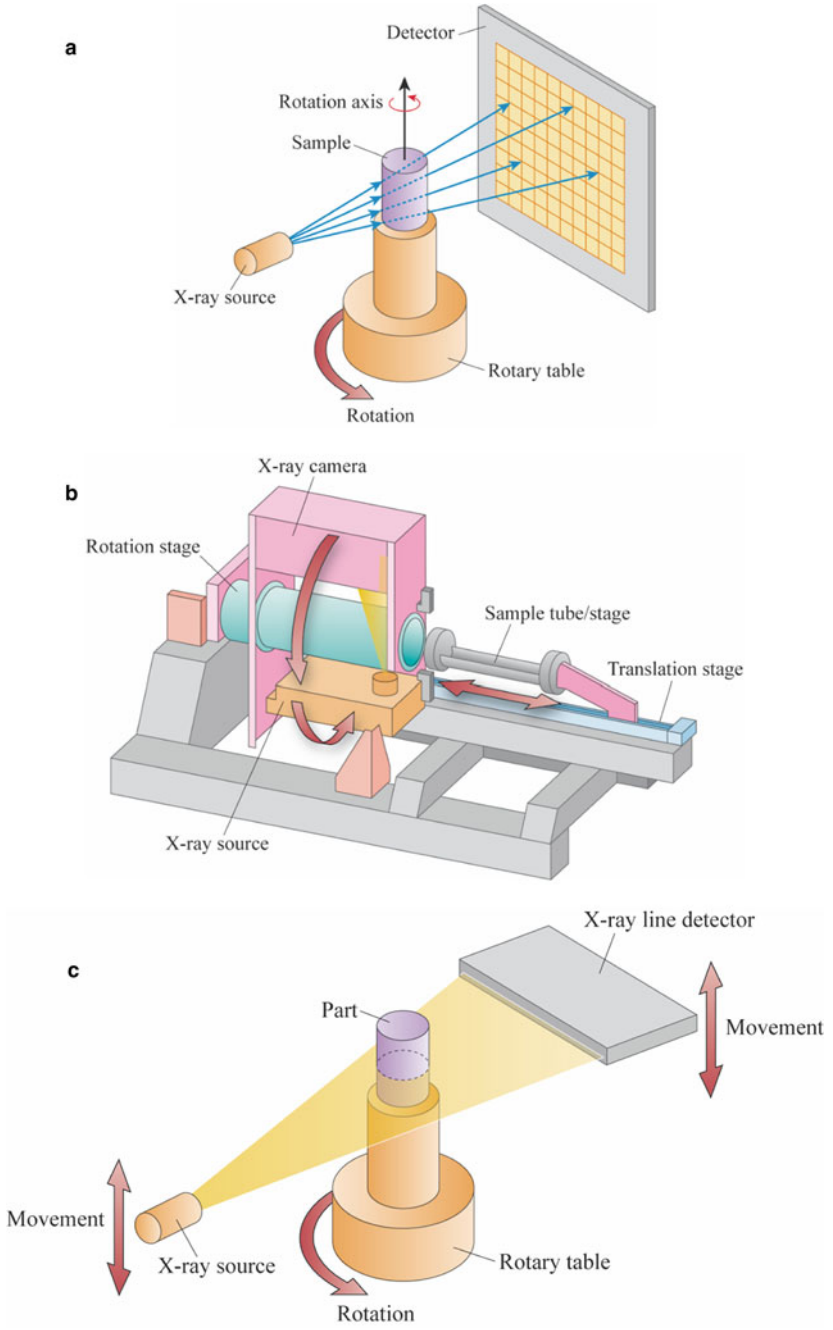

Fig. 3.1 Common X–ray computed tomography configurations **a** cone beam system typical of many laboratory systems **b** small animal μCT scanner configuration **c** set–up for an industrial X–ray CT line scanner. Illustrations courtesy of Vicky Eves, UK

obtain a projection image of the required quality dependent on the signal–to–noise ratio and obtaining a good dynamic range of contrast. The X–ray flux and exposure time will determine the number of X–ray photons incident per image pixel. It is important that the detector is not over–saturated by photons. The contrast sensitivity is determined by the characteristics of the specimen and also the instrument characteristics.

A typical laboratory μCT system with the configuration shown in Fig. 3.1a is shown in Fig. 3.2.

The noise in the reconstructions can be decreased by using frame averaging as long as the incident X–ray beam is stable. Essentially, this consists of acquiring multiple images at each rotation step which are then averaged to get the final image projection that is used for reconstruction with an improved signal–to–noise ratio. Depending on the detector, four frame averages with a 12 bit detector are comparable to a 14 bit detector i.e. in terms of the ability to discriminate between pixels of different grey levels. It is not possible to get a valid reconstruction if the detector saturates at any point in the image.

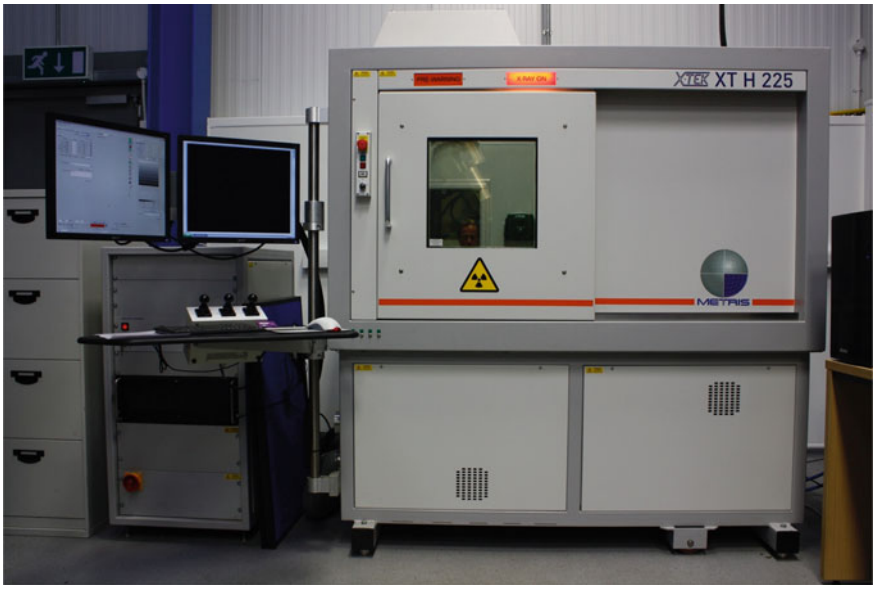

Fig. 3.2 A Nikon XT H225 micro computed tomography scanner in the Department of Engineering at the University of Leicester showing the sample chamber and control monitors for setting up the scans

Magnification, Resolution and Quantification

The magnification M in a μCT system is is defined as the ratio of the focus–to–detector distance over the focus–to–sample distance, i.e. M = FDD/FOD as shown in Fig. 3.3.

The spatial resolution of X–ray CT systems is influenced by a number of factors including the focal spot size, X–ray detector performance, system magnification, number of projections, filtering and the reconstruction algorithms that are used.

The spatial resolution is usually defined by the voxel size which is a function of the pixel size divided by the magnification. The spatial resolution is defined by how far two features of the object need to be separated to be distinguishable in the measured image [25]. This can either be determined by visual resolution tests using line group test patterns (which are observer dependent) where the resolution is defined by when two distinct lines cannot be separated or by using modulation transfer functions [26].

If μCT is being used for metrology purposes to derive quantitative data from the images, then it is important that the spatial resolution and other sources of error in the data are well understood. Additionally, it is important for the validity of measurements and their interpretation that measurements are both reproducible and repeatable i.e. that here is agreement of results from experiments performed in the same way under the same conditions and also for repeated measurements of a single sample under the same conditions. It is important that appropriate calibrations are performed [20, 27]. Additionally, variables during the measurements should be carefully controlled. These can include factors related to the CT systems:– the measurement object itself, the analysis method of the scans, the environment for scanning such as temperature and, humidity, and finally the operator using the same scanning parameters for repeated measurements.

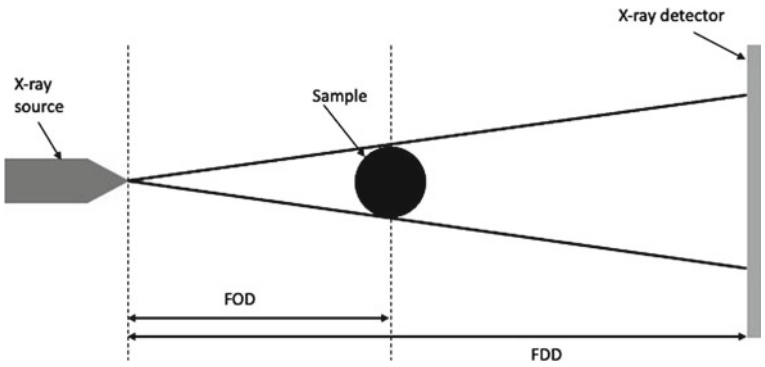

Fig. 3.3 Image magnification for μCT. FOD is the focus to sample distance and FDD is the Focus to detector distance

Software

An important part of any analysis by X–ray CT is image reconstruction. The reconstruction of images is challenging as every voxel has between 8–16 bits of grayscale information and a 3D volume image may have between 500^3 and 2000^3 voxels. This tends to lead to large files and a need for considerable computing power for image storage, transfer and display.

Most X–ray CT manufacturers have their own proprietary software for reconstruction. Most of these use a reconstruction method based on filtered back–projection which is based on an algorithm developed by Feldkamp [28]. In addition, there are a number of commercial software packages such as VGStudio MAX (Volume Graphics, GmbH) Avizo (VSG Visualization Sciences Group, Mérignac, France), and Simpleware (Simpleware Ltd., UK) which is a volumetric data processing software that can export volumetric data into CAD and finite element models. There are also a number of valuable freeware resources including Drishti [29], Image J [30] and Dragonfly (Object Research Systems Inc., Montreal, Canada) although others are also freely available.

Potential Sources of Error

There are several potential sources of error in μCT. These can be physical–based, scanner–based, or sample–based.

In scanners where the source and detector rotate around the sample, it is critical that the source and detector rotate so that deviation from the required ideal trajectory around the axis of rotation is smaller than the detector pixel size. Sample mounting is also important to avoid motion artefacts from the sample moving during scanning or dynamic changes occurring during scanning through for example heating or a hydrated sample drying out. Motion artefacts can also arise during dynamic scanning from the sample itself moving (such as a fly hatching).

Beam Hardening

X–ray beams have photons of different energies. Beam hardening is an artefact that occurs as the X–ray beam passes through an object as the lower energy X–rays are absorbed preferentially and higher energy X–ray photons remain. This means that the beam becomes "harder," i.e. its mean energy increases since lower energy photons are absorbed more rapidly than the higher–energy photons. Beam hardening can lead to uneven contrast from the outside to the inside of the sample. This is known as a cupping artefact (Fig. 3.4). Beam hardening can be reduced by using a physical filter of a material that absorbs the lower energy X–rays placed between the X–ray

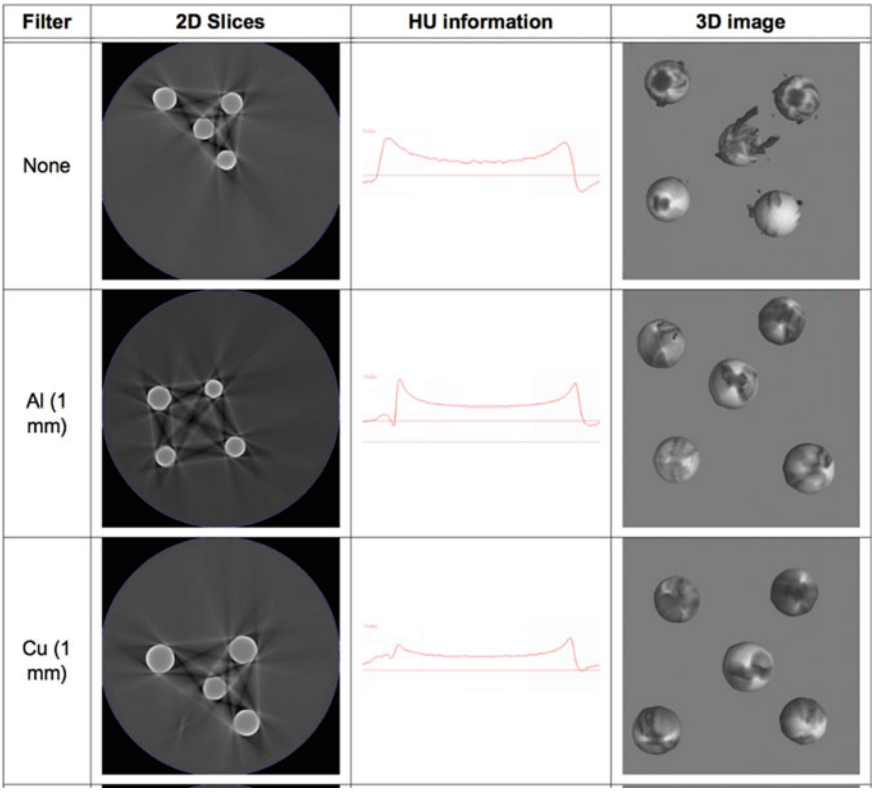

Fig. 3.4 CT number profile across the centre of a phantom (containing uniform shotgun pellets) showing cupping (brighter edges to the pellet) and streaking artefacts and the effect of using different filters on the profile obtained

source and the sample. These filters are typically thin (0.5–mm– thick) metal sheets of copper, tin or aluminium. An example of a cupping artefact from imaging shot–gun pellets is shown in Fig. 3.4, and the way in which filters change the shape of the artefact can also be seen. The disadvantage of using physical filters is that it reduces the signal–to–noise ratio.

Beam hardening artefacts can also be reduced by using correction algorithms in the image analysis.

Another type of artefact is a streak artefact. These usually occur when the X–ray beam is completely attenuated by high–density objects, but can also be caused by detectors with limited dynamic range, those with a limited number of discrete levels of measurement between the maximum and minimum signal that can be registered, such that peak white and peak black are readily reached and useful information from the image is lost.

Noise artefacts arise from two sources: structured noise from instrument artefacts such as electronic noise and detector inefficiency and random statistical noise from

background radiation [31]. Noise artefacts can be reduced by increasing the signal to noise ratio (SNR) i.e. by increasing the number of X–rays the sample is exposed to. Image processing methods such as averaging can also be used when using reconstruction software. One of the concerns about noise (in both medical and industrial CT) is that it can lead to false positive readings (for example, noise can appear as dots which could be mistaken for nodules in tissue samples [32] or pores or cavities in castings in industrial components [33]).

Partial Volume Artefacts

Each voxel in a CT image represents the attenuation properties of the specific material within the voxel. Partial volume effects or artefacts occur when a single voxel is filled by substances of two widely different absorptions. This gives a beam attenuation that is reflective of the average HU value of the substances. This can cause challenges in interpreting images quantitatively, particularly around boundaries. In materials and geology these effects can be used to highlight cracks or porosity and can add value; however, the image interpretation can be more challenging. Sutton et al. [34] suggest that partial volume effects are most problematic when the anatomical structure is close to the voxel size and that the way of reducing the issue is either increased magnification or else a detector with greater dimensions.

Scanner–based Sources of Error

There are a number of different errors that can arise from the μCT system itself. One of these is beam drift, where the spatial location of the X–ray focal spot can move or drift as the X–ray tube thermally expands. X–rays are typically generated by heating a filament of a material, usually tungsten that generates an electron beam that hits a target that then emits the X–rays. The temperature of the X–ray tube has to be controlled by cooling so that any errors from thermal drift are eliminated. Another issue related to the detectors, are concentric ring artefacts. These occur either from defects in the detectors themselves, poor detector calibration or non–uniform output from channel to channel in the detector array. Ring artefacts can be removed by carefully controlling the sensitivity across the whole detector to be uniform or using a numerical algorithm to correct for the issue.

Radiation Damage

Micro–computed tomography is largely considered to be non–destructive but as voxel sizes become smaller, the X–ray dose required to produce a high–quality radiograph increases. The high radiation dose can lead to radiation artefacts and damage to samples which might otherwise be considered to be macroscopically undamaged. The dose can cause damage to DNA, lead to discoloration or create chemical or structural damage for example. The radiation exposure of the object being studied increases with the voxel side dimension to the 4^{th} power. Thus, higher spatial resolutions give increased radiation exposure. The higher energy X–rays in tube source μCTs are considered less damaging than X–rays used in nano-CT from synchrotron sources which are usually lower energy X-rays with energies in the range soft (<1 keV) or moderate (5–30 keV) [18] but when also combined with the higher X-ray flux from a synchrotron source leads to a higher dose on the sample.

Immel et al. [35] studied subfossil bones and identified that a dose of <200 Gy was the safe limit to prevent DNA damage. In order to achieve doses less than this the CT voxel sizes needed to be >1 μm. Immel et al. [35] also suggested that a metallic filter should be used between the source and the sample to filter out the lowest energy and most damaging X–rays from the whitebeam radiation. McCollough et al. [36] found that the dose for a head scanned in a medical scanner is typically of the order of 0.06 Gy which should be low enough to avoid denaturing any DNA. For a 100 kV tube source CT with a 10 μm voxel size, Meganeck et al. [37] showed that the dose is ~0.4 Gy which again should be within acceptable limits.

Selected Applications

Bones and Toolmarks

Thali et al. [38] showed that μCT could be used for investigating knife marks in bones. The shape and size of the mark could indicate the type of tool used to make the mark. 3D analysis of the marks could be used to generate a “digital virtual knife”, and hence bone injuries could be correlated to the knife that made them. General class characteristics such as size, profile, shape, direction of travel and movement in the wound could also be visualised. Pounder and Sim [39] used μCT to investigate the serrations left by serrated knifes in stab wound tracts. Rutty et al. [19] demonstrated how the 3D sectioning of images through saw tracts could be used to differentiate between knife and saw marks from the shape of the bottom of false start kerfs and also showed the advantage that μCT has in reducing specular reflection (from mirror–like reflection of visible light) that is common in optical microscope images of tool marks on bone. Further work on investigating the use of μCT on marks made with different saws was performed by Norman et al. [40], who made cut marks with hand and electric saws and analysed the information that could be obtained. They found that

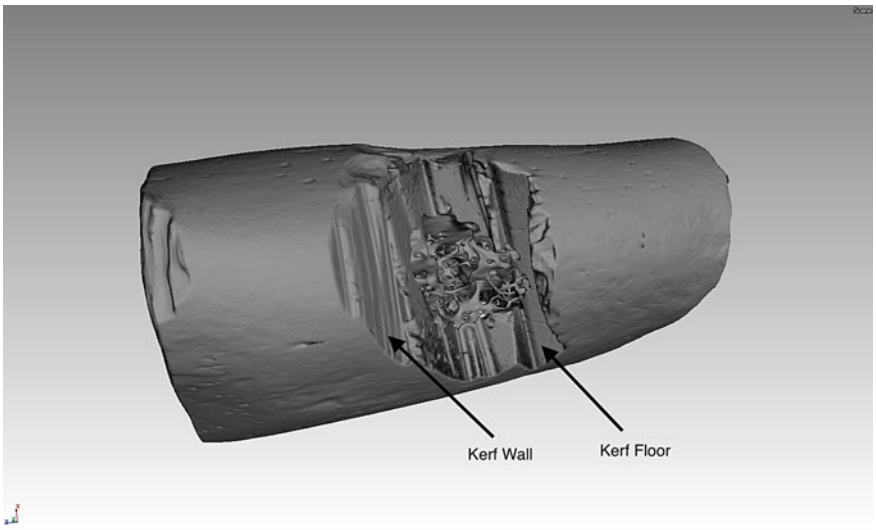

Fig. 3.5 Reconstruction of a μCT image of a partial cut through a jaw bone with an electrically powered circular saw. A number of steps can be seen in the kerf wall and the kerf (cut) floor is clearly visible. Partial cuts such as this can be used to potentially determine the thickness of the cutting blade

the width of the tool marks obtained from μCT could be consistently matched to the saw blade width and that marks made in fleshed bone were different to those made in defleshed bone. Norman et al. also produced an extended study of tool marks in bone from various different knives [41]. μCT analysis of weapon marks on bones can also be applied to archaeological cases such as analysis of the weapon marks on the remains of Richard III [42].

Figure 3.5 gives an example of the information that can be obtained from a μCT image.

The image shows a 3D reconstruction of a μCT image of a partial cut made with an electrically powered circular saw through a jaw bone. A number of steps can be seen in the kerf wall and the kerf (cut) floor is clearly visible. Partial cuts such as this can be used to potentially determine the thickness of the cutting blade. An additional advantage of using μCT in dismemberment cases is that the images are reconstructions and therefore can be shown in court in a way that pathology photographs cannot be shown. A further advantage of the 3D data is that it can be used along with 3D printing to provide replicas which again can be shown in court [43].

Larynx Fractures

Strangulation is a challenging cause of death to diagnose and a common homicide method, particularly for women who are commonly strangled by their partners. One of the challenges for the forensic pathologist is that the injuries can be subtle with no obvious bruising or compression of the neck and with a lack of features that can be attributed to asphyxia.

A number of authors have used μCT for analysing strangulation cases [44]. Baier [45] performed a comprehensive set of scans in which larynxes from a control group were imaged using μCT and compared to the current "gold standard" of histology. They examined two larynges from suspected strangulations and showed a strong correlation between the histology and the μCT images.

An example of a fractured larynx is shown in Fig. 3.6 (image courtesy of Prof Mark Williams of the University of Warwick). The fractures are labelled as A for a fracture on the posterior right greater horn and B for a fracture on the thyroid laminae. There was also a possible fracture identified at the base of the left superior horn of the thyroid cartilage.

The disadvantage of μCT for analysing injuries such as this is that the soft–tissue injuries cannot be readily visualised but it does show the benefit of using this technique for analysing fractures that cannot be seen on a conventional MDCT used for post–mortem virtopsys.

Fig. 3.6 An antero-lateral view of the volume-rendered μCT scan of a larynx A = hyoid fracture, B = fracture on left inferior margin of thyroid lamina, C = possible fracture of left superior thyroid horn

Gunshot

Analysis of gunshot residue is important for understanding the firing range in fatalities from gunshot. μCT has been used for detection of gunshot residue (GSR) in firearm wounds [46] and also for estimating firing distances from residue around gunshot wounds [47]. This work showed how μCT was able to generate a 3D reconstruction of the spatial distribution of GSR particles.

Giraudo et al. [48] performed detailed studies on the analysis of gunshot residue on wounds from a 0.32ACP pistol (Berretta Mod. 81) when the shots were made through fabrics as most shooting injuries are made when the victim is clothed. The shots were fired into sections of human calves at three different muzzle–to–target distances. All entrance wounds showed evidence of radio–opaque materials, whereas no exit wounds showed any evidence of GSR. This showed the value of μCT as a potential screening tool for differentiating between entrance and exit wounds.

μCT can also be used to evaluate the distribution of shot gun pellets into a sample. Figure 3.7 shows how the distribution of pellets from a shot gun discharged into a butchered pig's leg can be determined using μCT. The image shows the results from a test shot made using a Spanish Laurona 12–Bore Over/Under 28″ barrel shotgun with the lower barrel having a quarter choke. The ammunition was a twelve–gauge shot cartridge with plastic wadding. The figure shows that the pellets stop at differing distances into the leg, with a band of pellets towards the bottom of the figure at the point at which the pellets do not have sufficient energy to penetrate further into the

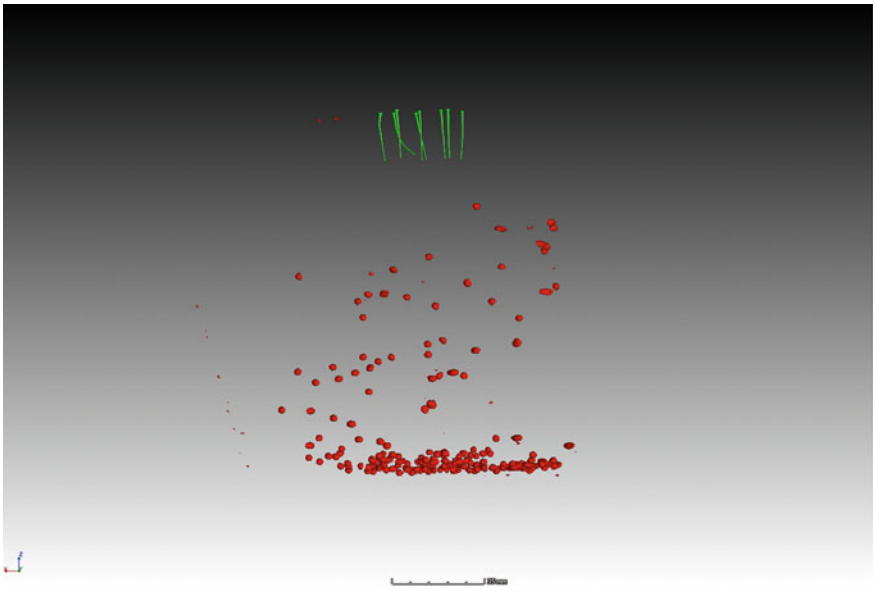

Fig. 3.7 μCT image of shotgun pellets into a pig's legs. Pellets are shown in red. The entrance wound position is marked by the green pins

flesh. The surface of the skin which was difficult to see with the μCT analysis, was marked by pins which are shown in green. The surface was not straightforward to determine as it was difficult to manipulate the image because of the large contrast range between the flesh and pellets. The pins therefore gave a convenient way of accurately determining the position of the entrance wounds.

A range of experiments were undertaken with differing firing distances into a butchered pig's leg from contact (0 m), 1 m, 2 m, 3 m, and 4 m and these could be correlated against the depth of penetration of pellets into a victim with closer–range shots penetrating to further distances. The spread (scatter) of the pellets also increased as the distance of the muzzle from the leg increased.

Entomology

Benecke [49] suggested that forensic entomology became identifiable as a discipline after the first use of insects and other arthropods as forensic indicators in Germany and France in the late by Reinhard and Hofmann; although there are case reports from China as early as the 13th Century of flies being found on deceased bodies. Bergeret, a French physician, is attributed as the first to use blow–fly pupae and larval moths [49] for determining postmortem interval (PMI) which is defined as the period between the time of death of a cadaver and when it was discovered. PMI is challenging to determine accurately as there are a large number of variables that affect the rate of decomposition of a cadaver, but forensic entomology is deemed useful in estimating the time since death with an acceptable degree of confidence to aid investigation [50]. Different insects and animals are interested in the cadaver at different stages of the cadaver decomposition [51].

Calliphora vicinia and *Calliphora vomitoria* [50] are the most common blowfly species in the UK and are the first to conquer a fresh cadaver [52].

It is often difficult to determine the age of a blowfly during the pupation stage as the fly is cocooned in a casing and the external features of the cocoon look very similar over the entire developmental stage. Figure 3.8 shows the different developmental stages of the pupae.

The traditional method for determining the pupal development stage is to use an invasive technique where the pupae is killed, stained, and dissected [52–54].

μCT is ideal for investigating the different stages of the pupal development as the internal 3D structure of the cocoon can be examined. Richards et al. [55] used μCT to scan *Calliphora vicina (Diptera: Calliphoridae)* during metamorphosis and reconstructed the internal structures of the pupae. Their work showed that μCT was a viable and a better alternative to the traditional methods. Martín–Vega et al. [56] were able to track the development of pupae, determine the critical periods in its development, and understand the role of the gas bubble during the structural development of the flies with unprecedented detail.

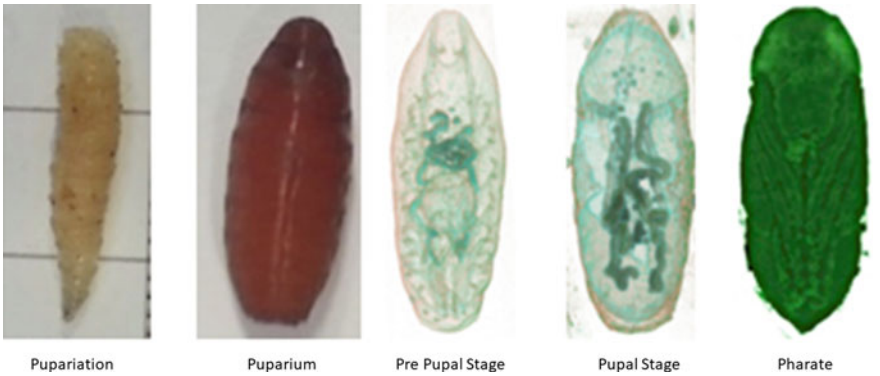

Fig. 3.8 The different phases of the pupal development

A series of images of blow–fly larvae at different stages of development were scanned in a Nikon XT H 225 industrial micro–CT scanner controlled by Nikon Inspect–X software with the parameters below:

1. 60 kV and 70 μA
2. 700 ms exposure
3. 0.5 mm tin filter

Pupae were held in place in the scanner by inserting them into a paper drinking straw which was found to give a way of obtaining images of several pupae in a single scan with good mechanical stability of the pupae.

The images were pre-processed using the scanner software and then uploaded to VGI Studio MAX where the air phase of the sample was removed. These files were then uploaded to Image-J to remove any noise and to create sharper and better-contrasted stacks of images. The image stacks were then uploaded to Drishti where the stacks of images were compiled into a 3D model that could be rendered and processed. In Drishti the scans were put through a series of morphological operations to expose the external and internal features of the fly within the pupae. Images of the scans were then collected and arranged to show the progression in the development of the pupae. Pupae were developed at a range of temperatures and for a varying number of days.

Figure 3.9 shows the development of a pupae at 2, 7 and 8 days. The μCT scans gives an understanding of the internal structure within the epidermis. This was especially convenient during the first few days after the puparium formation where the early tracheal tube structure (A), coiled tubular cluster (B) and gas bubble (C) is easily seen.

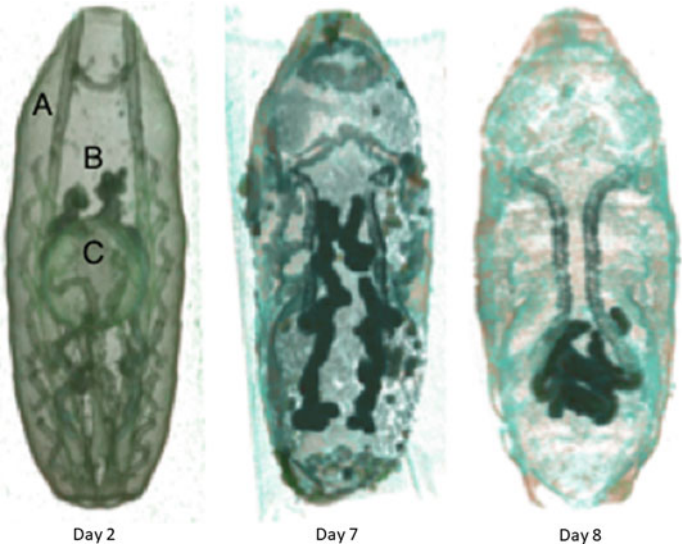

Fig. 3.9 Pupae development from μCT imaging illustrating the change in the tracheal tube and coiled tubed cluster as the pupae mature. A is the early tracheal tube, B the coiled tubular cluster and C the gas bubble

The point where the change from pre–pupal stage to pupal stage was also definite, and allowed the apolysis to be observed and the change in the tracheal tube structure to be visualised. Additionally, the progression of the coiled tubular cluster as well as its change in position overtime can be seen in the images.

However, in comparison to features that can be identified by traditional methods there are a number of structures that are not visible on the μCT images:– for example, the central nervous system, the peripheral nervous system, and the muscles along the body are not readily visible [57].

The full power of μCT as a visualisation tool for the internal structures can be seen in images in Fig. 3.10.

One of the advantages of μCT scanning is that in many instances, for example, in the imaging of blow–fly internal structures, the evolution of structure whilst an organism is growing can be tracked with multiple scanning sessions over a period of time.

A previous study on the radiation of Mexican fruit–fly suggests that the third –instar larvae and prepupal stage pupae have low sensitivity to irradiation, and the pupae are thought to be able to recover after each dose [58]. However, scans by us found that only small numbers of irradiated pupae emerged compared to their non–radiated counterpart, when each sample was only scanned once. Our scans were conducted to minimise exposure to radiation and therefore the image quality is less than if longer scans were used and therefore there is a compromise between development and quality of information obtained during μCT scanning.

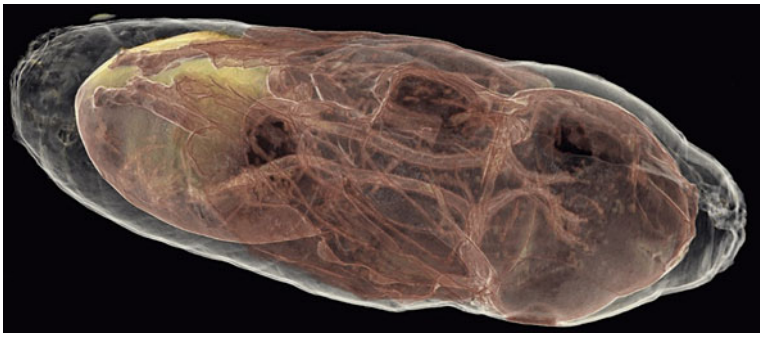

Fig. 3.10 Image of a blow fly pupae from X–ray μCT images using Drishti post processing to reveal and colour the structures that have developed

The scans in Figs. 3.8 and 3.9 were obtained without the use of staining as would be required in traditional studies using reflected light microscopy. Stains are not always required for μCT investigations. However, some researchers, such as Metscher, Kang et al. and Swart et al. [59–61] have used staining to provide additional contrast which improves the discrimination of the internal structure for studies of blow–flies and barnacles. Not all contrast stains are inert, and some may damage the specimen. Pauwels et al. [62] noted that acids such as phosphotungstic acid (PTA), dodeca molybdophosphoric acid (PMA) and $FeCl_3$ solution when used in high concentrations can dissolve calcified tissues such as bones and thereby destroy the specimen being examined.

The choice of staining therefore depends on what the aim of the investigation is. For fundamental science or entomology staining may be desirable but there will be instances where a forensic sample must remain unchanged unless experts for both prosecution and the defence agree that staining is an acceptable method from both parties' perspective.

Summary

Micro X–ray Computed Tomography has developed over the last 30 years as digital X–ray detectors have allowed the capture of multiple radiographs that can be reconstructed to give a 3D representation of the sample.

During this period, the time required to obtain the scans has reduced, and the computing power of the systems to generate the 3D images has evolved at pace. The power of the technique means that it has found multiple practical applications in the areas of forensic science and engineering. Continuous improvements in the image resolution and image contrast are likely to for the foreseeable future.

One particular advantage of the technique for forensic applications is that the images are traceable and easily shared, and the data can readily be stored. By comparison to multi–detector computed tomography scans that are commonly used for autopsy, μCT offers access to higher magnifications and higher resolutions, which means that it offers additional functionality and possibilities for forensic applications.

As access to scanners improves and the software and interpretation of images becomes more accessible, the diversity of applications in forensic science continues to grow. μCT therefore adds powerful additional insights for the forensic practitioner to interpret and understand forensic case work.

Acknowledgements Professor Mark Williams and Dr Waltrud Baier of Warwick Manufacturing Group, from the University of Warwick are thanked for the provision of Fig. 3.6. Jessica Lam of the University of Leicester is thanked for the provision of Fig. 3.4. Dayang Liyana Hj Awang Lamat and Graham Clark, also from the Department of Engineering at the University of Leicester, are acknowledged for the work that led to various other of the case studies and images referred to within this Chapter. Professor Michael Fitzpatrick of Coventry University is thanked for his constructive comments on the manuscript.

References

1. Mould RF. The early history of X-ray diagnosis with emphasis on the contributions of physics 1895–1915. Phys Med Biol. 1995;40(11):1741–87. https://doi.org/10.1088/0031-9155/40/11/001.
2. DenOtter TD, Schubert J. Hounsfield unit. Treasure Island (FL): StatPearls Publishing; 2022.
3. Glide-Hurst C, Chen D, Zhong H, Chetty IJ. Changes realized from extended bit-depth and metal artifact reduction in CT. Med Phys. 2013;40(6):61711. https://doi.org/10.1118/1.4805102.
4. Eckert WG, Garland N. The history of the forensic application in radiology. Amer J Forensic Med Pathol. 1984;5(1).
5. Blakeley C, Hogg P. Manchester medical society (imaging section) presidential address 2008. Radiography; 2009. https://doi.org/10.1016/j.radi.2009.10.001.
6. Di Chiro G, Brooks RA. The 1979 nobel prize in physiology or medicine. J Comput Assist Tomogr. 1980;4(2):241–5. https://doi.org/10.1097/00004728-198004000-00023.
7. Tempany CMC, McNeil BJ. Advances in biomedical imaging. J Am Med Assoc. 2001;285(5):562–7. https://doi.org/10.1001/jama.285.5.562.
8. Kalender WA. X-ray computed tomography. Phys Med Biol. 2006;51(13):R29–43. https://doi.org/10.1088/0031-9155/51/13/r03.
9. Saunders SL, Morgan B, Raj V, Rutty GN. Post-mortem computed tomography angiography: past, present and future. Forensic Sci Med Pathol. 2011;7(3):271–7. https://doi.org/10.1007/s12024-010-9208-3.
10. Leth P. The use of CT scanning in forensic autopsy. Forensic Sci Med Pathol. 2007;3:65–9. https://doi.org/10.1385/FSMP:3:1:65.
11. Flohr TG, Schaller S, Stierstorfer K, Bruder H, Ohnesorge BM, Schoepf UJ. Multi–detector row CT systems and image-reconstruction techniques. Radiology. 2005;235(3):756–73. https://doi.org/10.1148/radiol.2353040037.
12. Rutty GN, Morgan B. Virtual autopsy. Forensic Sci Med Pathol. 2013;9(3):433–4. https://doi.org/10.1007/s12024-013-9450-6.

13. Brüllmann D, Schulze RKW. Spatial resolution in CBCT machines for dental/maxillofacial applications-what do we know today? Dentomaxillofac Radiol. 2015;44(1):20140204. https://doi.org/10.1259/dmfr.20140204.
14. Pauwels R, Araki K, Siewerdsen JH, Thongvigitmanee SS. Technical aspects of dental CBCT: state of the art. Dentomaxillofac Radiol. 2015;44(1):20140224. https://doi.org/10.1259/dmfr.20140224.
15. Dawood A, Patel S, Brown J. Cone beam CT in dental practice. Br Dent J. 2009;207(1):23–8. https://doi.org/10.1038/sj.bdj.2009.560.
16. O'Connell A, et al. Cone-beam CT for breast imaging: radiation dose, breast coverage, and image quality. Am J Roentgenol. 2010;195(2):496–509. https://doi.org/10.2214/AJR.08.1017.
17. Ritman EL. Current status of developments and applications of Micro-CT. Annu Rev Biomed Eng. 2011;13(1):531–52. https://doi.org/10.1146/annurev-bioeng-071910-124717.
18. Withers PJ, et al. X-ray computed tomography. Nature Rev Methods Primers. 2021;1(1):18. https://doi.org/10.1038/s43586-021-00015-4.
19. Rutty GN, Brough A, Biggs MJP, Robinson C, Lawes SDA, Hainsworth SV. The role of micro-computed tomography in forensic investigations. Forensic Sci Int; 2013. https://doi.org/10.1016/j.forsciint.2012.10.030.
20. Sun W, Brown S, Leach R. An overview of industrial X-ray computed tomography; 2011.
21. Carmignato S, Dewulf W, Leach R. Industrial X-ray computed tomography. Springer International Publishing; 2018.
22. du Plessis A, le Roux SG, Guelpa A. Comparison of medical and industrial X-ray computed tomography for non-destructive testing. Case Stud Nondestruct Testing Eval. 2016;6:17–25. https://doi.org/10.1016/j.csndt.2016.07.001.
23. Christensen A, Smith M, Gleiber D, Cunningham D, Wescott D. The Use of X-ray computed tomography technologies in forensic anthropology. Forensic Anthropol. 2018;1:124–40. https://doi.org/10.5744/fa.2018.0013.
24. Bolliger SA, Oesterhelweg L, Spendlove D, Ross S, Thali MJ. Is differentiation of frequently encountered foreign bodies in corpses possible by hounsfield density measurement? J Forensic Sci. 2009;54(5):1119–22. https://doi.org/10.1111/j.1556-4029.2009.01100.x.
25. McCullough EC, et al. Performance evaluation and quality assurance of computed tomography scanners, with illustrations from the EMI, ACTA, and delta scanners. Radiology. 1976;120(1):173–88. https://doi.org/10.1148/120.1.173.
26. Rueckel J, Stockmar M, Pfeiffer F, Herzen J. Spatial resolution characterization of a X-ray microCT system. Appl Radiat Isot. 2014;94:230–4. https://doi.org/10.1016/j.apradiso.2014.08.014.
27. Schladitz K. Quantitative micro-CT. J Microsc. 2011;243(2):111–7. https://doi.org/10.1111/j.1365-2818.2011.03513.x.
28. Feldkamp LA, Davis LC, Kress JW. Practical cone-beam algorithm. J Opt Soc Am A. 1984;1(6):612–9. https://doi.org/10.1364/JOSAA.1.000612.
29. Limaye A. Drishti: a volume exploration and presentation tool. In: Proceedings SPIE, 2012, vol. 8506, pp. 85060X–8506–9. https://doi.org/10.1117/12.935640.
30. Schneider CA, Rasband WS, Eliceiri KW. NIH Image to ImageJ: 25 years of image analysis. Nat Methods. 2012;9(7):671–5. https://doi.org/10.1038/nmeth.2089.
31. Cherry SR, Sorenson JA, Phelps MEBT. Physics in nuclear medicine, 4th Editio. Philadelphia: Elsevier, 2012. https://doi.org/10.1016/B978-1-4160-5198-5.00033-2.
32. Kamiyama H, et al. Unusual false-positive mesenteric lymph nodes detected by PET/CT in a metastatic survey of lung cancer. Case Rep Gastroenterol. 2016;10(2):275–82. https://doi.org/10.1159/000446579.
33. Fuchs P, Kröger T, Garbe CS. Defect detection in CT scans of cast aluminum parts: a machine vision perspective. Neurocomputing. 2021;453:85–96. https://doi.org/10.1016/j.neucom.2021.04.094.
34. Sutton M, Rahman I, Garwood R. Techniques for virtual. Palaeontology. 2014. https://doi.org/10.1002/9781118591192.

35. Immel A, et al. Effect of X-ray irradiation on ancient DNA in sub-fossil bones—Guidelines for safe X-ray imaging. Sci Rep. 2016;6:32969. https://doi.org/10.1038/srep32969.
36. McCollough CH, Bushberg JT, Fletcher JG, Eckel LJ. Answers to common questions about the use and safety of CT scans. Mayo Clin Proc. 2015;90(10):1380–92. https://doi.org/10.1016/j.mayocp.2015.07.011.
37. Meganck JA, Liu B. Dosimetry in micro-computed tomography: a review of the measurement methods, impacts, and characterization of the quantum GX imaging system. Mol Imag Biol. 2017;19(4):499–511. https://doi.org/10.1007/s11307-016-1026-x.
38. Thali M, et al. Forensic microradiology: micro-computed tomography (Micro-CT) and analysis of patterned injuries inside of bone. J Forensic Sci. 2003;48:1336–42. https://doi.org/10.1520/JFS2002220.
39. Pounder DJ, Sim LJ. Virtual casting of stab wounds in cartilage using micro-computed tomography. Amer J Forensic Med Pathol. 2011;32(2). [Online]. Available: https://journals.lww.com/amjforensicmedicine/Fulltext/2011/06000/Virtual_Casting_of_Stab_Wounds_in_Cartilage_Using.1.aspx.
40. Norman DG, Baier W, Watson DG, Burnett B, Painter M, Williams MA. Micro-CT for saw mark analysis on human bone. Forensic Sci Int. 2018;293:91–100. https://doi.org/10.1016/j.forsciint.2018.10.027.
41. Norman DG, Watson DG, Burnett B, Fenne PM, Williams MA. The cutting edge—Micro-CT for quantitative toolmark analysis of sharp force trauma to bone. Forensic Sci Int. 2018;283:156–72. https://doi.org/10.1016/j.forsciint.2017.12.039.
42. Appleby J, et al. Perimortem trauma in King Richard III: a skeletal analysis. The Lancet. 2015;385(9964):253–9. https://doi.org/10.1016/S0140-6736(14)60804-7.
43. Biggs M. 3D printing applied to forensic investigations. In: Essentials of autopsy practice 2019, pp. 19–49. https://doi.org/10.1007/978-3-030-24330-2_2.
44. Fais P, et al. Micro computed tomography features of laryngeal fractures in a case of fatal manual strangulation. Leg Med. 2016;18:85–9. https://doi.org/10.1016/j.legalmed.2016.01.001.
45. Baier W, Mangham C, Warnett JM, Payne M, Painter M, Williams MA. Using histology to evaluate micro-CT findings of trauma in three post-mortem samples—First steps towards method validation. Forensic Sci Int. 2019;297:27–34. https://doi.org/10.1016/j.forsciint.2019.01.027.
46. Cecchetto G, et al. MicroCT detection of gunshot residue in fresh and decomposed firearm wounds. Int J Legal Med. 2012;126(3):377–83. https://doi.org/10.1007/s00414-011-0648-4.
47. Cecchetto G, et al. Estimation of the firing distance through micro-CT analysis of gunshot wounds. Int J Legal Med. 2011;125(2):245–51. https://doi.org/10.1007/s00414-010-0533-6.
48. Giraudo C, et al. Micro-CT features of intermediate gunshot wounds covered by textiles. Int J Legal Med. 2016;130(5):1257–64. https://doi.org/10.1007/s00414-016-1403-7.
49. Benecke M. A brief history of forensic entomology. Forensic Sci Int. 2001;120(1):2–14. https://doi.org/10.1016/S0379-0738(01)00409-1.
50. Gennard DE. Forensic entomology: an introduction. Chichester, England: Wiley; 2012.
51. Anderson GS. The use of insects in death investigations: an analysis of cases in British Columbia over a five year period. Canadian Soc Forensic Sci J. 1995;28(4):277–92. https://doi.org/10.1080/00085030.1995.10757488.
52. Greenberg B. Flies as forensic indicators. J Med Entomol. 1991;28(5):565–77. https://doi.org/10.1093/jmedent/28.5.565.
53. Sukontason KL, et al. Morphological observation of puparia of Chrysomya nigripes (Diptera: Calliphoridae) from human corpse. Forensic Sci Int. 2006;161(1):15–9. https://doi.org/10.1016/j.forsciint.2005.10.013.
54. Sert O, Ergil C. An examination of the intrapuparial development of Chrysomya albiceps (Wiedemann, 1819) (Calliphoridae: Diptera) at three different temperatures. Forensic Sci Med Pathol. 2021;17(4):585–95. https://doi.org/10.1007/s12024-021-00411-y.
55. Richards CS, Simonsen TJ, Abel RL, Hall MJR, Schwyn DA, Wicklein M. Virtual forensic entomology: improving estimates of minimum post-mortem interval with 3D micro-computed tomography. Forensic Sci Int. 2012;220(1):251–64. https://doi.org/10.1016/j.forsciint.2012.03.012.

56. Martín-Vega D, Simonsen TJ, Hall MJR. Looking into the puparium: Micro-CT visualization of the internal morphological changes during metamorphosis of the blow fly, Calliphora vicina, with the first quantitative analysis of organ development in cyclorrhaphous dipterans. J Morphol. 2017;278(5):629–51. https://doi.org/10.1002/jmor.20660.
57. Chyb S, Gompel N. Atlas of drosophila morphology : wild-type and classical mutants. Amsterdam: Academic Press; 2013.
58. Thomas DB, Hallman GJ. Developmental Arrest in Mexican Fruit Fly (Diptera: Tephritidae) Irradiated in Grapefruit. Ann Entomol Soc Am. 2011;104(6):1367–72. https://doi.org/10.1603/AN11035.
59. Metscher BD. MicroCT for comparative morphology: simple staining methods allow high-contrast 3D imaging of diverse non-mineralized animal tissues. BMC Physiol. 2009;9:11. https://doi.org/10.1186/1472-6793-9-11.
60. Kang V, Johnston R, van de Kamp T, Faragó T, Federle W. Morphology of powerful suction organs from blephariceridid larvae living in raging torrents. BMC Zoology. 2019;4(1):10. https://doi.org/10.1186/s40850-019-0049-6.
61. Swart P, Wicklein M, Sykes D, Ahmed F, Krapp HG. A quantitative comparison of micro-CT preparations in Dipteran flies. Sci Rep. 2016;6(1):39380. https://doi.org/10.1038/srep39380.
62. Pauwels E, van Loo D, Cornillie P, Brabant L, van Hoorebeke L. An exploratory study of contrast agents for soft tissue visualization by means of high resolution X-ray computed tomography imaging. J Microsc. 2013;250(1):21–31. https://doi.org/10.1111/jmi.12013.

Chapter 4
The Role of Fractography in Forensic Pathology and Anthropology Examinations

Ruth Machin and Angi M. Christensen

Introduction

The analysis of skeletal trauma is an important aspect of forensic death investigation. Often, skeletal fracture patterns and features are examined by pathologists or anthropologists to assess trauma type (for example, projectile, blunt, or sharp) as well as to understand other aspects of the trauma event (for example, timing, magnitude, and direction of force). These assessments have traditionally emphasized categorizing fractures into discreet types using features such as fragment shape and intersection of fracture margins. For example, the orientation of wedge-shaped fractures resulting from impact and bending forces in bone (such as when a pedestrian's leg is struck by a vehicle) have commonly been used to interpret the direction of force (see, for example, Cohen et al. [1], Holzhausen [2], Martens et al. [3], Messerer [4], Reber and Simmons [5], Tersinski and Madro [6]). It has been shown, however, that reliance on these fracture typologies can lead to erroneous or ambiguous conclusions [5, 7].

A better understanding of the bone failure event can be achieved by looking not only at these fracture types and fragment morphology, but by trying to understand the initial point of failure and its mechanical cause. In recent years, there has been a shift in skeletal trauma analysis from typological approaches to interpretation of

Disclaimer: This is publication number 22.16 of the Laboratory Division of the Federal Bureau of Investigation (FBI). Names of commercial manufacturers are provided for information only and inclusion does not imply endorsement by the FBI or the U.S. Government. The views expressed are those of the authors and do not necessarily reflect the official policy or position of the FBI or the U.S. Government.

R. Machin (✉)
Infirmary Square, University Hospitals of Leicester, Leicester L1 5WW, UK
e-mail: ruth.machin@uhl-tr.nhs.uk

A. M. Christensen
FBI Laboratory, Quantico, VA, USA
e-mail: amchristensen@fbi.gov

G. N. Rutty (ed.), *Essentials of Autopsy Practice*,
https://doi.org/10.1007/978-3-031-11541-7_4

the failure event based on bone's mechanical properties and its response to force and different loading regimes. One such example is the introduction of bone fractography in skeletal trauma analysis.

Fractography refers to the study of cracks and fractures in a material in order to understand the cause of failure. Fractography is often applied in the failure of engineering structures and products to help ensure future reliability and safety [8]. It is also widely used in forensic contexts to study failure in materials such as glass and ceramics (see, for example, Quinn [9]) as well as plastic and metals. The analysis of cracks and fractures in bone can reveal information about how, why, and where a failure occurred and a crack travelled.

The application of bone fractography in forensic investigations is relatively new. It is therefore not yet widely known or understood in the forensic pathology or forensic anthropology communities, nor regularly taught as part of academic or training programs. Although there are many aspects to fractography, here we emphasize the assessment of fracture surface features. We review some of the recent pertinent work in this area and discuss how bone fractography can be applied in forensic contexts using both visual assessments as well as computed tomography (CT) imaging.

Bone Fractography

One important aspect of bone fractography is the examination of fracture surface morphology, which will be the focus of this chapter. The fracture surface refers to the surface created by the separation of two portions of a material as a result of a propagating crack front. In theory, for simple fractures, the two fracture surfaces will be complements such that a ridge on one surface will correspond to a valley on the other. In practice, skeletal fractures are often complex, fragment may be missing, or surfaces may be contaminated or damaged in such a way that makes a thorough fractographic analysis challenging. However, a useful feature of fractography is that each fracture surface (even for small fragments) may have features that reveal information about the fracture event.

Fracture surfaces express features that reflect the mechanical properties of a material, as well as the speed and stability of the propagating crack front. These features can be used to determine the origin and direction of propagation of the fracture, identify the cause of the failure, and estimate stress levels at failure [8, 10]. The greater the stress in the fracture, the more stored energy, and the more prominent the fracture markings [9]. Glass tends to show fracture surface features very well due to its very fine microstructure. It therefore makes a useful introductory example. Three features in particular are well documented and usually very easy to identify: mirror, mist, and hackle (Fig. 4.1).

In brittle materials, fractures begin as a single origin point, propagating at first relatively slowly. The propagating crack front expands and accelerates outwards. This increasing speed is responsible for the changing pattern of the markings on

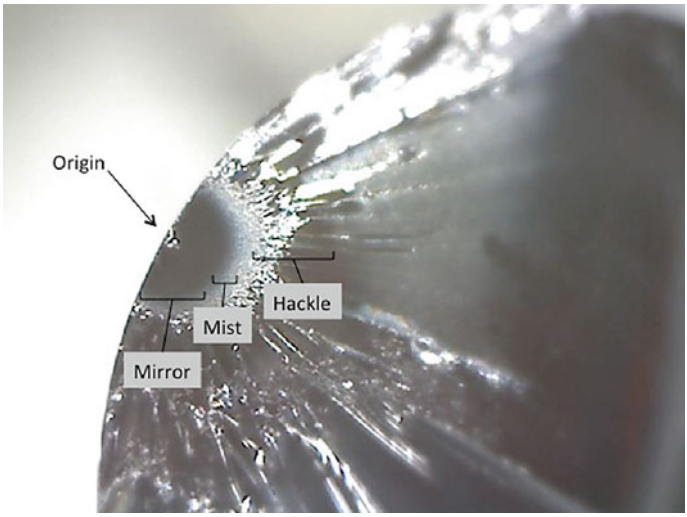

Fig. 4.1 Mirror, mist, and hackle shown on the fracture surface of a 5 mm glass rod; the fracture origin is indicated with an arrow (reprinted from Christensen AM, Hefner JT, Smith MA, Blakely Web J, Bottrell MC, Fenton TW. Forensic fractography of bone: a new approach to skeletal trauma analysis. Forensic Anthropol. 2018;1:32–51)

the fracture surface. Near the fracture origin, planar crack growth is associated with a relatively smooth fracture surface. As the crack accelerates away from the origin, microsteps and deviations begin to develop. These become rougher and more pronounced as the crack increases in speed and instability. The relative "roughness" of a fracture surface therefore indicates the direction of crack propagation, with smoother surface being associated with the fracture origin, becoming increasingly featured as the crack accelerates.

Features of bone fracture surfaces have been noted in a number of studies, including difference in the fracture surface appearance between fractured wet and dry bone [12, 13], and differences related to the postmortem interval [14]. Many researchers have also noted changes in fracture surface morphology across individual fracture surfaces, with the side of the fracture surface experiencing tension being noted as smooth or mottled, while compressive sides of bones are more jagged or sharp [13, 15–19]. While not described as such at the time, these observations were a form of bone fractography.

Forensic bone fractography, specifically the observation of fracture surface features and their relationship to fracture propagation and force direction, has been addressed in several recent papers beginning with Christensen et al. [11], and have found the approach to be reliable and easy to apply. The terminology used to refer to fracture surface features is somewhat standard in material science literature, but some variation exists between material types. Christensen et al. [11] developed terminology specific to the assessment of bone, noting that fractographic features in bone

Table 4.1 Fracture surface features commonly observed in bone (based on Christensen et al. [11], modified from Love and Christensen [20] and Christensen et al. [21])

Feature	Description
Bone mirror	A region at the fracture origin in bone that is relatively flat or featureless compared to the rest of the fracture surface due to relatively more stable crack growth
Bone hackle	Angular or rounded hackle on a bone fracture surface produced by increased crack speed and instability
Wake feature	The offset alignment of features on the following side of a large inclusion
Arrest ridges	Pronounced peaks aligned approximately perpendicular to the direction of crack propagation resulting from drastic changes in crack propagation velocity on the compressive side of the fracture
Cantilever curl	A curved lip just before terminal fracture of a body loaded in bending; also called *compression curl*

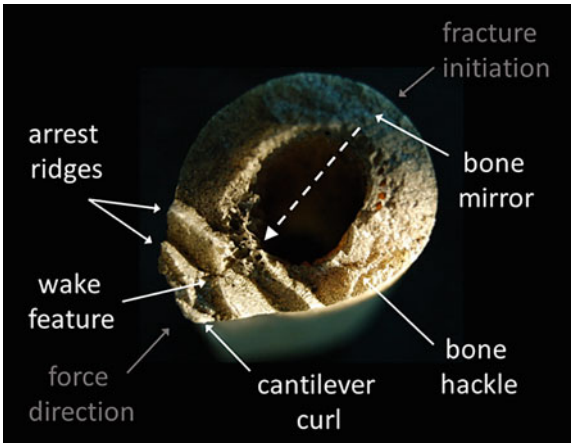

Fig. 4.2 Features of fracture surface morphology for a femur fractured in 3-point bending; solid white arrows indicate bone mirror, bone hackle, arrest ridges, wake feature, and cantilever curl; the dashed white arrow indicates the direction of crack propagation; grey arrows indicate force direction and fracture initiation (reprinted from Christensen AM, Decker SJ. Forensic fractography of bone using CT scans: a case review series. Forensic Anthropol. 2022;5(1):53–6)

appear somewhat differently in both quality and degree of expression than those previously described for other materials (Table 4.1 and Fig. 4.2).

Bone Mirror

Bone mirror is a region that occurs near the fracture origin prior to tilts and deviations from the original fracture plane and is relatively flat in comparison to the rest of

the fracture surface. Bone is a structurally complex material with a relatively large microstructure, so *bone mirror* will never be completely flat and smooth like in glass. It is generally the portion of the bone surface with the fewest features.

Hackle

Hackle is a broad category of fracture surface features, referring to any line on the surface of a fracture running in the local direction of cracking [9, 23], and resulting from increasing crack speed and instability. *Bone hackle* typically appears as rounded or angular ridges aligned in the direction of crack propagation. *Bone hackle* is sometimes sharp or angular and may also be more rounded.

Arrest Ridges

Arrest lines refer to lines on a fracture surface due to arrested or momentarily hesitated crack under an altered stress configuration [9]. *Arrest ridges* in bone result from drastic changes in crack propagation velocity as the crack reaches the compressive side of a bending fracture. They typically appear as pronounced ridges or peaks aligned approximately perpendicular to the direction of crack propagation, and are often very easy to identify.

Wake Hackle and Features

Wake hackle is a discreet line resulting from a split crack front passing an obstacle such as an inclusion or pore. When a crack wave reaches the other side of the obstacle, slight shifts in the angle may occur, with the two fronts of the crack wave ending up slightly out of sync on the following side. *Wake hackle* is aligned in the direction of crack propagation. *Wake features* in bone may be seen in the form of *wake hackle*, which has been noted in association with nutrient foramina or other small holes. *Wake features* may also present as the off-set alignment of larger features such as arrest ridges, which have been observed on the following side of large inclusions such as the medullary cavity.

Cantilever Curl

Cantilever curl forms at the terminus of a fracture of a structure loaded in bending, and presents as a curved lip (the positive portion of which is sometimes called a "breakaway spur" in anthropological literature). In fractured bone, it will be the final

feature in a fracture event. If there was a branching event (such as in the case of a "butterfly wedge") there may be two or more cantilever curls. *Cantilever curl* is typically associated with a load with a strong bending component, and may therefore not only be used to determine the direction of crack propagation, but also to interpret loading conditions.

A number of other fracture surface features have been documented and described for other materials, but are not seen (or are less often seen) in bone, including *Wallner lines* and other forms of *hackle*. These features may become more important and relevant as more is known about forensic bone fractography.

These features of fractured bone surfaces have been shown to be reliable indicators of the location of fracture initiation and therefore the direction of applied force in experimentally fractured bone [11]. Very strong agreement was found between assessors in identifying the point of fracture initiation and direction of crack propagation. It was also found that more experienced fractographers identified more features that those with less experience (even if those less experienced fractographers were highly experienced anthropologists). Visualization of fracture surface features were also noted to be enhanced through the use of aids such as oblique lighting, low-power microscopy, and the application of reversible coatings (such as fingerprint powder) on the fracture surface in order to decrease reflection and increase contrast. Overall, fractography was found to be a reliable, inexpensive, and user-friendly method for assessing fractured bone.

Other recent studies also support the reliability and utility of bone fractography. For example, Love and Christensen [20] retrospectively reviewed a series of blunt trauma cases from an autopsy sample, and found that fractographic features correlated well with autopsy findings (including soft tissue and radiologic findings) as well as with traditional skeletal trauma analyses. Isa et al. [24] studied complex fractures documented through high-speed video, and found that fractography findings were supported by ground truth. Fracture surface morphology was shown by Emerith et al. [25] to be more accurate for determining crack propagation direction than looking at wedge orientation in fractured sheep femora. While most studies have focused on blunt trauma, certain fracture surface features have also been noted in association with projectile trauma [26].

Bone Fractography Using Computed Tomography

In cases where remains are discovered or received skeletonized, the application of bone fractography is rather straightforward, since the bone fracture surfaces can be directly observed. Indeed, many of the previously mentioned studies involved the direct examination of defleshed, dry bone surfaces which were isolated and processed/macerated prior to assessment. In other contexts, such as autopsy cases involving skeletal trauma, remains are typically fresh with significant associated soft tissues. Direct examination of bone surfaces may be impossible or impractical, and assessment may be expedited if the fracture surfaces could be assessed without

maceration. Scheirs et al. [27] found that certain gross morphological features typically associated with perimortem fractures (including, for example, layered breakage, bone scale, flake defect, tension lines, and plastic deformation—some of which are similar to fracture surface featured described in bone fractography) could be identified using CT scans. Several studies and reviews have also specifically investigated the use of CT scanning to assess fracture surface features.

Christensen et al. [11] present several examples of bone fracture surfaces imaged using high-resolution micro-CT scanning. Perhaps unsurprisingly, the resolution of this imaging technology is sufficient to visualize many fracture surface features (Fig. 4.3). However, such instruments are not widely used and cannot be used for whole body imaging.

Christensen and Hatch [28] investigated whether fracture surface features could be observed using traditional medical CT scanners such as those commonly used in postmortem imaging. They reviewed postmortem CT scans performed at a large, high volume, centralized state medical examiner's office which were taken as part of routine forensic examinations. A single case was presented of an individual involved in a motor vehicle accident with a fractured femur. Imaging was performed using a large bore, 16 detector row CT, with thin slide data obtained of the lower extremities using a bone algorithm. The fracture surface was isolated using proprietary software to create a volume rendering, with surface details accentuated using lighting and shading tools. Fractographic features were found to be readily apparent, though the resolution was notably less than for fracture surfaces examined directly. Specifically, bone mirror, arrest ridges, and cantilever curl were all observed, and crack propagation direction could be easily determined (Fig. 4.4).

Christensen and Decker [22, 29] present a review of several clinical CT scans taken of patients with traumatic lower extremity injuries. Scans were performed with a 64-slice CT scanner using a standard trauma scan protocol. Scans had a

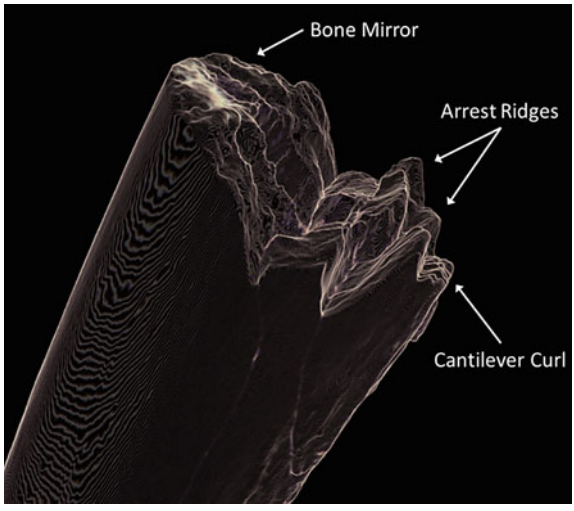

Fig. 4.3 High-resolution micro-CT scan of fractured femur surface; bone mirror, arrest ridges, and cantilever curl are all apparent (reprinted from Christensen AM, Decker SJ. Forensic fractography of bone using CT scans: a case review series. Forensic Anthropol. 2022;5(1):53–6)

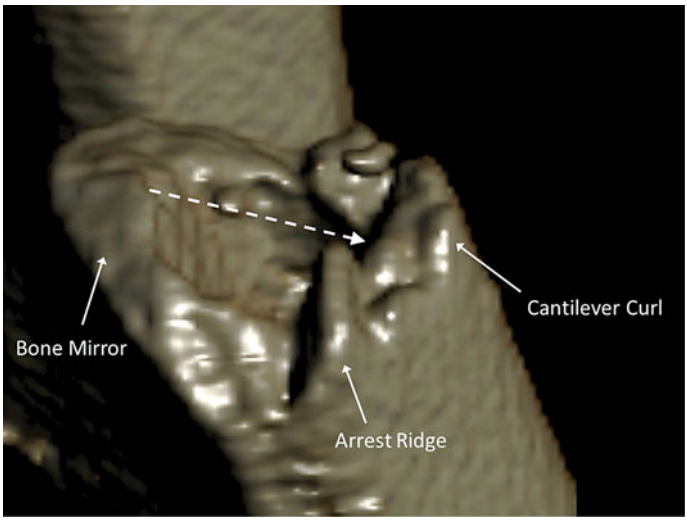

Fig. 4.4 Fracture surface features as seen in a postmortem CT scan; solid arrows indicate bone mirror, arrest ridge, and cantilever curl; dashed white arrow indicates direction of crack propagation (reprinted from Christensen AM, Hatch GM. Forensic fractography of bone using CT scans. J Forensic Radiol Imaging. 2019;18:37–9 with permission from Elsevier)

KVP of 120, mA was variable to patient size, all scans had a slice thickness of 1.25 mm and a slice increments of 0.75 mm. Data sets of the lower extremities were acquired using bone and soft tissue algorithms. Fracture surfaces were visualized as 3D computational models (volume and surface) in volume rendering software with a Hounsfield value of $\geq$226HU used to generate the initial surface models. Fragments were hand separated but maintained the same threshold value. The renders were overlain with a bone volume rendering. One case (Fig. 4.5) involved a motorcyclist struck by a car who suffered a fractured femur. Fracture surface features including bone mirror, arrest ridges, and cantilever curl are seen in the surface rendering, and clearly indicate the direction of crack propagation.

Machin [30, 31] examined the agreement between assessment of fracture surface morphology performed using CT scans and direct visual examination of the same bone specimens. Pig femora fractured in 3-point bending with axial loading were macerated and CT scanned. Bones were scanned using a 64-side scanner at 120 kV and 300 mA using 0.5 mm slices reconstructed with an interval of 0.33 mm. Reconstruction was performed using both a sharp "bone" kernel and a soft tissue kernel. CT images were assessed by a radiologist using a medical imaging viewer, and bones were examined directly by an anthropologist using a light and conventional light microscope. Both assessors examined the specimens for the presence of fracture surface features and interpretation of impact side/direction. Assessments were compared between the two groups as well as to ground truth for impact direction. The results showed perfect agreement between assessors and with ground truth for impact direction. There was also strong agreement between the assessors regarding the presence of arrest ridges (Fig. 4.6). There was less agreement between assessors

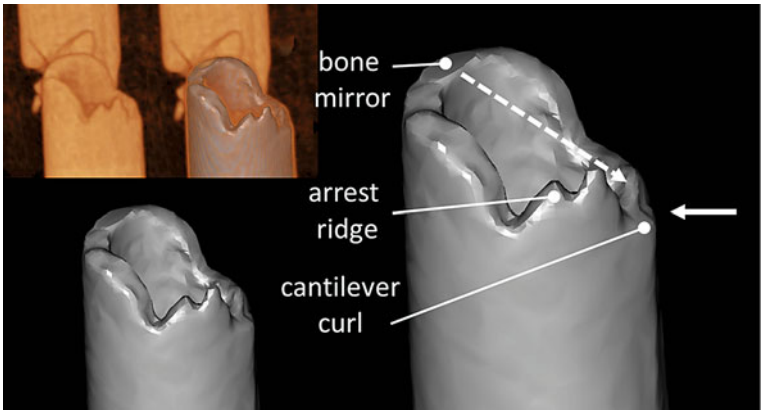

Fig. 4.5 Fracture surface features as seen on a clinical CT scan including volumetric rendering (top left), combined volumetric and surface rendering (top middle), and surface rendering (bottom left); several fracture surface features are apparent (far right); direction of crack propagation is indicated with a dashed arrow and the general direction of impact or loading (not necessarily a specific impact location or angle) is shown with the solid arrow (reprinted from Christensen AM, Decker SJ. Forensic fractography of bone using CT scans: a case review series. Forensic Anthropol. 2022;5(1):53–6)

regarding the presence of bone mirror (Fig. 4.7), bone hackle, wake features, and cantilever curl. Overall the results suggest that crack propagation direction can be reliably interpreted from CT scans although fewer fracture surface features are observed. Computed tomography images in combination with freeware such as Blender (see

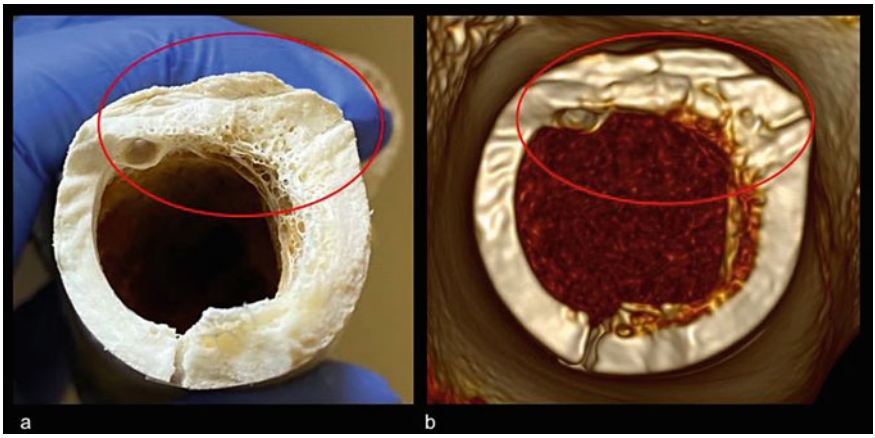

Fig. 4.6 Comparison of arrest ridges (indicated with red circles) between direct examination of the bone surface (left) and in a CT scan (right) (reprinted from Machin R. Can Computed tomography fracgtography determine the direction of fracture propagation? [MS Dissertation], University of Leicester; 2020)

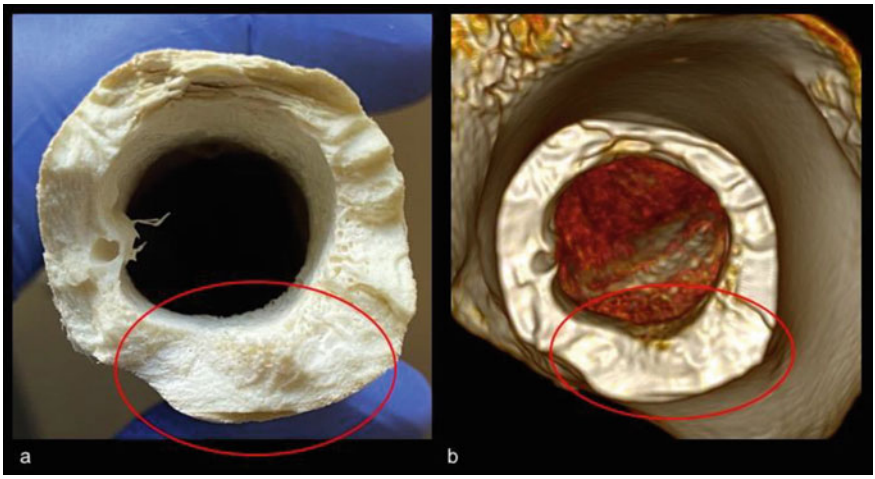

Fig. 4.7 Comparison of bone mirror (indicated with red circles) between direct examination of the bone surface (left) and in a CT scan (right) (reprinted from Machin R. Can Computed tomography fracgtography determine the direction of fracture propagation? (reprinted from Machin R. Can Computed tomography fracgtography determine the direction of fracture propagation? [MS Dissertation], University of Leicester; 2020)

Chap. 1; https://www.blender.org/ last visited March 2022) can also be used to virtually deflesh a fracture site and isolate individual fractured bones for fractographic analysis (Fig. 4.8).

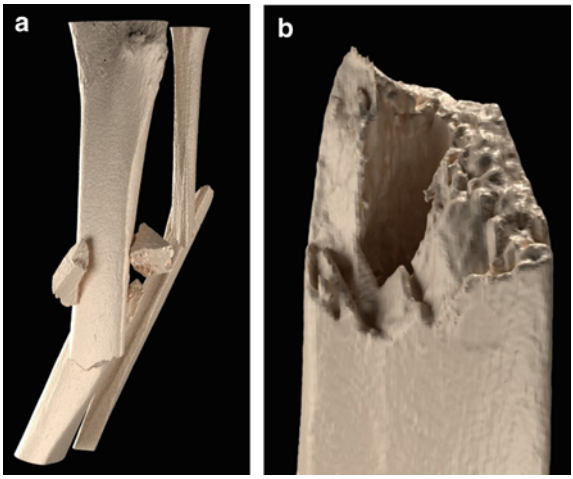

Fig. 4.8 **a** Postmortem computed tomography image of a fractured lower leg sustained in a pedestrian verses car incident using Blender (https://www.blender.org/.last visited March 2022) **b** The fracture through the tibia is then isolated for fractographic analysis

The amount of fracture surface detail is notably less in CT scans than direction observation of the bone (or using micro-CT) due to resolution limitations. However, features that are highly diagnostic of crack propagation direction, such as arrest ridges and cantilever curl, are still readily apparent. Smaller surface features such as hackle may be less likely to be observed due to this reduced resolution, though it is still considered possible. It may also be possible to increase the resolution of the scan in a region of interest if it is known prior to the scan that fractography may be utilized. The reduction in overall surface detail/resolution has also been noted to actually clarify the location of certain features such as bone mirror [28].

Scanner settings can impact the quality of the resulting model [22], which could potentially impact the detail expressed in the fracture surface. A CT slice thickness of $< / = 1.25$ allows for better visualization of the fractured region in 3D [32]. The selection of 3D modelling software may also affect results [22].

Although there are currently only a few studies that have addressed the use of bone fractography using CT scans, results strongly suggest that even with lesser surface detail available compared to direct examination, fracture surface features can be seen, and crack propagation direction can be reliably interpreted. This is significant because it not only potentially eliminates the need to macerate remains in order to apply fractography, but it also means that fractography may be applicable to a broader range of context than dry bones. Fractography may also have applications in clinical contexts, or forensic investigations involving the living. For example, fractography could be used to confirm or refute the circumstances of an injury incident such as an accident or abuse [28]. Moreover, CT scanners are now available in most clinical contexts, and increasingly in postmortem examinations, making it a practicable option in many settings.

Fractography in Practice

Forensic bone fractography is still a relatively new field. Few educational or training programs address it directly, and more research is needed to better understand the relationship between fracture surface features and skeletal trauma events. Notably, fewer fracture surface features are typically observed when evaluated by less experienced examiners [11]. Practitioners are therefore strongly encouraged undertake significant practice and study prior to applying fractography in casework.

Researchers have noted that features are less often identified when cortical area is smaller, and comminuted fractures also make feature identification more challenging. Caution should therefore be used in these potentially more challenging cases.

It is typical in anthropological examinations to physically re-fit fractured segments in order to reconstruct original bone dimensions or visualize overall fracture patterns. However, physical reconstruction of fragments for many other materials is discouraged because of the risk of altering or obliterating fine surface details through contact or abrasion. If physical reconstruction is to take place in an examination, it is recommended that fracture surface features be examined and documented first.

Based on what is known from fractography of other brittle materials, it is expected that higher energy events will have more features and be easier to interpret. Low energy fractures such as thermal fractures result in fewer surface features. Very porous or course-grained materials (such as bone) can also mask surface markings. More research is needed to fully understand the applications of fractography to forensic bone fractography.

Summary

Bone fractography has been shown to be an easy and reliable method for assessing skeletal trauma, specifically by observing the presence and orientation of fracture surface features. These features reveal information about the direction of crack propagation, and often correspondingly the direction of the impact or force. The presence of even one or two features, viewed directly on the bone surface or using CT scans, can be sufficient to interpret crack propagation direction.

It is hoped that the information presented here can be used by forensic practitioners to improve skeletal trauma analyses through the use of an additional method to interpret trauma patterns and better understand trauma events.

References

1. Cohen H, Kugel C, May H, Medlej B, Stein D, Slon V, et al. The influence of impact direction and axial loading on the bone fracture pattern. Forensic Sci Int. 2017;277:97–206.
2. Holzhausen G. Rekonstruktion des unfallherganges. In: Gerichtsmedizinische unterschungen bei Verkehrsunfällen. Leipzig; VEB GeorgThieme; 1966.
3. Martens M, Van Audekercke R, De Meester P, Mulier JC. Mechanical behaviour of femoral bones in bending loading. J Biomechanics. 1986;19:443–54.
4. Messerer O. Ueber die gerichtlich-medizinische Bedeutung verschiedener Knochenbruchformen. Friedreichs Bliitter f Gerichfl Med. 1885;36:81–104.
5. Reber SL, Simmons T. Interpreting injury mechanisms of blunt force trauma from butterfly fracture formation. J Forensic Sci. 2015;60:1401–11.
6. Teresinski G, Madro R. Evidential value of injuries useful for reconstruction of the pedestrian vehicle location at the moment of collision. Forensic Sci Int. 2002;128:127–35.
7. Patscheider H. Über Anprallverletzungen der untered Gliedmaßen beiStrassenverkehrsunfallen. Deutsche Zeitschrift für gerichtliche Medizin. 1963;54:336–66.
8. Hull D. Fractography. 1st ed. New York: Cambridge University Press; 1999.
9. Quinn GD. Recommended Practice Guide: Fractography of Ceramics and Glasses, 3rd ed. National Institute of Standards and Technology (NIST) Special Publication 960–16e3; 2007;2016;2020.
10. Bradt RC. The fractography and crack patterns of broken glass. J Failure Analysis Prevent. 2011;11(2):79–96.
11. Christensen AM, Hefner JT, Smith MA, Blakely Web J, Bottrell MC, Fenton TW. Forensic fractography of bone: a new approach to skeletal trauma analysis. Forensic Anthropol. 2018;1:32–51.

12. Johnson E. Current developments in bone technology. Adv Archeol Method Theory. 1985;8:157–235.
13. Symes SA, L'Abbe EN, Chapman EN, Wolff I, Dirkmaat DC. Interpreting traumatic injury to bone in medicolegal investigations. In: Dirkmaat DC, editor. A Companion to Forensic Anthropology. Chichester: John Wiley & Sons Ltd.; 2012. p. 340–89.
14. Hentschel K, Wescott DJ. Differentiating peri-mortem from postmortem blunt force trauma by evaluating fracture tension surface topography using geographic information systems. In: Proceedings of the 67th annual meeting of the American Academy of Forensic Sciences. Orlando, FL;2015.
15. Emanovsky P. Low-velocity impact trauma: an illustrative selection of cases from the Joint POW/MIA Accounting Command- Central Identification Laboratory. In: Passalaqua NV, Rainwater CW, editors. Skeletal trauma analysis: case studies in context. Boca Raton, FL: CRC Press; 2015. p. 156–66.
16. Galloway A, Zephro L. Skeletal trauma analysis of the lower extremity. In: Rich J, Dean DE, Powers RH, editors. Forensic medicine of the lower extremity: human identification and trauma analysis of the thigh, leg and foot. Totowa: Humana Press Inc.; 2005. p. 253–77.
17. Isa MI, Fenton TW, Deland T, Haut RC. Assessing impact direction in 3-point bending of human femora: incomplete butterfly fractures and fracture surfaces. J Forensic Sci. 2018;63(1):38–46.
18. L'Abbé EN, Symes SA, Raymond DE, Ubelaker DH. The Rorschach Butterfly: understanding bone biomechanics prior to using nomenclature in bone trauma interpretations. Forensic Sci Int. 2019;299:187–94.
19. Rainwater CW, Congram D, Symes SA, Passalacqua NV. Fracture surface characteristics for the interpretation of perimortem blunt force fractures in bone. In: Proceedings of the 71st annual meeting of the American Academy of Forensic Sciences. Baltimore, MD;2019.
20. Love JC, Christensen AM. Application of bone fractography to medical examiner sample: a case series. Forensic Anthropol. 2018;4:221–7.
21. Christensen AM, Isa MI, Smith MA, Hefner JT, Berryman HE, Saginor IS, Webb JB. Guide to Forensic Fractography of Bone (1.0). Zenodo. https://doi.org/10.5281/zenodo.6013748; 2022.
22. Christensen AM, Decker SJ. Forensic fractography of bone using CT scans: a case review series. Forensic Anthropol. 2022;5(1):53–6.
23. Fréchette VD. Failure analysis of brittle materials. In: Advances in Ceramics, vol. 28. Westerville, OH: American Ceramic Society; 1990.
24. Isa MI, Fenton TW, Antonelli L, Vaughan PE, Wei F. The application of fractography in trauma analysis of complex long bone fractures. In: Proceedings of the 72nd Annual Meeting of the American Academy of Forensic Sciences. Anaheim, CA; 2020.
25. Emrith TS, Mole CG, Heyns M. Interpreting impact direction: applying fractography to the analysis of butterfly fractures produced by blunt force trauma. Australian J Forensic Sci. 2020. https://doi.org/10.1080/00450618.2020.1781252.
26. Lillard K, Christensen AM. Fractography of long bones with high velocity projectile trauma. Forensic Anthropol. 2020;3(3):135–8.
27. Scheirs S, Cos M, McGlynn H, Ortega-Sanchez M, Malgosa A, Galtes I. Visualization and documentation of peri-mortem traits in long bone fractures using computed tomography. Forensic Sci Med Pathol. 2020;16:281–6.
28. Christensen AM, Hatch GM. Forensic fractography of bone using CT scans. J Forensic Radiol Imaging. 2019;18:37–9.
29. Christensen AM, Decker SJ. Forensic fractography of bone using CT scans. In: Proceedings of the 72nd Annual Meeting of the American Academy of Forensic Sciences. Anaheim, CA;2020.
30. Machin R. Can Computed tomography fracgtography determine the direction of fracture propagation? [MS Dissertation], University of Leicester;2020.
31. Machin R, Brough A, Morgan BM, Biggs M. Imaging impact: can computer tomography fractography determine direction of fracture propagation. In: Proceedings of the 73rd annual meeting of the American Academy of Forensic Sciences. 2021.
32. Ford JM, Decker SJ. Computed tomography slice thickness and its effects on three-dimensional reconstruction of anatomical structures. J Forensic Radiol Imaging. 2016;4:43–6.

Chapter 5
The Application of Radiographic Imaging in Forensic Odontology

Melanie Elizabeth Clarkson and Philip Haley Marsden

Introduction

Forensic odontology is the collection, analysis and reporting of dental evidence in the interest of the law and has long been recognised as a primary method of identification of deceased human remains, along with DNA and ridgeology (fingerprints) [1].

Radiographic imagery has always been a key feature in the application of forensic dental identification, especially in mass disaster scenarios. The saying, 'a picture is worth a thousand words' was framed by Henrik Ibsen in the 1900s and this applies particularly to a forensic dental identification report when read by parties such as the police, HM Coroner and even the deceased's family. The comparison of two-dimensional radiographic images Ante Mortem (AM) and Post Mortem (PM) have become part of the routine dental identification process, alongside evidence from AM and PM chartings. The radiographic images can give a distinctive pictorial understanding of the corresponding dental features which form the basis for a positive identification. Radiographs often can make the difference between a positive or established identification (as this is based on imagery) and a possible identification (based on the charting).

The use of PM computed tomography (PMCT) in forensic investigations and non-suspicious deaths investigated at the request of HM Coroner has increased [2]. As a result of these developments, forensic dental identification is now beginning to evolve to include the use of computed tomography (CT) scanning and its reconstructions to establish a positive human identification.

M. E. Clarkson (✉)
Headquarters Defence Medical Services, Coltman House, DMS Whittington, Lichfield, Staffordshire WS14 9PY, United Kingdom
e-mail: meclarkson@btinternet.com

P. H. Marsden
114 Cavendish Road, London SW12 0DF, United Kingdom

G. N. Rutty (ed.), *Essentials of Autopsy Practice*,
https://doi.org/10.1007/978-3-031-11541-7_5

This chapter will discuss the use of various conventional 2D radiographic techniques and their application in forensic odontology, along with the analysis and adaptation of PM medical CT scans to compare with AM clinical dental evidence. It will also describe how innovative three-dimensional comparative techniques can establish an individual's positive dental identification. These more contemporary CT techniques are paving the way forward to a new era of forensic odontology, where there is less reliance on invasive techniques to access the teeth and jaws. Where possible, with these novel imagery identification techniques, an intact body can be preserved, which helps to maximise the level of dignity and respect offered to an individual in death.

Part 1: An Introduction to Conventional Radiography Techniques and their Application in Forensic Dental Identification

No matter how detailed the description of a filling in the written dental records, no words could describe the unique outline of the floor of a cavity dictated by the extent of caries before the filling was applied. This is even more evident with root canal fillings, posts, amalgam pins and dental implants [3]. This is when radiographic imaging is extremely useful.

There are specific, commonly used, radiographic views taken of a patient in clinical practice (AM record), which can be replicated in the mortuary/hospital environment (PM record). INTERPOL recommend completing a full set of imaging including bitewings, periapicals of all teeth and particularly of any areas of interest (e.g. root fillings or crowns) [4]. Occlusals and lateral oblique mandibles can be completed as required. Every dental practice has access to intra-oral X-ray unit equipment. In practice, a small dental radiographic film or digital receptor is placed into the mouth and exposed to X-rays to produce imaging of the teeth, jaw and surrounding soft tissues. Hospital radiography departments more commonly provide access to extra-oral X-ray equipment such as panoramic radiographs which are positioned outside of the mouth and often surround the head and facial structures.

Many private or specialist dental practices, especially those offering orthodontic treatment or dental implant surgery will also have facilities for extra-oral imaging techniques, similar to within a larger hospital environment and this equipment may also include cone beam CT (CBCT) [5] which will be discussed later on in this chapter.

No matter what type of radiographic image is produced the image quality should be of the highest standard and evaluated and graded in accordance with the College of General Dentistry UK (CGDentUK) guidelines [6]. The production of such an image may be challenging in the deceased when rigor can hinder the mouth being opened. In the past, the tissues surrounding the jaws may have been cut to enable access to be gained; however, this practice may now be unnecessary. PMCT has the

advantage over radiographic imaging in these circumstances and its benefits can be exploited to obtain the required dental imaging, without the mouth being physically accessed.

It is essential for anyone undertaking radiography that they are fully trained in the various imaging techniques. In the field of forensic odontology, most odontologists are registered dental practitioners, working in the general dental practice environment, where taking radiographs is standard practice. In clinical practice, paralleling techniques are now more common than bisecting angle techniques [7], however depending on the view AM it may be necessary to try to replicate the image PM and hence experience and adaptation of all planar radiography techniques are required by the operator.

When completing any radiographic imaging, some key principles must be considered, and radiation protection rules must be adhered to as per Ionising Radiation Regulations 1999 (IRR 99) [8] and Ionising Radiation (Medical Exposure) Regulations 2017 (IR(ME)R17) [9]. In PM imaging, and particularly in temporary mortuaries, the protection of staff is the main consideration and the use of a controlled area to protect staff from direct exposure to the path of the X-ray beam is applied. Clinical principles of infection prevention must be followed. In addition, the following radiographic principles should be considered

- Radiographic film and image receptors should be covered when completing intraoral radiographs. Barrier envelopes can be purchased for this purpose and are usually part of the odontologist's consumable kit.
- Intraoral films/receptors should be placed carefully to avoid damaging the deceased.
- Intraoral films/receptors should not be bent in the mouth as this will distort the image and the cable attached to the sensor should be out of the field of view. Using film/receptor holders and teamwork when positioning will help with this.
- Paralleling technique should be used unless AM radiographs are available and need to be replicated.
- If using film (rarely done these days), consideration must be given to how they will be processed and mounted, as well as the safe use and storage of the photo chemicals.
- Clinically, patients can be asked to bite on the film holder to keep it in place. Those completing the PM imaging need to be creative to achieve the same results e.g. the use of sandbags or elastic bands to close the upper and lower jaws together (Fig. 5.1).

Fig 5.1 A periapical radiograph being taken in the mortuary, using a hand-held X-ray unit on tripod (black and arrowed) and the use of shield-wrapped sandbag and elastic bands to close the upper and lower jaws

Bitewing Radiographs

These are the most commonly used dental intra-oral radiographs in practice and are an individual film designed to capture images of the clinical crowns of the molars, premolars and occasionally canine teeth on one side of both of the jaws. The bitewing image is the most relevant one for the diagnosis of dental caries and serial bitewings can be used to monitor the progression of dental caries, to assess existing restorations and review the stability of the surrounding alveolar bone and periodontal tissues. It is recommended that any new patients registering with a practice have bitewings taken as a baseline view of a patient's dentition, so that any new or existing disease can be fully diagnosed, monitored and/or treated [10]. Depending on the level of caries risk, these bitewing radiographic views are repeated at 6 monthly, 12 monthly or two-yearly intervals, as a regular check on dental health [11]. This guideline has relevance when collecting AM radiographic evidence from a dental practice. Figure 5.2 shows a classic set of bitewing radiographs taken on a patient and some common features are labelled.

The radiograph should include the upper and lower premolars and molars on each side of the mouth and include all teeth from the distal surface of the canine to the distal surface of the second molar or mesial surface of the third molar, if present. In some cases, with digital radiography, if the digital sensor does not incorporate all premolars and molars in a single image, two bitewing images on each side of the mouth may be necessary to capture all surfaces of the premolar and molar teeth.

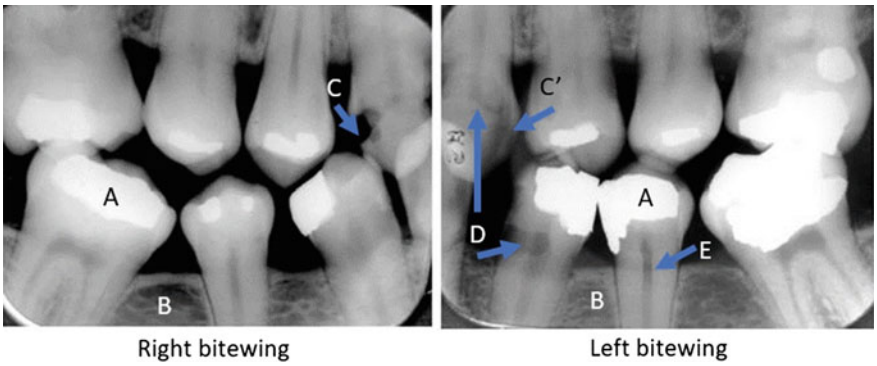

Fig 5.2 Examples of right and left horizontal adult bitewing radiographs (BWs). **A** represents Amalgam fillings (silver-mercury alloy/metallic filling material), **B** represents Bone, **C** represents a prepared cavity on the right BW. (This can be shown by the crisp margins, the definite rounded cavity base and the overlap of enamel gingivally). On the left BW, C' in the left BW represents dental caries or decay. **D** represents clearly prepared class V cavities [12] on the smooth surfaces of the tooth root and E represents the tooth pulp

The bitewing radiograph is extremely useful [13] for identification purposes, as it is not only the most regularly and routinely taken radiographic image (thus images for comparison are often available) but also because each bitewing radiograph will contain information about several teeth and their restorations. They are also routinely performed in pairs to capture dental information on both the left and right sides of the dentition, hence providing the forensic odontologist with potential evidence regarding between 16-24 teeth on two separate images. When taking the radiograph (Fig. 5.3).

Fig 5.3 Positioning of a patient for a bitewing radiograph

a. For ease of image replication, film holding beam-aiming devices are used, compatible with the receptor.
b. Image receptor/film positioned with its long axis horizontally and its short axis vertically within the mouth.
c. The long axes of posterior teeth and the image receptor should be parallel.
d. The central ray is perpendicular to the teeth and image receptor and angled downwards (caudad) approximately 5-8° and parallel to the beam-aiming device of the image receptor.

Figure 5.4 shows comparison of AM and PM bitewing radiographs, as part of a forensic dental identification. Note the similarities in shape and size of the metallic (amalgam) restorations in the teeth.

Similarly, Fig. 5.5 shows an additional example of left bitewing AM and PM comparison for identification purposes.

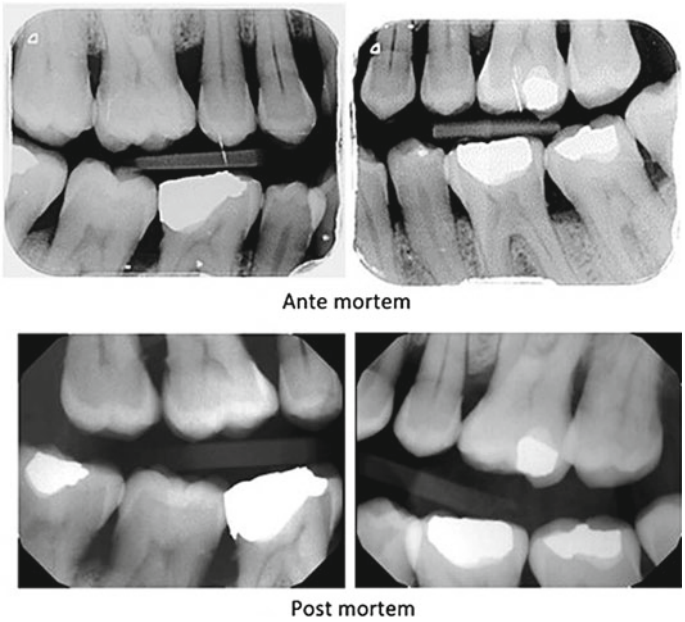

Fig 5.4 PM bitewing radiographs taken March 2021 (lower set of images) compared to AM bitewing radiographs taken 3 years earlier in Oct 2018 (upper set of images). Note the shape of the distinctive amalgam (metallic) restorations in multiple teeth. The PM radiographs are digital images and the ante mortem images are wet films, which accounts for the slight difference in appearance and size

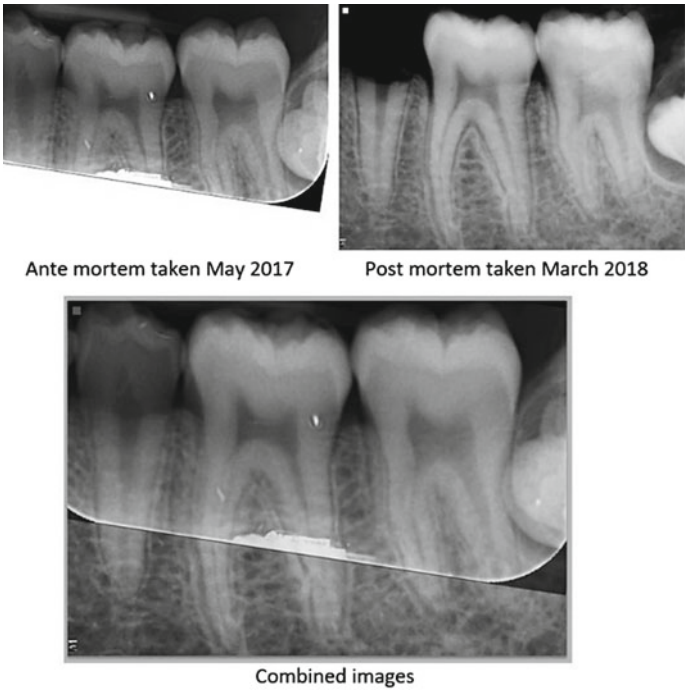

Fig 5.5 A further AM and PM Bitewing comparison and the lower image shows AM and PM superimposed onto one another, which shows corresponding root shape and form followed and the slight further movement upwards of the lower left 8 [14] as it slowly starts to move through the alveolar bone during eruption (Images courtesy of Dr P H Marsden—odontology casework)

Periapical Radiographs

Periapical radiographs are an intra-oral technique designed to provide detailed imagery of 2-4 teeth and the surrounding alveolar bone and periodontal tissues. The film/receptor are placed inside the mouth parallel to the long axis of the teeth and x-ray tube. Figure 5.6 shows positioning for a lower right periapical radiograph.

The quality of periapical radiographs can vary and is dependent on the skill of those taking the images. This is made more difficult when imaging the deceased and those taking the radiographs need to be able to adapt techniques to achieve the imaging. Positioning the plate, and keeping it in place, can be challenging and result in images not routinely seen in clinical dental radiography (an example is shown in Fig. 5.7 with the PM image (b) rotated compared to the AM image (a)).

Fig 5.6 Positioning of a patient for a lower right periapical radiograph

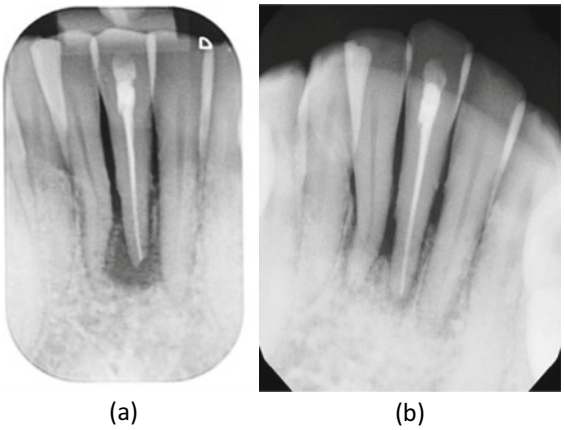

Fig 5.7 **a** A root filled lower incisor LL1 (31) and the LR1 (41) with a distinct distal curvature of the apical 1/3 of root (root tip) shown AM. **b** A similar shaped root-filling in the 31 and a corresponding distal curvature in 41 PM

Figure 5.8 shows how it is not just the teeth in a periapical that can provide evidentiary value in a radiographic comparison, but the trabecular bone patterns as well. Periapical images can be essential when teeth are missing (as shown in Fig. 5.8), as they can look at the surrounding tooth anatomy, in this case the trabecular bone pattern. The corresponding patterns were able to establish a positive identification in this disaster victim identification case.

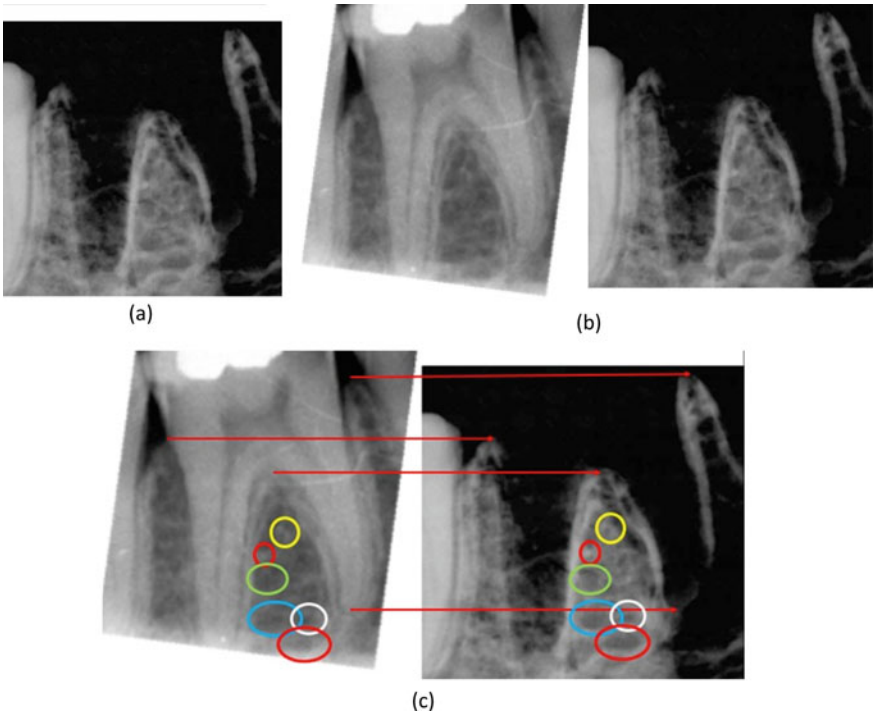

Fig 5.8 **a** PM periapical radiograph of lower right first molar socket. **b** AM image on the left of lower right 6 (first molar) with tooth in situ and its socket PM on the right. (**c**) Shows corresponding radiopaque and radiolucent spongy pattern of trabecular bone AM and PM compared. Each coloured circle corresponds to the concordant trabecular feature AM and PM (Images courtesy of Dr P H Marsden—odontology casework)

Occlusal Radiography

Occlusal Radiography is where the image receptor is placed in the occlusal or horizontal plane. The most common of these types of radiographs is the upper anterior occlusal, but lower occlusals and upper oblique occlusals are alternatives of this radiographic view. These images routinely show sections of the maxilla or mandible, with related teeth. They are indicated in orthodontics, particularly to locate the position of unerupted or ectopic (displaced) canines and supernumerary (extra) teeth. Figure 5.9 shows how the x-ray tubehead is positioned for an upper occlusal radiograph. Figure 5.10 provides an example of the type of image produced as a result of taking this type of radiograph.

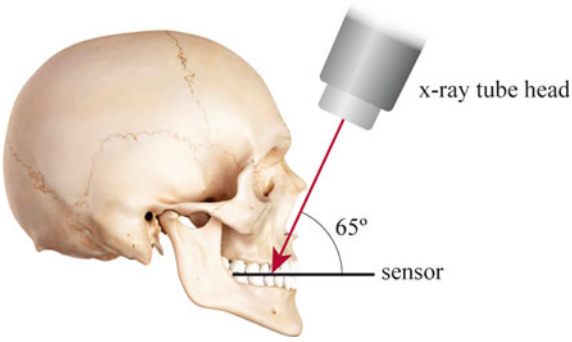

Fig 5.9 An image of an upper occlusal radiograph being taken (ideally the tube head needs to be positioned at 65° to the horizontal plane of the upper dentition). Illustration courtesy of Vicky Eves, UK

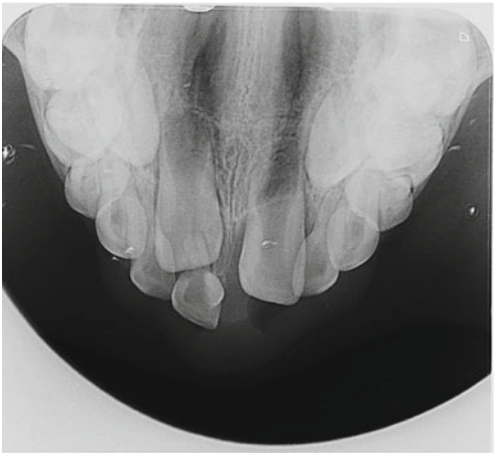

Fig 5.10 A typical upper anterior occlusal and the eruption of the two permanent upper anterior incisors, whilst the upper right baby incisor remains in situ and has not yet exfoliated (fallen out). The deciduous (baby teeth) can be seen in situ, with their permanent successors developing in the maxilla (upper jaw)

Lateral Oblique Radiography

Oblique lateral radiographs are extraoral views of the jaws that can be taken using dental radiographic equipment, whether that is in an x-ray room or department, or using a mobile x-ray unit. Before the development of panoramic equipment, these were the routine extraoral radiographs used both in hospitals and in general practice. In recent years, their popularity has reduced, but can still be used in forensic identification, especially PM, as hospitals will have equipment to produce them (if the odontologist does not have their own hand-held, portable radiography unit). Depending on the condition of the PM dental remains, it may be easier to take an extraoral image, without disruption to the head and facial structures, as they may be extremely fragile, in fire for example.

Lateral radiographs of the head and jaws are divided into:

- True laterals (Positioning for this type of radiograph shown in Fig. 5.11a).

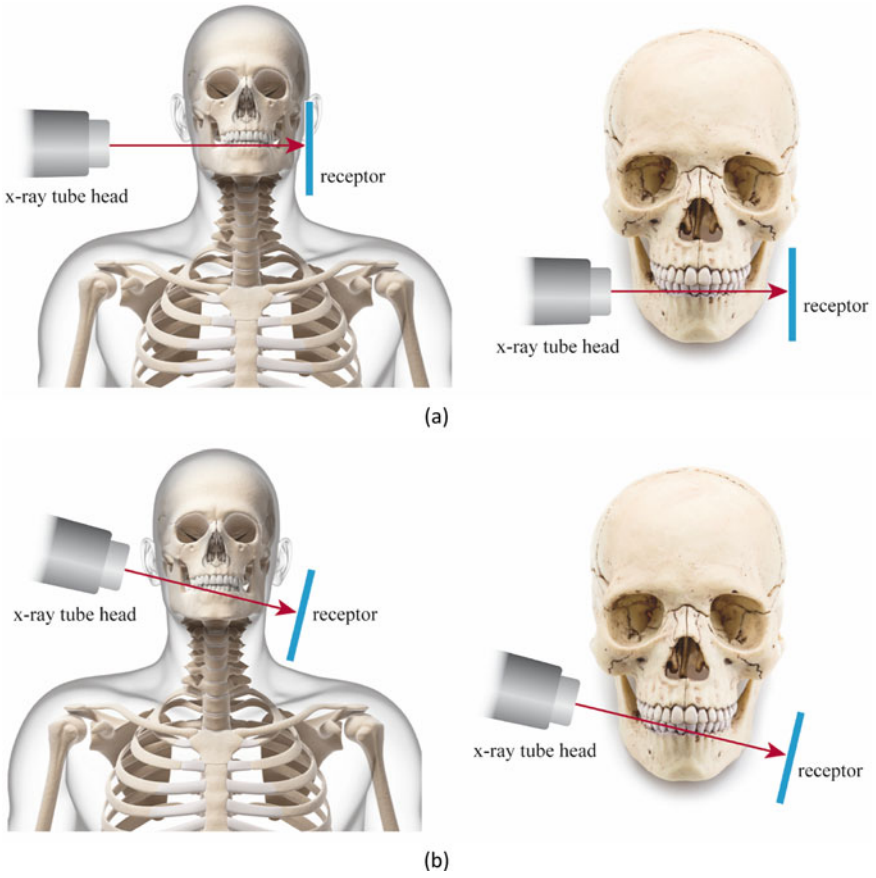

Fig 5.11 **a** Positioning for a true lateral radiograph. **b** The positioning of an oblique lateral. The images illustrate what is meant by the terms *true* and *oblique* lateral. Illustrations courtesy of Vicky Eves, UK

- Oblique laterals (the term bimolar was used historically to describe the image incorporating left and right oblique laterals on the same film taken as separate exposures). Figure 5.11b demonstrates positioning for this type of radiograph.

The adjectives true and oblique are used to indicate the relationship of the image receptor, patient and path of the X-ray to one another

The main reasons why these types of images may be taken (AM) include assessment of the presence and/or position of unerupted teeth; detection of fractures of the mandible; evaluation of lesions or conditions affecting the jaws including cysts, tumours, giant cell lesions, and other bone lesions; for specific views of the salivary glands or for temporomandibular joint assessment. They may also be used as an alternative when intraoral views are unobtainable because of a strong gag reflex, or if the patient is unable to open the mouth or is undergoing general anaesthesia.

In one forensic odontology case, lateral obliques were taken PM in the hospital radiography department, as the odontologist did not have his own hand-held radiography equipment. These images were compared against the AM radiographic images (bitewings in this case). Although not ideal, as the lateral obliques did not provide a reproducible view PM of the individual's dentition AM, due to the significant dentistry in the individual's dentition, a positive identification was still able to be established (Fig. 5.12).

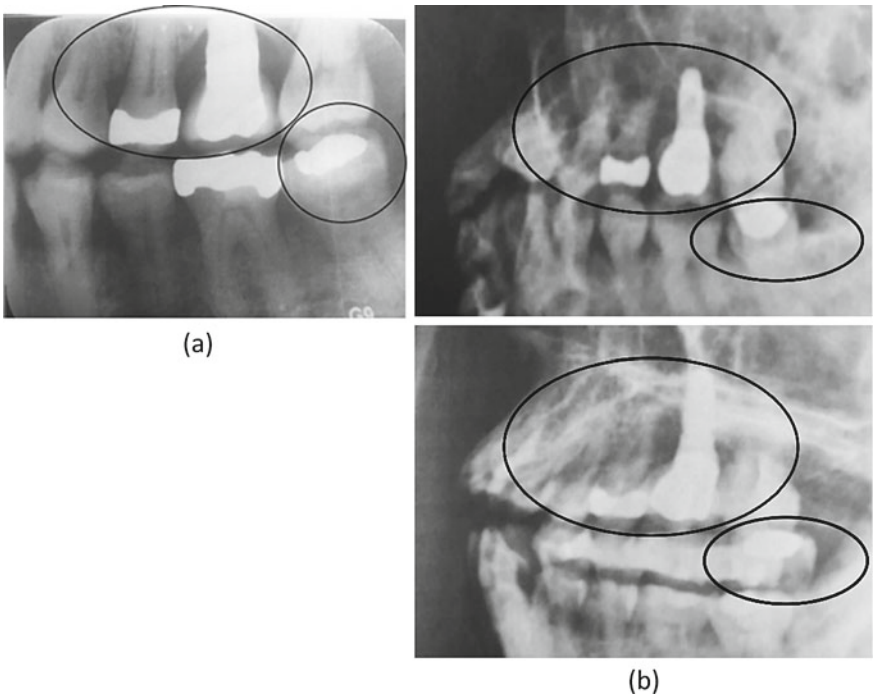

Fig 5.12 **a** A comparison of an AM left bitewing with **b** 2 x PM lateral oblique images. Although it is quite difficult to chart the full lower dentition in any detail from the PM radiographic views, particular features do stand out. The implant in the upper left 6, with its associated angular bone loss and the mesio-occluso-distal amalgam restoration in the upper left 5 have very distinctive shapes, PM and AM. The figure also shows the distinctively shaped occlusal amalgam restoration in the lower left 7 and the cavity outline in the LL6 PM is a concordant shape, covering the same surfaces as the lower left 6 amalgam restoration AM

Dental Panoramic Tomograph (DPT)

Tomography is a specialised, extra-oral 2D radiographic technique that produces radiographs of a section patient slice. Each individual tomographic image (or slice) shows the tissues within that section sharply defined and in focus. The surrounding tissues and structures are blurred and out of focus, created by the x-ray tube and film/receptor moving while taking the x-ray. To be viewed clearly, the area of interest must be positioned in the correct location, known as the focal plane or focal trough.

By varying the size of the X-ray beam and the type of equipment used, the shape of the tomographic layer can be altered from a straight or linear slice to a curved one. A curved slice is beneficial as it follows the curve of a dental arch, providing an overall panoramic view of all the teeth and their supporting structures –what we refer to in dentistry as the dental panoramic tomograph or DPT (previously referred to as an orthopantomograph or OPG (named after the machine that produced it).

Panoramic tomography is a commonly used examination in clinical dentistry and is an important diagnostic tool. It covers a wider area than a conventional intra-oral radiograph and, as a result, provides valuable information about the maxillary sinuses, presence and condition of the teeth and bone abnormalities. It is also used to treatment plan for full and partial dentures, orthodontics, extractions, implants and orthognathic surgery. Figure 5.13 shows an example of a patient positioned in a DPT machine and Fig. 5.14 shows an example of the image produced.

Fig 5.13 The positioning of the patient when taking a DPT (or CBCT scan)

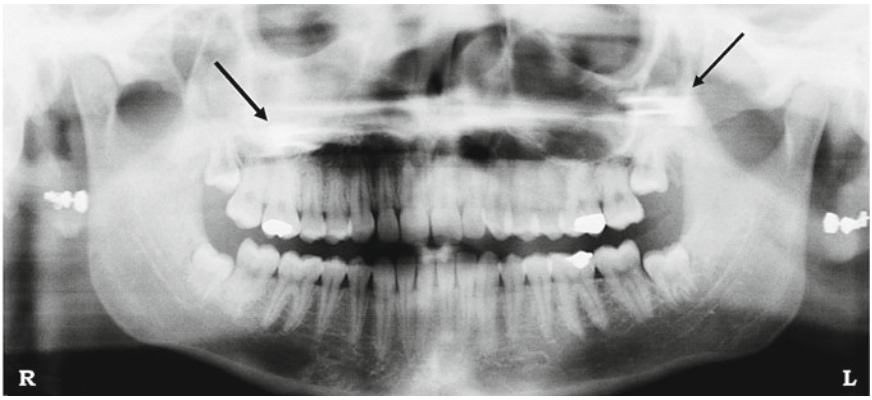

Fig 5.14 A DPT of a patient. *Note* best practise is to ensure patients have removed all jewellery prior to having the DPT taken. In this case the patient left their earrings in when the radiograph was taken which can create ghost shadows (arrowed)

A panoramic radiograph can also reveal dental and medical problems such as:

- Advanced periodontal disease.
- Bone cysts.
- Tumours and oral cancer.
- Unerupted and/or impacted teeth including wisdom teeth.
- Temporomandibular joint or disorders [5].

Ante-mortem panoramic radiographs are an immensely useful tool for the forensic odontologist as a single image will often cover the full dentition providing identifiable details on all teeth, bone structure, sinuses etc [5]. Even small post-mortem fragments may show points of concordance to the detail on such radiographs which can be invaluable in a mass disaster. However, it is worth bearing in mind that due to the equipment and most DPT machines requiring the patient to be erect, DPTs are not used in DVI (as Post Mortem, the patients will be supine and therefore not in a suitable position for radiographic exposure).

It is these 2-D radiographs, particularly that can provide the most favourable comparisons with PMCT scans. A scan of the jaw can be reconstructed to appear like a DPT. The AM and PM images can be compared, often producing several prominent dental characteristics which can be married up to establish a positive dental identification. This can be seen later on in the chapter.

Part 2: An Introduction to Post Mortem CT Scanning (PMCT) and Its Application in Forensic Dental Identification

CT Scanning

In the past 20 years, the use of PMCT in forensic death investigations has increased [15, 16] and its potential for disaster victim identification was tested both in actual and simulated mass disaster scenarios [17–19]. Today, PMCT has an established role in disaster victim identification (DVI) [20].

With an increase in Cone Beam CT (CBCT) scanning in dentistry additionally AM, due to the abundance of implant provision in the private sector, CBCT could also be used to compare AM 3D imagery of teeth with PMCT of teeth in a similar way that conventional radiography can be compared currently.

There are several advantages of using CT scanning in DVI. The image acquisition is much quicker (5 minutes for a CT scan and 60 minutes or more in difficult cases for a full dental series). The deceased does not have to be removed from the bag for CT, but the head does for radiography, hence CT reduces the infection risk. Also, not viewing the deceased, who may be badly disfigured in a DVI incident, is less stressful for those completing the scanning; and a CT scanner, whether using a static scanner or a mobile CT unit, is in a lead-lined box, minimising the radiation risk to all of the DVI team.

Scans of the head include all the details attainable on dental radiographs and soft tissues that radiographs do not demonstrate. The scans can be reconstructed to demonstrate teeth as they would be seen on any dental radiograph and into 3D images of bone, teeth and soft tissue, something that 2D radiographs simply cannot do.

CT scanning acquisition protocols need to be specifically designed for PM imaging. Clinical scanning parameters produce diagnostic quality images balanced with radiation dose received by the patient. As radiation dose is not a concern in PM imaging, parameters can be increased in PMCT scanning to improve the image quality. In dental imaging this is important as scans are degraded by high density amalgam (silver filling material) that creates streak artefacts and photon depletion. Increasing kilovoltage and milliamperage can reduce artefact; minimising the scan area (the field of view) can also help.

CT scans can be reformatted in various ways using the scanner workstation or reformatting software some of which are freely available. Clinically, sagittal and coronal reformats are the most common, but these may be of limited use in dental imaging. Scans can be reformatted in an oblique plane to replicate lateral oblique radiographs. To replicate DPTs, a curved multi-planar reformat (cMPR) is required. Reformats can be created in various thicknesses or ‘slabs’. The focal troughs in clinical DPTs are a set thickness, depending on the manufacturer, and this technique can increase the thickness of a reformat to appear like a DPT. Increasing the thickness will decrease the detail seen in the image, so a compromise has to be reached.

Volume rendering, a technique not frequently used in clinical imaging, enables 3D images of the dentition to be produced. The images can be presented demonstrating teeth, bone or soft tissues enhancing CT scans' ability to support identification. These reformats are helpful if comparing dentition to AM open-mouth photographs.

In DVI, an optimal dental protocol may be a volume rendered image, lateral oblique reformats and a cMPR for DPT comparison. However, these will take time to produce, and it may be more practical for these to be made when it is known what AM dental records or imagery the PM records need to be compared to.

Medical CT Scan and Manipulation for Dental Identification Purposes to Simulate a DPT

Recently, PMCT has become a reality in PM investigation, providing a wealth of information that is relevant not only to the pathological and wider investigation but also for the purpose of identification [21, 22]. PMCT scans can be reconstructed to use as comparative imaging with 2D AM dental images or cone-beam CT images.

There are two such techniques:

(a) The first being the comparison of selected reconstructed PMCT images with 2D AM dental radiographic images (Fig. 5.15).
(b) The second being the production of 3D PMCT evidence such as a 3D print to compare with the AM 2D radiographic images, dental records or even a smile photographic image (Fig. 5.22).

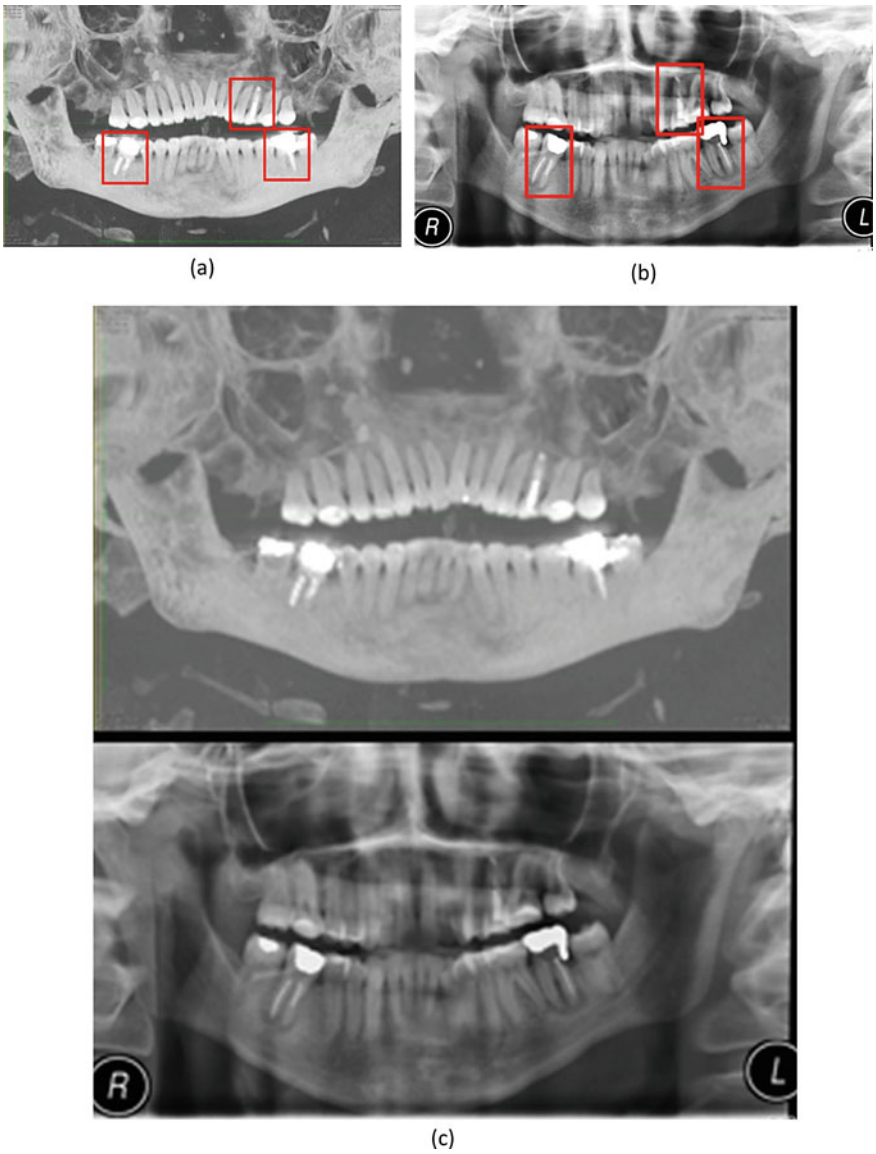

Fig 5.15 **a** A PMCT curved multi-planar reformat (cMPR) for a fire victim that was created to look like a DPT. Although the quality is not the same as conventional radiography, characteristic detail can be seen in three teeth. **b** The AM DPT where correspondent characteristics are seen in the same teeth as the image above. **c** The comparison between PM and AM images, with the distinctive characteristics in the LR7, LL7 and UL5 clearly evident, which resulted in a positive dental identification and non-invasive dental examination

Methodology of PMCT Development

Manipulation of a CT Section to Replicate a 2D Dental Panoramic Tomograph (DPT)

Volume Rendering

A cMPR can be created to replicate a DPT from a 3D volume of CT data.

Producing quality DPT equivalent cMPRs can be time consuming and the resultant images are reliant on the skill of those creating them. The orientation of the dentition needs to be corrected in the first instance to mimic the position the clinical imaging would have been obtained in.

The length needs to provide the same coverage as the DPT, so start and end posteriorly to the mandibular condyles. The thickness of the cMPR needs to be considered as increasing the thickness decreases the detail in the image. The authors' experience have found a thickness of approximately 10mm to be ideal, although thicker reformats may be required for some. The preferences of those interpreting the imaging needs to be expressed to those creating the cMPRs.

The path of the cMPR can be plotted starting and ending 20–25 mm posteriorly to the mandibular condyles. The path needs to follow the dentition and be centred within the teeth. It can be tempting to place fewer markers for speed, but time spent placing more accurate markers on most teeth will improve the resultant image quality.

Clinically the mandible and maxilla are at different focal depths, corrected in all but Class III [23] malocclusions by posturing the mandible forward, so that the upper and lower teeth are edge-to-edge. This problem can be addressed in the deceased by producing cMPRs centred for the maxilla and mandible individually.

Care needs to be taken to ensure the reformats do not miss any dentition or unique identifying features. Unerupted '8s' (also known as wisdom teeth) can easily be missed if the cMPR is not carefully positioned. Orthodontic devices may not be in a 10mm thick cMPR but need to be visualised as they can be highly individual. Including the mandible, maxilla and orbital floor can demonstrate previous healed or surgically repaired fractures.

Once a cMPR is produced, it will need to be saved. There are options available such as JPEGs of individual images, but if later analysis may be required it is recommended the cMPR path is saved in an appropriate format so that it can be accessed and reapplied to the data set later. If this is not done, the cMPR path will be lost and have to be recreated later. Figure 5.16 shows the stages of a cMPR being created.

Following an aviation crash and flash fire, victims were recovered and removed to a local DVI mortuary established to investigate the incident. The DVI process included CT scanning. The scans were completed on a Toshiba 64 slice scanner (120kD, 300–350 mA, 64×0.5 mm slice thickness, 0.6–0.8 pitch and 512×512 matrix). The head scans were reconstructed at 1mm slice thickness with 0.8mm scan intervals on bone sharp and soft tissue kernels.

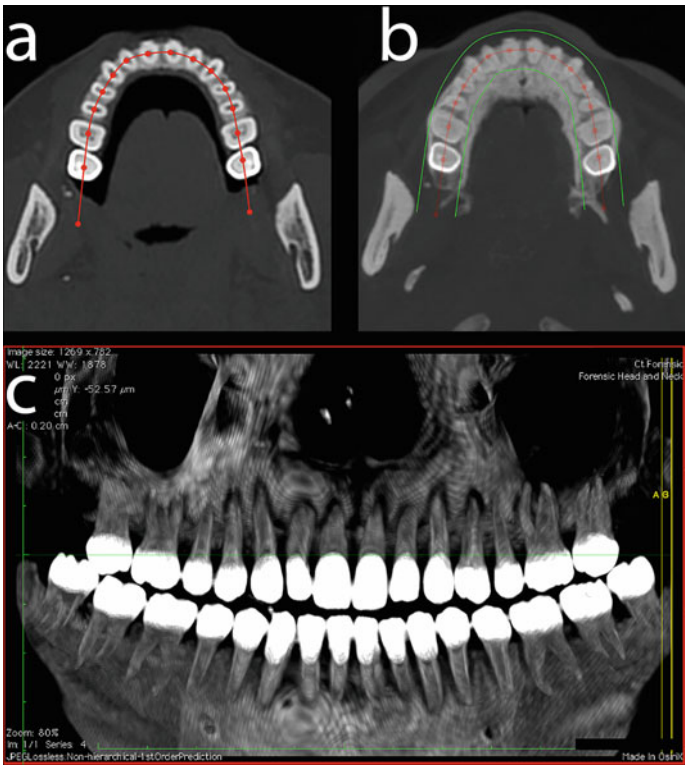

Fig. 5.16 **a** The "path" (*red line*) is created by placing "points" (*red dots*) along the required route, **b** The thickness of the image "slab" (*green*) can be increased until all teeth are included to their full extent, **c** The resulting reformatted image can then be adjusted for optimal display of the anatomical features of interest (Images reproduced courtesy of Dr Mike J P Biggs).

PMCT image sections were compared against AM radiographic images (of different views: some DPTs, some periapicals and bitewing radiographs) which also resulted in 80% of victims being identified positively by dental evidence. Figures 5.17 and 5.18 show such examples.

With one of the victims, there was no AM dental evidence, but PMCT evidence did reveal a key supportive feature, where two upper left anterior teeth were missing from the individual's dentition and there had been a centre-line shift to the left, where the upper right teeth had drifted and had partially narrowed the residual space. Figure 5.19 shows this supportive PM evidence.

Figure 5.20 shows a comparison of the AM photos of the missing individual compared with the PMCT images of the aviation crash victim, showing similarities in the centre-line shift observed in the PM evidence.

When comparing the centreline and the shift of the upper teeth PM compared to AM, supportive evidence was able to be provided to HM Senior Coroner as indicated above. Figure 5.21 shows a further comparison of AM DPT radiography and PMCT.

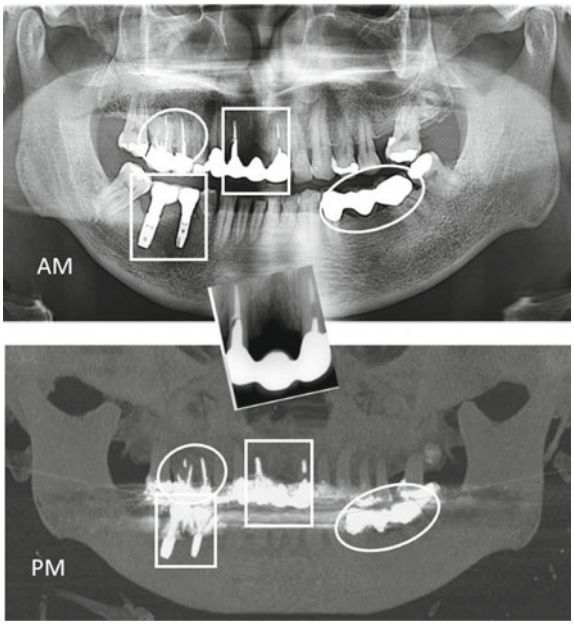

Fig 5.17 A comparison of AM and PM images showing key concordant features PM and AM between the DPT and PMCT radiographic images. The upper anterior bridge was also able to be radiographed intra-orally through gaining conventional access (without dissection) by placing a digital radiography sensor behind the upper anterior teeth (Images courtesy of Dr P H Marsden—odontology casework)

In this case the two images have been amalgamated together to show AM and PM dentition similarities all in one place.

The image was created by first generating separate curved MPR images for both the upper and lower dentition, and then superimposing these individual images onto the original conventional radiographic DPT that was available as part of the AM record. This montage was produced initially for convenience, to make the comparison process as easy as possible by arranging all of the required information side by side, but also now serves as a permanent record of the process undertaken.

Fig 5.18 A comparison of the upper left odontome with centralised area of demineralisation on the PMCT scanned image with artefacts, and the AM comparison, which has a ring shape (Images courtesy of Dr P H Marsden and Dr Mike J P Biggs—DVI casework)

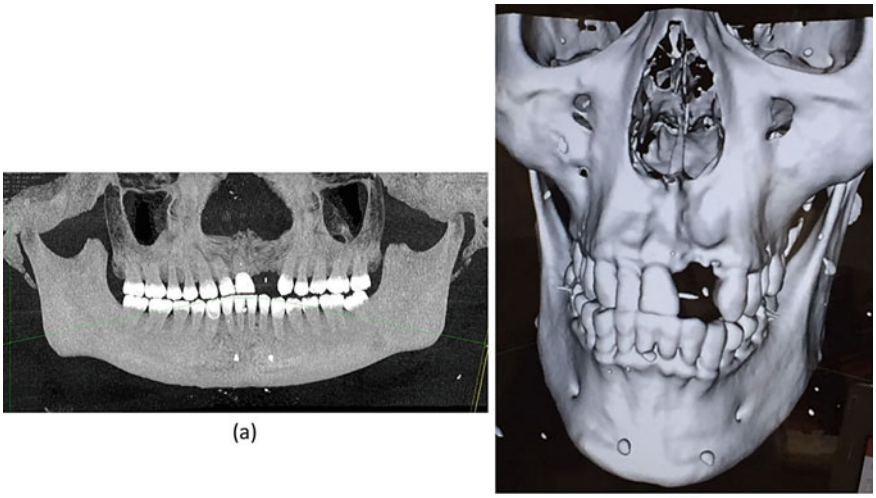

Fig 5.19 **a** and **b** above show supportive evidence from the PMCT of one of the individuals in the case. a shows a cMPR image and b a 3D scanned image of the skull. The 3D scanned image of the skull was able to indicate a centre-line shift of the upper anterior teeth to the left, where the upper left central incisor and lateral teeth was missing. These missing teeth and centre-line shift could also be identified from AM open-mouth photographs and the dimensions of the centre-line shift compared (Images reproduced courtesy of Dr P H Marsden and Dr Mike J P Biggs—DVI Casework)

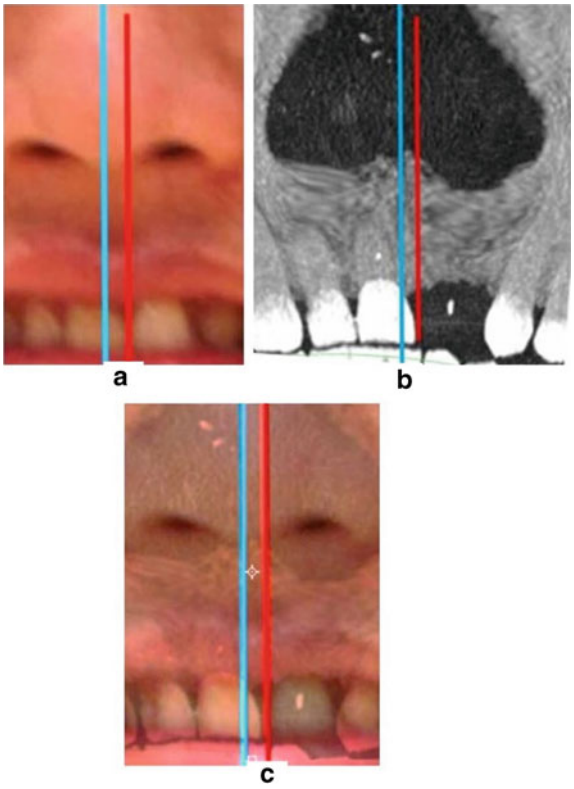

Fig 5.20 **a–c** show the PMCT scans of one of the individuals indicating a centre-line shift of the upper teeth to the left-hand side, as a result of the upper left central and lateral incisor teeth being missing and a prosthetic replacement of the upper left 1 not being worn regularly. Photographs of the individual AM show the UL1 prosthetic tooth to be a different shade to the rest of the teeth and spacing distally, indicating a poorly manufactured and fitted denture, but also this could be as a result of the upper left lateral incisor space not fully closing with time (Images courtesy of Dr P H Marsden and Dr Mike J P Biggs)

Fig 5.21 The comparison undertaken here enabled an established identification of an individual. Note the supernumerary (no. 9 upper left arrowed pink in the PM image and yellow in the AM image). Also, the distinctive distal angulation of the lower 8s, the consistent shapes of the metallic (amalgam) restorations in the molar teeth and the angulation of the lower left 5 root. In the PMCT image the lower left first molar (6) has been root-filled and a post placed in the distal canal. This is explainable as the individual will have seen a dentist for endodontic treatment since the AM dental radiographic image was taken. (Image courtesy of casework from Dr M E Clarkson and Dr M J P Biggs)

Creation of a 3D Printed Model From PMCT Scan

In another DVI response to a case that involved multiple traumatised and burned victims, one individual had no significant AM dental identifiers, but a suitable open-mouth photograph had been provided by the next of kin. Fire damage meant that access to the dentition would not have been possible without disfiguring dissection, and so a decision was made to attempt to create a facsimile by 3D printing the data contained within the PMCT scan. A 3D virtual model was extracted from the scan data using the surface rendering module of the imaging software, and this was cropped to include only that part of the dentition visible within the smiling photograph. The on-site availability of a Formlabs Form 2 3D printer enabled the complete production of this model (Fig. 5.22) within approximately 2 hours, and therefore no undue delay was introduced into the DVI mortuary process.

The pathologist presented the 3D printed model (Fig. 5.22) to the odontology team for review and comparison with the AM dental documents and the open mouth photograph. Due to the generally unrestored nature of the suspected individual's dentition (teenager), which only included four fissure sealants on the four first molar teeth (sealants can be viewed as unreliable dental evidence due to the surface nature and clinical survival rates of this type of restoration), the most valuable evidence was that of the smiling photograph, provided by the individual's family. Additionally, the incinerated nature of the PM remains was such that direct clinical access was prevented, without significant dissection of the orofacial tissues, which HM Senior Coroner had requested wherever possible, be avoided. This provided a challenge to the odontology team.

Comparing the 3D model to the 2D smiling photograph requires an experienced forensic odontologist, who is also capable of applying a certain degree of judgement for explainable differences between AM and PM evidence and the nature of the presentation of the evidence (2D compared to 3D). Quality assurance in this scenario is also key and wherever possible, the evidence should be verified by a second

Fig 5.22 3D printed model of a burn victim's upper teeth

odontologist or sometimes, in the case of DVI scenarios, a whole odontology team, which happened here.

"The advantage of having a physical 3D model over simply viewing simulated 3D representations of CT scan data on a 2D screen was that the fine-tuning of viewing angle and perspective to appreciate subtle variations of surface relationships and depth in real time was possible, even within the mortuary environment". By viewing screen-based imagery alone would have created an additional level of difficulty and by being able to palpate the model and its physical parameters, viewing it from all angles, this vastly increased the confidence of odontological corresponding features [21].

This case has introduced an innovative way of working in forensic odontology, that is non-invasive and enables a detailed comparison of salient comparative features AM and PM. On-site availability of a high-quality 3D printer facilitated this process within a timely manner, enabling reconciliation of evidence on the same day as production and is key to its success.

Where there may be multiple models produced for different individuals, the model can be labelled by a debossed unique identifying number (Fig. 5.23), much like study models would be labelled for patients in dentistry or denture marking for patients wearing oral prostheses.

The scanning in this case was carried out for general DVI mortuary purposes, and dental identification had not been a specific intention at the time of scanning. Although the parameters set in the above case produced an entirely usable model, given the significance of the dental data available following PMCT scanning, the potential for improving feature definition over that routinely obtained in DVI scanning was considered. Scan quality is dependent on the scan parameters and the reconstruction parameters. Clinical parameters are restricted by the need to limit radiation exposure to patients which is not a concern in PMCT scans. Restraint is however advised, to balance the image quality with the number of images produced,

Fig 5.23 Shows unique identifier debossed for audit trail of evidence [19]. Licensed by Springer Nature, License Number 5280780965869

and subsequent storage costs, and the potential damage to the CT scanner such scanning could cause. Body position, tube current and voltage [24], slice thickness and the size of the field of view [25] can all be used to improve the image quality. For dental scanning, our protocol is now 120kD, 350 mA, 64/80×0.5 mm slice thickness, 0.6–0.8 pitch and 512×512 matrix with the scan collimated to the area of interest. The scans were reconstructed at 0.5mm slice thickness with 0.3 mm scan intervals on bone sharp and soft tissue kernels. With the introduction of digital intra-oral scanners in dentistry, the 3D printed PMCT model will act as a useful comparator against a 3D AM intra-oral scan [26].

Artefacts in PMCT

One of the main drawbacks of using PMCT for dental identification is artefacts. Streak artefact inconsistencies in a single measurement [27] are the most common in dental CT and are due to the high density of metallic restorations [28–30]. They are a result of a combination of beam hardening, photon starvation and metal streak artefacts.

Beam Hardening

Beam hardening derives its name from the underlying cause: the increase in mean x-ray energy, or "hardening" of the x-ray beam as it passes through the scanned object. As lower-energy x-rays are attenuated more readily than higher-energy x-rays, a polychromatic beam passing through an object preferentially loses the lower-energy part of the spectrum. Metallic dental restorations severely attenuate the x-ray beam which significantly degrades image quality seen as dark bands or streaks and may have adjacent bright streaks [27] (Fig. 5.24).

Metal Streak Artefacts

Metal streak artefacts are created by beam hardening and photon starvation (a lack of photons due to the density of the metal that produce errors in the image reconstruction) and create further dark and white streak artefacts on the images [28] (Fig. 5.24). Both streak and beam-hardening artefacts are confined to the area of the dentition and are kept away from the alveolar bone area.

The effects can be reduced during the scan and during the image reconstruction. Increasing the exposure factors used, using narrow collimation or by angling the gantry (only a feature in some scanners) can help. Metal artefact reduction algorithms can be applied during the processing of the scan data and can notably improve image

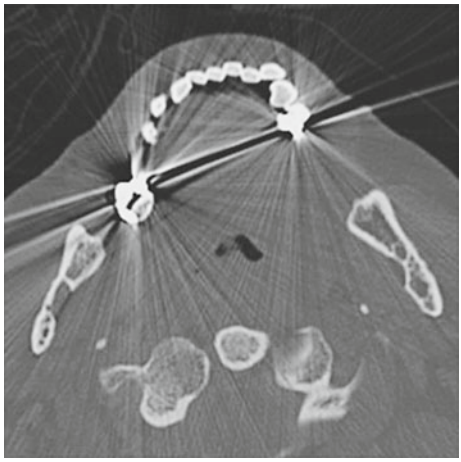

Fig 5.24 Shows the dark bands between two restorations and white streak artefacts most commonly found in CT scans. [33] Licensed by Springer Nature, License Number 5302927651

quality. The use of an extended CT scale has been shown to reduce beam-hardening artefacts produced by metal implants [30] and has also been applied in minimising artefacts caused by dental filling materials [31, 32].

A proposed guideline for PMCT as part of dental identification was developed and later published in July 2019 by the Section of Forensic Pathology, Department of Forensic Medicine at the University of Copenhagen, Denmark [33]. During the period, 475 autopsies were performed, and of these, 15 were selected in which dental findings known to be important for identification were present.

The guideline referenced shows how various filling materials appear on CT. Table 5.1 provides a summary of these.

At Leicester Royal Infirmary, the radiographer would employ the scanner software's metal artefact reduction algorithms at the time of performing the scan reconstructions (i.e. turning the raw data into images) to reduce this phenomenon.

Table 5.1 Outlines how the different restorative materials are seen on PMCT and the type of artefacts that result from the varying characteristics of the materials, dependent on their composition and density. Metallic restorations generally create more beam-hardening and streak artefacts compared to non-metallic restorations such as composites or gutta-percha in root fillings [33]. Licensed by Springer Nature, License Number 5302927651

Dental restorative (Filling) material	Observations {Reference Guideline}
Amalgam (alloy of Copper, Zinc, Silver, Tin and Mercury). Elements have high Atomic Numbers therefore produce significant beam-hardening artefacts	These produce beam-hardening and streak artefacts on the PMCT which can cause problems when determining their extent in the tooth and make it difficult to detect adjacent fillings (Fig. 5.25a)
Composite	These produce little or no beam-hardening or streak artefacts (Fig. 5.25b)
Gold Crowns (high atomic number) or extra-coronal metallic restorations incorporating whole crown of tooth	These can be recognised by their more rounded circumference (Fig. 5.25c)
Root fillings	These are easy to identify due to the radiopacity of gutta-percha filling material. There can be some beam-hardening due to heavy metal sulphates used as radiopacifiers (Fig. 5.26a, b and c show)
Metallic post and cores	These cause beam-hardening and streak artefacts, but they have high radiopacity and are seen as metallic structures anchored in the bone (Fig. 5.27)
Titanium implants	These produce very few beam hardening artefacts, but they have high radiopacity and are seen as metallic structures anchored in the bone (Fig. 5.27)

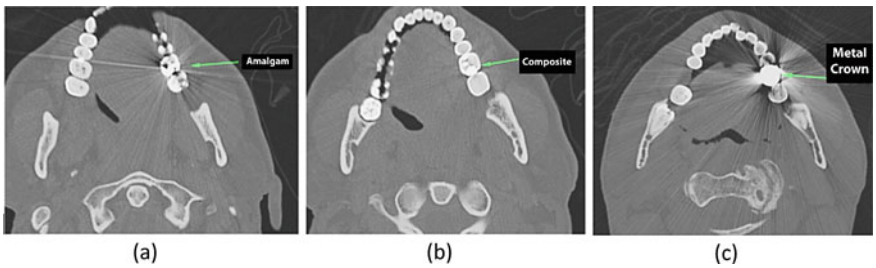

Fig 5.25 **a** streak artefacts radiating from an amalgam filling. **b** shows composite exhibiting much lower streak artefacts than amalgam in **a**. **c** the more rounded, distinctive nature of an extra-coronal gold or metallic restoration, covering the whole tooth surface above the gum (crown) e.g. a gold crown, compared to an amalgam filling or inlay. [33] Licensed by Springer Nature, License Number 5302927651

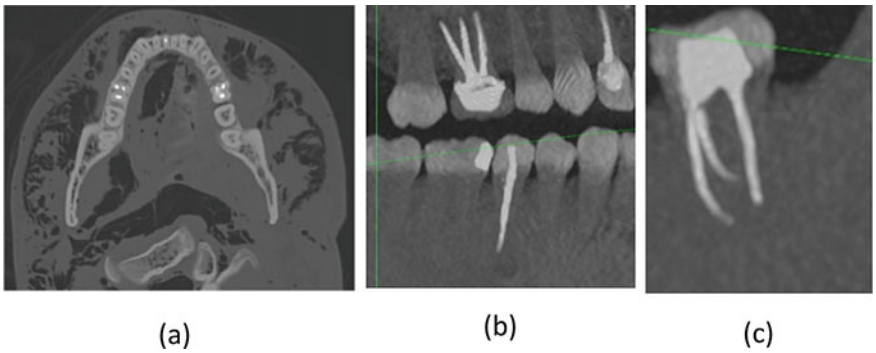

Fig 5.26 **a** shows the appearance of root fillings from an axial view. **b** and **c** show the appearance of root fillings from the coronal view. **a** [33] Licensed by Springer Nature, License Number 5302927651

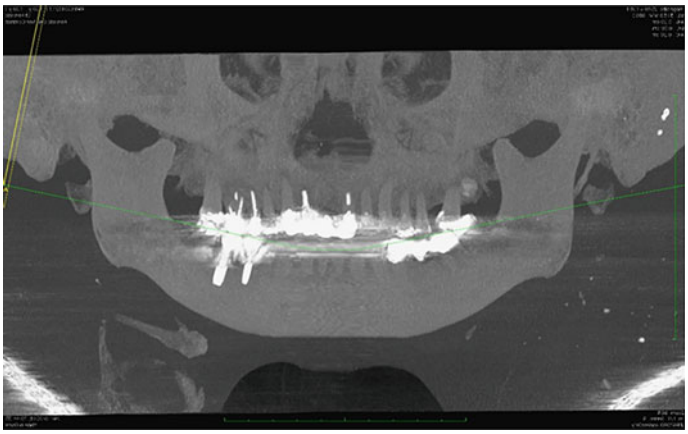

Fig 5.27 Implants lower right 5 and 6, root fillings upper left 1, upper right 2, upper right 5 and 6. Upper right 5 and 6 also have metallic post and cores. Note the beam-hardening and white-streak artefacts from the metallic crowns and amalgam restorations

A Comparison Between 3-Dimensional and 2-Dimensional Imaging in Forensic Odontology

There are numerous advantages and disadvantages to both 3D and 2D imagery to be considered when comparing like with like imagery or when comparing the two. These can be found listed in Table 5.2.

Table 5.2 Comparison of the advantages and disadvantages between 3D CT and 2D imagery

3D CT		2D imagery	
Advantages	Disadvantages	Advantages	Disadvantages
Multiplanar reformatting and data manipulation allowing anatomy/pathological conditions to be viewed in different planes (including 3D model production)	Imagery requires experienced practitioners to interpret, especially when comparing 2D against 3D [34, 35]	Can provide enhanced or 'close-up' detail in an identification, to consolidate information found on medical CT image e.g. periapical of upper anterior porcelain bonded to metal conventional bridge	Invasive in a PM setting, if intra-oral radiography used and requires access for intra-oral sensor positioning in the mouth (difficult in incinerated remains or during rigor mortis)
Can provide relatively geometrically accurate images, but this is dependent on resolution applied	Create artefacts with radiodense materials e.g. white streak artefacts and beam-hardening, especially making restoration shapes difficult to compare, unless adjustments made	Relatively geometric accurate images e.g. endodontics, give or take a relative amount of technique distortion when taking the radiograph	Technique sensitive
Good spatial resolution	Requires manipulation of software for comparison with similar 2D imagery i.e. DPT	2D radiography imagery better spatial resolution compared to 3D CBCT or PMCT	2D image of 3D object so limited plane view and requires experience to interpret imagery
Non-invasive	Generally confined to mortuary environment or hospital radiography unit/can get mobile CT in DVI scenarios however	Applicable in field conditions (hand-held radiography machine e.g. NOMAD Pro 2™)	Create artefacts but to a lesser extent than CT i.e. more technique-related rather than due to subject matter
Axial tomographic sections are obtainable	Higher dose of radiation compared to conventional dental radiography, although less of an issue in Post Mortem setting	Much lower dose of radiation compared to Medical CT Scanning and Cone-Beam CT Scanning	Axial sections not available unless take an additional radiograph
	CT mandible/maxilla = 0.25–1.4 mSv (Effective Dose), however this is significantly less than e.g. CT Abdomen = 5.6 mSv [36]	Bitewing/Periapical = 0.0003-0.022 mSv,	
		DPT = 0.0027–0.075 mSv	
		Upper Standard Occlusal = 0.008 mSv, Lateral Ceph = 0.0022–0.0056 mSv.	
		Skull Radiograph (PA) = 0.02 mSv [36]	

(continued)

Table 5.2 (continued)

3D CT		2D imagery	
	The equipment is expensive	In comparison the equipment is relatively cheap	

Summary

From this chapter, it is clear that CT scanning has a significant place within the realms of dental identification. It creates not only a less invasive and more dignified method of determining a positive dental identification, by avoiding incisions, especially when incinerated remains are involved, but could also allow remote identification. By looking at the PMCT scans in advance, the odontologist has a better idea on which dental characteristics to focus their examination, following confirmation that those characteristics are present for comparison with the AM dental records. Therefore, PMCT can also assist as a rapid screening method for identification purposes. For example, an upper anterior bridge which is present AM can easily be verified as present on a PMCT cMPR section.

The ability to print 3D models of the teeth is also useful in determining additional characteristics AM and PM, which cannot be gleaned through 2D imagery. The 3D PMCT models can be compared to AM study models or photos of the teeth.

More research is no doubt required regarding PMCT in dental identification, and this can be acquired through increased usage and analysis of dental identification casework, shared experiences within the forensic community and the evolution of PMCT technology.

Acknowledgments Grateful acknowledgements for their contribution to this chapter go to Dr M J P Biggs, University of Leicester and Dr Claire Robinson, University Hospitals of Leicester.

References

1. Annexure 12: Methods of Identification. In: E DVI Guide 2018 Annexure 12.pdf INTERPOL. 2018. https://www.interpol.int/content/download/5759/file/E%20DVI_Guide2018_Annexure12.pdf. Accessed 01 Apr 2022.
2. Grabherr S, Heinemann A, Vogel H, Rutty G, Morgan B, Woźniak K, et al. Post-mortem CT angiography compared with autopsy: a forensic multicenter study. Radiology. 2018;288(1):270–6.
3. Carabott R. Radiography in Dental Identification. In: Adams C, Carabott R, Evans S, editors. Forensic Odontology, An Essential Guide. WILEY Blackwell, 2014. p. 87–93.
4. INTERPOL DVI guide 2018 part B, annexure 5 https://www.INTERPOL.int/en/How-we-work/Forensics/Disaster-Victim-Identification-DVI. Accessed 01 Apr 2022.
5. Viner MD, Robson J. Post-mortem forensic dental radiography—a review of current techniques and future developments. J Forensic Radiol Imag. 2017;8:22–37. https://doi.org/10.1016/j.jofri.2017.03.007.

6. CGDent(UK). Quality assurance in dental radiology. In: Guidance notes for dental practitioners on the safe use of X-ray equipment. 2nd ed. Public Health England. FGDP(UK);2020. p. 82–94.
7. Whaites E, Drage N. Periapical radiography. In: Essentials of dental radiography and radiology, 6th ed. Elsevier Limited;2021. p. 106–115.
8. The Ionising Radiations Regulations 1999. https://www.legislation.gov.uk/uksi/1999/3232/contents/made. Accessed 01 Apr 2022.
9. The Ionising Radiation (Medical Exposure) Regulations 2017. https://www.legislation.gov.uk/uksi/2017/1322/contents/made. Accessed 04 Apr 2022.
10. College of General Dentistry, Drage A, Walker A. The new patient to the practice. In: Horner K, Eaton K A. Selection criteria for dental radiography, 3rd ed. London: Faculty of General Dental Practice (UK);2018. p. 22.
11. College of General Dentistry, Pitts N, Ricketts, D. Radiographs in dental caries diagnosis. In: Horner K, Eaton K A. Selection criteria for dental radiography, 3rd ed. London, Faculty of General Dental Practice (UK);2018. p. 43–64.
12. Banerjee A, Watson Timothy F. Clinical operative procedures—a step-by-step guide. In: Pickard's Manual of Operative Dentistry, 9th ed. Oxford University Press;2011. p. 102. https://toaz.info/doc-view. Accessed 12 April 2022.
13. Kogon S, MacLean D. Long-term validation study of bitewing dental radiographs for forensic identification. J Forensic Sci. 1996;41(2):230–2. https://doi.org/10.1520/JFS15418J (ISSN0022-1198).
14. Dental Charting. NEBDN. 2015. https://www.nebdn.org/app/uploads/2019/05/NEBDN-Dental-Charting-Book-October-18.pdf. Accessed 16 Apr 2022.
15. Baglivo M, Winklhofer S, Hatch GM, Ampanozi G, Thali MJ, Ruder TD. The rise of forensic and post mortem radiology—analysis of the literature between the year 2000 and 2011. J Forensic Radiol Imaging. 2013;1:3–9.
16. Rutty GN, Biggs MJP, Brough A, Morgan B, Webster P, Heathcote A, Dolan J, Robinson C. Remote post-mortem radiology reporting in disaster victim identification experience gained in the 2017 Grenfell Tower disaster. Int J Legal Med. 2020;134:637–43.
17. Sidler M, Jackowski C, Dirnhofer R, Vock P, Thali M. Use of multislice computed tomography in disaster victim identification—advantages and limitations. Forensic Sci Int. 2006;169(2/3):118–28.
18. O'Donnell C, Lino M, Mansharan K, Leditscke J, Woodford N. Contribution of post-mortem multi-detector CT scanning to identification of the deceased in a mass disaster: experience gained from the 2009 Victorian bushfires. Forensic Sci Int. 2011;2011(205):15–28.
19. Ruder TD, Kraehenbuehl M, Gotsmy WF, Mathier S, Ebert LC, Thali MJ, Hatch GM. Radiological identification of disaster victims: a simple and reliable method using CT of the paranasal sinuses. Eur J Radiol. 2012;81:e132–8.
20. Hofman P, Alminyah A, Apostol M, Boel LWT, Brough A, Bouwer H, O'Donnell C, Fujimoto H, Iino M, Kroll J, Lee CT, Levey DS, Makino Y, Oesterhelweg L, Ong B, Ranson D, Robinson C, Rutty G, Singh MKC, Villa C, Viner M, Woodford N, Watkins T, Wozniak K. Use of post-mortem computed tomography in disaster victim identification. Updated positional statement of the members of the Disaster Victim Identification working group of the International Society of Forensic Radiology and Imaging. J Forensic Radiol Imag. 2019;19: https://doi.org/10.1016/j.jofri.2019.100346
21. Biggs M, Marsden P.H. Dental identification using 3D printed teeth following a mass fatality incident. J Forensic Radiol Imag. 18:1–3. https://doi.org/10.1016/j.jofri.2019.07.001
22. Caplova Z, Obertova Z, Gibelli DM, De AD, Mazzarelli D, Sforza C, et al. Personal identification of deceased persons: an overview of the current methods based on physical appearance. J Forensic Sci. 2019;63(3):662–71.
23. Proffit WR, Fields HW, Sarver DM. Malocclusion and dentofacial deformity in contemporary society. The changing goals of orthodontic treatment. In: Contemporary orthodontics. 5th ed. Elsevier Mosby;2013. p. 7.
24. Gascho D, Flach PM, Schaerli S, Thali MJ, Kottner S. Application of 3D image fusion for radiological identification of decedents. J Forensic Radiol Imag. 2018;13:12–16.

25. Ford JM, Decker SJ. Computed tomography slice thickness and its effects on three-dimensional reconstruction of anatomical structures. J Forensic Radiol Imag. 2016;4:43–6.
26. Reesu VG, Woodsend B, Mânica S, Revie GF, Brown NL, Mossey PA. Automated Identification from Dental Data (Auto IDD): A new development in digital forensics. Forensic Sci Int. 2020;309:1–9. https://doi.org/10.1016/j.forsciint.2020.110218.
27. Barrett JF, Keat N. Artefacts in CT: recognition and avoidance. Radiographics. 2004;24:1679–91. https://doi.org/10.1148/rg.246045065.
28. Boas EF, Fleischmann D. CT Artifacts: causes and reduction techniques. Imaging Med. 2012; 4(2):229–240. http://www.edboas.com/science/CT/0012.pdf. Accessed 16 Apr 2022.
29. Boas EF, Fleischmann D. Evaluation of two iterative techniques for reducing metal artifacts in Computed Tomography. Radiology 2011; 259(3):894–902. https://pubs.rsna.org/doi/epdf/10.1148/radiol.11101782. Accessed 16 Apr 2022.
30. Ese Z, Kressmann M, Kreutner J, Schaefers G, Emi D, Zylka W. Influence of conventional and extended CT scale range on quantification of Hounsfield units of medical implants and metallic objects. tm-Technisches Messen 2018;85:343–50.
31. Jackowski C, Lussi A, Classens M, Kilchoer T, Bolliger S, Aghayev E, et al. Extended CT scale overcomes restoration caused streak artifacts for dental identification in CT-3D colour-encoded automatic discrimination of dental restorations. J Comput Assist Tomogr. 2006;30:510–3.
32. Jackwoski C, Wyss M, Persson A, Classens M, Thali MJ, Lussi A. Ultra-high-resolution dual-source CT for forensic dental visualisation-discrimination of ceramic and composite fillings. Int J Legal Med. 2008;122:301–7.
33. Jensen ND, Arge S, Hansen NF, Lynnerup N. Post-mortem computed tomography as part of dental identification—a proposed guideline. Forensic Sci Med Pathol. 2019;15:574–9.
34. Pretty IA, Pretty RJ, Rothwell BR, Sweet D. The reliability of digitized radiographs for dental identification: a web-based study. J Forensic Sci. 2003;48:1325–30.
35. Ruder TD, Thali YA, Rashid SNA, Mund MT, Thali MJ, Hatch GM, Christensen AM, Somaini S, Ampanozi G. Validation of post-mortem dental CT for disaster victim identification. J Forensic Radiol Imag. 2016;5:25–30.
36. Whaites E, Drage N. Radiation dose, dosimetry and does limitation. In: Essentials of Dental Radiography and Radiology. 6th ed. Elsevier Limited;2021. p. 61.

Chapter 6
Disaster Victim Identification: Traditional Approaches and Changing Practices

Soren Blau, David Ranson, and Hans de Boer

Introduction

Mass fatalities may result from natural environmental events such as fires, floods, landslides, avalanches, earthquakes, as well as human induced incidents, either intentional (e.g., a terrorist attack) or accidental (e.g., a train or aircraft accident, building collapse, industrial explosion). A vital component of disaster management is the identification of the deceased, which involves the comparison of information about the individual when they were alive (ante-mortem data) with information obtained during the post-mortem examination of the deceased person (post-mortem data). Confirmation of an individual's name (i.e., identification) can be seen as forming part of the legal right to identity, as outlined in Article 24 of The International Covenant on Civil and Political Rights [1], and facilitating a variety of legal processes as set out in Article 6 of The Universal Declaration of Human Rights which states that "Everyone has the right to recognition everywhere as a person before the law" [2]. The confirmation of the identity of a deceased person is also of paramount importance for compassionate and health and welfare reasons since the certainty of the death of a loved one allows family and friends of a deceased person to grieve and can support them in their bereavement [3, 4].

From a social and legal perspective, the recording of who has been born into a society and who has died has profound implication for social order, community services and the economic and social planning process of governments. Systems to

S. Blau (✉) · D. Ranson · H. de Boer
Victorian Institute of Forensic Medicine / Department of Forensic Medicine, Monash University Victoria, Southbank, VIC, Australia
e-mail: soren.blau@vifm.org

D. Ranson
e-mail: david.ranson@vifm.org

H. de Boer
e-mail: Hans.de.Boer@vifm.org

G. N. Rutty (ed.), *Essentials of Autopsy Practice*,
https://doi.org/10.1007/978-3-031-11541-7_6

record the deaths of persons are found in most societies. However, personal identification in the inherently chaotic circumstances following a disaster is invariably challenging. Recognizing the importance of establishing standards for identification, regardless of where and how the disaster occurred, who is involved, or the preservation of the remains, the International Criminal Policing Organization (INTERPOL) produced a Disaster Victim Identification (DVI) Guide in 1984. This Guide, which is available in four languages (Arabic, English, French and Spanish) and has been revised regularly over the past thirty years, outlines the procedures used to positively identify victims of mass casualty incidents [5]. The aim of the Guide is to promote best practice and encourage all 194 members of INTERPOL to follow a common process to increase the effectiveness and timelines of identification efforts [6].

DVI operations are usually overseen by a legal official (e.g., a judicial officer, who, depending on the jurisdiction may be a coroner or a prosecutor) and managed by police officials. However, forensic specialists including forensic pathologists, forensic anthropologists, forensic odontologists, and molecular biologists have key responsibilities during the operation. This chapter is primarily aimed at those medico-legal specialists, and provides an up-to-date overview of personal identification, the phases that occur in a DVI, and some of the developments and challenges that have arisen in the investigation of mass fatalities and the identification of human remains.

The Basics of Personal Identification

The personal identification of a deceased individual, in any context, is based on two sources of information. First, the information that can be obtained from, or around the body, regardless of preservation or completeness, must be considered. This information, since it relates to a post-mortem examination, is also referred to as 'post-mortem' (PM) data. Secondly, there is information that can be obtained from sources relating to a missing individual. Since this information dates back to the missing individual was still alive, this information is referred to as ante-mortem (AM) data. An unknown individual is confirmed as identified when the PM and AM data match to such a degree that they are considered sufficiently similar as to only relate to one and the same individual. Because no commonly accepted threshold of agreement exists; an identification is eventually at the discretion of a responsible official. Depending on the jurisdiction and context, this can be a police officer, a medical specialist, or a legal/administrative official.

The various types of PM and AM data that are compared are called 'identifiers', and they often require specific forensic expertise for their recording and interpretation. INTERPOL distinguishes between two classes of identifiers, or identification methods. The three identifiers that are currently considered to be most reliable are DNA, fingerprints, and odontology. These methods are considered to be so specific, that a PM-AM match is accepted as sufficient proof of identity [5]. Therefore, INTERPOL classifies these identifiers as 'primary' identifiers and are the preferred means for identification. All other identifiers are currently considered inferior and

are in the DVI Guide referred to as 'secondary'. Examples of secondary identifiers are scars, moles, tattoos, medical devices (pacemakers, joint replacements), and anatomical variations. Less-specific information, for instance sex, height, hair colour, ethnical affinity, and personal effects (e.g., jewellery, clothing) are also secondary identifiers. INTERPOL advises against identifications based on secondary identifiers alone. However, if primary identifiers are not available, a (combination) of highly specific secondary identifiers may be the only option and the decision to rely on such secondary identifiers to conclude identity is the responsibility of the official charged with the legal determination of identity. The use of secondary identifiers, and their value in personal identification is further discussed later in this chapter.

The ability to compare PM and AM data relies on the existence of an identification hypothesis i.e., a presumed identity of the deceased. From a probabilistic point of view, the identifiers are the evidence to help differentiate between two mutually exclusive hypotheses: the presumed identity is correct, or the presumed identity is wrong. This aligns well with the Bayesian method of evidence interpretation, which is currently becoming the standard in most fields of forensic science [7, 8]. However, in the early phases of an DVI operation, detailed PM or AM data may not yet be available, and a direct comparison of AM and PM data may not yet be possible. In such a situation, secondary identifiers can be used to reduce the list of possible matches, and thereby appropriately direct the identification process [9]. In other fields of forensic science this may be referred to as the 'investigative' phase of the operation [7], but in a DVI context, the word 'triage' is generally used (e.g., [10]. For instance, estimation of age may be used to separate young individuals and therefore, assist in a more timely identification. Similarly, cases can be prioritized based on radiological screening (e.g. elaborate dental work, signs of previous surgery). Such triaging does not require a presumptive identity and is often based on non-specific 'secondary' identifiers. This shows that the value of an identifier is not only determined by its specificity, and that the potential value of secondary identifiers for human identification should not be overlooked.

The Phases of DVI: A Summary

As outlined in the INTERPOL DVI Guide, there are four official phases of the DVI process (the scene, post-mortem, ante-mortem, and reconciliation) and one unofficial (debrief).

Phase 1: The Scene

Phase 1 involves an evaluation of the disaster site and the subsequent search for and collection, preservation and transportation of human remains. Detailed mapping of the scene during the recovery process is required to ensure the location of

human remains and associated evidence are appropriately recorded and systematically collected. Management of the scene and recovery process is overseen by police and, depending on the preservation of the remains, may involve forensic experts such as anthropologists, odontologists, pathologists and archaeologists [9].

Phase 2: Post-mortem (The Mortuary)

Phase 2 involves the examination in the mortuary of human remains, regardless of preservation, to obtain information pertinent to establish identification, and where required, establish cause and mechanism of death. Personnel involved in phase 2 typically include photographers, scribes, mortuary technicians, and a range of forensic experts including forensic pathologists, radiologists [11, 12], anthropologists [9], odontologists [13, 14], fingerprint experts [15], and molecular biologists [16]. All information observed in the mortuary potential pertinent to the identification process is recorded on post-mortem (pink colored) DVI recording forms.

Phase 3: Ante-mortem (Data Collection)

Phase 3 of the DVI process involves the collection of information from friends and family of the missing person that may potentially assist with identification. Common sources of antemortem data include dental information (including charts, records, clinical photographs, models, casts etc.), fingerprint records, family reference DNA samples, and medical records. The collection of this information is typically undertaken by police personnel [17] and recorded on ante-mortem (yellow) INTERPOL DVI forms. These forms mirror the information obtained on the pink postmortem forms, facilitating the comparison of identifiers.

Phase 4: Reconciliation

The fourth phase of the DVI process involves comparing ante and post-mortem data to attempt to obtain a match and ultimately confirm a positive identification. Depending on the preservation, this process typically involves so-called primary identifying information: dental records [18], fingerprint data [19], and/or DNA [20]. However, in selected cases, identifications can be suggested based on secondary identifiers. When a match between the ante- and post-mortem data is confirmed, the findings are presented to a reconciliation board who are responsible for reviewing all the evidence, performing a final quality check, and confirming the identification. Depending on the

jurisdiction overseeing the DVI, the board may include a coroner, magistrate, police, military, and government officials Often, the main forensic specialties involved are also represented at the board.

Phase 5: Debrief

Although not yet officially described as a phase in the INTERPOL DVI Guide, the Guide recommends a debrief after the operation is complete. The aim of a debrief is to review the effectiveness of the DVI process and make recommendations for future incidents (often referred to by practitioners as Phase 5) [21, 22]. The debrief is usually performed at three levels: a day-to-day operational debrief is conducted during the DVI operation, in an attempt to handle *ad hoc* issues and streamline the identification process. In long-lasting operations, the frequency may eventually diminish, and these debrief may be held every couple of days or every week. The second level of debrief involves a full review of the entire process, after the DVI operation has been completed. The third level of debrief pertains to the exchange of information between DVI teams and forensic specialists, for instance through conferences, workshops and publications.

From an occupational health and safety (OHS) perspective the welfare of disaster responders is a critical aspect of a debriefing process. While debriefing needs to be considered at a personal level as part of all the phases of the DVI operational response it also needs to be addressed particularly in the weeks, months and years following an incident. A DVI debriefing system needs to ensure that response agencies maintain their personnel support services for staff, but also that staff who leave the agency following being involved in a disaster response continue to be followed up.

The wider aspects of the resolution of a DVI response do not end with the unofficial ‘debriefing phase’. From an emergency management perspective, other post-incident processes are necessary to ensure that the capacity and capability of a jurisdiction to respond to future disasters is maintained and developed. This involves evaluating and reviewing capacity and capability, implementing improvements, and testing and training new systems, with further regular evaluation of modified systems. This cycle is a never-ending ‘circle of preparedness’ involving ‘impact evaluations’ that needs to be maintained and actively resourced [23, 24].

Although the various phases outlined above are generally described as a strict sequence, they often coincide or overlap. For instance, the AM data collection ordinarily runs simultaneously with the mortuary activities, and the mortuary phase may well overlap with the latter stages of the scene investigation and the early phase of reconciliation.

Different Types and Scales of Disasters

The DVI process has been implemented following different scale mass fatalities ranging from two [25] to thousands of deceased persons [26]. The benefits of following the DVI guide have been well demonstrated in so called "closed disasters", that is, where the exact number of missing individuals is known, for example, aviation and shipping accidents [27]. DVI protocols have also been applied to so-called "open disasters", that is, where anyone could be a victim, such as terrorist attacks [28] and natural disaster such as earthquakes, bushfires, floods, mudslides, hurricanes etc. [29].

However, challenges associated with implementing DVI protocols in large scale disasters where the number of deceased may be in the tens of thousands, or a criminal investigation coincides with the identification efforts have been noted [30, 31]. Such challenges include managing and recording large scale human remains (often in varying states of preservation) and associated evidence [32], as well as the data created following examination [18], often in contexts where the existing infrastructure has been impacted severely by the disaster. Another challenge is provided by protracted disasters, such as those related to the thousands of deaths of individuals on migrant routes towards Europe or North America. Challenges in the identification of these individuals are for instance related to severe underfunding and understaffing, or the general lack of reliable AM data [33, 34].

The relationship between human-made civil disasters, terrorist acts, and military and quasi-military action can be complex and overlays the medical and scientific efforts of DVI teams with political and diplomatic considerations that can be both disruptive and supportive. With mass fatality events, especially those associated with transport incidents, involving deceased persons of many different nationalities and from widely different legal and political jurisdictions, finding a common set of values and cultural expectations for the management of the dead can be problematic [35]. Indeed, diplomatic issues can arise where victims have dual or multiple nationalities, an issue that can complicate the repatriation of remains. Legal and jurisdictional differences can include variations in the degree of proof and the validity of the evidence required for legal determination of identity in a particular jurisdiction. This can impact on the scientific and medical teams with them being required to meet and document different evidential standards. While the INTERPOL processes provide a degree of consistency, changes and modifications to the international standards they proscribe may take some time to be accepted by the individual identification officials in some jurisdictions.

Another feature of some 'modern' disasters is the risk of contamination of the scene and the human remains by chemical, biological, radiological, and nuclear (CBRN) hazards. These can result in the scene and mortuary phases having to be undertaken in a setting of high OHS risk [36, 37]. The expanding use of postmortem imaging in DVI scenarios (see below) provides an opportunity to manage the examination of contaminated human remains while reducing the risk of exposure of the examiners to hazardous materials. Such radiological studies can be undertaken within

'hot zones' or with deceased stored in 'HazMat' containers that have been decontaminated. In the case of a 'hot zone,' reviewing of the radiological images may be undertaken on a remote location that is a designated place of safety [38].

The abovementioned challenges have resulted in re-thinking about how, and to what extent, identifications can be achieved and in turn, the need in many contexts, to initially manage the dead body appropriately with the idea of facilitating identification at some time in the future. Dead body management has largely been promoted by the International Committee of the Red Cross [39]. However, representatives from the ICRC are members of the INTERPOL working groups (see below), and their experiences in dealing with humanitarian crises therefore also inform the INTERPOL DVI guide.

Changing Practices

While DVI is police-led, the importance of forensic medical specialists in the process is widely recognized. This importance is demonstrated by the inclusion of discipline-specific specialist sub-working groups which support DVI activities. There are currently four scientific sub-working groups within INTERPOL: Pathology and Anthropology, Odontology, Ridgeology (fingerprints), and Molecular Biology (DNA). These working groups are made up of discipline-specific representatives from around the world who meet annually to "discuss how DVI procedures and standards can be improved and to help develop training programmes" [40]. Contributions from the sub-working groups have seen a number of changes to the ways in which DVI practice is undertaken.

Technological Advances in Identification Processes and Methods

Identifying deceased persons has long been of importance to a range of stakeholders including families of the victims, death registration authorities, legal practitioners in the field of Wills and Succession, commercial insurance providers, law enforcement agencies, and forensic medical practitioners. Technological advances in a range of fields have significantly improved identification capabilities [41, 42].

At The Scene

Not all fatality events will involve the human remains being located at a single site. Natural disasters such as flooding or earthquakes and transport disasters, involving

the breakup of aircraft at altitude, may result in human remains being distributed over a large area. The exact location of remains may be of critical importance in determining the circumstances of the incident. The numbering systems for registering the recovered remains need to be capable of recording the location and the identity of the scene examiners involved. Modern techniques including the use of hand-held global positioning system (GPS) recording devices, or GPS-enabled Drone or related unmanned aerial vehicles (UAVs) to survey scenes and locate regions of interest for further investigation, are now starting to be used in disaster victim identification scenarios [43].

Implementation of Medical Imaging as a Triage Tool and for Identification

While the use of medical imaging in the form of X-rays to assist with identifying victims of mass fatalities has a relatively long history [44], it was not until 2006 that the use of a mobile computer tomography (CT) scanner was first used in a DVI operation [45]. Since this time, radiology has been employed in a number of DVI operations including in Australia [46], Japan [12], the Netherlands [47], France [48] and the UK [49]. While purchasing and maintaining CT scanners is expensive and requires a high level of skill and infrastructure, the contributions of radiology are significant, as has been highlighted in the various positional statements by the DVI working group of the International Society of Forensic Radiology and Imaging (ISFRI) (e.g. [45, 50]). As a triage tool, medical imaging allows for a non-invasive analysis, which means there is no requirement to prepare or clean the remains, or even open the body bag, in case of potentially hazardous/contaminated remains. Also, medical imaging has the ability to provide a timely and efficient opinion on the presence of commingling and potentially identifying items and bony features. For instance, the presence of jewellery, dental elements (with or without restoration) and medical devices are readily visible [46]. This can help the recovery and recording of such identifiers. In selected cases, radiological images can be used for identification, for instance through comparison of frontal sinuses [51], or anatomical variations (e.g. [52–54]). Further, CT data can be stored indefinitely and transferred digitally to remote sites for storage or later reexamination of the images [49].

The Pathology and Anthropology Sub-working Group (PASWG) worked with forensic radiologists to develop a recording form for radiologists involved in DVI [55]. This form provides an intuitive and quick way to record the most pertinent information, such as used modality, the type and state of remains, and the presence of possible identifiers. This form has been included as an appendix in the DVI Guide which means it can be used as and when required by DVI teams across the globe.

Dental Identifications

In cases where comparative ante-mortem dental records can be located, dental evidence in the form of treatments and information about individualities in teeth structures is commonly used by forensic odontologists to positively identify individuals in DVI operations [56, 57]. Where the infrastructure exists, technological advances in imaging have seen an increase in the use of post-mortem computer tomography (PMCT) for dental identification [18, 58]. The ability to reconstruct standard CT images to emulate conventional panoramic dental radiographs (orthopantomagrams -OPGs) has proven helpful in this regard [59].

DNA

As technologies advance, the application of more powerful DNA methods using a range of different samples of varying preservation levels are being explored. For example, while it is well known that fire denatures DNA [60], successful DNA identifications were achieved following the 2009 Victorian (Australian) bushfires. Despite many of the victims being extensively burnt such that samples typically selected for DNA analysis failed, samples obtained from the bladder (a relatively protected anatomical area) provided successful identifications [61]. The very high yield of the DNA sampling in the context of the DVI following the July 2014 MH17 airplane disaster also attests to the great sensitivity of current DNA techniques [62]. In that particular operation, the relatively protected deep muscle tissues of the upper leg, femoral cortical bone, and femoral bone marrow swabs were used. The increased sensitivity of current DNA recovery methods however poses new challenges, as it increases the risk of contaminated samples, which may hamper interpretation of the recovered data considerable.

Another innovation in identification is the use of so-called rapid DNA. This kit, which is portable and can be operated by a non-specialist, has the ability to analyse several tissue types at once with the estimated time from sample to profile available anywhere from 2–3 h [63]. Such ‘lab on a chip’ technologies are starting to appear in routine forensic work in a number of fields with digitised result from ‘on scene’ analysis being able to be transferred back to major forensic laboratories for expert analysis and comparisons [64]. While promising as a future technology, currently the number of runs is very limited (e.g., 4–5) and the required equipment is expensive. Also, the results seem to be highly dependent on preservation, with problems quickly arising when post-mortem interval increases [63]. For some tissue types (e.g., bone and decomposed soft tissue) the results are poor. Some countries require specialised accreditation before use. Many countries have tried rapid DNA using different samples [65] and the application of so called rapid-DNA to DVI operations has also been discussed [66].

Fingerprints

Depending on the preservation of the hands and the availability of ante-mortem fingerprint records, identification via fingerprint comparison is also employed in DVI operations [67]. As technology has developed, fingerprint experts have been able to obtain prints from relatively poorly preserved remains [68] and kits have become more portable with an increased use of digital capture of prints [69]. The digital capture of fingerprints allows for a quick and automated comparison with digitally stored AM prints. There have also been developments in training of fingerprint experts involved in post-mortem fingerprint collection, with resources such as the open access online training videos developed by the Federal Bureau of Investigation of the United States (https://www.fbibiospecs.cjis.gov/Home/TrainingPostmortem).

Ante-mortem Data Collection

The increased mobility of populations on a worldwide basis with people having homes in different jurisdictions at varying times of the year has significantly complicated the collection of timely contemporaneous ante-mortem data on the missing. This change in mobility has resulted in an increased need to assess people's biometrics quickly and efficiently. While improvements in biometric databases facilitate timely and widespread sharing of data, there is also an increased awareness about the issues associated with such databases including the rights of the individual and national security [70].

Reconciliation

New technologies supporting this phase of operations include: the digital tagging of remains and samples for testing as well as documentary and other evidential material collected during the various phases of the DVI response [32]; the implementation of systems for rapid data communications and integration of remote datasets with any central incident dataset (an area where blockchain technologies may have a future role [71], and use of information communication technology (ICT) systems designed to provide automated comparison of AM and PM datasets for potential identification matches. INTERPOL currently uses a ICT system known as "PlassData" [72]. For automated DNA comparison, the software "Bonaparte" is available [73].

Re-thinking Primary Versus Secondary Identification Methods

The INTERPOL classification of primary and secondary identifiers is useful from a practical point of view, in the sense that it allows for a clear-cut identification of three very reliable identification methods. However, this classification is not without problems, and various recent publications have focused on a repositioning of secondary identifiers or advocated for a more holistic approach to identification [74, 75].

In general, these papers conclude that although primary identifiers are generally accepted to be the most reliable means of identification, it should be kept in mind that the value of an identifier is as much dependent on the context as on the method of identification itself. First of all, because in the absence of AM data, all PM data is worthless. Therefore, situations in which no next of kin can be identified, or no dental records or fingerprints are available, primary identifiers cannot be used [76]. This limitation is especially encountered in mass fatality incidents pertaining to migrants/refugees and in developing countries where many individuals are not formally registered. In such situations a 'circumstantial' identification, based on secondary identifiers may be the only option [77].

Furthermore, in certain contexts, secondary identifiers can be as reliable as primary identifiers. For example, in closed disasters, with a known list of missing persons, a relatively uncommon secondary identifier can be sufficient proof of identity. Consider for instance a car crash with 6 individuals, of which one is a sub-adult. Or a plane crash in which it is known that only one of the victims underwent a total hip replacement and pacemaker insertion. In both situations the presence (or combination of) particular traits rules out all possible identifications but one. As noted, this approach usually requires a limited list of missing persons. In open disasters the approach is more problematic, since there continues to be limited knowledge about the frequency of many anatomical traits, the specificity of a particular secondary identifier cannot, therefore, be calculated. The lack of a standardized method of recording for many secondary identifiers also impacts on the utility. For instance, many secondary identifiers have a level of subjectivity not encountered in more numerical identifiers, such as fingerprints and DNA. When identifications are based on secondary identifiers, it is good practice to retain a DNA sample, nonetheless. This is not only useful to corroborate the identification at a later moment if required, but also to re-associate other fragmented remains that lack any other identifier.

Managing Operations with Fragmented Human Remains

Preservation of human remains following a disaster will be dependent on the type of disaster and the accompanying forces that impact the body. There are, however,

numerous examples of disasters which have resulted in severely fragmented, compromised and/or commingled human remains, and these cases come with specific challenges. Amongst others, the recovery of such remains from the scene requires specialized knowledge, to prevent further commingling, and make sure that the remains are transported in a manner that reduces the risk of further physical damage prior to their arrival at the mortuary [78, 79]. Also, difficult decisions pertaining to the extent and mandate of the identification efforts must be made as soon as possible. For instance, is the aim of the investigation to account for all missing persons, or to identify each fragment? This decision will depend to some extent on the type of disaster (open vs. closed), but also is dependent on political, religious, or ethical consideration. A related decision that must be made at the outset of the DVI operation is the definition of a 'fragment', as no commonly accepted definition exists at this moment in time. Furthermore, the identification of heavily fragmented remains often relies heavily on DNA analysis. The logistical and financial requirements for the sampling, processing and reporting of a large number of DNA samples must therefore be considered.

In recognition of these logistical, practical, and ethical challenges, in 2017, the PASWG developed a series of recommendations specifically related to fragmentary remains as an addition to the general recommendations provided in the INTERPOL DVI Guide. These recommendations included the importance of having a detailed strategy for managing human remains as part of the disaster preparedness plan. This plan promotes establishing: who will advise those responsible for making decisions about fragmentary remains; which experts with expertise in the identification and recovery of human remains should attend the scene; the extent to which post-mortem examination of fragments will be undertaken and ultimately identified, and how information about preservation will be conveyed to families of the victims. The PASWG also developed a dedicated recording form to improve the documentation and utility of fragments in the identification process [80].

The Impact of DVI on DVI Responders

As mentioned above, the debrief following a DVI is of considerable valuable. As well as contributing to the preparedness for future DVI operations, assessing the mental and physical wellbeing of those involved in DVI is of great importance. In recent years, there has been increased attention for the psychological effects of the extraordinary images, stories, and experiences DVI workers may be confronted with. It is now well-recognized that this occupational trauma exposure can adversely impact on a worker's physical health and psychological wellbeing, which in turn, can significantly affect their professional performance and personal life. Naturally, not every worker is affected the same way, and many are not affected at all, but various studies have noted that a considerable percentage (between 1.9 and 24%) of DVI workers experience traumatization [81–85]. The degree of traumatisation seems, amongst other, dependent on both organisational and personal factors, and the degree in which the workers were performing duties that align with their normal

daily profession. Persons who dealt with family members of the dead, or who had not received training in DVI also appeared to be particularly affected. While psychological support is an important welfare support service for those engaged in responding to a disaster, the value of debriefing services is difficult to prove and, counter-intuitively, there have been examples where engagement with debriefing services has increased the stress on particular individuals [86].

The effects of trauma may not manifest directly upon trauma exposure. It is therefore imperative to not only consider psychological support during the actual operation, but also to consider the follow-up after the operation. In this regard, it is important to note that occupational health and safety is always a shared responsibility, between employer and employee.

Summary

The processes involved in attempting to identify a deceased person/s following a disaster are well described in the INTERPOL DVI Guide. As discussed in this chapter, the extent to which the processes can be implemented in full is, to some extent, influenced by the type and scale of the disaster. The success of a DVI requires a collaborative approach and while police-led, forensic medical specialists play an invaluable role. Continued advances in technology will inevitably see improvements in the identification processes and methods and ensure that identifications following a disaster are completed in the timeliest manner as possible.

References

1. International Covenant of Civil and Political Rights, Art. 24(2), 999 U.N.T.S. 171;(1966).
2. Universal Declaration of Human Rights, G.A.
3. Blau S, Hill T. Disaster victim identification: a review. Minerva Medicoleg. 2009;129:35–46.
4. Ranson D. The role of forensic pathology in bereavement support and in promoting public health through a modern medical death investigation system. Grief Matters Austr J Grief Bereavem. 2016;19(2):41–6.
5. Interpol. Interpol Disaster Victim Identification Guide. Interpol Working Group on Disaster Victim Identification;2018.
6. Sweet OCD. INTERPOL DVI best-practice standards—An overview. Forens Sci Int. 2010;201(1):18–21.
7. Jackson G, Jones S, Booth G, Champod C, Evett IW. The nature of forensic science opinion—a possible framework to guide thinking and practicce in investigation and in court proceedings. Sci Justice. 2006;46(1):33–44.
8. Berger EH, van Wijk M, de Boer HH. Bayesian inference in personal identification. In: Obertová Z, Stewart S, Cattaneo C, editors. Statistics and probability in forensic anthropology. London: Academic Press;2020. p. 326–37.
9. Mundorff AZ, Black S, Blau S, Drawdy SM, Kosalka Shore RC. Disaster Victim Management—the role of the anthropologist. In: Payne-James J, Byard RW, editors. Encyclopedia of Forensic and Legal Medicine. 2nd ed. London: Elsevier; 2016. p. 288–304.

10. Mundorff AZ. Anthropologist-directed triage: three distinct mass fatality events involving fragmentation of human remains. In: Adams B, Byrd J, editors. Recovery, Analysis, and Identification of Commingled Human Remains. Totowa: Humana Press; 2008. p. 123–44.
11. O'Donnell C, Iino M, Mansharan K, et al. Contribution of postmortem multidetector CT scanning to identification of the deceased in a mass disaster: experience gained from the 2009 Victorian bushfires. Forensis Sci Int. 2011;205:15-28.
12. Iino M, Aoki Y. The use of radiology in the Japanese tsunami DVI process. J Forensic Radiol Imaging. 2016;4:20–6.
13. Taylor J. A brief history of forensic odontology and disaster victim identification practices in Australia. J Forensic Odontostomatol. 2009;27(2):64–74.
14. Zikir A, Manica S. Forensic dentistry and disaster victim identification (DVI) in Indonesia. Aust J Forensic Sci. 2021;53(1):75–83.
15. de Souza MA, Urtiaga GdO, Ferreira RCG, da Silva LM, Umbelino JKG, de Melo FR, et al. Friction ridge analysis in disaster victim identification (DVI): Brazilian case studies. Forensic Sci Res. 2021:1–7.
16. Montelius K, Lindblom B. DNA analysis in disaster victim identification. Forensic Sci Med Pathol. 2012;8(2):140–7.
17. De Valck E. Major incident response: collecting ante-mortem data. Forensic Sci Int. 2006;159:S15–9.
18. Forrest A. Forensic odontology in DVI: current practice and recent advances. Forensic Sci Res. 2019;4(4):316–30.
19. Kahana T, Grande A, Tancredi DM, Penalver J, Hiss J. Fingerprinting the deceased: traditional and new techniques. J Forensic Sci. 2001;46(4):908–12.
20. Sozer AC. DNA analysis for missing person identification in mass fatalities. Boca Raton: CRC Press; 2014.
21. Bassed R, Leditschke J. Forensic medical lessons learned from the Victorian bushfire disaster: recommendations from the phase 5 debrief. Forensic Sci Int. 2011;205:73–6.
22. Winskog C, Tonkin A, Byard RW. The educational value of disaster victim identification (DVI) missions—transfer of knowledge. Forensic Sci Med Pathol. 2012;8(2):84–7.
23. Archer F, Spencer C, McArdle D, Cross S, Boyd L. Emergency management evaluations: beyond the lessons-learned paradigm. Austr Emerg Manag Instit;2021. 33–4.
24. Landahl MR, Muffet-Willett SL. Preparedness and planning for law enforcement operations. In: Landahl MR, Thornton TE, editors. The role of law enforcement in emergency management and homeland security. Community, environment and disaster risk management, vol. 24, Emerald Publishing Limited;2021. p. 171–91.
25. Blau S, Robertson S, Johnston M. Disaster Victim Identification: new applications for postmortem computed tomography. J Forensic Sci. 2008;53(4):1–6.
26. Wright K, Mundorff A, Chaseling J, Forrest A, Maguire C, Crane DI. A new disaster victim identification management strategy targeting "near identification-threshold" cases: experiences from the Boxing Day tsunami. Forensic Sci Int. 2015;250(null):91–7.
27. Przybyłowski M. Problematic aspects of the identification of the dead bodies of aviation crash victims in Poland. The role of the forensic medicine expert in an external examination group and a Disaster Victim Identification (DVI) team. Arch Med Sadowej Kryminol. 2020;70(2–3):136–48.
28. Arrighi E, Charlot AM. Identifying terrorist attack victims. Forensic Sci Res. 2020;5(3):236–41.
29. Cordner SM, Woodford N, Bassed R. Forensic aspects of the 2009 Victorian bushfires disaster. Forensic Sci Int. 2011;205(1–3):2–7.
30. Winskog C, Tsokos M, Byard RW. The progression from disaster victim identification (DVI) to disaster victim management (DVM): a necessary evolution. Forensic Sci Med Pathol. 2012;8(2):81–3.
31. Acharya J, Shrestha R, Shrestha PK, Kanchan T, Krishan K. When protocols become fairy tales and gods remain buried under: excerpts from the diary of forensic experts at Ground Zero during the Mega Quake that hit Nepal. Am J Forensic Med Pathol. 2017;38(1):5–8.

32. Lovell D, Vella K, Muñoz Sáez D, McKague M, Brereton M, Ellis P. Exploring technologies to better link physical evidence and digital information for disaster victim identification. Forensic Sci Res. 2022.
33. Olivieri L, Mazzarelli D, Bertoglio B, De Angelis D, Previderè C, Grignani P, et al. Challenges in the identification of dead migrants in the Mediterranean: the case study of the Lampedusa shipwreck of October 3rd 2013. Forensic Sci Int. 2018;285:121–8.
34. Reinke R, Anderson BE. Missing in the US–Mexico Borderlands. In: Congram D, editor. Missing persons: multidisciplinary perspectives on the disappeared. Toronto: Canadian Scholars' Press; 2016. p. 249–68.
35. Ranson D. The loss of Malaysia Airlines Flight MH17: a forensic and humanitarian task. J Law Med. 2015;22(4):745–50.
36. Ramesh AC, Kumar S. Triage, monitoring, and treatment of mass casualty events involving chemical, biological, radiological, or nuclear agents. J Pharm Bioallied Sci. 2010;2(3):239–47.
37. Jacocks J, Danley R, Green L, Gavin M. Consequence management–what do we do with the contaminated dead. Joint Center Operat Anal J. 2008;11(1):53–60.
38. Rutty GN, Robinson C, Morgan B, Black S, Adams C, Webster P. Fimag: the United Kingdom disaster victim/forensic identification imaging system. J Forensic Sci. 2009;54(6):1438–42.
39. Anon. Guiding principles for the dignified management of the dead in humanitarian emergencies and to prevent them becoming missing persons. ICRC;2020.
40. Anon. Disaster Victim Identification (DVI) INTERPOL. 2022. https://www.interpol.int/en/How-we-work/Forensics/Disaster-Victim-Identification-DVI.
41. Ellis P. Modern advances in disaster victim identification. Taylor & Francis;2019. p. 291–2.
42. Levinson J, Domb A. Applying new police technologies to disaster victim identification. Forensic Res Criminol Int J. 2016(5).
43. Mohd Daud SMS, Mohd Yusof MYP, Heo CC, Khoo LS, Chainchel Singh MK, Mahmood MS, et al. Applications of drone in disaster management: a scoping review. Sci Just J Forensic Sci Soc. 2022;62(1):30–42.
44. Brough AL, Morgan B, Rutty GN. The basics of disaster victim identification. J Forensic Radiol Imaging. 2015;3(1):29–37.
45. Rutty GN, Alminyah A, Cala A, Elliott D, Fowler D, Hofman P, et al. Use of radiology in disaster victim identification: positional statement of the members of the disaster victim identification working group of the international society of forensic radiology and imaging; May 2013. J Forensic Radiol Imaging. 2013;1(4):218.
46. O'Donnell C, Iino M, Mansharan K, Leditscke J, Woodford N. Contribution of postmortem multidetector CT scanning to identification of the deceased in a mass disaster: experience gained from the 2009 Victorian bushfires. Forensic Sci Int. 2011;205(1–3):15–28.
47. De Boer HH, Maat GJR. The Dutch approach in Disaster Victim Identification. J Forensic Med Conflict Disast Human Situat. 2016;59(1):85–91.
48. de Jong LW, Legrand L, Delabarde T, Hmeydia G, Edjlali M, Hamza L, et al. Experience with postmortem computed tomography in the forensic analysis of the November 2015 Paris attacks. Forensic Sci Res. 2020;5(3):242–7.
49. Rutty GN, Biggs MJP, Brough A, Morgan B, Webster P, Heathcote A, et al. Remote postmortem radiology reporting in disaster victim identification: experience gained in the 2017 Grenfell Tower disaster. Int J Legal Med. 2020;134:637–43.
50. Hofman P, Alminyah A, Apostol M, Boel LWT, Brough A, Bouwer H, et al. Use of postmortem computed tomography in disaster victim identification. Updated positional statement of the members of the disaster victim identification working group of the International Society of Forensic Radiology and Imaging; July 2019. J Forensic Radiol Imaging 2019;19:100346.
51. Souza LA Jr, Marana AN, Weber SAT. Automatic frontal sinus recognition in computed tomography images for person identification. Forensic Sci Int. 2018;286:252–64.
52. Mundorff AZ, Vidoli G, Melinek J. Anthropological and radiographic comparison of vertebrae for identification of decomposed human remains. J Forensic Sci. 2006;51(5):1002–4.
53. Verna E, Piercecchi-Marti MD, Chaumoitre K, Bartoli C, Leonetti G, Adalian P. Discrete traits of the sternum and ribs: a useful contribution to identification in forensic anthropology and medicine. J Forensic Sci. 2013;58(3):571–7.

54. Verna E, Piercecchi-Marti MD, Chaumoitre K, Adalian P. Relevance of discrete traits in forensic anthropology: from the first cervical vertebra to the pelvic girdle. Forensic Sci Int. 2015;253(134):e1-7.
55. Rutty G, Alminyah A, Apostol M, Boel L, Brough A, Bouwer H, et al. Positional Statement radiology disaster victim identification reporting forms. J Forensic Radiol Imaging 2018;15.
56. Pretty IA, Sweet D. A look at forensic dentistry–Part 1: the role of teeth in the determination of human identity. Br Dent J. 2001;190(7):359–66.
57. Al-Amad SH. Dental evidence as a sole human identifier in world disasters. A literature review with emphasis on the 2004 tsunami disaster. Arab J Forensic Sci Forensic Med. 2018;1(7).
58. Nguyen E, Doyle E. Dental post-mortem computed tomography for disaster victim identification: a literature review. J Forensic Radiol Imaging. 2018;13:5–11.
59. Thali MJ, Markwalder T, Jackowski C, Sonnenschein M, Dirnhofer R. Dental CT imaging as a screening tool for dental profiling: advantages and limitations. J Forensic Sci. 2006;51(1):113–9.
60. Heinrich A, Schwark T, Simeoni E, Wurmb-Schwark N. Genetic identification of fire deaths. Forensic Sci Int Genet Suppl Ser. 2009;2:253–4.
61. Owen R, Bedford P, Leditschke J, Schlenker A, Hartman D. Post mortem sampling of the bladder for the identification of victims of fire related deaths. Forensic Sci Int. 2013;233(1–3):14–20.
62. de Boer HH, Maat GJR, Kadarmo DA, Widodo PT, Kloosterman AD, Kal AJ. DNA identification of human remains in Disaster Victim Identification (DVI): an efficient sampling method for muscle, bone, bone marrow and teeth. Forensic Sci Int. 2018;289:253–9.
63. Turingan RS, Brown J, Kaplun L, Smith J, Watson J, Boyd DA, et al. Identification of human remains using Rapid DNA analysis. Int J Legal Med. 2020;134(3):863–72.
64. Cornelis S. Forensic Lab-on-a-Chip DNA analysis. Ghent University;2019.
65. Erlich H, Calloway C, Lee SB. Recent developments in forensic DNA technology. In: Erlich H, Stover E, White TJ, editors. Silent witness: forensic DNA analysis in criminal investigations and humanitarian disasters. Oxford: Oxford University Press; 2020. p. 105–27.
66. Wickenheiser R, Sozer A. Disaster Victim Identification (DVI): rapid DNA response operations workshop. Forensic Sci Int Synergy. 2019;1:S1–2.
67. Tamisier L, Nicolas T, Prat L, Malo M, Ledroit P. The fingerprint disaster victim identification toolkit: from powder to biometrics. JFI. 2019;69:2019–413.
68. Knobel GJ. Taking fingerprints from a decomposed body using the "indirect cadaver hand skin-glove method." S Afr Med J. 2005;95(9):665–6.
69. Johnson BT, Riemen JAJM. Digital capture of fingerprints in a disaster victim identification setting: a review and case study. Forensic Sci Res. 2019;4(4):293–302.
70. Bikker J. Disaster victim identification in the information age: the use of personal data, post-mortem privacy and the rights of the victim's relatives. SCRIPTed. 2013;10:1(1):57.
71. Alsalamah S, Alqahtani S, Aschheim K, Alimam A, AlAdullatif A, AlAmri A, et al. Towards a unified blockchain-based dental record ecosystem for disaster victims identification. 2019.
72. Torpet LA. DVI System International: software assisting in the Thai tsunami victim identification process. J Forensic Odontostomatol. 2005;23(1):19–25.
73. Slooten K. Validation of DNA-based identification software by computation of pedigree likelihood ratios. Forensic Sci Int Genet. 2011;5(4):308–15.
74. Salado Puerto M, Abboud D, Baraybar JP, Carracedo A, Fonseca S, Goodwin W, et al. The search process: Integrating the investigation and identification of missing and unidentified persons. Forensic Sci Int Synerg. 2021;3: 100154.
75. de Boer HH, Obertová Z, Cunha E, Adalian P, Baccino E, Fracasso T, et al. Strengthening the role of forensic anthropology in personal identification: Position statement by the Board of the Forensic Anthropology Society of Europe (FASE). Forensic Sci Int. 2020;315: 110456.
76. Blau S. Missing persons investigations and identification: Issues of scale, infrastructure, and political will. In: Morewitz SJ, Sturdy Colls C, editors. Handbook of Missing Persons. Switzerland: Springer; 2016. p. 227–35.

77. Baraybar J-P. When DNA is not available, can we still identify people? Recommendations for best practice. J Forensic Sci. 2008;53(3):533–40.
78. Blau S, Sterenberg J. The use of forensic archaeology and anthropology in the search and recovery of buried evidence. In: Payne-James J, Byard R, editors. Encyclopaedia of forensic and legal medicine. 2nd ed. London: Elsevier; 2015. p. 236–45.
79. Dirkmaat DC. Forensic anthropology at the mass fatality incident (commercial airliner) crash scene. In: Dirkmaat DC, editor. A companion to forensic anthropology. Chichester: John Wiley and Sons;2012. p. 136–56.
80. de Boer HH, Roberts J, Delabarde T, Mundorff A, Blau S. Disaster victim identification operations with fragmented, burnt, or commingled remains: experience-based recommendations. Forensic Sci Res. 2020;5(3):191–201.
81. Gabriel R, Ferrando L, Cortón ES, Mingote C, García-Camba E, Liria AF, et al. Psychopathological consequences after a terrorist attack: an epidemiological study among victims, the general population, and police officers. Eur Psychiatry. 2007;22(6):339–46.
82. Perrin MA, DiGrande L, Wheeler K, Thorpe L, Farfel M, Brackbill R. Differences in PTSD prevalence and associated risk factors among World Trade Center disaster rescue and recovery workers. Am J Psychiatry. 2007;164(9):1385–94.
83. Misra M, Greenberg N, Hutchinson C, Brain A, Glozier N. Psychological impact upon London Ambulance Service of the 2005 bombings. Occup Med (Lond). 2009;59(6):428–33.
84. Wilson LC. A systematic review of probable posttraumatic stress disorder in first responders following man-made mass violence. Psychiatry Res. 2015;229(1–2):21–6.
85. Motreff Y, Baubet T, Pirard P, Rabet G, Petitclerc M, Stene LE, et al. Factors associated with PTSD and partial PTSD among first responders following the Paris terror attacks in November 2015. J Psychiatr Res. 2020;121:143–50.
86. Deahl M. Psychological debriefing: controversy and challenge. Aust N Z J Psychiatry. 2000;34(6):929–39.

Chapter 7
Examining an Already Autopsied or Exhumed Body

Krzysztof Jerzy Woźniak, Artur Moskała, Marta Barszcz, and Ewa Rzepecka-Woźniak

Introduction

Experienced forensic pathologists would acknowledge that the outcome of a case cannot be predicted with any certainty at the initial stage of the investigation. What may initially present as a complicated case requiring a lengthy autopsy examination with extended procedures may be resolved through autopsy without the need for further opinion. On the other hand, what appeared to be an uncomplicated case at the beginning may raise additional questions during the course of examination requiring additional investigation or opinion. Additional pieces of evidence may cause one to consider or undertake supplementary analyses, including the use of unpredicted kinds of evidence. This chapter considers the value of the further examination of a body that has already undergone an invasive autopsy as well as the examination of the exhumed body.

It is not the responsibility of a forensic pathologist to decide about the nature or extent of the forensic post-mortem examination although, depending upon where they work in the world, they may contribute to the decision-making process. The final decision is made by the relevant legal authority which for many but not all countries around the world is by a magistrate. Each country will likely have legislation related to the medico-legal examination of the dead. As an example, for the authors own

K. J. Woźniak (✉) · A. Moskała · M. Barszcz · E. Rzepecka-Woźniak
Department of Forensic Medicine, Jagiellonian University Medical College, Grzegórzecka 16, 31-531 Kraków, Poland
e-mail: krzys.wozniak@uj.edu.pl

A. Moskała
e-mail: artur.moskala@uj.edu.pl

M. Barszcz
e-mail: marta.barszcz@doctoral.uj.edu.pl

E. Rzepecka-Woźniak
e-mail: ewa.rzepecka-wozniak@uj.edu.pl

G. N. Rutty (ed.), *Essentials of Autopsy Practice*,
https://doi.org/10.1007/978-3-031-11541-7_7

country of work this is covered by Chap. 23 ("Inspection. Post Mortem. Procedural Experiment") of the Code of Criminal Procedure Act of 6 June 1997 of the Republic of Poland [1]:

"Article 209.

§ 1. *If it in suspected that death has been caused by criminal means, an examination of the corpse and an autopsy shall be ordered.*

§ 2. *An examination of the corpse shall be conducted by a state prosecutor, and, in court proceedings—the court, with the participation of a physician who is whenever possible a specialist in forensic medicine. In cases not amenable to delay, the examination is done by the Police with an obligation to notify the state prosecutor without delay.*

§ 3. *The examination of the corpse shall be done at the place of its discovery. Before the arrival of an expert, a state prosecutor or the court, the corpse may be moved or relocated only in exigent circumstances.*

§ 4. *An autopsy should be made by an expert with the state prosecutor or the court present (…)*

§ 5. *If necessary, a physician who has recently treated the deceased may be summoned to be present at the examination of the corpse and the autopsy, in addition to the court expert. The expert shall then prepare an opinion about the examination and autopsy (…)*

Article 210.

§ 1. *In order to conduct an examination of the corpse or an autopsy, adisinterment (exhumation) may be ordered by the state prosecutor or the court."*

It seems obvious that due to economical and organizational issues it is impossible to perform a forensic post-mortem examination for every death. A thorough inspection of the place of where the body was discovered may offer a good bases for the relevant decision of directing a body to forensic autopsy examination. However, in some countries this may still prove problematic due to bias and economic pressure placed upon the public prosecutor's office.

One problem that may be encountered is a relative paucity of specialists in the field of forensic medicine. Again, using Poland as an example, for a country of approximately 38 million citizens, there are only about 150 forensic medical specialists [2]. Because of this in a considerable number of cases, especially in more remote areas to university centres, forensic medical duties may be fulfilled by another specialists. This can result in a risk of diagnostic error [3], (Fig. 7.1).

In any society it is inevitable that unless every deceased person is subject to invasive forensic autopsy that a proportion of homicides will go undetected. If the original autopsy is not to a forensic standard, even if the entire deceased population was autopsied then homicides would still be missed. We know this from the experience of pre-cremation examinations in Germany [4] and a dip sample audit of second autopsies undertaken in the United Kingdom [5].

A consequence of this is that there is a potential necessity to perform a re-examination of the body i.e., a so-called "*second autopsy*". This examination may

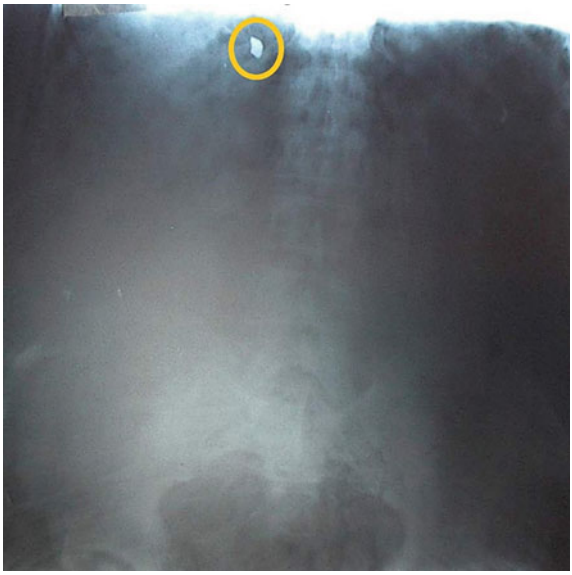

Fig. 7.1 A conventional X-ray of the torso of an exhumed corpse a couple of months after death (and primary autopsy), showing the presence of a foreign body—an out-shaped projectile (encircled) lodged inside the brain which was put in the body cavity during body restoration. The primary autopsy was performed by a general pathologist, who outlined craniocerebral injuries as referring to the appliance of a blunt force

discover important evidence missed at the first examination. Depending upon the case, the main purpose of the second autopsy or a post mortem of an exhumed corpse may be limited such as to obtain samples for: DNA profiling (ex. disputed paternity/maternity cases, doubtful previous body identification) [6, 7], toxicological investigation (due to lack of material already secured), physicochemical analyses regarding explosives, forensic science weapon identification (ex. fractured bones' pieces, lodged foreign objects) [8–10].

General Limitations

It is a duty of a forensic pathologist to fully describe the body's external and internal condition related to the primary autopsy examination procedures [11]. This is important as the first invasive autopsy examination will limit the opportunities to reassess the contents of the body cavities fluid and gas spaces as well as structures such as the ventricles of the brain, stomach, gall bladder, intestines and urinary bladder the integrity of which will be changed by the first examination. The anatomical structure of the internal organs may be extensively altered by the primary examination procedures including previous collecting of specimens for further laboratory analyses. The primary examination may affect the interpretation of broken bones and presence and location of foreign bodies. Sometimes the primary autopsy examination may be so

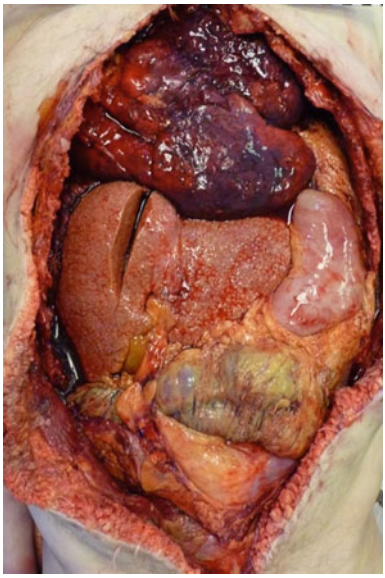

Fig. 7.2 An example of a primary autopsy where there has been limited examination such that the internal organs are practically unexamined

limited and the conclusions drawn questionable that a secondary autopsy examination is required to address the inadequacies of the first examination and undertake the examination that should have been undertaken in the first place (Fig. 7.2). With the passage of time between the primary and second autopsy, decomposition may affect the identification and interpretation of findings that were or could have been observed at the first autopsy [12]. In cases where cremation of the body was performed, all possibilities are lost forever.

Application of Post-mortem Procedures—Their Potential Gains and Weaknesses

Post-mortem Imaging—Radiology—Post-mortem Computed Tomography (PMCT)

Even with the variety of abovementioned limitations there are still possibilities of discovering important evidence through a second examination. In cases of exhumed bodies which have not undergone an autopsy examination, even in the presence of advanced decomposition, it is still possible to perform post-mortem computed tomography (PMCT), even with the use of contrast medium (CA) administration [13, 14]. CA administration and performance of PMCT angiography (PMCTA) can reveal

additional findings such as organ/vessel rupture or malformations. Before the application of CA, it is recommended to perform an unenhanced PMCT examination first. Even in cases of previously autopsied bodies, it is advised to perform unenhanced PMCT first as this will inform the examiner as to the general state of the remains and provide information regarding the nature and extent of the previous examination procedures (Fig. 7.3), as well as provide information related to body identification, bone fractures (Fig. 7.4) and previously unidentified metal foreign objects (Fig. 7.5). It is good practice to perform the imaging prior to opening the transportation bag. Due to post-mortem alteration (which may be estimated with the use of the so-called "*RAI—index*" [15]) it may be more problematic to find injuries of smaller bones (ex. both hands and feet), especially due to the fact that the post-mortem processes may influence the loss of soft tissue continuity. It is rather unlikely that we could be successful in the evaluation of soft tissues—perhaps the only possible findings identified would be changes due to calcification of the aorta, coronary arteries etc.

Even when post-mortem imaging methods are applied during the primary examination of the corpse, it is still recommended to perform a PMCT examination at the second examination for the purpose of registration of the state of the corpse before opening the transportation bag. This can be achieved even when the remains are within a metal coffin, as confirmed during the Smolensk plane crash investigation by Professor Grzegorz Teresiński [16].

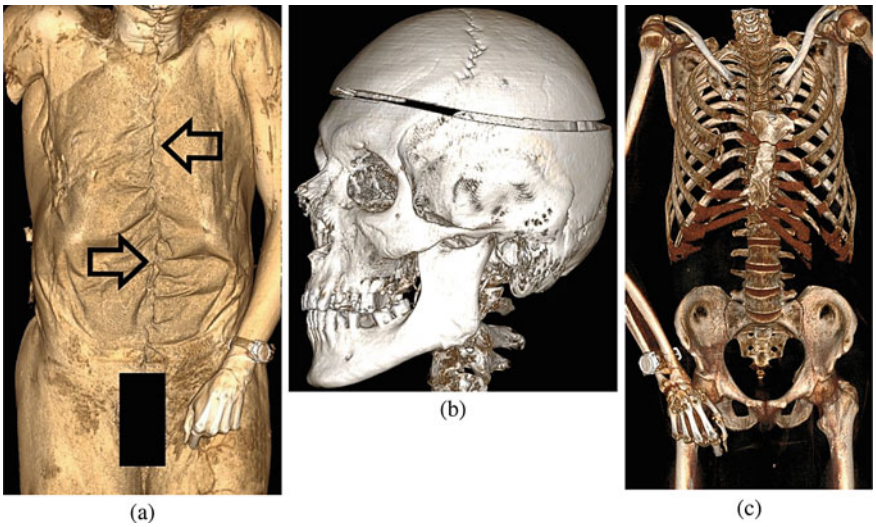

Fig. 7.3 PMCT imaging of previously autopsied cadavers. **a** 3D surface image showing the sutured midline opening of the chest and abdomen. **b** 3D cranial bone image showing the site of opening of the cranial cavity. **c** 3D bone reconstruction showing displacement of the sternum due to opening of the ribcage

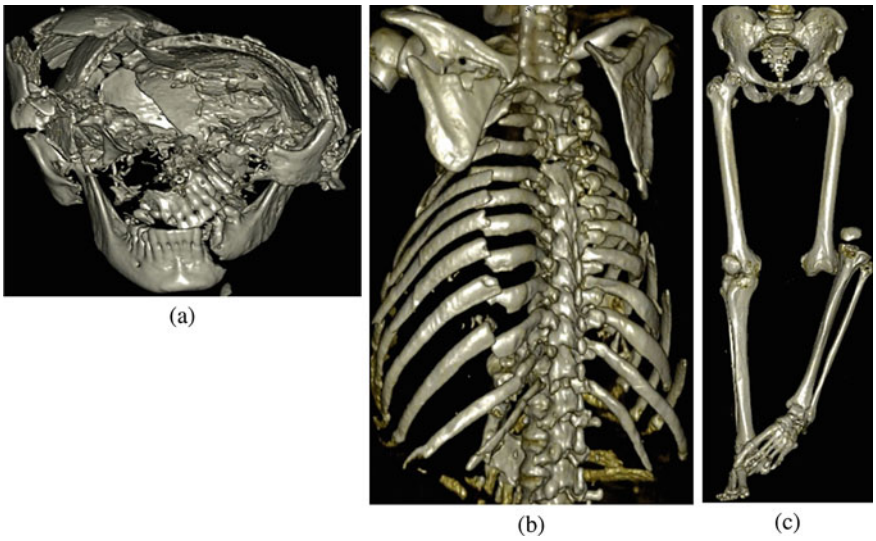

Fig. 7.4 PMCT imaging of 3D bone reconstructions of skeletal injuries sustained in a high energy transportation incident in a previously examined cadaver. **a** Cranial bone disruption. **b** Bilateral posterior rib fractures, upper thoracic spine disruption and fractures of both scapulae. **c** Disruption of the left knee joint anatomy

Conventional Autopsy Examination—External Examination

On occasion the secondary autopsy examination will be performed a short time after primary procedures. Under such circumstances the opportunity to revisit the external body injuries is quite high. However due to the previous autopsy and cosmetic procedures for example washing the body, reconstruction and changes due to drying the appearances of any external findings may alter. Unfortunately, the chances for successful identification and recovery of subtle material evidence will have been lost for example due to the removal of clothing or washing of the body during the primary autopsy external examination. The examiner however must not make this assumption or neglect a normal order of examination—a meticulous, unbiased approach to the examination is still valid.

In the case of exhumed bodies without previous autopsy, in most situations late post mortem changes will influence the examination and findings. External abrasions and bruises may be lost completely. Changes to the skin due to post mortem alteration processes are to be expected. Wounds may remain visible although with more advanced late post mortem changes and fragility of tissues it may be problematic to

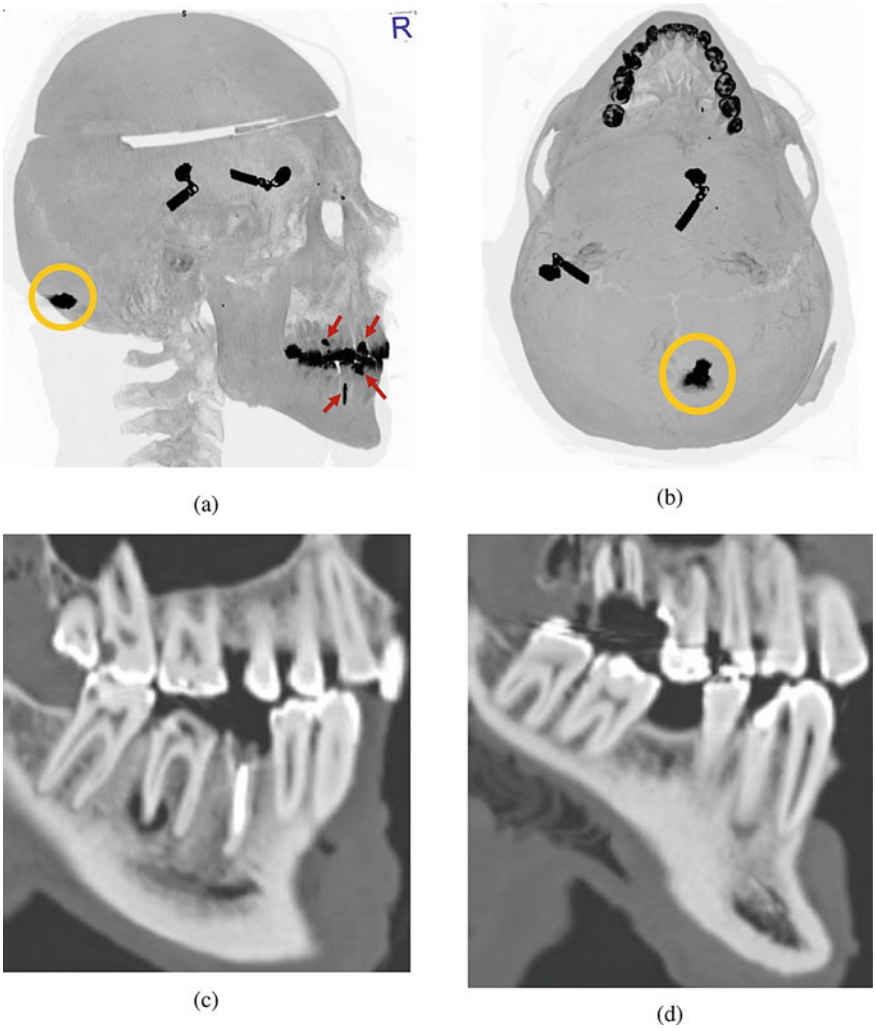

Fig. 7.5 **a** and **b** PMCT 3D MIP images showing the position of a metal projectile (circle) within the occipital region of the skull in a previously autopsied cadaver where the brain had been removed. Also seen are two zips (central skull) related to fabric filling of the cranial cavity for the purpose of cosmetic restoration after primary autopsy as well as dental restoration to the teeth of the upper and lower jaw (arrows). **c** and **d** illustrate magnified views of the dental restoration

determine their nature and exclude that they are not simply post mortem changes or artefacts. These can still be sampled for histopathological examination including the use of special staining methods.

Conventional Autopsy Examination—Internal Examination

As discussed above, the procedures of the primary autopsy will affect the assessment of body cavity gas/fluid content. When the timeframe between the primary and secondary examination is short then there remains the opportunity to re-examine the internal organs. However, with the passage of time and the effect of the previous autopsy procedures (missing parts from tissue sampling, fragmentation) as well as post-mortem alteration this task becomes more challenging [17, 18], (Fig. 7.6).

Specimens Obtained for Further Evaluation

Material for Physicochemical Examination

Obtaining specimens where there has been the potential use of explosives and firearms is a specialist area of evidence recovery. It requires collaboration with dedicated specialists, which may be from the uniformed services. Relevant procedures should be conducted at the beginning of examination activities by appropriately trained individuals ideally in the presence of the forensic pathologist.

Fig. 7.6 A putrefied body **a**, please note almost completely "liquified" soft tissues of the head due to late post-mortem processes; autopsy specimen in the same case **b**—the border between the stomach and duodenum: a deep ulceration which was combined with the high volume of blood clots inside intestines, giving the clarification of the cause of death due to a disease

Specimens for DNA Sampling

Throughout the stages of post-mortem alteration, there are opportunities for collecting a variety of material for DNA analysis [19–22]. Fresh corpses may still present the possibility of sampling blood depending upon the extent of the first examination. There is a wide variety of other materials which can be used for DNA analysis including hair, deep muscle, teeth (preferably without previous medical intervention), pieces of shafts of long bones, small bones and rib cartilages, even fingernails and other pieces of soft tissue. It is recommended to adhere to one's local DNA laboratory needs, and that the assistance of a laboratory worker during sampling should be considered.

In cases of previously autopsied bodies the examiner should be aware of the risk of contamination. It may even be the case that the internal organs may have their origin from another individual. Thus it is advisable to collect samples from regions that were not autopsied earlier.

Samples for Toxicological Investigation

Modern toxicological investigation methods prefer body fluid analysis. In cases of fresh bodies, it may be still possible to obtain blood from distal vessels, especially from the limbs. At different stages of post-mortem alteration regarding corpses without previous autopsy examination it may be possible to obtain blood, urine, bile, and gastric content. Intraocular or cerebrospinal fluid however become unobtainable with the passage of time. Again, as with DNA sampling, it is advisable to adhere to the needs of the toxicology laboratory as to which biological material can be utilized for examination [23–26].

Microscopic Evaluation of Specimens Including Special Staining Methods

Results of forensic medical post-mortem examination are based not only on gross anatomy diagnosis. It is also important to support the conclusions of the examination through the microscopic examination of relevant samples.

In cases regarding corpses without excessive late post-mortem alterations such evaluation may not differ considerably from opportunities available at the primary autopsy examination. Due to the effect of late post-mortem changes it may be problematic to identify viable tissue for histological sampling, specifically in the case of smaller internal organs such as the thyroid gland. Missing parts of tissues due to previous autopsy procedures may also limit diagnostic opportunities. Specimens that are taken for evaluation may be examined using traditional histochemical staining as

well as special staining methods, including immunohistochemistry methods such as glycophorin A (GPA) as a marker of bleeding by using anti-human GPA monoclonal antibody immunohistochemically [27], (Figs. 7.7 and 7.8).

Material for Microbiological Evaluation

In both situations of previously autopsied and/or exhumed corpses it is problematic to distinguish between a real pathogen and postmortem body saprophytes through microbiology examination. Prior to undertaking such an examination it is recommended that the microbiology laboratory is consulted with regards to the realistic chances of gaining a meaningful result through such an examination [30].

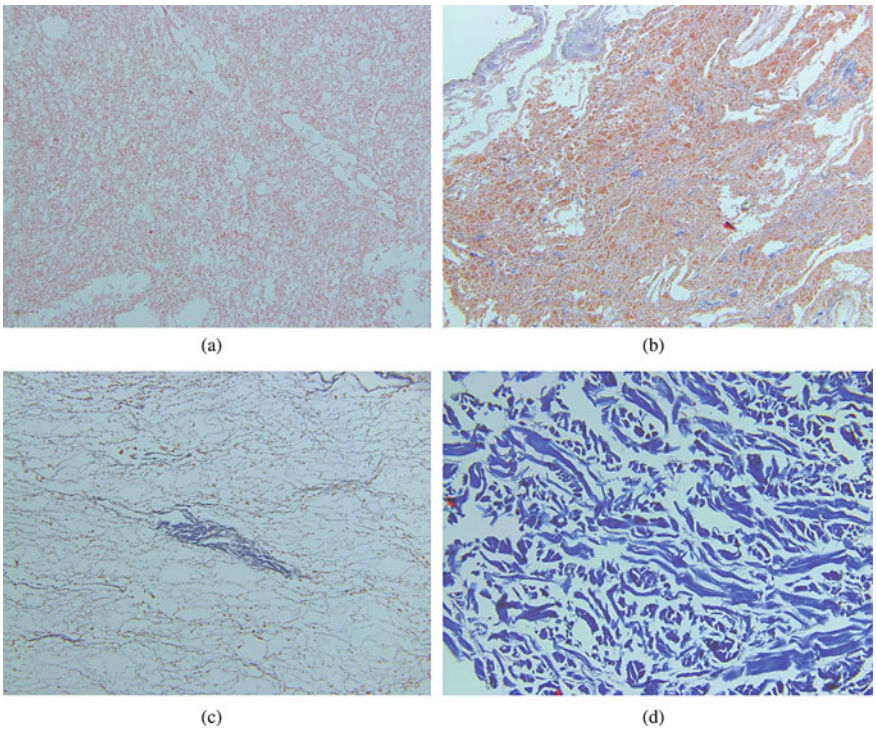

Fig. 7.7 Histopathological specimens of soft tissues obtained during the first post-mortem examination of an exhumed corpse after about 65 years from the time of death [28, 29]. The body seemed to be fixed after death for a long-distance naval transportation, then was buried in an earth grave and finally, in a tomb for the last period of 15 years before examination: **a** the brain, magnification 400x; **b** the heart, magnification 200x; **c** the liver, magnification 200x; **d** the skin, magnification 200x. Masson's trichrome staining

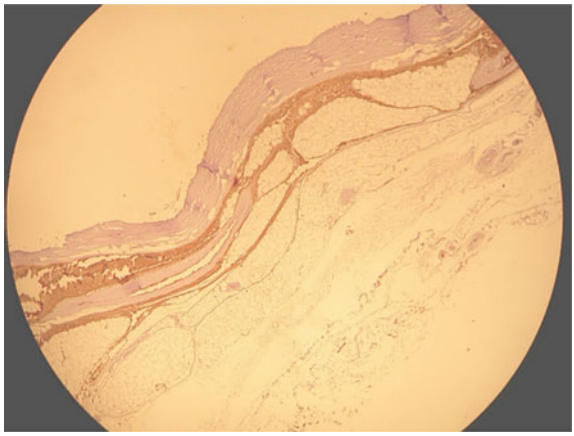

Fig. 7.8 Positive immunohistochemical staining against glycophorin A (GPA) as a marker of bleeding within a tissue sample derived from the dorsal side of the hand obtained during a second autopsy undertaken several years after the death. Magnification 40x

Material for Criminalistics (Mechanoscopy)

It may be that fragments of broken bones and/or foreign bodies [31] remain in the body (Figs. 7.1 and 7.5) and thus constitute a vital piece of evidence, especially if a previous examination has not identified this evidence or has not given appropriate consideration to such findings. As discussed above the examination of the body with PMCT is an essential step in trying to identify such potential evidence within the body.

Presentation of Findings

It is important to present the results of post mortem examination in an objectified, comprehensive written report that details the procedures and findings including traumatic injuries, natural disease, and post-mortem alterations. The findings can be captured and presented through conventional autopsy photography, and reconstructions based on the results of post-mortem imaging acquisition [32–36]. In cases of previously autopsied corpses where the competency of the original pathologist is in question then the report, photographs and PMCT images can be used to support one's observations and opinion.

Summary

The examination of already autopsied and/or exhumed bodies is one of the biggest challenges in forensic medicine and requires vast knowledge and experience of a forensic pathologist. Unfortunately, in a considerable number of cases it cannot

recover all diagnostic opportunities. Hence, the most important aspect of such examination is to be aware of all its limitations and pitfalls. Almost all procedures that are used in a standard forensic post-mortem examination can be used in cases of already autopsied and/or exhumed bodies. However, the results should be very carefully and critically analysed to avoid misinterpretation and false conclusions.

References

1. Code of Criminal Procedure of the Republic of Poland Act of 6 June 1997. https://www.legislationline.org/documents/action/popup/id/17669.
2. Naczelna Izba Lekarska, Zestawienie nr 04. https://nil.org.pl/uploaded_files/1641220880_za-grudzien-2021-zestawienie-nr-04.pdf.
3. Gunasekera RS, Brown AB, Costas EH. Tales from the grave: opposing autopsy reports from a body exhumed. J Forensic Leg Med. 2012;19(5):297–301. https://doi.org/10.1016/j.jflm.2012.02.011.
4. Behrens LM, Sperhake J-P, Püschel K, Schröder AS. The postmortem examination prior to cremation: still a necessary safety measure? Leg Med (Tokyo). 2020;43: 101664. https://doi.org/10.1016/j.legalmed.2019.101664.
5. Jones D. Fatal call-getting away with murder: a study into influences on decision making at the initial scene of unexpected death. The doctoral thesis, School of Criminology and Criminal Justice, University of Portsmouth;2016. https://researchportal.port.ac.uk/en/studentTheses/fatal-call-getting-away-with-murder.
6. Dorozynski A. Yves Montand to be exhumed to test paternity. BMJ. 1997;315(7120):1398. https://doi.org/10.1136/bmj.315.7120.1397b.
7. Ossowski A, Kuś M, Kupiec T, Bykowska M, Zielińska G, Jasiński ME, March AL. The Polish genetic database of victims of totalitarianisms. Forensic Sci Int. 2016;258:41–9. https://doi.org/10.1016/j.forsciint.2015.10.029.
8. Szleszkowski Ł, Thannhäuser A, Szwagrzyk K, Kawecki J, Jurek T. Gunshot wounds (resulting from execution) of exhumed victims of the communist regime in Poland. Leg Med (Tokyo). 2014;16(4):201–7. https://doi.org/10.1016/j.legalmed.2014.03.009.
9. Szleszkowski Ł, Thannhäuser A, Szwagrzyk K, Jurek T. The possibility of establishing causes of death on the basis of the exhumed remains of prisoners executed during the communist regime in Poland: the exhumations at Powązki Military Cemetery in Warsaw. Int J Legal Med. 2015;129(4):801–6. https://doi.org/10.1007/s00414-014-1084-z.
10. Wojciechowski A, Fudalej M, Skowronek P. Assessment of head gunshot wounds by means of post-mortem computed tomography in exhumed anonymous cadaver. BJR Case Rep. 2016;2(4):20150304. https://doi.org/10.1259/bjrcr.20150304.
11. Ríos L, Martínez B, García-Rubio A, Herrasti L, Etxeberria F. Marks of autopsy and identification of victims of human rights violations exhumed from cemeteries: the case of the Spanish Civil War (1936–1939). Int J Legal Med. 2014;128(5):889–95. https://doi.org/10.1007/s00414-013-0896-6.
12. Varlet V, Bruguier C, Grabherr S, Augsburger M, Mangin P, Uldin T. Gas analysis of exhumed cadavers buried for 30 years: a case report about long time alteration. Int J Legal Med. 2014;128(4):719–24. https://doi.org/10.1007/s00414-014-0998-9.
13. Bolliger SA, Thali MJ. Decomposition. In: Thali MJ, Dirnhofer R, Vock P, editors. The virtopsy approach. 3D optical and and radiological scanning and reconstruction in forensic medicine. Boca Raton: CRC Press;2009. p. 188–94.
14. Franckenberg S, Flach PM, Gascho D, Thali MJ, Ross SG. Postmortem computed tomography–angiography (PMCTA) in decomposed bodies–a feasibility study. J Forensic Radiol Imaging. 2015;3:226–34.

15. Egger C, Vaucher P, Doenz F, Palmiere C, Mangin P, Grabherr S. Development and validation of a postmortem radiological alteration index: the RA-Index. Int J Legal Med. 2012;126(4):559–66. https://doi.org/10.1007/s00414-012-0686-6.
16. Teresiński G, Unarski J, Wach W. [Wypadki i katastrofy lotnicze] in Polish. In, [Medycyna sądowa t.1. Tanatologia i traumatologia sądowa] in Polish. Warszawa: PZWL;2019. p. 777–88.
17. Ambade VN, Godbole HV, Batra AK. Atherosclerosis: a medicolegal tool in exhumed decomposed bodies. Am J Forensic Med Pathol. 2008;29(3):279–80. https://doi.org/10.1097/PAF.0b013e31817e792b.
18. Omalu B, Hammers J, Luckasevic T. Diagnosis of hemorrhagic stroke in an exhumed brain after three years of burial in a deep grave. J Forensic Sci. 2012;57(6):1665–8. https://doi.org/10.1111/j.1556-4029.2012.02214.x.
19. Rocchi A, Presciuttini S, Chiti E, Pierotti S, Spinetti I. Identification of an exhumed corpse by DNA extraction from bulb swab. A disputed parentage case report. Sci Justice. 2019;59(2):214–6. https://doi.org/10.1016/j.scijus.2018.10.001.
20. Agostini V, Bailo P, Chiti E, Linarello P, Gentile G, Primignani P, Giriodi M, Piccinini A. Ocular swabs on exhumed bodies: an alternative to the collection of "classical" tissue samples in forensic genetics. Forensic Sci Int Genet. 2020;44: 102206. https://doi.org/10.1016/j.fsigen.2019.102206.
21. Emmons AL, Davoren J, DeBruyn JM, Mundorff AZ. Inter and intra-individual variation in skeletal DNA preservation in buried remains. Forensic Sci Int Genet. 2020;44: 102193. https://doi.org/10.1016/j.fsigen.2019.102193.
22. Simoes Dutra Correa H, Cortellini V, Brescia G, Verzeletti A. Human identification through DNA analysis of restored postmortem teeth. Forensic Sci Int Genet. 2020;47:102302. https://doi.org/10.1016/j.fsigen.2020.102302.
23. Käferstein H, Sticht G, Madea B. Chlorprothixene in bodies after exhumation. Forensic Sci Int. 2013;229(1–3):e30–4. https://doi.org/10.1016/j.forsciint.2013.03.051.
24. Cippitelli M, Mirtella D, Ottaviani G, Tassoni G, Froldi R, Cingolani M. Toxicological analysis of opiates from alternative matrices collected from an exhumed body. J Forensic Sci. 2018;63(2):640–3. https://doi.org/10.1111/1556-4029.13559.
25. Bolte K, Dziadosz M, Kono N, Vennemann B, Klintschar M, Teske J. Determination of drugs in exhumed liver and brain tissue after over 9 years of burial by liquid chromatography-tandem mass spectrometry-part 1: cardiovascular drugs. Drug Test Anal. 2021;13(3):595–603. https://doi.org/10.1002/dta.2940.
26. Bolte K, Dziadosz M, Kono N, Vennemann B, Klintschar M, Teske J. Determination of drugs in exhumed liver and brain tissue after over 9 years of burial by liquid chromatography-tandem mass spectrometry-part 2: Benzodiazepines, opioids, and further drugs. Drug Test Anal. 2021;13(7):1318–30. https://doi.org/10.1002/dta.3029.
27. Tabata N, Morita M. Immunohistochemical demonstration of bleeding in decomposed bodies by using anti-glycophorin a monoclonal antibody. Forensic Sci Int. 1997;87(1):1–8. https://doi.org/10.1016/s0379-0738(97)02118-x.
28. Woźniak K, Gross A, Konopka T, Pohl J, Kłys M. [Report from the medico-legal autopsy of the exhumed corpse of general Władysław Sikorski] in Polish. Arch Med Sadowej Kryminol. 2009;59(1):15–21.
29. Rzepecka-Woźniak E, Furgał-Borzych A. [Histological examination of specimens obtained during autopsy of the exhumed corpse of general Władysław Sikorski] in Polish. Arch Med Sadowej Kryminol. 2009;59(1):22–6.
30. Plenzig S, Holz F, Bojkova D, Kettner M, Cinatl J, Verhoff MA, Birngruber CG, Ciesek S, Rabenau HF. Detection and infectivity of SARS-CoV-2 in exhumated corpses. Int J Legal Med. 2012;135(6):2531–6. https://doi.org/10.1007/s00414-021-02670-4.
31. Ebner L, Flach PM, Schumann K, Gascho D, Ruder T, Christe A, Thali M, Ampanozi G. The tip of the tip of the knife: stab sequence reconstruction using postmortem CT in a homicide case. J Forensic Radiol Imaging. 2014;2(4):205–9. https://doi.org/10.1016/j.jofri.2014.08.002.
32. Bolliger SA, Thali MJ. Sharp trauma. In: Thali MJ, Dirnhofer R, Vock P, editors. The virtopsy approach. 3D optical and and radiological scanning and reconstruction in forensic medicine. Boca Raton: CRC Press;2009. p. 304–17.

33. Bolliger SA, Kneubuehl BP, Thali MJ. Gunshot. In: Thali MJ, Dirnhofer R, Vock P, editors. The virtopsy approach. 3D optical and and radiological scanning and reconstruction in forensic medicine. Boca Raton: CRC Press;2009. p. 318–31.
34. Dedouit F, Mokrane F-Z, Savall F, Faruch M, Grimm JM, Grabherr S, Mangin P, Rousseau H, Rougé D, Telmon N. Blunt trauma. In: Grabherr S, Grimm JM, Heinemann A, editors. Atlas of postmortem angiography. Cham: Springer;2016. p. 345–409.
35. Woźniak K, Moskała A, Grabherr S. Sharp trauma. In: Grabherr S, Grimm JM, Heinemann A, editors. Atlas of postmortem angiography. Cham: Springer;2016. p. 411–51.
36. Woźniak K, Moskała A, Grabherr S. Gunshot trauma. In: Grabherr S, Grimm JM, Heinemann A, editors. Atlas of postmortem angiography. Cham: Springer;2016. p. 453–90.

Chapter 8
Death Associated with Trees

Deland Weyrauch

Introduction

As large, heavy, abundant, living parts of the terrestrial environment, trees are so widely distributed and useful to humans that direct interactions between people and trees are common all over the world. Trees are regularly sawed, felled, harvested, and climbed by people, and people are occasionally struck by falling trees, branches, or fruits. This chapter reviews human fatalities in the context of these events, most of which are due to accidental blunt force traumatic injuries. The circumstances, epidemiology, injuries, autopsy findings, and investigative considerations of these cases are discussed.

What is a "Tree-Related" Death?

This chapter *will cover*:

- Fatalities resulting from a person physically altering a tree, for purposes of harvesting, landscaping, etc.
- Fatal descents from height, whether the decedent fell directly from a tree or from an elevated position while working on a tree.
- Other deaths where the presence of a tree is fundamental or central to an activity, such as deaths associated with tree stands used for hunting.
- Fatalities due to falling trees or tree parts ("tree failures"), including deaths in motor vehicles struck by a fallen tree and in vehicles that struck trees which had fallen onto a roadway.

D. Weyrauch (✉)
Yale School of Medicine, 333 Cedar Street, New Haven, CT 06510, USA
e-mail: deland.weyrauch@yale.edu; djweyrauch1@gmail.com

G. N. Rutty (ed.), *Essentials of Autopsy Practice*,
https://doi.org/10.1007/978-3-031-11541-7_8

This chapter *will not cover*:

- Suicidal hangings on trees—The tree may be an available means of suspension, but the characteristics of these deaths relate more to the hanging method and suicidal nature.
- Motor vehicle collision fatalities in which the vehicle veered off a roadway before happening to collide with a tree.
- Other deaths where the presence of a tree is best classified as incidental.
- Sawmill fatalities—At this juncture, the raw material is best considered lumber/timber as opposed to a tree.
- Other deaths involving products derived from trees, but not the perennial woody plant as such. In other words, once a tree is successfully harvested, it is no longer considered a tree and deaths associated with the processing or consumption of products sourced from trees will not be discussed.

Background—The Case of Lucy

One of the most ancient and famous human ancestors likely died while interacting with a tree. The fossilized skeletal remains of A.L. 288-1, better known as "Lucy," were studied by researchers at The University of Texas at Austin, who examined both the original specimen as well as computed tomographic scans of the skeleton to assess for a possible cause of death for the 3.2-million-year-old adult member of *Australopithecus afarensis.* This research was undertaken in a particular context: the discovery of Lucy in 1974 in the Afar Depression of what is now Ethiopia sparked a vigorous and ongoing debate about whether this erect-walking species—a capable terrestrial biped—spent time in trees. This question is important to the field of paleoanthropology as it relates to the role of arboreal locomotion in hominin evolution.

Lucy is approximately 40% of a complete skeleton, and analyzing these available elements the researchers described a set of likely perimortem fractures present in a pattern consistent with trauma produced by a vertical deceleration event. This included a four-part fracture of the proximal right humerus, an injury commonly seen when someone stretches out their arm while attempting to break a fall or descent from height. The left humerus was also fractured, and while infrequent, bilateral compressive proximal humerus fractures are usually associated with high-energy trauma from impact on outstretched arms. There were multiple additional fractures in Lucy's skeleton involving the distal shaft of the right radius, left femur, right tibia and fibula, right talus, cranium, bilateral ribs, and pelvis.

The findings were published in a 2016 article in the scientific journal *Nature* and the authors concluded that Lucy's most likely cause of death was blunt trauma from falling out of a tall tree [1]. To support the inference that tall trees would have been part of Lucy's environment and accessible to her, the authors cite lines of evidence from the fossil record and dating of paleosol carbonates suggesting the region where Lucy was found would have been a grassy woodland with sizable

trees. Like many other small primates, Lucy may have foraged in trees or sheltered in them at night. Chimpanzees, similar in body size to the extinct *Australopithecus afarensis*, have been documented sleeping in tree nests at heights equating to a 16-storey building (50 m), and the search for food and provisions can occur at even greater heights. Unimpeded falls with impact from such heights produce a wide range of concomitant fractures in humans similar to those found in Lucy and often cause fatal damage when vital internal organs are violently compressed and/or penetrated by broken bones. Taken together with the paleohabitat information and resemblance with known clinical cases in humans, the authors propose the overall pattern of fractures—considering specific anatomic locations and fracture types—suggests Lucy fell from of a tree of considerable height and impact progressed sequentially from feet and legs to the hip, then arms, then thorax and head, causing injuries likely to be rapidly lethal.

This vignette is to say that as long as humans have existed, trees have been prominent features of our natural environment and our culture, simultaneously a way of survival and a figure of demise. As we have found more uses for trees, the range and frequency of our interactions with them have grown. It is the editor's and my opinion that tree-related activities, with the injuries and deaths that may be associated with them, are a subject receiving little attention to date within forensic and autopsy textbooks. This chapter is written in the hopes of covering this topic for an international readership.

Deaths in Logging, Forestry, Tree Care Operations, and Recreational Tree Care

Cutting, pruning, sawing, lopping, trimming, felling, removing, or any version of physically altering a tree is an inherently dangerous thing for a person to do. Several occupations have these activities as integral parts of the job description:

- Logging—Harvesting trees as a raw material.
- Forestry worker—May refer to a logger or someone who creates and maintains forests [2].
- Tree felling—Making an entire tree fall down.
- Tree lopping—Cutting a branch, limb, or other protrusion off the main trunk of a tree.
- Landscaper, arborist, or amenity tree service worker—Professional involved in tree removal, maintenance, or other tree care operations (Fig. 8.1) [3].

These occupations are notorious for unusually high exposure to hazards with resulting high rates of fatalities and severe injuries [4]. Although labor statistics vary by time period, region, and methodology, it is generally accurate to say that logging and forestry workers have continually experienced one of the highest fatality rates all over the world for decades, at over 100 deaths per 100,000 person-years, more than

Fig. 8.1 Example of urban tree care operations in New Haven, Connecticut, U.S. **a** Worker removing tree limb segments with a chainsaw while elevated via boom lift bucket truck. **b** Aerial work platform at height of about 20 m. **c** Worker carrying cut segments to a woodchipper

10 times the all-industry average and 2–3 times higher than other notably dangerous sectors like construction and mining/quarrying [2–8]. Similar observations have been made in multiple studies spanning Australia, Canada, New Zealand, Russia, Sweden and the Nordic countries, and the United States (U.S.), underscoring the universality of these hazards. The fatality risk for logging is extremely high, even greater than that for commercial fishing [2].

Recreational tree care—"non-occupational" or so-called "do-it-yourself" projects—involves similar hazards, but in the amateur setting. Non-professionals commonly undertake these tasks for reasons including aesthetics, removal of a dead or rotten tree, firewood collection, physical fitness, pride and satisfaction in completing home maintenance, and self-sufficiency; older and retired persons are overrepresented in these accidents, and they have also reported limited ability to afford the specialized labor costs as a factor in choosing to do the work themselves [3, 9]. Since there is substantial overlap in the characteristics of professional and recreational cases, they will be discussed together unless otherwise specifically noted.

One difference is in demographics, where the average age of professionals suffering fatal injury is about 20 years younger than non-professionals (40 years vs. 60 years, respectively) [2, 3, 8, 10]. However, whether occupational or non-occupational, these deaths overwhelmingly occur to males, who have to date comprised 90–100% (usually closer to 100%) of tree cutting-related fatalities in every country they have been investigated [2, 3, 5, 7, 8, 10].

Hazards

The preeminent hazard in working with trees is the unintended release of large amounts of kinetic energy, which takes several forms. Hardwood trees can be 25 m tall and weigh in excess of 10 metric tons, with individual limbs weighing 450 kg or more, and portions of a tree may be under immense gravitational stress [4]. Some parts may be weakened by decay or otherwise unstable in unpredictable ways. Sawing, cutting, or hammering wedges into a tree can release this stored energy directly, or manifest as falling objects. When felling, a tree's trunk can suddenly and violently split vertically into two or more pieces as the forces shift and internal pressure is sent up the stem (colloquially called "barberchairing," a reference to the sliding action of the old-style barber chair), creating potentially massive and horizontally fast-moving tree fragments as well as haphazardly falling fragments from above (Fig. 8.2). Most fatalities result from being struck by moving trees or branches (about 60–75% of deaths) [2–4, 6, 8, 10], and quite often these are not from the tree being felled, but rather originate from a second nearby tree which is disturbed by the felling of the intended tree [2, 4, 10]. Falling trees can knock the branches off neighboring trees and connecting vines can pull branches in the same canopy down upon the worker. Since the questions of when, where, and how a tree will fall are so multifactorial, predicting the fall trajectory is difficult and planning for all contingencies takes great expertise. Experienced loggers are aware of these dangers and know very well that any error in judgement can carry lethal consequences.

Fig. 8.2 Recreational tree felling accident. **a** The decedent's frozen body was discovered in his wooded backyard, with adjacent sawed and fragmented tree trunk and chainsaw. **b** Scene likely depicting "barberchair"-type incident, where the trunk splits vertically as the tree falls, generating great lateral force when it suddenly snaps (instead of hinging at the base, the hinge point is higher up on the tree when it tilts and falls). **c** Left-sided depressed skull fracture, which upon further examination was associated with bilateral fractures of the skull base, subdural and subarachnoid hemorrhage, and intraventricular hemorrhage

Apart from splintering tree fragments and falling tree limbs, other hazards include uneven terrain, extremes of weather, working at elevated heights, contact with overhead power lines, chainsaws and other sharp instruments, working with woodchippers and heavy mechanical equipment, and isolated environments (Fig. 8.1).

Injuries

Regarding type and distribution of injuries in these deaths, the head is the most frequent primary and lethal impact site (40–60% of cases), usually when it is struck by moving/falling tree parts [2–4, 8, 10]. It is common for the decedent to have been wearing a helmet at the time of the accident; helmets may be broken or completely shattered as they can fail under the tremendous impact forces seen in many events [2]. Investigation should document the presence and condition of any helmet involved in these fatalities. Skull fractures with associated lacerations of the brain are often encountered at autopsy, as are subdural, subarachnoid, and intraventricular hemorrhages. Atlanto-occipital dislocation and cervical spine trauma may also result.

After isolated head/neck injuries, lethal thoracic or abdominal trauma is the next most common body site (about 20–30% of cases) (Fig. 8.3), followed by severe combined multisite trauma (10–20%) [8, 10].

About 10% of deaths are due to traumatic compression asphyxia, usually when the worker's chest is crushed and/or pinned by tree limbs [2, 3, 8]. Autopsy findings to support traumatic asphyxia may include cutaneous or mucosal petechiae, generalized visceral congestion, and pulmonary edema.

Descent from Height

Descent from height is another distinct event leading to fatal injury. Incidence is somewhat variable in the literature, but it appears there is a significant risk difference based on labor type. While industrial loggers typically cut a tree down from the base, landscapers and urban tree professionals will start at the top and delimb sections until there is nothing left but the stump (Fig. 8.4), and consequently falls from elevation mostly occur in landscaping-type tasks [4]. These events account for something between 5–35% of overall deaths depending on the labor activity being measured, and can include descents from the tree itself, ladders, or the aerial work platform of a boom lift bucket truck [2–5, 8]. One case involved a landscaper who fell out of a tree while trimming branches with ensuing 9 m descent, resulting in skull fracture, subdural hemorrhage, brain contusion, rib fractures, lung contusion, T12 vertebral fracture with spinal cord transection, and sacro-iliac dislocation. (See "Overview of Injuries in Descent from Height Fatalities"—for more discussion of this topic). It is

Fig. 8.3 Severe blunt trauma of the torso sustained when a tree fell onto a non-professional tree cutter, including: extensive bilateral rib fractures; T5/T6 and L1 vertebral fractures; and lacerations of the heart, aorta, liver, and spleen associated with marked hemothorax and hemoperitoneum (not pictured)

Fig. 8.4 Landscaping fatality. **a** The decedent was felling a tree by delimbing the trunk from top to bottom in large segments, and his body was discovered suspended by the waist high on the tree. **b** Blunt impact by the cut segment resulted in multiple lethal injuries in this case, including a classic type I hinge fracture of skull (pictured), brainstem injury, atlanto-occipital dislocation, and aortic laceration

occasionally difficult to determine the primary reason for fatal injury when there are combined elements of moving tree/branch-inflicted trauma and descent from height injuries [8].

Electrocution

Although rare, electrocution deaths are dramatic and more likely to represent fatalities in which a serious workplace safety violation or egregious error in judgement was committed. Alternatively, they may occur in the context of clearing tree debris near damaged power lines in close temporal proximity to storms, reflecting particularly hazard-laden work conditions. Contact with electric current accounts for about 5–10% of fatalities, often from chainsaw or bodily contact with a power line [3, 5, 8]. Thermal electrical burns should be documented if present in a case where electrocution caused or contributed to death.

Chainsaws

Also rare, perhaps surprisingly, is fatal direct chainsaw trauma. Many studies in countries all over the world have shown that while a common source of non-lethal injuries, chainsaw or circular saw accidents seldom result in death, accounting for less than 5% of cases [2, 3, 6, 8, 10]. Engineering safety controls in chainsaw design and effective personal protective gear may explain this non-lethality to some degree [6]. The most common reason for accidental contact with the chainsaw's blades, and the most dangerous, is "kickback"—sudden uncontrolled backwards jerking toward the operator when the chain abruptly stops as a link encounters more solid wood [11]. A fatal case usually involves chainsaw kickback causing lethal injury to the neck region (Fig. 8.5) [12].

There are a couple reports of more unusual chainsaw accidents in the literature. One teenage forestry worker fell upon his chainsaw, with the autopsy report stating death was due to extensive disruption of the brain associated with markedly comminuted skull fracture [13]. Another paper details the case of an 80-year-old farmer who was engaged in felling a tree [14]. His chainsaw was found jammed in the tree, with the chain broken but still in place. A single bloody wound of the mid-anterior chest was present, a penetrating wound described as having one sharp end and one blunt end, with greater depth than length, mimicking a stab wound. It penetrated the aortic arch causing a 1,500 mL left hemothorax. Examination of the chainsaw revealed a missing chain link, and a pelvic radiograph obtained at autopsy revealed a metallic foreign body near the head of the right femur. Dissection uncovered a broken chain link measuring 1.7 cm in greatest dimension within the right femoral artery that matched the missing link of the chainsaw in question. This chainsaw link

Fig. 8.5 Chainsaw accident. **a** The decedent was cutting a log when a "kickback"-type chainsaw incident occurred, creating a traumatic open wound of the left neck and chest with massive blood loss, causing him to stagger about 4 m before collapsing. **b** The wound extended through skin, soft tissue and muscle, with partial transection of the left carotid artery (pictured) and unidentifiable internal jugular vein

embolization changed certification of both the cause and manner of death, as without this finding the death could have easily been determined to be due to a penetrating stab wound of the chest of probable homicidal origin.

Logs/Trunks

If the worker is involved in loading or unloading a log truck, large piles of logs are a well-known hazard and fatalities may occur when workers are struck by rolling logs causing massive blunt trauma [2, 15].

One case was a boom-claw tree trunk removal mishap. The decedent was working on a two-person crew for a tree removal company, using a boom truck with a giant claw to move large limbs and trunks. He was on the ground while the boom operator was lifting a trunk. The claw lost grip, the trunk fell, and the worker was inappropriately positioned underneath the clear hazard. He was crushed by the falling trunk with lethal blunt injuries of the head and torso.

Drugs/Alcohol

Impairment from drugs or alcohol is not a common factor in these fatalities [8, 10], but rates of alcohol intoxication in fatal occupational injury do appear to be higher in forestry compared to other sectors and the degree of alcohol intoxication has been found to be directly correlated to risk of fatality [7]. Alcohol has been implicated in both recreational and professional tree cutter fatalities. Some notable cases include a 36-year-old who felled a large tree onto his own head while pulling it by a wire with a tractor (0.19 gm% ethanol concentration) and a 32-year-old trimming branches while elevated via boom truck whose chainsaw made contact with a power line, electrocuting him and causing him to fall about 6 m to the ground (0.09 gm% ethanol concentration in addition to positive postmortem tests for benzoylecgonine and oxycodone) [8].

Working in Isolation

Non-occupational deaths usually happen when the person is working alone, with only about 20% of these events being witnessed. In contrast, professionals are rarely alone, but may be outside visual contact with coworkers when the incident occurs [5, 8]. In most cases death occurs at the place of injury before any medical assistance is given, but a minority involve injuries likely survivable if timely treatment is administered; in some of these fatalities, delay in treatment due to worksite remoteness and/or working alone has been identified as a probable contributing factor to the death [2, 10].

Bystander Deaths

Quite often the person who dies is not the person actively cutting, but instead a fellow worker or bystander who is struck by the falling tree or tree parts. Laborers and onlookers have died when they were:

- Working under the influence of alcohol (0.04 gm% ethanol concentration) on the ground when a coworker in the tree above cut a large branch which fell and crushed him [8].
- Struck by a felled tree while driving past in a vehicle [3].
- A child watching from the seat of a nearby tractor whose father misjudged the fall angle, leading to a dead tree falling directly on top of the child [8].
- Walking down a long driveway adjacent an urban tree care operation when professionals cut a large branch at the exact moment he was underneath [8].

Human Factors and Prevention

Investigations have suggested the main human factors contributing to fatal accidents are misjudgment of a hazardous situation, failure to preplan an escape route when felling, and improper felling techniques [2, 4, 10].

For prevention of serious injury and death, there is a particularly useful document published by WorkSafe Victoria of the government of Victoria, Australia, which outlines safety measures to mitigate many of the hazards discussed here including overhead powerlines, working at height, chainsaws, falling objects, and more (https://www.worksafe.vic.gov.au/resources/working-safely-trees) [16]. Since the most dangerous activity is felling an entire tree, safety ought to be especially stressed for these workers. Any measure that puts more physical distance between the worker and the tree being felled will improve safety, such as mechanized logging methods that decrease the need for chainsaws [4]. Widespread fatalities from falling trees and tree parts imply those in felling operations should be taught to "look up" and consider hazards from above [4]. It has also been suggested that ideally, non-professionals should not participate in tree felling [10]. This may also extend to "non-timber workers," those employed outside a relevant tree profession who nevertheless participate in these activities while often considered insufficiently qualified or experienced to do so. These workers, often employed in farming, construction, utilities or general labor, comprise at least one quarter of tree care or landscaping-type work fatalities [3, 5].

Death from Tree Failures

Unlike deaths while purposefully interacting with a tree, fatalities due to accidental impact by falling trees or branches during a storm or from "spontaneous" failures appear to be more "act of God"–type events. A simple web query using a search engine demonstrates how easy it is to find news reports of people killed by falling trees, seemingly at random or inexplicably, from a 55-m-tall redwood in the western U.S. collapsing in unremarkable weather to a tree uprooted by high winds falling on a moving car in Tasmania. Images of horizontal trees, crushed vehicles, obstructed roadways, and damaged houses are visually dramatic and readily shared via electronic media. A study in Australia has provided evidence of just how newsworthy journalists consider these deaths, as the researchers' database showed that since the beginning of the twenty-first century the media reported almost all, if not all fatalities from tree failures in that country [17].

Of course, trees and branches fail for an underlying reason, even if the reasons are not entirely discernible. Inclement weather conditions such as storms and high winds are without question the most significant identifiable factor in tree failures, accounting for up to 90% of fatal incidents [17]. The risk of being killed or seriously injured is greatest during or immediately after a severe weather event, as even healthy

and structurally sound trees can be broken or felled by strong winds or water/ice accumulations [18]. So-called "widow-makers" are broken-off tree limbs initially trapped at high levels, only to fall to the ground later. Therefore some "spontaneous" failures represent a delayed consequence of storm-induced damage. This makes cleaning up debris during or after a storm in a wooded area a hazardous activity. Drought, fire, and insect infestations also render trees more susceptible to failure, and weakened or dead trees can cause fatalities in the absence of severe weather [8, 18].

The specifics of disease data collection such as broad categories that subsume all deaths and injuries related to falling objects of many types, not just trees and branches, mean most if not all governments worldwide cannot simply analyze accidental tree failures. Epidemiologic and other data rely on targeted, time-intensive research projects. The available studies suggest death from these incidents is very rare [19], and that if you live in Australia, mortality from accidental tree failure is 250 times less likely than death from driving in a vehicle [17]. From years 1995–2007 in the U.S., there were about 30 deaths per year from wind-related tree failure in a country with about 280,000,000 population, equating to a little less than one death for every 10,000,000 people [18].

Depending on the country and region, the most common scenario is either tree strike while in a moving vehicle (U.S. and United Kingdom) or while engaged in outdoor activities (Australia) [17, 18, 20], a difference possibly explained by the climate and lifestyle of the region. In certain places such as the New England region of the U.S., it is not necessarily uncommon to see motor vehicle incidents involving trees falling onto the travel portion of a roadway (Fig. 8.6) [8]. Other settings include tents and, exceedingly rarely, death by tree failure while cycling. Perhaps surprisingly,

Fig. 8.6 Examples of tree failures involving trees falling onto roadways, all causing fatal accidents in motor vehicles. **a** A tree which fell due to high winds, landing on the roof of a moving mail delivery truck, crushing the cabin and entrapping the driver, ultimately resulting in death due to chest compression with traumatic asphyxia. **b** Large oak tree which failed during torrential rain and high winds, landing upon and crushing a sport utility vehicle **c.** Fragment of a large tree with attached fragment of a school bus, which broke off the main trunk when failing for unclear reasons, striking the bus on the driver's compartment; the bus then coasted off the roadway before striking a utility pole

Schmidlin reported about 20% of wind-related events in the U.S. were deaths while the person was inside their house, with half being mobile homes and half frame houses [18].

To my awareness, only one published study has described injuries and autopsy findings in tree failure deaths [8]. The lethal injury site is a roughly even mix of head trauma, severe combined multisite trauma, torso injuries, and even isolated neck injuries. Two deaths were due to atlanto-occipital dislocation, an injury involving the ligaments and/or bony structures connecting the skull to the cervical spine which leads to secondary brainstem and upper cervical spinal cord damage (Fig. 8.7); atlanto-occipital dislocation is also a common cervical spine injury in motor vehicle collision fatalities [21]. Another case was that of a driver navigating a rural road in high winds when a 55 cm long tree limb smashed through the windshield, penetrating the right side of the neck and exiting on the left upper back, causing a C7 vertebral fracture as well as a severed right external jugular vein (Fig. 8.8) [8]. This case highlights how vehicles may not be able to withstand these forces, as even a falling 55 cm branch can shatter a windshield and still possess sufficient energy to perforate the total anteroposterior depth of an adult neck/thorax.

The pruning and removal of trees discussed in the previous section are often performed at least partly to reduce risk of accidental tree failure [17]. Tree risk assessment and management programs have been suggested, especially for parks and along roadways [18]. However, given the hazards of physically altering a tree combined with the very low frequency of injuries to persons not interacting with trees, it has also been proposed that pushing over or cutting down trees is obviously more dangerous than leaving them alone, limiting the benefit of these programs [19].

Fig. 8.7 Death due to atlanto-occipital dislocation. **a** Heavy rain and wind uprooted a 15-m-long tree, which fell on a parked vehicle. **b** At autopsy, this decedent had minimal head injury, and cause of death was attributable to isolated atlanto-occipital joint dislocation

Fig. 8.8 Lethal penetrating blunt force trauma due to a falling branch. **a** The decedent was driving in windy conditions when a 55-cm-long tree limb smashed through the windshield and pierced the right side of her neck, exiting at the left upper back. **b** The wound after removal of the branch, where examination revealed a C7 vertebral fracture and severed vasculature including the right external jugular vein

In severe storms and high winds shelter ought to be sought in sturdy buildings and, if outdoors, openings are much safer than sheltering under trees (coincidentally, this is also valuable advice to avoid being killed by lightning if the inclement weather happens to be a thunderstorm) [17, 18].

Overview of Injuries in Descent from Height Fatalities

Before further discussion in particular tree-related contexts, there are general concepts in fatal descents from height worth summarizing.

Injuries sustained in falls from height are a distinct form of blunt trauma. Most cases in developed areas are accidental or suicidal falls from buildings, bridges, construction sites, or ladders. For purposes of this section, falls onto solid impact surfaces will be considered, as opposed to descending into water. There are two broad injury categories [22]:

- Direct impact injuries—Damage caused by direct contact between tissue and impact surface. These are predominantly fractures.
- Deceleration type injuries—Occur when tissue is forcefully displaced upon motion arrest during impact. These are predominantly internal organ lacerations, including large vessels. Another important indirect-type injury is cervical spine hyperflexion or hyperextension.

Factors influencing the distribution and severity of injuries in descents from height include [23–26]:

- Fall height—Directly relates to velocity at impact.
- Orientation of the body at impact.
- Composition of the impact surface—Relates to duration of impact. Surfaces such as rocks or concrete allow minimal deformation which decreases impact duration, thus increasing force and injury severity. To the contrary, soil or snow are more deformable, resulting in decreased injury risk [27].
- Secondary impacts with other objects.
- The individual's age and body mass.
- The individual's psychological/neurological state—May affect body tone or behavioral response to the fall. Examples include drug or alcohol intoxication.

Of these, the height of the fall is a major contributor to the pattern and extent of injuries in fatal descents, for both direct and deceleration type injuries [24–26, 28–30]. At lower fall heights, lethality is more closely linked to the body orientation at impact such that head/neck injuries are the typical cause of death and may even be the sole significant injury. As fall height increases, injuries increase, and polytrauma with multiple fatal injuries predominates. One autopsy study found that about 30% of fall deaths from less than 10 m showed multiple lethal injuries, while this figure increased to 90% when fall height was greater than 30 m [24]. Although the frequency of head fractures does not appear to be significantly correlated with descent height, the greater magnitude of impact from higher falls results in more comminuted skull fractures. Injury to the rest of the body is more dependent on fall height than the head/neck region; the frequency and extent of fractures to the thorax, pelvis, and extremities all increase, and with additional fractures come adjacent tissue damage, particularly lung lacerations accompanying multiple bilateral rib fractures. Deceleration injuries are directly proportional to fall height, and some cases are marked by death due to a single organ laceration with internal bleeding.

The head is the most commonly injured site and often traumatized regardless of fall height or even site of primary impact in cases presenting to autopsy. In one series, more than half of decedents who had been known to land on their feet had evidence of brain damage due to secondary impact of the head [29]. Direct impact is usually to the frontal and parietal regions with associated cranial lacerations and hematomas [31]. Subdural and subarachnoid hemorrhages are frequent, and it is common to see a combination of skull base and cranial vault fracture [30]. In feet- or buttocks-first impact, force transmitted upward through the pelvis and spine may cause a classic pattern ring fracture of the skull base [26, 29]. Those who land head-first tend not to reach medical care alive. Craniocerebral trauma is also more common in children because their center of gravity is more superior due to larger head: body size ratio [30].

The neck is an important anatomic region in these autopsies, for a couple specific reasons:

- *Cervical hyperextension injuries*—Falls with primary impact on the face or forehead can cause cervical vertebrae injury due to neck hyperextension. Osawa and colleagues describe 14 cases of isolated cervical hyperextension as a cause of death in falls of low height [32]. All decedents had abrasions and bruises of the upper part of the face at autopsy, but there were often no other external injuries.

Internal examination revealed linear tears of the anterior longitudinal ligament in the cervical vertebra with associated hemorrhage into prevertebral fascia in all 14 cases. 12 decedents had inter-vertebral disc space disruptions at the ligament tear site characterized by dislocated small bone fragments, evident upon sectioning the cervical vertebral column. An anterior-inferior corner fracture of the vertebral body may also be present behind the anterior longitudinal ligament tear, typically appearing as a thin avulsed bone fragment. The lower cervical vertebrae tend to be affected, with disc disruptions and bone fractures usually located between C4 and C7. Sectioning the spinal cord usually reveals gross evidence of trauma in the form of a linear or round central cord hemorrhage, although this is not always present. Histopathologic examination in a subset of these cases demonstrated, based on microscopic findings of edema and macrophage invasion in the cord, that some decedents may have survived for several hours after the accident before death occurred.

- *Laryngohyoid fractures*—Important from a forensic perspective, laryngohyoid fractures have been discovered in about 10% of autopsied non-homicidal falls from height, with incidence of hyoid bone fracture corresponding to increasing fall height and thyroid cartilage fracture increasing with decedent age [33]. Hyoid and thyroid cartilage fractures are also seen accompanying cervical spine fractures in these cases. It is also possible to have cervical soft tissue/muscle hemorrhage or bruising without laryngohyoid fracture [34]. The predominant mechanism is probably indirect fracture secondary to cervical hyperflexion or hyperextension, or mandible or cervical vertebral fractures. One study found that these particular neck injuries were limited to fall heights of more than 10 m, and were not present in autopsied cases of falls from less than 10 m [26]. Therefore, although these findings normally direct the pathologist's thoughts toward homicide, in these instances they do not in isolation suggest strangulation prior to the descent.

Spinal injury is common. Feet- or buttock-first impacts can cause axial loading, transmitting force upward through the spine, resulting in compression or burst fractures of the vertebrae. Spinal cord injury is associated more strongly with thoracic vertebrae fractures as the spinal canal has a relatively small diameter in this region [22].

The sternum can be broken by either direct impact or, interestingly, by the decedent's own mandible secondary to extremely forceful hyperflexion of the neck [22]. Sternal fractures are strongly associated with myocardial contusion.

For visceral injuries, aortic laceration is a classic autopsy finding in descents from height, and damage to the aorta or heart may be due to deceleration injury, compression between skeletal components of the thorax, or penetration by fractured bone ends [26, 29]. The liver appears to be the most vulnerable abdominal organ.

Pelvic fractures are often associated with life-threatening hemorrhage and may be caused by direct impact or force transmitted through the femur across the hip joint. The latter is seen when primary impact is on the feet or knees [35]. A great amount of force is required to disrupt the strong junctures of the posterior pelvic ring, so fractures of the posterior aspect are more indicative of high falls [25].

Finally, while landing on both feet is more common in intentional jumpers committing suicide, it may also occur in accidental falls [22, 25]. Primary impact onto both feet has some specific findings like calcaneus fracture and fracture of bilateral lower extremities. While open fractures of the soles of the feet or splitting of the bilateral heels has been described as a classic or even pathognomonic pattern, this external examination finding is present in less than 20% of cases where a feet-first landing is known [26, 29]. Overall, because so many factors potentially influence the injury distribution, attempting to reconstruct the circumstances of death based on autopsy findings alone is not advised [36]. Fortunately, it does not appear that suicidal descent from height involving a tree has been reported, and only deaths due to accidental falls from trees are known.

Tree-Related Deaths and Injuries in Melanesia and Tropical Regions

Tropical regions of Earth, located near the Equator between the Tropic of Cancer and the Tropic of Capricorn, are characterized by latitudes at which the Sun can be directly overhead. Land in these areas receives more direct sunlight, and the tropics are on average warmer with more precipitation compared to other climates. Tropical plant life is particularly biodiverse and includes a number of culturally and economically important fruit-bearing trees, some of which grow to considerable heights with the fruit located high in the crown of the tree.

Tropical regions are home to a large and actively increasing percentage of the world's population. As an illustration, there are 400 million people who live on just nine tropical islands—Sumatra, Java, Sulawesi, Luzon, Mindanao, Borneo, Hispaniola, Sri Lanka, and New Guinea. The encompassed countries are essentially all of low- or middle-income, where injuries represent a neglected problem in global public health; greater than 90% of deaths and 94% of disability-adjusted life years from injuries worldwide occur in low- and middle-income countries [37]. High population growth rates accompany progress in economic development and public infrastructure in most areas. Still, many individuals and families rely on subsistence agriculture. For example, as of year 2016, an estimated 85% of the Solomon Islands population are subsistence farmers reportedly living a traditional Solomon Islander lifestyle [38].

The available literature on tree-related mortality and morbidity mainly comes from rural Melanesia, a geographical subregion of islands in the southwestern Pacific Ocean [38–43]. Tree-associated injuries, especially involving coconut palm trees, are an enduring and leading cause of trauma here, accounting for about 20–40% of trauma-related hospital admissions [38, 39].

A few trees are worth emphasis:

- Coconut palm trees—Coconut trees are ubiquitous in coastal tropical regions and are among the most useful trees in the world to humans, providing a source of food, fuel, cosmetics, and building material. They are integral to life in the Solomon

Islands given the widespread dependence on subsistence agriculture [42]. The coconut fruits grow in clusters and hang from the top of a tall, smooth, slender trunk. The trees can grow to 30–35 m tall. With this height and slender trunk in combination with fruits and long pinnate leaves at the very top, the trees will sway in high winds.

- Betel palm trees—Also known as the areca nut palm. It is a medium-sized palm, usually growing to about 20 m tall. Like the coconut tree, it has a long, smooth, slender trunk. If a climber falls from a coconut or betel palm there is seldom anything to grasp on the way down [39].
- Mango trees—Mangoes are the national fruit of the Philippines. These are large trees which may reach heights up to 40 m [41]. They have a greater trunk circumference and are closer in resemblance to an oak tree than a coconut palm tree.
- Breadfruit trees—Another important and ubiquitous tropical fruit tree which can grow to heights of 20–25 m. It is not a palm type of tree.

Deaths and injuries will be divided into two general categories for discussion: those occurring when climbers fall out of the tree, and those resulting from either fruits or tree limbs falling and striking people underneath the tree.

Falls of Climbers While Harvesting from Fruit Trees

Climbing trees is important to rural life in many developing tropical regions and is frequently performed as a harvesting method, making falls from trees a significant public health problem and occupational hazard [44]. This is uniquely true given how many of these harvesters are children and adolescents. In the tropics, falling out of trees is a more common cause of trauma than being hit by falling objects. Many tree types have been implicated including coconut, mango, betel palm, guava, apple and nut trees [39, 43].

Coconut palms have received the most attention in the literature and may be the most common and fatal descents from height. The physical features of the tree are such that climbers must ascend a slender unbranched trunk to retrieve fruits at the very top. This is a cultural tradition requiring skill. The person assumes a body posture that enables them to exert pressure on the tree trunk with their feet, sometimes with the assistance of looped rope, twine, or cloth around the ankles. This helps the climber keep their feet close together as they advance up the tree using their hands and the soles of their feet [39]. Workers on some islands use a variant method whereby they tie a bolo knife or similar machete-type cutting tool to their waste, notching grooves in the coconut tree trunk to serve as a ladder and protective measure against falling. Another sharp instrument may be introduced if the harvester uses a blade to cut the coconuts free instead of merely plucking them manually. Harvesting coconut sap sometimes entails a system of bamboo or rope bridges connecting the canopies, and the worker moves from tree to tree on these high bridges [45].

As for mango trees, falls may be more likely to occur when branches break as the climber works their way distal from the trunk, toward the fruit [41].

There is a sex and age predisposition which varies somewhat depending on societal norms. About 75% of those injured in falls from trees are male, and about 75% are less than 16 years of age. Not many studies have documented fall height. One prospective study of emergency department visits in Burkina Faso showed a mean fall distance of 5.2 m, although these were mostly from mango and other trees with fruit accessible at lower elevations compared to palm trees [44]. In this study, the most common circumstances reported for the accidents were slipping on a branch (60%) and the breaking of a branch (35%), with an interesting cause being insect bites leading to loss of balance (3%).

The most frequent injury across all tree types is upper extremity fracture, especially of the distal radius, suggesting falls on outstretched arms predominate. This is consistent with the patient population skewing young and fit with better reflexes relative to older individuals, with attempts to break their falls by reaching out with their arms. However, thoracic injuries appear to be rare, possibly due to greater costal grid flexibility in childhood [44]. Abdominal trauma is more likely and may include splenic laceration.

Information on deaths has seemingly gone almost entirely uncaptured. Barss and colleagues created a questionnaire for their 1984 study in Papua New Guinea and distributed it to regional health centers in an attempt to acquire some data on prehospital mortality [39]. The responses revealed at least 28 deaths in a four-year period due to falls from trees, where death occurred prior to reaching medical care. Every case was reported as a lethal head injury, and a few also had thoracic, abdominal, or spinal injuries. One climber fell after accidently cutting his arm with a bush knife. Another case involved a harvester with an epileptic condition who fell from a mango tree during a seizure and died. Further characteristics of the fatalities were not described.

If women and girls are tasked with climbing trees to collect fruit, an important population to consider is pregnant females. Dakouré and colleagues report three of these patients who fell and while they survived, all three suffered secondary abortions [44].

Being remote and rural settings in developing countries, time interval to medical treatment for these injuries is a persistent issue. The skeletal fractures are often complicated by osteomyelitis at presentation if the climber survives, and it is not uncommon for the interval to last multiple days to weeks [39, 44].

Although safety harnesses and head protection have been recommended, many village tree climbers do not employ any safety equipment [45]. Some countries have pioneered the use of mechanical tree climbing devices and robots as an alternative to manual fruit harvesting.

Deaths and Injuries from Falling Coconuts and Tree Limbs

While less common in the tropics than climbers falling out of trees, trauma to those on the ground from being struck by falling trees/limbs and fruits is still a hazard. These will be discussed separately, as the falling coconut injuries are fairly idiosyncratic.

Falling Trees and Tree Limbs

Clearing land for traditional rainforest gardens usually requires tree felling. When these large tropical trees fall, very often they will pull down branches from adjacent trees by numerous connected vines, generating dangerous falling objects [39]. Instead of cutting them down, large trees are occasionally burnt or ring-barked and left standing, leaving them damaged and more susceptible to failure. Weather can play a factor, as tropical cyclones sometimes uproot even massive rainforest trees and blow them over or cause wind-induced breaks of tree limbs.

Escoffery and Shirley report a death in Jamaica which came to autopsy [46]. The decedent was a previously healthy 10-year-old female who was sitting under a tree in a park when a branch broke for unspecified reasons, fell, and hit her on the head. She arrived at the emergency unit with fixed and dilated pupils. She was bleeding from the nostrils, ears, and mouth. She died soon after presentation. Autopsy showed bruising over the left side of the forehead. There were extensive basilar skull fractures and diffuse subgaleal, subdural, and subarachnoid hemorrhages with accompanying marked cerebral edema. Additional findings included disrupted supraspinous and interspinous ligaments between the C1 and C2 vertebrae. The size of the tree limb and the type of tree were not specified.

Falling Coconuts

For a 1984 paper, Dr. Peter Barss enlisted the help of a clerk to weigh immature and mature and wet and dry coconuts, and had astronomer A.E. Whitford assist in calculating the physical forces of these dropping fruits [40]. They ranged from 1–4 kg. The paper states that a coconut weighing two kilograms which falls 25 m will be traveling 80 km/hour upon impact with a victim's head. Although the impact force depends on direct versus glancing strike angles as well as the distance over which the coconut decelerates, they calculated that for a direct blow with a stopping distance of 5 cm, the force would be 1,000 kg.

Coconuts are the seeds of the tree and so naturally fall to the ground when they mature, or occasionally get knocked down during high winds or heavy rain. Being positioned under a coconut palm therefore makes a hit by a falling coconut possible,

and this happens with some frequency wherever the trees and people coexist. The events are rarely fatal, as a direct strike to the head represents a spatiotemporal improbability.

Nonetheless, the sheer oddity of such accidents has made them fodder for news outlets. Several media reports have spotlighted the concern for death by falling coconut. Some articles warn travelers to the tropics, cautioning them about camping underneath coconut trees. Cities in northeastern Australia have removed or de-fruited coconut palms in populated areas to prevent the dreaded falling-drupe fatality. The phenomenon of getting hit on the head by a coconut has even been depicted for comedic effect on popular American television shows, including *Gilligan's Island* and *SpongeBob SquarePants*.

The fatal cases likely suffer the same problem of underreporting due to pre-hospital mortality and survivorship bias in the existing literature as the deaths due to climbers falling from trees [38, 39, 42]. Escoffery and Shirley again have the only published autopsy case I could find [46]. The decedent was a 79-year-old female standing under a coconut tree when she was struck on the head by a plummeting coconut. She was unconscious upon presentation to the emergency unit. A 4 cm stellate laceration was present on the right parietal scalp with associated palpable skull defect. Status epilepticus ensued, and the patient died on the third day of admission. Autopsy revealed subgaleal hemorrhage associated with the scalp laceration and a subjacent depressed skull fracture, cerebral edema, and cerebellar tonsillar herniation.

In 1973, a 2-year-old died during a diaper change in the shade of a coconut tree in Hawaii, U.S. A cluster of 57 coconuts fell and landed on the child [47].

In addition to Jamaica and Hawaii, deaths from falling coconuts have been reported in Sri Lanka, Singapore, Papua New Guinea, Vanuatu, Thailand, India, and Colombia.

As a combination of circumstances, coconuts sometimes fall and strike people who are actively climbing the trunk of the tree [39].

On a final and bizarre note, there is a harvesting method employed by some farmers in Thailand and Malaysia whereby trained macaques pick the fruits. In 2001 in Malaysia, an adult male reportedly died instantly when one of these monkeys dropped a coconut on his head [48].

Deaths and Injuries Associated with Falls from Walnut Trees in the Agricultural Setting

Walnut trees are native to large swaths of land ranging from southeast Europe to southwest Asia, central Asia and southwestern China, and the fruit of the walnut tree is a key feature of several regional economies as it has uses in the food and drug industries. Especially in rural areas where walnut harvesting is an important source of income, falls have been widespread among farmers who climb the trees to harvest the fruit [49–51].

Walnut trees are large deciduous trees growing to about 15–30 m with some attaining heights of 35 m. They typically have a broad crown and most fruits are located toward the distal end of long branches. Characteristics of the walnut tree unfavorable to climbers include a surface of smooth bark which is commonly described as slippery, and air space-containing chambered piths in the branches which make them especially frangible if the tree's health is compromised [49–51].

Where studied, greater than 90% of farmers who fall from walnut trees are male, mean age is about 35 years, and many harvesters are classified as illiterate [49–51].

Most falls occur when the branches break during climbing. Some harvesting methods include standing on a branch while dislodging nuts with a stick and vigorously shaking branches to force the nuts free, both of which increase risk of fracturing a tree limb [50]. Falls also occur due to loss of balance on the slippery surface of the branch [49, 51]. A disproportionate number of cases present to hospitals during the evening shift, suggesting loss of visibility and worker fatigue may play significant roles [50].

The most frequent serious injuries to surviving patients are of the spinal column, particularly of the lumbar spine in the form of burst and wedge compression fractures. A subset of these have caused complete paraplegia. There appears to be an approximately equal mixture of upper and lower extremity trauma in these walnut tree falls.

In studies from Iran, Turkey, and the Kashmir region of the Indian subcontinent, mortality in these falls ranges from about 5–25% [51–53]. This is likely an underestimate given most methodologies do not account for pre-hospital deaths. Therefore, mortality is considerable even though fall victims tend to be relatively young and fit males. In a study of 127 patients referred to a trauma center, five patients died on the day of admission, all due to traumatic brain injuries [50]. In another study, there were two deaths attributed to complete paraplegia complicated by pressure ulcers with superimposed infection and bacteremia [51]. Deaths due to dislocations and fractures of the cervical spine have also been reported [49].

One possible prevention measure is to eliminate the need to climb trees by use of a mechanized walnut harvesting device; of course, preventing injury and death from walnut tree falls requires these machines to be available and affordable [49].

Deaths and Injuries Associated with Tree Stands Used for Hunting

Tree stands, also known as hunting stands or deer stands, are elevated platforms affixed to trees upon which someone perches to gain an advantage while hunting. These stands are commonly used for hunting deer, a popular recreation in many regions of North America. A tree stand gives the hunter an expanded field of vision, removes the hunter from the deer's normal line of sight, reduces ground scent, and decreases the likelihood of being struck by stray projectiles launched by other hunters.

Most deer hunters in the U.S. employ tree stands, and time trends of trauma registries from two U.S. states suggest there is an increasing number and rate of serious tree stand-related injuries which likely reflect the growing popularity of these stands [54, 55].

Concomitantly, there is a small but distinct literature in the U.S. dedicated to the epidemiology and features of tree stand-associated injury, as falls from stands actually represent the leading cause of hunting-related accidents in the country, even when restricting the analysis to only those injuries severe enough to warrant admission at a major trauma center [54–63]. This contradicts the prevailing stereotype, which views hunting injuries as intoxicated friends accidently shooting themselves or each other. The classic case is a male, about 40 years of age, hunting with a bow and arrow who presents to a small- or medium-sized hospital with a skeletal fracture after falling from a tree stand, without involvement of alcohol or drugs of abuse. A survey of over 38,000 visits to U.S. emergency departments for hunting stand injuries found that patients were 93% male [60].

Although it is somewhat unclear why these falls occur and naturally the reasons will vary on a case-by-case basis, there are some reported common factors precipitating the events:

- Structural failures—Include both failures of the stand itself (e.g., broken stand parts) and failures of the tree to which the stand was attached. Structural failures are typically due to poor design or construction of the perch. Although commercial tree stands are now available, some hunters still make their own. One study reported a high rate of falls were attributable to homemade stands [62]. These rudimentary stands often consist of an elevated wooden platform nailed to the tree, with either a wooden ladder or wooden steps nailed to the trunk (Fig. 8.9) [64]. Even with industry-constructed stands, errors in placement may result in failure. Evidence of structural failure at a scene might include a collapsed or broken stand at the base of the tree, snapped or broken cables or carabiners, two pieces of a climbing tree stand that are separated (not tethered together), cracked or damaged tree limbs, and loose or unstable fastenings.
- Loss of balance while entering or exiting the stand—The moment of climbing into or getting out of a hang-on platform type tree stand appears to be especially prone to slips and loss of control. Assembling and disassembling the stand while elevated can also be difficult to navigate. However, ascertaining this information is reliant upon history provided by the victim or a witness.
- Descending a tree in the evening—A disproportionate percentage of falls occur in the evening hours [63]. There are some interesting points to consider. Aside from the loss of visibility, intrinsic factors related to the hunter may play a significant role. As an example, to maximize the hunt's potential, some hunters will perform an "all-day sit" where they are perched in the tree stand nearly continuously from dawn until nightfall. Physical and mental fatigue at the end of a marathon day may contribute to accidents as they are exiting the stand and descending the tree. Furthermore, hunters may view the act of eating in the stand as detrimental to the success of the hunt due to excess movement and scent, and so hunger may

Fig. 8.9 A tree stand located north of Ray, North Dakota, U.S. **a** The hunter constructed this stand in his youth, creating an elevated wooden platform and nailing wood steps to the trunk **b** Closer view of the homemade tree stand

exacerbate the fatigue. These hunts in tree stands can be physiologically strenuous activities requiring constant diligence, prolonged time spent in one body position, and possible exposures to frigid environments, wind, and other taxing weather conditions.

These factors can occur in combination. For example, a lapse in judgment in the context of fatigue may lead to a hunter choosing a suboptimal tree branch for balance while exiting a stand.

In most cases, alcohol is not a factor. Nearly all studies show alcohol involved at rates of less than 10%. However, one study demonstrated that for 325 victims with available data, 7% were legally intoxicated with blood alcohol content >0.1% [55]. Alcohol use appears to be overrepresented in severe and lethal injuries. Drugs of abuse are involved in less than 5% of cases.

It is no surprise that falls causing severe injury occur when the hunter does not wear a safety harness. As deadly or life-altering injuries are largely preventable, proper use of a full-body fall restraint device is now routinely recommended and promoted by hunter education programs, as well as public awareness campaigns in some U.S. states.

People can hunt from quite high elevations in these tree stands. Average fall heights are between 4–6 m; it is not uncommon to see stands positioned greater than 6 m above the ground, and falls from over 9 m have been reported [59].

The most frequent serious injuries are fractures of the spinal column and long bones of the lower extremities. Paraparesis to complete quadriplegia may result from spinal cord injury, depending on location and extent of the traumatic central nervous system lesion. Fractures of the thoraco-lumbar spine appear to vastly outnumber

those of the cervical spine; while survivorship bias may skew this proportion in the literature, the overall evidence suggests impact forces in most cases predominantly involve the torso and lower extremities, suggesting a preponderance of lower body-first falls. Incapacitating injuries may be peculiarly relevant as hunting by its very nature occurs in rural, remote areas. This is borne out in the literature, where the average time between the fall and presentation to a medical facility is about four hours, with very few victims arriving in less than one hour [55, 63].

Fatalities in tree stand incidents are nevertheless presumably rare. Usually, the injuries are not lethal. When they are, they may include the expected blunt trauma-associated vertebrae and rib fractures, solid organ lacerations, and head injuries. Shields and Stewart report a medical examiner case of a typical death for the forensic pathology literature [64]. The decedent was a 65-year-old male discovered under a tree in the early morning by his fellow hunters. He had fallen approximately 6 m to the ground from a homemade tree stand and was not secured by any safety equipment. He was pronounced dead upon arrival at a neighboring county's emergency department. Pertinent autopsy findings were limited to evidence of blunt force trauma, including superficial abrasions and contusions, multiple rib fractures, a left superior ramus pelvic fracture, 1,000 mL left-sided hemothorax, and 500 mL hemoperitoneum. Cause of death was truncal blunt force injuries, and manner of death was accident.

Interestingly and worth highlighting, Shields and Stewart also report a second tree stand-associated death in the same article, this one by an appreciably different cause and mechanism [64]. This decedent was a 65-year-old male with significant obesity discovered in the evening while hanging upside-down from a tree. He was tethered by a rope around his waist extending from a homemade hunting stand, which was wedged between two trees in a rudimentary fashion. At autopsy, there was evidence of asphyxiation including dark red–purple suffusion of the face, dark purple livor mortis with petechial hemorrhages of the upper torso, scleral injection, and palpebral conjunctival petechial hemorrhages. The heart weighed 900 g, with left ventricular hypertrophy and dilation. Microscopic examination demonstrated myocardial fibrosis. Postmortem toxicological and electrolyte studies were unremarkable. The cause of death was attributed to positional asphyxia due to reverse suspension from the tree stand, and ischemic heart disease was judged a significant contributing condition. The manner of death was accident.

The asphyxia death is intriguing for a couple reasons. First, it is conceivable that this type of event represents an underreported tree stand-associated injury, as these accidents are likely not medically attended and therefore may not be captured by study methods. Second, these deaths occur in the presence of harnesses and safety devices, likely makeshift or worn improperly. The paper by Shields and Stewart appears to be the only report of tree stand-related injury tailored for the forensic literature to date, and their review found only two previously published cases describing asphyxiation as a cause of death. These were a teenager wearing an ill-fitting harness which compressed too tightly around his waist [65] and a man who fell while using a belt-type safety harness which slid up around his neck [61]. Falling with a harness on still necessitates both an uncontrolled fall and a sudden termination or alteration of momentum. There are online anecdotes of hunters who fell while wearing safety

harnesses only to then swing into the sharp edges of affixed climbing sticks or slam into the tree trunk. As demonstrated in the reverse suspension case, the fallen hunter can be effectively trapped in the harness while hanging from the tree, with no dependable mode of extrication.

Additional topics of greater uncertainty include the involvement of firearms, such as unintentional discharges while hunters carry firearms up to or down from a tree stand, or discharge upon impact after a fall. Only rarely have gunshot wounds been reported in these cases, and it is unclear whether the injured was shot by another hunter, suffered a self-inflicted gunshot wound prior to falling out of the stand, or shot themselves upon hitting the ground after the fall. While these hunts tend to make use of bows and arrows and therefore the risk of firearm incidents may be reduced, hunters will often carry accessories such as shears and folding saws for pruning any tree branches that might interfere with the archery, and therefore introduce a potentially tricky activity with a sharp object executed at a considerable height.

In addition to properly utilizing a full-body safety harness, other practices to reduce the risk of hunting stand accidents include using a commercial model instead of a homemade stand, proper methods of stand placement, careful assessment of tree branch strength prior to applying any weight to the branch, avoidance of fatigue and alcohol, and proper methods of stand entrance and exit. If a firearm is used instead of a bow and arrow, anticipation of recoil is pertinent. Equipment ought to be lifted or lowered to or from the tree stand with a haul line, as opposed to being carried on the hunter.

Summary

Hopefully this chapter has addressed a gap in the available literature on environmental and occupational deaths. The global scope of this writing almost guarantees that certain types of tree-related deaths and injuries have been overlooked. Still, for events with such worldwide prevalence, it seems worthwhile to start somewhere.

References

1. Kappelman J, Ketcham RA, Pearce S, Todd L, Akins W, Colbert MW, Feseha M, Maisano JA, Witzel A. Perimortem fractures in Lucy suggest mortality from fall out of tall tree. Nature. 2016;537(7621):503–7. https://doi.org/10.1038/nature19332.
2. Driscoll TR, Ansari G, Harrison JE, Frommer MS, Ruck EA. Traumatic work-related fatalities in forestry and sawmill workers in Australia. J Safety Res. 1995;26(4):221–33. https://doi.org/10.1016/0022-4375(95)00018-L.
3. Brodie LR, Ibrahim JE. Fatal injury in tree felling and related activities, Victoria, Australia 1992–2007. Inj Prev. 2010;16(1):53–6. https://doi.org/10.1136/ip.2009.021683.
4. Michael J, Gorucu S. Occupational tree felling fatalities: 2010–2020. Am J Ind Med. 2021;64(11):969–77. https://doi.org/10.1002/ajim.23286.

5. Centers for Disease Control and Prevention (CDC). Work-related fatalities associated with tree care operations–United States, 1992–2007. MMWR Morb Mortal Wkly Rep. 2009;58(15):389–93.
6. Lindroos O, Burström L. Accident rates and types among self-employed private forest owners. Accid Anal Prev. 2010;42(6):1729–35. https://doi.org/10.1016/j.aap.2010.04.013.
7. Varakina ZhL, Vyazmin AM, Sannikov AL, Nygard CH, Grjibovski AM. Fatal occupational injuries in the Arkhangelsk region. Northwest Russia Occup Med (Lond). 2010;60(6):470–5. https://doi.org/10.1093/occmed/kqq068.
8. Weyrauch D, Gill JR. Accidental deaths involving trees: professional and nonprofessional woodcutting and tree failures with autopsy findings. Am J Forensic Med Pathol. 2021;42(4):350–3. https://doi.org/10.1097/PAF.0000000000000686.
9. Ashby K, Ozanne-Smith J, Fox B. Investigating the over-representation of older persons in do-it-yourself home maintenance injury and barriers to prevention. Inj Prev. 2007;13(5):328–33. https://doi.org/10.1136/ip.2006.012328.
10. Centers for Disease Control and Prevention (CDC). Nonoccupational logging fatalities–Vermont, 1997–2007. MMWR Morb Mortal Wkly Rep. 2008;57(10):260–2.
11. Dąbrowski A. Kickback risk of portable chainsaws while cutting wood of different properties: laboratory tests and deductions. Int J Occup Saf Ergon. 2015;21(4):512–23. https://doi.org/10.1080/10803548.2015.1095547.
12. Koehler SA, Luckasevic TM, Rozin L, et al. Death by chainsaw: fatal kickback injuries to the neck. J Forensic Sci. 2004;49(2):345–50.
13. Macfarlane I, Harry N. Severe chainsaw injuries. Aust N Z J Surg. 1977;47(2):183–5. https://doi.org/10.1111/j.1445-2197.1977.tb04264.x.
14. Choi CS, Jordan FB, Balding LE. The missing link. an unusual case of embolization. Am J Forensic Med Pathol. 1994;15(3):211–2. https://doi.org/10.1097/00000433-199409000-00006.
15. Myers JR, Fosbroke DE. Logging fatalities in the United States by region, cause of death, and other factors—1980 through 1988. J Safety Res. 1994;25(2):97–105. https://doi.org/10.1016/0022-4375(94)90021-3.
16. WorkSafe Victoria. Working safely with trees. State Government of Victoria;2020. https://www.worksafe.vic.gov.au/resources/working-safely-trees. Last Accessed 22 Nov 2021.
17. Hartley MA, Chalk JJ. A review of deaths in Australia from accidental tree failures. Arboriculture Australia;2019. https://arboriculture.org.au/getassets/a2bd3064-7acd-ea11-90fb-00505687f2af/A%20Review%20of%20Deaths%20in%20Australia%20from%20Accidental%20Tree%20Failures.pdf. Last Accessed 19 Nov 2021.
18. Schmidlin TW. Human fatalities from wind-related tree failures in the United States, 1995–2007. Nat Hazards. 2009;50:13–25. https://doi.org/10.1007/s11069-008-9314-7.
19. Walsh RA, Ryan L. Hospital admissions in the Hunter Region from trees and other falling objects, 2008–2012. Aust N Z J Public Health. 2017;41(2):121–4. https://doi.org/10.1111/1753-6405.12614.
20. Ball DJ, Watt J. The risk to the public of tree fall. J Risk Res. 2013;16(2):261–9. https://doi.org/10.1080/13669877.2012.737827.
21. Hall GC, Kinsman MJ, Nazar RG, et al. Atlanto-occipital dislocation. World J Orthop. 2015;6(2):236–43. https://doi.org/10.5312/wjo.v6.i2.236.
22. Teh J, Firth M, Sharma A, Wilson A, Reznek R, Chan O. Jumpers and fallers: a comparison of the distribution of skeletal injury. Clin Radiol. 2003;58(6):482–6. https://doi.org/10.1016/s0009-9260(03)00064-3.
23. Buckman RF Jr, Buckman PD. Vertical deceleration trauma. Principles of management. Surg Clin North Am. 1991;71(2):331–44. https://doi.org/10.1016/s0039-6109(16)45383-1.
24. Li L, Smialek JE. The investigation of fatal falls and jumps from heights in Maryland (1987–1992). Am J Forensic Med Pathol. 1994;15(4):295–9. https://doi.org/10.1097/00000433-199412000-00003.
25. Petaros A, Slaus M, Coklo M, Sosa I, Cengija M, Bosnar A. Retrospective analysis of free-fall fractures with regard to height and cause of fall. Forensic Sci Int. 2013;226(1–3):290–5. https://doi.org/10.1016/j.forsciint.2013.01.044.

26. Türk EE, Tsokos M. Pathologic features of fatal falls from height. Am J Forensic Med Pathol. 2004;25(3):194–9. https://doi.org/10.1097/01.paf.0000136441.53868.a4.
27. Gupta SM, Chandra J, Dogra TD. Blunt force lesions related to the heights of a fall. Am J Forensic Med Pathol. 1982;3(1):35–43. https://doi.org/10.1097/00000433-198203000-00008.
28. Çakı İE, Karadayı B, Çetin G. Relationship of injuries detected in fatal falls with sex, body mass index, and fall height: An autopsy study. J Forensic Leg Med. 2021;78: 102113. https://doi.org/10.1016/j.jflm.2020.102113.
29. Goonetilleke UK. Injuries caused by falls from heights. Med Sci Law. 1980;20(4):262–75. https://doi.org/10.1177/002580248002000407.
30. Türkoğlu A, Sehlikoğlu K, Tokdemir M. A study of fatal falls from height. J Forensic Leg Med. 2019;61:17–21. https://doi.org/10.1016/j.jflm.2018.10.008.
31. Thierauf A, Preuss J, Lignitz E, Madea B. Retrospective analysis of fatal falls. Forensic Sci Int. 2010;198(1–3):92–6. https://doi.org/10.1016/j.forsciint.2010.01.010.
32. Osawa M, Satoh F, Hasegawa I. Acute death due to hyperextension injury of the cervical spine caused by falling and slipping onto the face. J Forensic Leg Med. 2008;15(7):457–61. https://doi.org/10.1016/j.jflm.2008.02.006.
33. Eş H, Şahin MF, Özdemir E. Laryngohyoid fractures in fatal nonhomicidal falls from a height. Am J Forensic Med Pathol. 2017;38(4):289–93. https://doi.org/10.1097/PAF.0000000000000350.
34. de la Grandmaison GL, Krimi S, Durigon M. Frequency of laryngeal and hyoid bone trauma in nonhomicidal cases who died after a fall from a height. Am J Forensic Med Pathol. 2006;27(1):85–6. https://doi.org/10.1097/01.paf.0000201104.10652.08.
35. Lowenstein SR, Yaron M, Carrero R, Devereux D, Jacobs LM. Vertical trauma: injuries to patients who fall and land on their feet. Ann Emerg Med. 1989;18(2):161–5. https://doi.org/10.1016/s0196-0644(89)80107-6.
36. Gill JR. Fatal descent from height in New York City. J Forensic Sci. 2001;46(5):1132–7.
37. Hyder AA. Injuries in low- and middle-income countries: a neglected disease in global public health. Injury. 2013;44(5):579–80. https://doi.org/10.1016/j.injury.2013.01.028.
38. Rehan R, Jones PD, Abdeen H, Rowas H, Dhaliwal J. The dangers to children from coconut tree trauma, in KiraKira, Solomon Islands: a retrospective clinical audit. Arch Public Health. 2016;74:14. https://doi.org/10.1186/s13690-016-0125-0.
39. Barss P, Dakulala P, Doolan M. Falls from trees and tree associated injuries in rural Melanesians. Br Med J (Clin Res Ed). 1984;289(6460):1717–20. https://doi.org/10.1136/bmj.289.6460.1717.
40. Barss P. Injuries due to falling coconuts. J Trauma. 1984;24(11):990–1. https://doi.org/10.1097/00005373-198411000-00012.
41. Gupta A, Reeves B. Fijian seasonal scourge of mango tree falls. ANZ J Surg. 2009;79(12):898–900. https://doi.org/10.1111/j.1445-2197.2009.05141.x.
42. Mulford JS, Oberli H, Tovosia S. Coconut palm-related injuries in the Pacific Islands. ANZ J Surg. 2001;71(1):32–4. https://doi.org/10.1046/j.1440-1622.2001.02021.x.
43. Negin J, Vizintin P, Houasia P, Martiniuk AL. Barking up the wrong tree: injuries due to falls from trees in Solomon Islands. Med J Aust. 2014;201(11):698–700. https://doi.org/10.5694/mja14.01083.
44. Dakouré PW, Diallo M, Traoré AC, et al. Trauma related to falls from trees treated in a specialized trauma centre in Burkina-Faso-one hundred and six cases treated in one year. Int Orthop. 2015;39(12):2451–6. https://doi.org/10.1007/s00264-015-2966-5.
45. International Labour Organization: tropical tree and palm crops;2011. https://www.iloencyclopaedia.org/part-x-96841/agriculture-and-natural-resources-based-industries/tree-bramble-and-vine-crops/item/548-tropical-tree-and-palm-crops. Last Accessed 14 Oct 2021.
46. Escoffery CT, Shirley SE. Fatal head trauma from tree related injuries. Med Sci Law. 2001;41(4):298–300. https://doi.org/10.1177/002580240104100404.
47. Baby dies after being hit by falling cluster of coconuts. In: Honolulu star-bulletin;1973. https://www.newspapers.com/clip/18012093/baby-dies-after-being-hit-by-falling/. Last Accessed 12 Oct 2021.

48. Monkey kills man with coconut. In: New Straits Times;2001. https://www.news24.com/News24/Monkey-kills-man-with-coconut-20010813. Last Accessed 12 Oct 2021.
49. Ersoy S, Sonmez BM, Yilmaz F, et al. Analysis and injury paterns of walnut tree falls in central anatolia of turkey. World J Emerg Surg. 2014;9:42. https://doi.org/10.1186/1749-7922-9-42.
50. Hoseini Azizi T, Hejazi SS, Kameli A. Frequency of complications of falling from the walnut tree, as an occupational-seasonal injury. J Inj Violence Res. 2018;10(2):91-96. https://doi.org/10.5249/jivr.v10i2.980.
51. Nabi DG, Rashid TS, Kangoo KA, Ahmed DF. Fracture patterns resulting from falls from walnut trees in Kashmir. Injury. 2009;40(6):591–4. https://doi.org/10.1016/j.injury.2008.11.013.
52. Baba AN, Paljor SD, Mir NA, et al. Walnut tree falls as a cause of musculoskeletal injury–a study from a tertiary care center in Kashmir. Ulus Travma Acil Cerrahi Derg. 2010;16(5):464–8.
53. Javadi SA, Naderi F. Pattern of spine fractures after falling from walnut trees. World Neurosurg. 2013;80(5):e41-3. https://doi.org/10.1016/j.wneu.2012.12.014.
54. Crockett A, Stawicki SP, Thomas YM, et al. Tree stands, not guns, are the midwestern hunter's most dangerous weapon. Am Surg. 2010;76(9):1006–10.
55. Smith JL, Lengerich EJ, Wood GC. Injuries due to falls from hunters' tree stands in Pennsylvania. Am J Prev Med. 2009;37(5):433–6. https://doi.org/10.1016/j.amepre.2009.06.019.
56. Centers for Disease Control (CDC). Tree stand-related injuries among deer hunters–Georgia, 1979–1989. MMWR Morb Mortal Wkly Rep. 1989;38(41):697–700.
57. Gates RL, Helmkamp JC, Wilson SL, Denning DA, Beaver BL. Deer stand-related trauma in West Virginia: 1994 through 1999. J Trauma. 2002;53(4):705–8. https://doi.org/10.1097/00005373-200210000-00014.
58. Lawrence DW, Gibbs LI, Kohn MA. Spinal cord injuries in Louisiana due to falls from deer stands, 1985–1994. J La State Med Soc. 1996;148(2):77–9.
59. Lazzara AA Jr, Ditmer BI, Doughty KW, Reynolds KR. Tree stand-related injuries in nonadmitted and admitted patients at a level 2 trauma center in Michigan: 2015–2019. Wilderness Environ Med. 2021;S1080–6032(21):00160–5. https://doi.org/10.1016/j.wem.2021.08.006.
60. Loder RT. Epidemiology of hunting stand injuries presenting to US emergency departments, 2008–2013. Wilderness Environ Med. 2015;26(3):387–94. https://doi.org/10.1016/j.wem.2014.07.004.
61. Metz M, Kross M, Abt P, Bankey P, Koniaris LG. Tree stand falls: a persistent cause of sports injury. South Med J. 2004;97(8):715–9. https://doi.org/10.1097/00007611-200408000-00003.
62. Urquhart CK, Hawkins ML, Howdieshell TR, Mansberger AR Jr. Deer stands: a significant cause of injury and mortality. South Med J. 1991;84(6):686–8.
63. VanWormer JJ, Holsman RH, Petchenik JB, Dhuey BJ, Keifer MC. Epidemiologic trends in medically-attended tree stand fall injuries among Wisconsin deer hunters. Injury. 2016;47(1):220–5. https://doi.org/10.1016/j.injury.2015.09.012.
64. Shields LB, Stewart D. Deer stand fatalities in Kentucky: two cases of reverse suspension and blunt force trauma. Am J Forensic Med Pathol. 2011;32(1):39–43. https://doi.org/10.1097/PAF.0b013e3181eafe05.
65. Forks TP. Hunting injuries in Mississippi. J Miss State Med Assoc. 2002;43(11):339–43.

Chapter 9
Mountain Death Revisited: Mass Slope Movements, Mountain Associated Suspension and Volcanos

Guy N. Rutty

Introduction

Landscape can be defined as a *mountain* based on its elevation and slope. Using the 7 classes defined by Blyth et al., mountains account for approximately 27% of the Earth's surface [1]. An estimated 1 in 10 people live in a mountainous region with an estimated 100 million tourists worldwide visiting mountainous areas annually [2]. All year round both adults and children alike will suffer morbidity or death due to living in or visiting mountainous regions across the world [3]. This is not only because of the nature of the activity undertaken but because of the physiological challenges placed upon the individual due to a combination of falling barometric pressure, temperature, and humidity, together with increased solar radiation and wind speed [4].

Mountain associated deaths fall into four broad categories: trauma, cold injury, high altitude illness, and sudden cardiac death [4] of which only high altitude illness is specific to mountainous regions i.e. the other three categories are not dependent upon altitude. The 2019 edition of Essentials of Autopsy Practice contained a chapter related to death due to high altitude illness [5] as well as one related to extreme aerial sports, a cause of traumatic death in the mountains [6]. Thus, these subjects are not revisited here. In terms of mountain associated sudden cardiac death [SCD], 50% occur on the first day of downhill skiing or mountain hiking [2]. Males are 15 times more affected than females with 90% of all mountains associated SCD occurring in those aged 34 and above [7]. It is reported that triggers for mountain associated SCD include unusual physical exertion, late morning hours, dehydration and depletion of carbohydrate stores.

As the Essentials series is intended to focus on subjects not covered in detail in the general forensic pathology textbooks, this chapter will concentrate on the trauma

G. N. Rutty (✉)
East Midlands Forensic Pathology Unit, University of Leicester, Leicester Royal Infirmary, Robert Kilpatrick Building, Leicester, UK
e-mail: gnr3@le.ac.uk

G. N. Rutty (ed.), *Essentials of Autopsy Practice*,
https://doi.org/10.1007/978-3-031-11541-7_9

category of mountain deaths. As the pathology related to falls such as occur with rock/ice climbing or canyoning, drowning as may occur with white water sports or collision with objects such as trees, as could occur when skiing or cycling in the mountains, will be familiar to forensic pathologists, for this chapter I have decided to consider deaths related to the general subject of mass slope movements and associated events, suspension related to mountain activities and deaths related to volcanic activity as these areas gain lesser attention in general reference sources. I hope that by focusing on these areas this will provide a reference source for those not used to encountering a death under such circumstances.

Mass Slope Movements

Each year thousands of individuals suffer morbidity and mortality as a result of the sudden and unexpected movement of the surface within the immediate environment of their geographical location. Although this need not be restricted to mountaneous areas, two different types of mass slope movements and asscoiated events which can be associated with mountains will be considered within this section.

Landslides

The term "landslide" is considered equivalent to the word "landslip", a term first introduced by Lyell in 1833 to describe when "*a portion of land that has slid down in consequence of disturbance by an earthquake or from being undermined by water washing away the lower beds which supported it*" [8]. The word landslide itself was first used in March 1838 in the Jeffersonium Magazine in the reporting of an incident that occurred to the City of Natchez. This was followed later in the year in October 1838 in the Niles National Register in relation to an incident in Vicksburg. The first classification of landslides is attributed to Dana who, in 1862, classified landslides into debris flows, earth spreads and rock slides [9]. The word itself was redefined by Sharpe in 1938 as the perceptible downward slide or fall of a relatively dry mass of earth, rock or mixture of the two. This definition and term were adopted and updated by Varnes in 1958 [10]. Although today there are several classifications related to landslides [10, 11] they arise as variations of the 1996 classification of Cruden and Varnes [12]. In their 1996 document they define a landslide as "*the movement of a mass of rock, debris or earth down a slope*", and go on to explain how a landslide can be described by a word describing the material, where the material is either rock, debris or earth, and a second word describing the type of movement, which can be one of five types; falls, flows, slides, spreads and topples (Fig. 9.1).

Every year several thousand people die as a result of a landslide [13]. Mortality is reported to be higher in developing countries, with males outnumbering females, and the younger age groups at greater risk than the elderly [14]. People can die as either

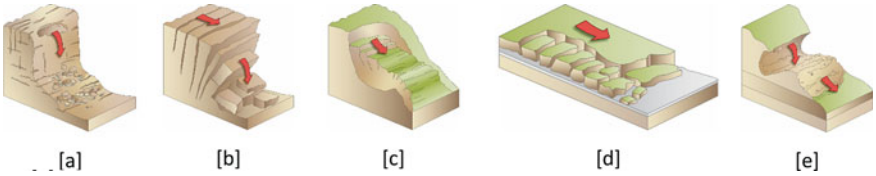

Fig. 9.1 The principal types of landslides. **a** Fall, **b** topple, **c** slide, **d** spread and **e** flow. The arrow indicates the direction of mass slope movement. Illustrations courtesy of Vicky Eves, UK

pedestrians or drivers/passengers in vehicles when the road is struck by a landslide, as well as in trains, or at work, for example, as lumberjacks or shepherds. Deaths can occur in the mountains, on beaches, or in the countryside. The commonest scenario is to be killed within a building which can partially or completely collapse when engulfed by a landslide.

Ph et al., provide a description of the autopsy findings of six people killed when a landslide struck a minibus they were travelling in [15]. Five sustained a head injury in the form of skull fractures, brain lacerations and intracranial bleeds. All six sustained chest injuries in the form of rib fractures, lung and heart injuries. Abdominal organ injuries and limb mutilation were also described. The main cause of death was considered to be traumatic/compression asphyxia with one case attributed to mechanical asphyxia due to clogging of the entire airway with soil as well as multiple fractured ribs. Asphyxia as the principal cause of death in landslide victims has also been reported by Pereira et al. [16].

A death has been reported related to the rescue of a victim of a landslide. In this case a 41-year-old female was working in the bottom of a hole when a landslide occurred. She was completely buried under earth and sand. A power shovel was used in an attempt to rescue her. This resulted in her sustaining a fatal injury to her head as well as an injury to her left axilla from the claws of the shovel. In addition to these injuries she sustained rib fractures, lung lacerations, left arm bone fractures as well as conjunctival and internal organ petechiae which were all attributed to the landslide [17].

Avalanches

Avalanches can be considered as a mass of snow sliding, tumbling or flowing down an inclined surface [18]. Several types are described (Fig. 9.2). "*Slab avalanches*" account for nearly all avalanche deaths in North America. These are cohesive plates of snow that slide as a unit on the snow underneath. They are typically about the size of half a football pitch, about 30–80 cm deep and reach 30 km/h within 3 s, accelerating to 130 km/hr within 6 s. When loose snow slides down a mountainside it is known as a "*loose snow avalanche*". Small versions of this type are known as "*sluffs*". As they start at a point and fan outwards as they descend, they are also known as "*point releases*". Few people are killed by this type, mainly climbers, although

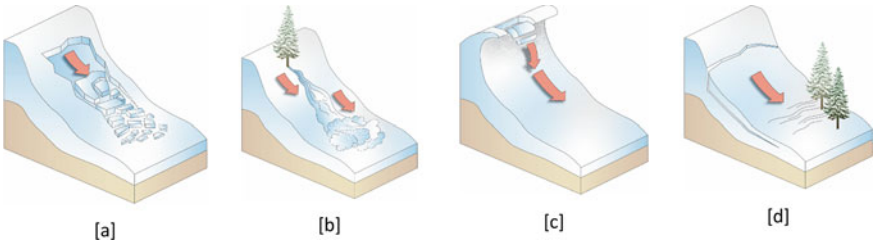

Fig. 9.2 The principal types of avalanches. **a** Slab, **b** loose snow, **c** falling cornice, and **d** slab. The arrow indicates the direction of avalanche movement. Illustrations courtesy of Vicky Eves, UK

houses may be buried by them and people can be swept by them over cliffs, into crevasses or become buried in gullies. After these two main types, a number of lesser types, in terms of their potential to cause fatalities, are described. "*Icefall avalanches*" occur when blocks of ice fall from an icefall, the ice equivalent to a waterfall. Few people are killed by these, again mainly climbers. Cornices i.e. cantilevered snow structures formed by wind drifting snow onto the downside of an obstacle such as a ridgeline can break into pieces resulting in a "*cornice fall avalanche*". As with icefall avalanches, few deaths are associated with cornice fall avalanches. "*Glide*" occurs over several days and is when the entire snowpack slides slowly as a unit, similar to a glacier on the ground. Occasionally there can be a catastrophic release resulting in a "*glide avalanche*". Finally, the "*slush avalanche*" is seen in the Brookes Range, Alaska or northern Norway where there is impermeable permafrost soil. These are seen on gentle slopes and rarely occur on slopes steeper than 25 degrees. The slush can run for long distances. As few people live in high altitude, permafrost mountains, few are killed by this type of avalanche.

The type of snow that constitutes the avalanche is important [19]. Avalanches are described as being composed of wet or dry snow. Both can occur as slab or loose snow avalanches. Wet snow avalanches typically travel at slower speeds [15–30 km/h] and account for fewer deaths, usually climbers compared to dry snow avalanches, which can travel at 100–130 km/hr catching the person in a tumbling mass of snow. During their passage they may encounter not only blocks of snow but also rocks, trees and cliffs. When they halt, they may be partially or fully buried under snow, in a variety of positions, disorientated with regards to where the surface is [20]. Time to extrication then becomes a critical factor as to whether one survives or not. There is a reported 80% survival if uncovered immediately, with the chance of survival reduced by one half for every hour they continue to be buried [21] Factors that affect survivability are the depth of burial, duration of burial, severity of any trauma, presence of an air pocket and the presence of a patent airway [22].

Approximately 150 persons a year die in Europe and North America due to avalanches [22]. The median age for death is suggested at 35 years with recreational backcountry [outside the normal boundaries of a ski resort] skiers, snowboarders and snowmobiles accounting for 90% of deaths [23]. More males die than females [24]. The overall mortality rate is around 23% with a 40% mortality rate for partial

burial and 52% for complete burial [25]. Survival in those buried deeper than 1 m is rare due to difficulty in finding them and the effect of the weight of snow upon them [26]. Snow can weigh 800 kg/m^3 and can freeze solid around the victim once the avalanche stops [27].

Trauma accounts for up to 24% of avalanche associated deaths [28]. These deaths are associated with wet snow, and rocky, forested terrain with the deaths mainly occurring in the first 30 min after burial [22, 29]. The chest and head represent the commonest anatomical areas of traumatic injury.

Although trauma causes death in the immediate period after an avalanche, asphyxia is the overall commonest mode of death following avalanches [22, 28, 30]. Several different modes of asphyxia may account for the death. In the first 10 min death can be due to complete airway obstruction by snow. If no air pocket has been created, then there may be no available breathable air. Dry powder snow has more available oxygen than wet snow. If an air pocket is present, after approximately 30 min hypoxia ensues with associated hypercarbia due to a build-up of CO_2 within the air pocket. Humidified exhaled air can condense around the nose and mouth forming an ice mask which prohibits ventilation [25]. The position of the victim under the snow as well as the weight of the snow of the chest and abdomen may result in compression/positional asphyxia. Finally, the airway may become compromised by gastric contents.

Although the victim is buried under snow, hypothermia accounts for as little as 1% of deaths [28]. Death may be caused by drowning if a person is swept into water and on occasion may be due to natural cardiac disease [31].

As the victim would be expected to wear winter outdoor clothing, there are often few injuries seen on external examination. These are described to be confined to the head and face area, comprising abrasions, bruises or lacerations depending upon what has made contact during the avalanche [24, 32]. Those dying of asphyxia may show little, if any, external traumatic injuries. If positional/compression asphyxia is the principal form of asphyxia they may show marked congestion of the facial and chest areas [21] which may be accompanied by congestion of the chest and abdominal organs internally. Brain oedema is reported in cases dying of asphyxia. A range of internal skeletal and organ trauma may occur including base of skull fracture, neck fractures, rib fractures, haemothorax, liver and splenic laceration, pelvic fractures and upper and lower limb fractures [21, 22, 25, 26, 28, 32, 33]. Ligament injury of the knees is common. Injuries to the upper limbs are thought to arise as the victim swings their arms or puts their hands up during the avalanche. Injuries to the lower limbs may be caused as the limbs become entangled in skis. Skis and snowboards can also act as an anchor, trapping the victim [25].

Lung congestion and pulmonary oedema with froth within the tracheobronchial tree is described along with acute pulmonary emphysema and an increase in lung weight [21, 22, 32, 34]. Two mechanisms are proposed. The first is negative pressure oedema as a result of upper airway obstruction [34]. The second, and more favoured, is one of acute cardiac failure. This is thought to arise due to a combination of the effects of hypoxia, peripheral surface cooling and compression of the body by the weight of snow. The net effect results in pulmonary artery hypertension, increased

peripheral arterial resistance due to vascular contraction and net transfer of fluid to the blood. Arrest of respiratory movement abolishes the haemodynamic pump effect of the lungs. The resulting effect is centralisation of the blood with high-pressure gradient over the pulmonary capilliary-alveolar membrane causing acute pulmonary oedema, and haemorrhage [21, 34, 35].

Radiology of Avalanche Victims

The papers of Wick et al., and Grosse et al., describe the radiological findings associated with avalanche fatalities [25, 33]. A wide range of musculoskeletal injuries are described within these and the general avalanche trauma literature including base of skull, humerus and radial bone fractures, shoulder subluxation and scapholunate dissociation. Lower limb injuries include bone fractures as well as medial meniscal tear, medial and lateral collateral ligament rupture, posterior cruciate ligament sprain and knee cartilage defects. Spinal fractures include transverse process fractures, compression fractures at the level of T9 and L2-4 as well as C6/C7 dislocation fractures. Sternal, rib and pelvic fractures are all described. In terms of extra skeletal injury, within the cranial cavity cerebral contusion, epidural haematoma, and cerebral oedema and ischaemia are reported. Within the thorax one may observe pulmonary contusion, pneumo and/or haemothorax and hypoxic pulmonary oedema. Although Cohen et al., illustrate the computed tomography [CT] findings of ground glass opacities typical of pulmonary oedema, this is a non-ventilated scan and I caution readers concerning the risk of over interpreting postmortem CT lung findings [34]. Finally, cardiac, liver and kidney contusion as well as splenic and small intestinal rupture are described.

Non-avalanche-Related Snow Immersion Deaths

First reported in 1994 by Kizer et al. [36], non-avalanche-related snow immersion deaths [NARSID], also known as *tree well* and *deep snow immersion* asphyxiation, is a rare cause of death of often experienced, backcountry skiers and snowboarders, predominately in western North America although deaths have been reported from the Tatra Mountains of Poland [37–39]. A *tree well* is a void or depression that forms around the base of a tree. The branches of the tree may disguise the presence of the void which may contain a mix of loose snow, air and tree branches. Deaths usually occur during or immediately after large snowstorms when snow is soft and deep [a tree well may be 10 feet deep or more], particularly in association with coniferous trees although death can occur in deep snow on open slopes. Tree branches may hide the well and be the source of additional snow which can deposit onto the victim.

The skier or snowboard falls into the well or hole, such that they are upside down (Fig. 9.3). Snow then falls onto them from the sides as well as from overhead branches.

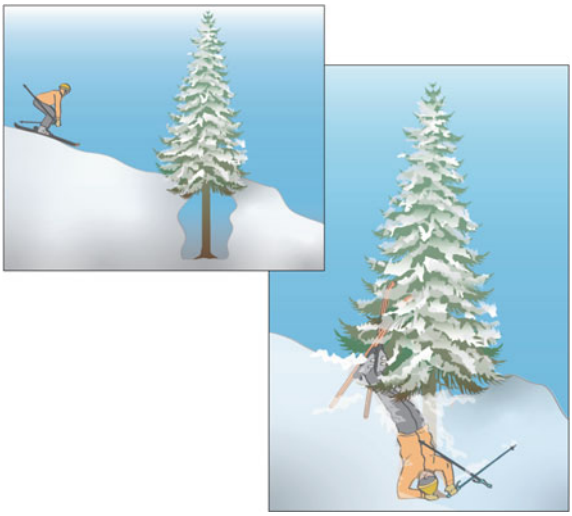

Fig. 9.3 A skier approaches a tree well [left]. They go head first into it ending up in an inverted position. From which they cannot escape. Illustrations courtesy of Vicky Eves, UK

Snow may also enter their clothing due to their inverted position. Movement, in an attempt to escape, causes them to go deeper into the well. Spatial orientation is lost. In experiments undertaken in 1998–1999 volunteers placed inverted into a snow well could not escape. Unfastening of skis was found to cause them to go deeper into the well whereas snowboarders were unable to unfasten their bindings [37].

Injuries and hypothermia are not reported in these deaths, as death is due to asphyxiation. As with avalanches, asphyxia may result from airway obstruction due to snow or gastric contents, the formation of an ice mask, CO_2 rebreathing and their position. As an air pocket is not present, death is reported to occur within 5–10 min although some may survive as long as 15–30 min.

Suspension

Both head-down and head up supension deaths may occur in relation to mountains.

Head-Up Suspension

From time to time individuals may become trapped, suspended in a vertical or near-vertical, motionless position. An early example of death associated with position is head-up crucifixion. Today, typically this occurs where a rope and harness is used to prevent a fall in activities related to occupational work on high structures such as buildings, pylons bridges, dams or off-shore platforms as well as recreational sports such as climbing or caving. Sitting in a harness can be tolerated for hours at

a time as long as the person remains mobile. If they suffer injury, exhaustion, hypoglycaemia, hypothermia, mental or technical problems and thus become motionless in a suspended position this can lead to pathophysiological complications which, if uncorrected, can result in death in the absence of traumatic injuries.

A number of terms are used to describe the loss of consciousness that may occur whilst suspended; *harness-induced pathology*, *orthostatic shock while suspended*, *suspension syncope*, *suspension trauma* and *suspension syndrome.*

Motionless suspension in a harness results in orthostatic pooling of blood to the lower limbs (Fig. 9.4). Twenty percent of circulatory volume can be lost due to this pooling resulting in a relative hypovolaemic state [40]. It is hypothesised that the motionless state results in a loss of a muscle pump which in turn causes a reduction of cardiac preload and subsequent decrease in cardiac output. A fall in heart rate and blood pressure indicates the onset of a pre-syncope state which is suggested to be a vagally driven mechanism with mixed vasodepressive and cardioinhibitory pattern [41]. Various authors have reported this stage can be reached in volunteers between 5 and 59 min of motionless suspension [40–42]. Continued reduced cardiac output results in reduced tissue perfusion with resultant cerebral hypoperfusion. This can lead to loss of consciousness and, after several hours, death [42].

Progressive limb engorgement also leads to loss of vascular tone, capillary leak and limb swelling. This in turn will result in limb ischaemia. If the suspended person is then released in an uncontrolled manner, "*rescue cardioplegia*" can occur. Here, the sudden uncontrolled release of cold, pooled blood causes a sudden increase in preload on the right heart whilst at the same time afterload and systemic vascular resistance falls. The released pooled blood contains a mix of toxic metabolites with reduced pH and increased potassium, magnesium, calcium, phosphate and amino acids. The combination of pre and afterload strain with the toxic blood mix can result in an alteration of cardiac conduction properties resulting in asystole. Limb ischaemia of 2–3 h duration has also been reported to result in rhabdomyolysis which can lead to acute renal failure [43].

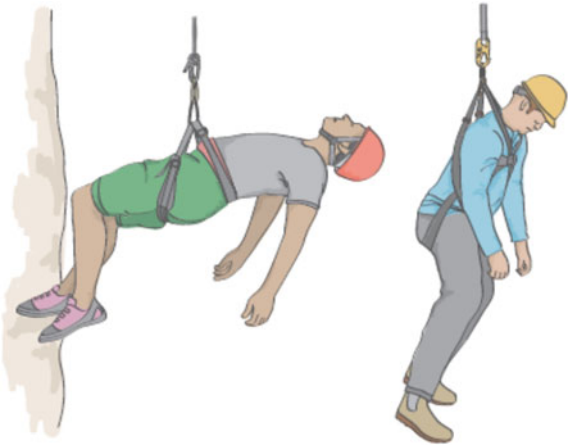

Fig. 9.4 Motionless suspension in with a rope and harness in a climber [left image] and an occupational worker working at height [right image]. Note the different type of harness worn affects the way that the unconscious person is suspended. Illustrations courtesy of Vicky Eves, UK

Those suspended at a height, for example by gripping onto a ledge or rail, can sustain bruising and tears to the upper anterior and posterior muscles of the thorax.

Although unrelated to mountain environments, for completion of the subject"*reverse hanging*", a head-up suspension torture technique also known as "*Palestinian hanging*", "*strapped*", "*Scorpion Position*" or "*Akreb*" is where the victim is suspended by their hands tied together behind their back. It can result in muscle and tendon injuries, brachial plexus injury and shoulder joint injury. A single case is reported where death followed prolonged reverse hanging. In this case shoulder muscle necrosis lead to rhabdomyolysis and myoglobinuric renal failure [44].

Head-Down Suspension

Humans are designed to function vertically and horizontally, not upside down although they are able to tolerate an inverted state for prolonged periods of time [45]. An example of this was the Scirocco rollercoaster incident in Belgium, 1997 when 26 passengers were suspended upside down for 1.5 h when the coaster became stuck at the top of the middle loop. All were young and healthy, and none sustained any life-threatening injury. Inversion stimulates a range of physiological reflexes that try to compensate for the abnormal gravitational effects of inversion, specifically related to blood pooling and impaired venous return [46]. As with head-up suspension, if an individual remains in a head-down position for a protracted period of time, as occurs in non-avalanche-related snow immersion deaths, death can ensue.

Death following head-down suspension is commonly referred to as a form of positional asphyxia although Sauvageau et al., in their review of the literature suggests that it is a distinct pathological entity [47]. One of the earliest examples of death following head-down suspension is that of the crucifixion of St. Peter which is depicted in religious themed paintings across the world. St Peter is reported to have requested to be crucified in this position. The nineteenth century drawing of Francisco de Goya "One Cannot Watch" illustrates how the head-down position was used as a method of torture [48]. Inverted hanging as a form of public execution has been recorded since the fourteenth century. Sometimes referred to as "*Jewish execution*", although not specific to those of the Jewish faith, the hanging of individuals in the inverted position between two hanging dogs has become historically associated with the punishment of Jews [49].

Death following head-down suspension is considered rare and usually accidental in nature although Hilgermann and Richter report a case of intentional head-down suspension where a male simulated his own slaughtering in a position similar to that of slaughtering a pig [50]. It can occur indoors, for example through intentional suspension [51], after falling through floorboards in a ceiling [51] or becoming suspended on broken boarding [46] or more commonly outdoors, for example from railings [52, 53], windows [51], or fences [54]. Typically, the deceased hangs trapped,

inverted by one foot or ankle, often fully suspended with the arms reaching down towards the ground and the non-trapped leg extended outwards at almost right angles to the body (Fig. 9.5). Intoxication with alcohol is a feature of some reported cases.

Schäffer suggests that males, possibly due to more risky behaviour, are at greater risk of death than females. The elderly, particularly those with pre-existing cardiovascular disease, are also at greater risk, although an infant of 11-months age is described as dying from been suspended head down from a crib with a foot stuck in the crib rods [55].

Typically, there is no pathoanatomical finding to account for death. The normal external observation is congestion of the head, neck and other dependent parts of the body, often described as being marked or "monstrous" in nature. In the work by Schäffer, a case is illustrated courtesy of Tsokos of the face demarcated into two distinct halves at the level of the nose by the demarcation between the congested and non-congested part. Trauma sufficient to cause death is usually absent although non-fatal traumatic injuries may occur, caused whilst coming into the position they are found in or during attempts to self-extricate themselves from the inverted position. In relation to the latter, their fingernails may be broken, and one case is described where abdominal wall muscle haemorrhage was attributed to the victims attempt to self extracate. Internally, congestion of the brain and dependent lobes of the lungs are usually observed. Brain and lung oedema is described as well as stress ulceration of the gastric mucosa.

Death in this position occurs over a protracted time frame. In the experimental work Uchigasaki et al., they report how rabbits suspended upside down took between

Fig. 9.5 Head down suspension. The deceased is typically found suspended by one leg with the ankle snagged on a structure such as a railing. The other leg is extended laterally with the arms and head hanging free of the ground [right image] or the airway compromised due to hyperflexion of the neck as the head rests on the ground [left image]. Illustrations courtesy of Vicky Eves, UK

17–44 h, mean 26 h, to die [56]. Other authors agree on a prolonged time frame and thus exhaustion is also suggested to be a factor in these deaths.

The exact mechanism to cause death remains disputed in the literature. Purdue suggested that the cause of death was one of asphyxia, hence it is often termed positional asphyxia [52]. He suggested that the inverted position likely caused a stretching effect resulting in tensing of the abdominal wall which in turn hindered expiration. Further, the weight of the arms and upper body induced fixation on inspiration. This net effect along both directions of the long axis of the body was proposed to fix or splint the chest, making breathing difficult in both phases of breathing. However, a year later Lawler suggested that the circulatory effects of inversion i.e. orthostatic blood pooling, impairment of venous return and physiological reflexes were the underlying cause of death [46]. This mechanism would be similar to that of head-up suspension. He also suggested that hypothermia may play a role in some deaths. Madea explored both theories further concluding that the head-down position resulted in marked depletion of venous return of blood to the heart, increase in transmural pressure in the venous part of the cerebral circulation and probable decrease in arterial blood pressure. Altered ventilation could also affect venous return to the heart [52]. More recently De Donno et al., favoured a respiratory mechanism [54] whereas Schäffer [55] and then Sauvageau et al. [47] draw upon clinical data involving the head down tilt position [HDT], as well as experiments with centrifuges and microgravity conditions to suggest a cardiac failure mechanism to explain the death. A HDT of more than 30° results in a significant increase in cardiac output due to an increase in stroke volume, increased passive filling of the left ventricle, increased arterial pressure, along with decrease in peripheral resistance, increase in venous return and increase in cerebral resistance. Oxygen saturation and pressure of carbon dioxide remains stable. Blood pressure was also significantly altered with the arms hanging downwards compared to when the arms remained alongside the body [47, 57] Both conclude that this supports that heart failure, not asphyxia is the important mechanism in these deaths.

Other mechanisms can explain the death. Heath et al., discuss a case where exsanguination occurred whilst in a head-down position as well as how, when the head is resting on the floor with the neck in a hyperflexed position, upper airway comprise is an important mechanism in the death (Fig. 9.5). The weight of the abdominal organs may also affect diaphragmatic movement and obesity as well as pregnancy may also be important factors in these deaths. Non-fatal traumatic abdominal injury sustained whilst suspended in an inverted position by a rope tied around the waist attached to a motor vehicle is described in the literature. In this case a worker was cutting vegetation from a cliff when the vehicle he was attached to sped off. The worker sustained traumatic injury to the small intestine and seromuscular layers of the ascending and descending colon [58].

Volcanos

A volcano, according to the Global Volcanism Program [GVP], is defined as "an accumulation of explosively or effusively erupted materials originating from single or multiple vents or fissures at the surface of the Earth or other planets" [59]. At any one time, for example as you read this chapter, they suggest that 20 volcanoes are erupting worldwide [59]. The GVP website illustrates 10 different types and features of volcanoes as follows [modified from source information found at [59]]:

1. Stratovolcanoes—also called composite volcanoes these are large complex volcanoes formed over tens of hundreds of thousands of years from accumulating lava flows, lava domes and explosive deposits.
2. Shield volcanoes—mostly created through low viscosity, low silica lava flows from effusive eruptions these are low-angled, broad volcanoes that may be part of a volcanic chain or field.
3. Calderas—large depressions formed by subsidence that can span up to 50 km in diameter.
4. Volcanic craters—the top surface opening of conduits formed by explosive excavation or ejection of rock and build-up of material around the vent.
5. Fissures—elongated vents with a range of activity from lava fountaining and flows to explosive events.
6. Scoria cones—also known as cinder cones these are the smallest and most abundant of volcanic features ranging from tens to hundreds of meters in height. Formed over a single eruption period of days to years, they occur in tens to hundreds in association with volcanic fields, as well as on shield volcanos and stratovolcanoes.
7. Submarine volcanoes
8. Geothermal features
9. Maar volcanoes—usually spanning tens to around 200 m deep with a diameter of several hundred kilometres these structures contain a crater which cuts into the ground surface, a diatreme [a volcanic pipe] and a tephra ring around the crater.
10. Volcanic fields—systems that can have numerous volcanic features such as scoria cones, larva flows, maar craters, stratovolcanoes and vents.

Brown et al., inform us that over 29 million people worldwide live within 10 km of active volcanos and around 800 million within 100 km of them which, as we will see, is within a distance where volcanic activity may result in death [60]. From their analysis of the updated volcano fatalities database they report that between 1500 and 2017AD there were 278,368 volcano related fatalities [60]. In the earlier paper of Auker et al., they noted that the count was dominated by a handful of disasters and that most fatal incidents were associated with 10 or less fatalities [61].

Fatalities may occur in towns or villages related to the summit or crater, on the cone or those climbing to the summit, from falls or jumps into acidic crater lakes or thermal pools, from quiescent gas emissions, non-eruptive avalanches, floods

earthquakes and tsunamis [60, 62]. In relation to an active volcano a number of different mechanisms can result in death [60, 63–68]. These are presented below in terms of the increasing mean distance from the event (Fig. 9.6).

Ballistics

Explosive eruptions which involve rapid expansion of gas can result in fragmentation of magma into solid fragments [also known as "blocks"] or fluid [also known as "bombs"] [59]. The projectiles can range in size from centimetres to meters in diameter. Approximately 40% of deaths occurring within 5 km of the volcanic event are due to individuals been struck by projectiles [maximum distance reported 7 km, mean distance 1.7 km] [60]. Ballistics related fatalities usually involve small numbers of people and account for <1% of total fatalities. Hot ejecta may also start local fires.

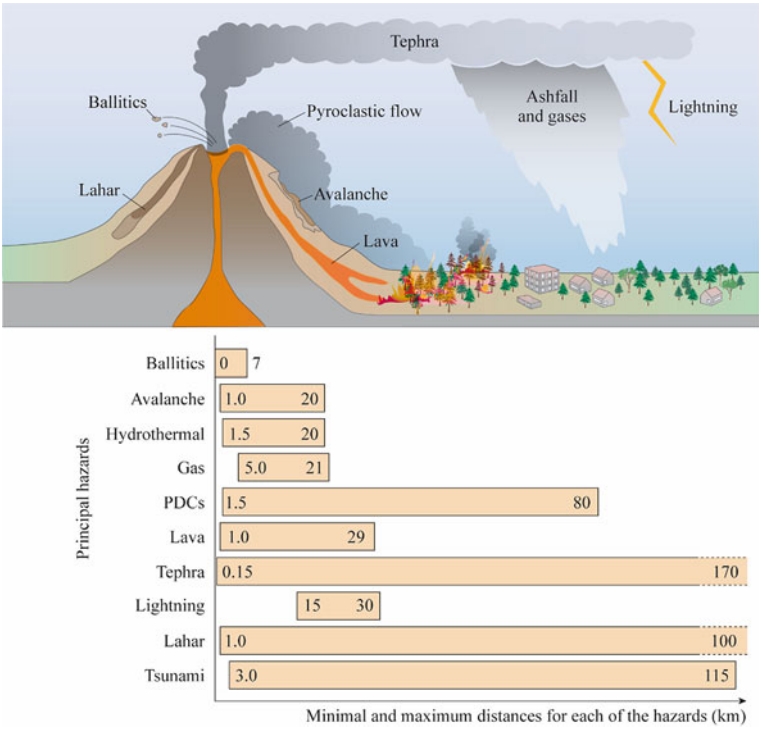

Fig. 9.6 Diagramatic reprsentation of the principal causes for death, with the exception of a tsunami, associated with vocanic activity. Underneath the image is a chart showing the minimal and maximum distances in kilometers from the event where deaths have been reporeted for each cause (*Source* [60]). Illustration courtesy of Vicky Eves, UK

Avalanche

Avalanches including debris avalanches, sector collapse and landslides resulting from unstable edifice collapse, seismic activity, eruption or intense rainfall have been reported to result in deaths up to 20 km from the volcano [minimum distance reported 1.0 km, mean distance 8.3 km] [60]. When the avalanche goes into water, there may be a resultant tsunami.

Hydrothermal

Fatalities associated with explosive hydrothermal incidents occur as a result of ejection of boiling water, mud, steam and ballistics. They are reported to occur around the explosion vent with deaths reported up to 20 km away [minimum distance reported 1.5 km, mean distance 9.3 km] [60].

Gas

Gases, in general, are not thought to pose a serious hazard [63]. The main gases associated with volcanic eruption are carbon dioxide [CO_2], sulphur dioxide [SO_2] and hydrochloric acid. Lesser gases of hydrogen fluoride, carbon monoxide and hydrogen sulphide [H_2S] may also be present [65]. Deaths associated with gases are reported up to 21 km from the eruption [minimum distance reported 5.0 km, mean 9.8 km] [60]. Deaths may also occur when the volcano is not erupting. So-called quiescent gas has been reported to result in deaths up to 74 km from the volcano [60].

Carbon dioxide is given off in large quantities during eruptions. It generally occurs in clouds or accumulations in low lying areas and may result in large numbers of deaths principally due to asphyxiation following exposure to high concentrations [66]. Victims have been described as falling asleep where they stand. Bullous and erythematous skin lesions have been described to the face [especially the cheeks], abdomen, back and legs. The blackened skin may resemble burns [66].

Sulphur dioxide exposure is associated with eye irritation and airway constriction, the latter of which has been reported to result in a small number of deaths in asthmatic tourists [66]. Similar eye and airway problems are reported due to exposure to sulphur dioxide, hydrochloric acid and hydrogen fluoride. Fluoride and heavy metal contamination may occur to local drinking water and vegetation [65].

Hydrogen sulphide, along with carbon monoxide, is a potential asphyxiant depending upon the concentration present [63]. Hydrogen sulphide is associated with respiratory tract problems as well as central nervous system disorders. The main health and mortality risk is reported in chronic exposure to the gas in those living near an active geothermal field [66].

Pyroclastic Density Currents

Pyroclastic density currents [PDC] or pyroclastic flows result in the largest number of deaths attributed to volcanic eruptions [60]. They are fast moving ground-hugging hot mixtures of dense rock, pumice, gas and ash from column or dome collapse, collapse of lava flow fronts, boiling over from a vent or phreatomagmatic eruptions [59, 63]. Death may be caused by the effects of heat [hundreds of degree Centigrade] and asphyxiation caused by the associated ash cloud up to 80 km from the eruption [minimal reported distance 1.5 km, mean distance 10.7 km] [60]. The word "blast" is often used in association with PDC's although the typical findings at autopsy of ruptured eardrums, and lung and organ contusions are often not present in the victims [64]. Although Baxter questions the reliability of the reports, it is suggested that PDC's may result in the peculiar phenomenon of whole body cadaveric spasm which could be enhanced by the effect of thermal coagulation or heat rigor [64]. Under such circumstances the person appears to have died instantaneously and remained frozen in the position they were in at the time of death.

Lava Flows

Lava is a mixture of molten rock, solid crystals and gas. It can have different flow velocities, lengths and thickness and may form domes and lakes. In general, it is slow moving but can travel a long way from the event [59]. As larva is slow moving, escape is possible and thus in general poses little risk to life. Having said that deaths have been reported up to 29 km from the volcano [minimal distance reported 1 km, mean distance reported 12.2 km] [60]. They can occur for example if an escape route is cut-off or an explosion occurs when larva interacts with vegetation, water or fuel [60].

Tephra

Tephra, also known as the ash cloud and associated ash fall has been associated with deaths up to 170 km from the eruption [minimal distance reported 0.5 km, mean distance reported 18.6 km] [60]. When the particle size is <10 μm the particles can enter the respiratory tract causing airway irritation particularly in those with asthma [63, 65]. Eye irritation and injury from foreign bodies may occur. Previous existing respiratory and cardiac conditions can be exacerbated resulting in death. The ash can be deposited on buildings resulting in roof collapse which in turn may cause fatalities [60]. In the long term, due to the minerals present within the cloud, patients may develop silicosis.

Lightening

Lightning is a common feature of volcanic ash clouds [60, 67]. As it may accompany the cloud as the cloud travels downwind deaths from lightning strikes have been reported up to 30 km from the eruption [minimum distance reported 15 km, mean distance 22.5 km] [60, 63].

Lahars

Lahars, also known as debris or mudflows, are a highly destructive, deadly volcanic phenomenon comprising of hot or cold mixtures of mud, water and volcanic rock that flow rapidly down channels that drain volcanoes [59, 63]. Their consistency has been described to resemble wet concrete [65]. They can flow for tens of hundreds of kilometres. Deaths, which may occur in the thousands, are reported up to 100 km from the event [minimum distance reported 1 km, mean distance reported 24.1 km] [60], principally due to drowning or trauma a result of being engulfed in the flow. When hot, thermal injury make occur.

Tsunami

Volcanic associated tsunami may occur due to debris avalanches and PDC's entering water along with eruption associated earthquakes, submarine eruptions, caldera collapse and volcanic shockwaves [60]. They account for the second total largest number of volcano associated deaths and can result in large numbers of deaths related to a single incident as exampled by the 1883 eruption of Krakatau where 36,000 deaths were attributed to the resulting tsunami [60]. Deaths have been reported up to 118 km from the eruption [minimum distance reported 3 km, mean distance 37.3 km] [60].

Indirect Deaths

In addition to direct deaths resulting from volcanic events, indirect fatalities are reported. Examples of this are road traffic related deaths caused during evacuation or unsafe driving conditions, sudden cardiac death, famine and disease for example by water contamination by lahars or mosquito-borne diseases such as malaria [60, 65]. Deaths have been reported from jumping or falling into geothermal pools, climbing the cone as well as falling into a volcanic fumarole whilst maintaining the protective fencing along its boarder [60, 62].

Postmortem Radiology of Volcano Fatalities

In 2015 selected images were released into the popular press from the postmortem computed tomography [PMCT] examination of 86 of the victims of the Mount Vesuvius eruption of 79AD [69]. Other than this and the radiological appearance of silicosis, a chronic adverse health effect associated with tephra, we have to apply the general known literature and experience of PMCT to volcano associated deaths rather than accessing a volcano specific reference list.

From the text above the principal mechanisms causing death in association with volcanos fall into the broad categories of trauma, thermal, asphyxia and drowning. These may range from single deaths to a mass fatality incident. In relation to the later PMCT can form part of a disaster victim identification response with the use of the INTERPOL radiology DVI form in conjunction with local or remote radiology reporting [70–72].

PMCT is recognised to be an excellent adjunct for the identification skeletal trauma. The work of Blau et al., is an excellent reference source to explore the range of skeletal trauma that can be identified through PMCT examination [73]. Both external and internal findings associated with the effect of heat can be observed using PMCT, from the effect of heat on the cranium, ribs, limb bones and digits to heat haematomas, the so-called "brainatoma" to chest and abdominal wall breaches and the protrusion of the small intestine outside the abdominal cavity [74–77]. Deaths due to asphyxia may show little if any findings using PMCT. Hyperinflation of the lungs may be observed in airway obstruction and asthmatics. Drowning on the other hand, although many of the changes may be viewed as nonspecific, has been reported to show a number of changes with PMCT examination from the presence of fluid within the facial sinuses, froth within the airways, hyperinflation of the lungs, haemodilution and layering of gastric contents [78–81].

Summary

Encountering a death related to a landslide, avalanche or volcano will depend upon where one practises in the world. In dealing with a death associated with such events it is important to have a general knowledge of the terminology applied to the event and the circumstances in which death may occur. This will allow one to predict the pathology that one may encounter. The pathology associated with and causing the death may not be unique to the event but rather fall into the broad categories of trauma, asphyxia, drowning, thermal/cold injury and sudden cardiac death. PMCT will play an increasing role in the investigation of the death, particularly in the case where multiple fatalities occur.

References

1. Blyth S, Groombridge B, Lysenko I, Miles L, Newton A. Environmental change and sustainable development in the mountains. https://wayback.archive-it.org/all/20080511044709/http://www.unep-wcmc.org/mountains/mountain_watch/pdfs/WholeReport.pdf. [last visited January 2022].
2. Niebauer J, Burtscher M. Sudden cardiac death risk in downhill skiers and mountain hikers and specific prevention strategies. Int J Environ Res Public Health. 2021; 1621. https://doi.org/10.3390/ijerph18041621.
3. Soule B, Lefevre B, Boutroy E. The dangerousness of mountain recreation: a quantitative overview of fatal and non-fatal accidents in France. E J Sport Sci. 2017;17:931–9.
4. Windsor JS, Firth PG, Grocott MP, Rodway GW, Montgomery HE. Mountain mortality: a review of deaths that occur during recreational activities in the mountains. Postgrad Med J. 2009;85:316–21.
5. Windsor J. Mountain deaths. In: Rutty G, ed. Essentials of Autopsy practice: reviews, updates and advances. Springer, London; 2019, pp. 111–128.
6. Feletti F. Fatalities related to extreme aerial sports. In: Rutty G ed. Essentials of Autopsy practice: reviews, updates and advances. Springer, London; 2019, pp. 129–142.
7. Burtscher M. Risk and protective factors for sudden cardiac death during leisure activities in the mountains: an update. Heart Lung Circ. 2017;26:757–62.
8. Lyell C. Principles of geology, being an attempt to explain the former changes of the Earth's surface, by reference to causes now in operation. London, vol. 3, 1833.
9. Cruden DM. The first classification of Landslides? Environmental & Engineering Geoscience 2003; IX, 605–608.
10. Li Y, Mo P. A unified landslide classification system for loess slopes: a critical review. Geomorphology. 2019;340:67–83.
11. Kazeev A, Postoev G. Landslide investigations in Russia and the former USSR. Nat Hazards. 2017;88:S81–101.
12. Cruden DM, Varnes DJ. Landslide types and processes. Transportation Research Board, U.S. National Academy of Sciences, Special Report. 1996; 247: 36–75.
13. Petley D. Global patterns of loss of life from landslides. Geology. 2012;40:927–30.
14. Salvati P, Petrucci O, Rossi M, Bianchi C, Pasqua A, Guzzetti F. Gender, age and circumstances analysis of flood and landslide fatalities. Sci Total Environ. 2018;610–611:867–79.
15. Ph M, Loyi M, Nabachandra H. Landslide fatalities: a study of six cases. J Indian Acad Forensic Med. 2012;34:182–4.
16. Pereira BMT, Morales W, Cardoso RG, Fiorelli R, Fraga GP, Briggs SM. Lessons learned from a landslide catastrophe in Rio De Janeiro. Brazil Am J Disaster Med. 2013;8:253–8.
17. Watanabe-Suzuki K, Nozawa H, Ishii A, Seno H, Suzuki O. A case of death due to rescue action by a power shovel after being buried alive. Legal med. 2001;3:241–5.
18. Avalanche.org http://avalanche.org/avalanche-encyclopedia/avalanche. Last checked January 2022.
19. International Association of Cryospheric Sciences. The International classification for seasonal snow on the ground. 2009. https://unesdoc.unesco.org/ark:/48223/pf0000186462. Last visited January 2022.
20. McIntosh SE, Grissom CK, Olivares CR, Kim HAS, Tremper B. Cause of death in avalanche fatalities. Wilderness Environ med. 2007;18:293–7.
21. Stalsberg H, Albretsen C, Gilbert M, Kearney M, Moestue E, Nordrum I, Rostrup M, Orbo A. Mechanism of death in avalanche victims. Virchows Archiv A Pathol Anat. 1989;414:415–22.
22. Kornhall DK, Martens-Nielsen J. The prehospital management of avalanche victims. J R Army Corps. 2016;162:406–12.
23. Berlin C, Techel F, Moor BK, Zwahlen M, Hasler RM. Snow avalanche deaths in Switzerland from 1995 to 2014—results of a nation-wide linkage study. PLoS ONE 14(12):e0225735.

24. McIntosh SE, Brant-Zawadzki G, Milliner BH, Christensen ED, Nyberg AA, Grissom CK, Olivares CR, Kim HS, Tremper B. Cause of death in Utah avalanche fatalities, 2006–2007 through 2017–2018 winter seasons. Wilderness Environ Med. 2019;30:191–4.
25. Grosse AB, Grosse CA, Steinbach LS, Zimmermann H, Anderson S. Imaging findings of avalanche victims. Skeletal Radiol. 2007;36:515–21.
26. Grossman MD, Saffle JR, Thomas F, Tremper B. Avalanche trauma. J Trauma. 1989;29:1705–9.
27. Gray D. Survival after burial in an avalanche. BMJ. 1987;294:611–2.
28. Boyd J, Haegeli P, Abbu-Laban RB, Shuster M, Butt JC. Patterns of death among avalanche fatalities: a 21-year review. CMAJ. 2009;180:507–12.
29. Sheets A, Wang D, Logan S, Atkins D. Causes of death among avalanche fatalities in Colorado: a 21-year review. Wilderness Environ Med. 2018;29:325–9.
30. Page CE, Atkins D, Shockley LW, Yaron M. Avalanche deaths in the United States: a 45-year analysis. Wilderness Environ Med. 1999;10:146–51.
31. Niedermeier M, Gatterer H, Pocecco E, Fruhauf A, Faulhaber M, Menz V, Burtscher J, Posch M, Ruedl G, Burtscher M. Mortality in different mountain sports activities primarily practised in the winter season—a narrative review. Int J Environ Res Public Health. 2020;17:259. https://doi.org/10.3390/ijerph17010259.
32. Kobek M, Skowronek R, Jablonski C, Jankowski Z, Pasz A. Histopathological changes in lungs of mountain snow avalanche victims and its potential usefulness in determination of cause and mechanism of death. Arch Med Sad Kryminol. 2016;66:23–31.
33. Wick MC, Weiss RJ, Holrieder M, Tecklenburg K, Jaschke W, Rieger M. Radiological aspects of injuries of avalanche victims. Injury Int J Care Injured. 2009;40:93–8.
34. Cohen JG, Grenier F, D'Alnoncourt SD, Reymond E, Blancher M, Peoc'h M, Scolan V, Ferretti G, Bouzat P. Asphyxia after complete avalanche burial: a new paradigm. Resuscitation 2017:118: e1–e2.
35. Schmid F. The pathogenesis of pulmonary edema after being buried by an avalanche. Schwiez med Wochenschr. 1981;111:1441–5.
36. Kizer KW, MacQuarrie MB, Kuhn BJ, Scannell PB. Deep snow immersion deaths: a snowboarding danger. Phys Sportsmed. 1994;22:48–61.
37. Cadman R. Eight nonavalanche snow-immersion deaths Physcian Sportsmed. 1999;27:31–43.
38. Kosinski S, Jasinski J, Krzeptowski-Sabala S, Gasienica J, Gorka A. Deep snow immersion suffocation—the deadly threat. Anaesthesiology Intensive Therapy. 2013;45:33–4.
39. Van Tilburg C. Non-avalanche-related snow immersion deaths: tree well and deep snow immersion asphyxiation. Wilderness Environ med. 2010;21:257–61.
40. Lee C, Porter KM. Suspension trauma. Emerg Med J. 2007;24:2378–3238.
41. Rauch S, Schenk K, Strapazzon G, Dal Cappello T, Gatterer H, Palma M, Erckert M, Oberhuber L, Bliemsrieder B, Brugger H, Paal P. Suspension syndrome: a potentially fatal vagally mediated circulatory collapse—an experimental randomised crossover trial. European J Applied Physiol. 2019;119:1353–65.
42. Pasquier M, Yersin B, Vallotton L, Carron P-N. Clinical update: suspension trauma. Wilderness Environ Med. 2011;22:167–71.
43. Wharton DR, Mortimer RB. Rhabdomyolysis after prolonged suspension in a cave. Wilderness Environ Med. 2011;22:52–3.
44. Pollanen M. Fatal rhabdomyolysis after torture by reverse hanging. Forensic Sci Med Pathol. 2016;12:170–3.
45. Jason van der Velde. Trauma: suspension and crush. In: Nutbeam T, Boylan MBMJ ed. ABC of prehospital emergency medicine. London, Books, 2013, pp. 98–102.
46. Lawler W. Death by reverse suspension. Am J Forensic Med Pathol. 1993;14:87–8.
47. Sauvageau A, Desjarlais A, Racette S. Deaths in a head-down position: a case report and review of the literature. Forensic Sci Med Pathol. 2008;4:51–4.
48. Smith Laing T. For Goya, the normal, the terrible, and the fantastical existed cheek by jowl. Apollo 2020. https://www.apollo-magazine.com/goya-drawings-prado-review/. Last visited January 2022.

49. Cohen E. The Crossroads of Justice: Law and Culture in late Medieval France. Netherlands: E.J. Brill; 1993. p. 92–3.
50. Hilgermann R, Richter O. Einige besondere Falle aus einem rechtsmedizinischen Obduktionsgut. Britr Gerichtl Med. 1973;30:163–74.
51. Madea B. Death in a head-down position. Forensic Sci Int. 1993;61:119–32.
52. Purdue B. An unusual accidental death from reverse suspension. Am J Forensic Med Pathol. 1992;13:108–11.
53. Heath KJ, Cala A, Byard RW. Metal railing fences and accidental death. J Forensic Sci. 2018;63:972–5.
54. De Donno A, De Fazio A, Greco MG, Introna F, Maglietta RAG. Death in head-down position in a heavily intoxicated obese man. Leg Med. 2008;10:204–9.
55. SchäfferA T. Death in a head-down position. In: Tsokos M ed. Forensic pathology reviews. Vol. 3. Ed, Humana press, Totowa, New Jersey, 2005, pp. 137–156.
56. Uchigasaki S, Takahashi H, Suzuki T. An experimental study of death in a reverse suspension. Am J Forensic Med Pathol. 1999;20:116–9.
57. Madea B, Doberentz E. Death upside down. In: Madea B ed. Asphyxiation, suffocation and neck pressure deaths. CRC Press Taylor & Francis Group, London, 2021, pp. 2450–248.
58. Katiyar A, Kherwal N, Kumar A, Azam Q, Rattan A. Reverse suspension syndrome: first report of a novel mechanism of severe trauma. Trauma Case Reports. 2019;24: 100264. https://doi.org/10.1016/j.tcr.2019.100264.
59. https://volcano.si.edu/. Last visited January 2022.
60. Brown SK, Jenkins SF, Sparks RSJ, Odbert H, Auker MR. Volcanic fatalities database: analysis of volcanic threat with distance and victim classification. J Appl Volcanol. 2017;6:15. https://doi.org/10.1186/s13617-017-0067-4.
61. Auker MR, Sparks RSJ, Siebert L, Crosweller HS, Ewert J. A statistical analysis of the global historical volcanic fatalities record. J Appl Volcanol. 2013;2:2. https://doi.org/10.1186/2191-5040-2-2.
62. Cantrell L, Young M. Fatal fall into a volcanic fumarole. Wilderness Environ med. 2009;20:77–9.
63. Baxter PJ, Bernstein RS, Falk H, French J, Ing R. Medical aspects of volcanic disaster: an outline of hazards and emergency response measures. Disasters. 1982;6:268–76.
64. Baxter PJ. Medical effects of volcanic eruptions. Bull Volcanol. 1990;52:532–44.
65. Baxter PJ. Health hazards of volcanic eruptions. J Royal Col Physicians Lon. 1983;17:180–2.
66. Hansell A, Oppenheimer C. Health hazards from volcanic gases: a systematic literature review. Arch Environ health. 2004;59:628–39.
67. McNutt SR, Williams ER. Volcanic lightning: global observations and constraints on source mechanisms. Bull Volcanol. 2010;72:1153–67.
68. Spence RJS, Kelam I, Baxter PJ, Zuccaro G, Petrazzuoli S. Nat Hazards earth Syst Sci. 2005;5:477–94.
69. https://www.dailymail.co.uk/sciencetech/article-3253660/Peering-inside-Pompeii-s-tragic-victims-Incredible-CT-scans-reveal-bodies-unprecedented-laying-bare-bones-delicate-facial-features-dental-cavities.html. Last visited January 2022.
70. Rutty GN, Alminyah A, Apostol M, Boel LWT, Brough A, Bouwer H, O'Donnell C, Fujimoto H, Iino M, Kroll J, Lee CT, Levey DS, Makino Y, Oesterhelweg L, Ong B, Ranson D, Robinson C, Singh MKC, Villa C, Viner M, Woodford N, Watkins T, Wozniak K. Positional statement: radiology disaster victim identification reporting forms. Positional statement of the members of the disaster victim identification working group of the international society of forensic radiology and imaging. J Forensic Radiol Imaging. 2018;15:4–7.
71. Hofman P, Alminyah A, Apostol M, Boel LWT, Brough A, Bouwer H, O'Donnell C, Fujimoto H, Iino M, Kroll J, Lee CT, Levey DS, Makino Y, Oesterhelweg L, Ong B, Ranson D, Robinson C, Rutty G, Singh MKC, Villa C, Viner M, Woodford N, Watkins T, Wozniak K. Use of post-mortem computed tomography in disaster victim identification. updated positional statement of the members of the disaster victim identification working group of the international society of forensic radiology and imaging. J Foresic Radiol Imag 2019. https://doi.org/10.1016/j.jofri.2019.100346.

72. Rutty GN, Biggs MJP, Brough A, Morgan B, Webster P, Heathcote A, Dolan J, Robinson C. Remote post-mortem radiology reporting in disaster victim identification: experience gained in the 2017 Grenfell Tower disaster. Int J leg Med. 2020;134:637–43.
73. Blau S, Ranson D, O'Donnell C. An atlas of skeletal trauma in medico-legal contexts. Academic Press, 2018.
74. Rutty GN, Hollingbury FE, Morgan B. Post-mortem computed tomography visualised fire related post-mortem changes of the head. J Forensic Radiol Imaging. 2015;3:235–7.
75. Henri M, de Bakker HM, Roelandt GHR, Soerdjbalie-Maikoe V, van Rijn RR, de Bakker BS. The value of post-mortem computed tomography of burned victims in a forensic setting. Eur Radiol. 2019;29:1912–21.
76. Hammarlebiod S, Farrugia A, Bierry G, Raul J-S, Willaume T. Thermal bone injuries: post-mortem computed tomography findings in 25 cases. Int J Legal Med 2021. https://doi.org/10.1007/s00414-021-02708-7. Online ahead of print.
77. Coty J-B, Nedelcu C, Yahya S, Dupont V, Rougé-Maillart C, Verschoore M, Ridereau Zins C, Aubé C. Burned bodies: post-mortem computed tomography, an essential tool for modern forensic medicine. Insights Imaging. 2018;9:731–43.
78. Raux C, Saval F, Rouge D, Telmon N, Dedouit F. Diagnosis of drowning using post-mortem computed tomography—state of the art. Arch Med Sadowej Kryminol. 2014;64:59–75.
79. Christe A, Aghayev E, Jackowski C, Thali MJ, Vock P. Drowning–post-mortem imaging findings by computed tomography. Eur Radiol. 2008;18:283–90.
80. Kawasumi Y, Kawabata T, Sugai Y, Usui A, Hosokai Y, Sato M, Saito H, Ishibashi T, Hayashizaki Y, Funayama M. Assessment of the relationship between drowning and fluid accumulation in the paranasal sinuses on post-mortem computed tomography. Eur J Radiol. 2012;81:3953–5.
81. Gotsmy W, Lombardo P, Jackowski C, Brencicova E, Zech W-D. Layering of stomach contents in drowning cases in post-mortem computed tomography compared to forensic autopsy. Int J Legal Med. 2019;133:181–8.